STRUCTURE AND WATER-OXIDIZING CAPABILITIES OF DIMERIC RUTHENIUM COMPLEX IONS

Jinzhong Zhou
B.A., University of Nanjing, 1964
M.S., Institute of Atomic Energy, 1981

A dissertation submitted to the faculty of the

Oregon Graduate Institute
of
Science and Technology

in partial fulfillment of the
requirements for the degree
Doctor of Philosophy
in
Inorganic Chemistry

July, 1990

The dissertation "Structure and Water-Oxidizing Capabilities of Dimeric Ruthenium Complex Ions" by Jinzhong Zhou has been examined and approved by the following Examination Committee:

James K. Hurst, Thesis Advisor
Professor

Thomas M. Loehr
Professor

Shankar B. Rananavare
Assistant Professor

Jack H. Devletian
Professor

DEDICATION

This dissertation is dedicated to all of those who have influenced and helped me throughout my academic career. I especially wish to thank my wife for emotional support and understanding. I would like to dedicate this work to my teacher, Dr. De-Xi Wang. This is also dedicated to my two children.

ACKNOWLEDGMENTS

I wish to express my thanks to Dr. James K. Hurst for his understanding and encouragement as well as providing me with the opportunity to do this work in the first place. I also wish to thank the Examination Committee for the time and effort they have put into refining this work.

Thanks also to David Thompson and William Barrette for their help. And I would like to acknowledge Eberhardt Kuhn, Brian Patterson, and Yabin Lei for their contributions to the understanding of this work.

ABSTRACT

Structure and Water-Oxidizing Capabilities of Dimeric Ruthenium Complex Ions

Jinzhong Zhou, Ph.D.
Oregon Graduate Institute, 1990

Supervising Professor: James K. Hurst

Several ruthenium-edta complexes were synthesized and their optical and electrochemical properties studied. The reduction potential for the $(edta)_2Ru_2^{III,IV}/(edta)_2Ru_2^{IV}$ couple was acid-insensitive over the pH range pH 2-10, suggesting that the dimer does not contain coordinated H_2O in either oxidation state. Resonance Raman (RR) spectra of $(edta)_2Ru_2^{III,IV}$ exhibited a prominent band at 433 cm^{-1}, which shifted to 431 cm^{-1} upon substitution of ^{16}O by ^{18}O in the bridging ligand. A second band at 324 cm^{-1} underwent a comparable isotope-dependent shift to lower energy. The RR spectra were insensitive to deuterium substitution. These features indicate that the dimer is a μ-oxo ion; from the magnitude of the isotopic shifts, the Ru-O-Ru angle was estimated to be 165°. Cyclic voltammographic and optical behavior suggested that the dimeric $(edta)_2Ru_2^{IV}$ was unstable with respect to decomposition. A reinvestigation of the water-oxidizing capabilities of this ion by Clark oxygen electrode, gas chromatography, and mass spectrometry revealed that CO_2 was the only detectable gaseous product, indicating that the ion is not a catalyst for water oxidation.

Bipyridine derivatives and their bis-bipyridyl ruthenium monomeric and dimeric complexes were also synthesized, and their optical and electrochemical properties studied. Electron-withdrawing substituents

on the bipyridine rings caused absorption spectra to shift to lower frequencies and reduction potentials to more positive values. The solvent dependence upon these properties varied quantitatively with the solvent donor number. RR spectra of $(bpy)_2(OH_2)Ru^{III}ORu^{III}(OH_2)(bpy)_2$ and its one-electron oxidation product indicated that no exchange took place between aqua ligands and water molecules in the solvent within a few hours or during catalytic turnover in water-oxidizing reactions. Given this observation, the oxygen isotope distribution from single-turnover experiments established that catalyzed water oxidation did not occur by oxidative elimination pathways involving coordinated water but rather by direct oxidation of free H_2O. A direct comparative study indicated that addition of an electron-withdrawing group to the bipyridine rings deactivated the catalyst.

LIST OF ABBREVIATIONS

bpy = 2,2'-bipyridine

$(bpy)_2(OH_2)Ru^{III}ORu^{III}$ = μ-oxobis[aquabis(2,2'-$(OH_2)(bpy)_2$ bipyridine) ruthenium(III)]

CPE = constant potential electrolysis

4,4'-diacid = 4,4'-dicarboxylic acid-2,2'-bipyridine

5,5'-diacid = 5,5'-dicarboxylic acid-2,2'-bipyridine

4,4'-diester = 4,4'-dicarbethoxy-2,2-bipyridine

5,5'-diester = 5,5'-dirbethoxy-2,2'-bipyridine

4,4'-dimethoxy = 4,4'-dimethoxy-2,2'-bipyridine

edta = ethylenediaminetetraacetate

$(edta)_2Ru_2{}^{III,IV}$ = μ-oxo[bis(ethylenediaminetetraacetato] ruthenium(III,IV)

(4,4'-ester)$_2(OH_2)Ru^{III}O$ = μ-oxobis[aquabis(4,4'-dicarbethoxy $Ru^{III}(OH_2)$(4,4'-ester)$_2$ 2,2'-bipyridine)ruthenium(III)]

(5,5'-ester)$_2(OH_2)Ru^{III}O$ = μ-oxobis[aquabis(5,5'-dicarbethoxy-$Ru^{III}(OH_2)$ (5,5'-ester)$_2$ 2,2'-bipyridine)ruthenium(III)]

GC = gas chromatography

GCE = glassy carbon electrode

MS = mass spectroscopy

(4,4'-methoxy)$_2(OH_2)Ru^{III}O$ = μ-oxobis[aquabis(4,4'-dimethoxy-2,2 $Ru^{III}(OH_2)$(4,4'-methoxy)$_2$ bipyridine)ruthenium(III)]

$Ru(bpy)Cl_2$ = cis-dichlorobis(2,2'-bipyridine)ruthenium(II)

$Ru(bpy)_3Cl_2$ = tris-(2,2'-bipyridine)ruthenium(II) chloride

ABBREVIATIONS (Continued)

$Ru^{III}(edta)(OH_2)$ = aqua(hydrogenethylenediaminetetraacetato) ruthenium(III)

$Ru(4,4'\text{-ester})_2Cl_2$ = cis-dichlorobis(4,4'-dicarbethoxy-2,2'-bipyridine) ruthenium(II)

$Ru(5,5'\text{-ester})_2Cl_2$ = cis-dichlorobis(5,5'-dicarbethoxy-2,2'-bipyridine) ruthenium(II)

$Ru(4,4'\text{-methoxy})_2Cl_2$ = cis-dichlorobis(4,4'-dimethoxy-2,2'- bipyridine) ruthenium(II)

SCE = saturated calomel electrode

TABLE OF CONTENTS

CHAPTER

LIST OF TABLES

LIST OF FIGURES

CHAPTER 1

INTRODUCTION

Recent figures estimate that the world's annual consumption of energy is the enormous value of about 10^{17} Kcal and is increasing, doubling each 15 to 20 years.[1] Fossil fuel reserves are limited. If we are to meet future energy requirements, we must develop alternative sources. Solar energy seems to be an important and attractive candidate because it offers the possibility of fulfilling energy cycles without polluting the environment and adding additional heat to the Earth.[1] However, wide use of solar energy is restricted by two factors: its low energy density and variability. Thus, it is necessary to collect and convert solar energy into a form convenient for practical use. Conversion into chemical energy seems to be one of the most promising methods under consideration. Some reactions which could possibly serve this purpose are listed in Table 1.1. Of these reactions, hydrogen production via photocatalytic water cleavage seems highly attractive because it is both a high energy and ecologically harmless fuel and a valuable material for chemical industry. In addition, from information accumulated to date concerning chemical reaction mechanisms, photocatalytic cleavage of water is expected to be the simplest to accomplish among all the reactions given in Table 1.1. Some successes in development of photocatalytic systems for water cleavage into molecular hydrogen and oxygen have already been reported.[2-5] These systems are conventionally divided into two types: semiconductor and molecular photocatalytic systems.

Table 1.1. Solar to Chemical Reaction Schemes[a]

Reaction[b]	n[c]	ΔG (Kcal/mol)	ΔH (Kcal/mol)	λ[d] (nm)
$H_2O = H_2 + 1/2\ O_2$	2	56.71	68.25	1008
$2H_2O + CO_2 = CH_4 + 2O_2$	8	195.54	212.8	1176
$2H_2O + CO_2 = CH_3OH + 3/2\ O_2$	6	167.92	173.64	1025
$3H_2O + 2CO_2 = C_2H_5OH + 3O_2$	12	318.34	336.82	1077
$3/2\ H_2O + 1/2\ N_2 = NH_3 + 4/3\ O_2$	3	81.09	91.44	1059
$2H_2O + N_2 = N_2H_4 + O_2$	4	181.33	148.74	629

[a] Abstracted from reference 1.

[b] Thermodynamic data are given for liquid H_2O, CH_3OH, C_2H_5OH, and N_2H_4.

[c] n, number of electrons transferred.

[d] λ is the threshold wavelength (maximum wavelength) for an n-photon mechanism.

Semiconductor systems use massive or highly dispersed semiconductors as photocatalysts. Systems of this type have been developed with an efficiency of several percent of solar light conversion into the chemical energy of the hydrogen-plus-oxygen pair.[2,6] Molecular photocatalytic systems are based loosely on modeling the scheme of natural photosynthesis. The work with these systems was started later than that with the semiconductor systems and has not yet yielded the capabilities for photcatalytic water splitting that match efficiencies already achieved with semiconductors. Nevertheless, because the efficiency of solar energy conversion by natural photosynthesis is quite high (as high as 5 to 10%) for a very complicated reaction between water and carbon dioxide,[7] we may hope that efficient artificial converters can be created for a much simpler reaction of water cleavage.

For several years, research in Dr. Hurst's laboratory has been directed at integrated systems for water photolysis. The sort of scheme we are concerned with is illustrated below:

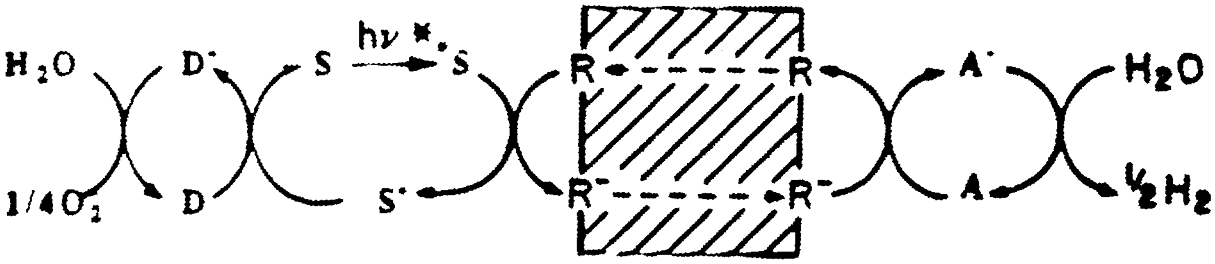

Scheme 1.

It includes:

1. A photosensitizer which undergoes oxidative quenching, leading to formation of a primary redox ion pair at an interface.

$$S + R \rightarrow S^{+} + R^{-} \qquad (1)$$

2. Secondary dark reactions which separate the charge across a physical barrier. (In the Hurst laboratory, the barrier is always a vesicle bilayer membrane.)

$$R^{-} + A \rightarrow R + A^{-} \qquad (2)$$

$$S^{+} + D \rightarrow S + D^{+} \qquad (3)$$

3. Terminal, i.e., irreversible, reactions involving catalyzed reduction and oxidation of water on the opposite sides of the membrane.

$$4D^+ + 2H_2O \rightarrow 4D + 4H^+ + O_2 \tag{4}$$

$$2A^- + 2H^+ \rightarrow 2A + H_2 \tag{5}$$

The overall process is described by the reaction:

$$2H_2O \rightarrow 2H_2 + O_2 \tag{6}$$

One of the major difficulties in achieving such a set of reactions for water splitting is that no good homogeneous catalysts exist for the oxidative half-cycle.

A few chemical oxidants, such as Ce^{4+}, MnO_4^-, and Co^{3+}, have thermodynamic potentials sufficient to oxidize water to oxygen, but the oxidative reaction does not take place rapidly because homogeneous oxidation of water in four consecutive electron-transfer steps involves the reactive and high energy species OH·, H_2O_2, and HO_2 as intermediates and, therefore, is associated with large activation energies. These physical constraints can be seen clearly from the sequential one-electron oxidation steps (given in the following Latimer diagram) involved with water oxidation in acidic media (potential vs. NHE; $a_{H^+} = 1$):

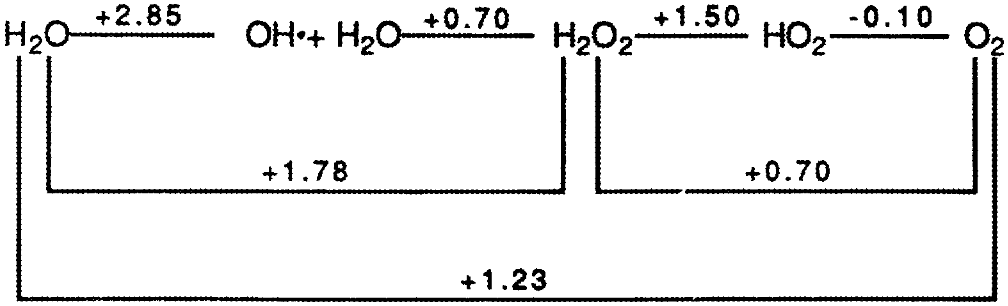

Any mechanism which proceeds by stepwise one-electron transfer steps must necessarily involve the intermediate, hydroxyl radical, which demands a very powerful oxidant if the reaction is to proceed at a reasonable rate. Thus, to achieve oxidation of water to oxygen, we must utilize catalysts that are able to bypass this step. Such catalysts must be capable of multiple electron transfer. This point is further illustrated in the following scheme where the energetic consequences of one-electron and multi-electron pathways are compared.

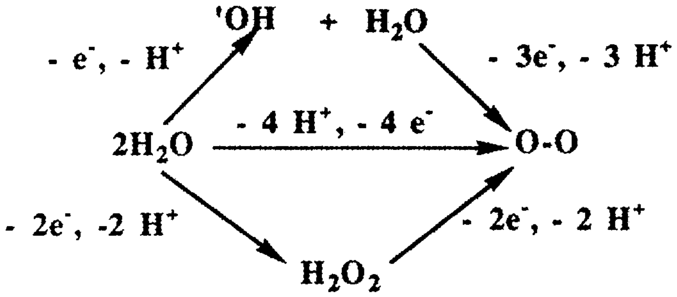

Scheme 2.

The direct four-electron pathway, which would avoid high energy intermediate radical formation, places a significant demand on the catalysts and requires the concerted loss of $4H^+$ and $4e^-$ from two water molecules with concomitant formation of an O–O bond. The two-electron pathway with H_2O_2 as an intermediate is able to avoid the high energy intermediate, OH·, and decreases the demand on the catalysts, but the reaction barrier is higher than the four-electron pathway.

Systematic search for catalysts began in the late 1970's.[1] Initial studies were made with heterogeneous catalysts comprising noble metals and their oxides,[9] and only more recently has the search been extended to soluble metal ion complexes[7] and multinuclear metal ion complexes.[10-17] Table 1.2 summarizes the different materials which have

Table 1.2. Oxygen Catalysts and Oxidizing Agents[a]

Catalysts	Oxidants
Pt foil	Ce^{4+} ion (2 mol H_2SO_4)
$RuO_2 \cdot xH_2O$ (powder, colloid)	$Ru(bpy)_3{}^{3+}$
$RuO_2 \cdot xH_2O$ (powder, colloid)	$Ru(bpy)^{3+}$
$RuO_2 \cdot xH_2O$ (powder, colloid)	$Fe(bpy)_3{}^{3+}$, Tl^{3+}, $BrO_3{}^-$, $MnO_4{}^-$
$RuO_2 \cdot xH_2O$ on various supports (TiO_2, Al_2O_3, clay, zeolite)	Ce^{4+}, $Ru(bpy)_3{}^{3+}$
PtO_2 (Adams)	Ce^{4+} (0.5 mol H_2SO_4)
IrO_2	Ce^{4+} (0.5 mol H_2SO_4)
$IrO_2 \cdot xH_2O$	Ce^{4+} (0.5 mol H_2SO_4)
MnO_2	$Ru(bpy)_3{}^{3+}$
Rh_2O_3	$Ru(bpy)_3{}^{3+}$
$Fe_4[Fe(CN)_6]_3$	Ce^{4+}, $Ru(bpy)_3{}^{3+}$
$[(bpy)_2Mn(\mu\text{-}O)_2Mn(bpy)_2](ClO_4)^b$	Ce^{4+}
$[(phen)_2Mn(\mu\text{-}O)_2Mn(phen)_2(ClO_4)^c$	Ce^{4+}
$[(NH_3)_4Ru(NH_2)Ru(NH_3)_4]Cl_4$	Ce^{4+}
trans-$Ru(bpy)_2(H_2O)^{2+}{}_2$	$Ru(bpy)_3{}^{3+}$
$(edta)_2Ru_2{}^{IVe}$	Ce^{4+}
$[(bpy)_2(H_2O)Ru^{III}ORu^{III}(OH_2)(bpy)_2]^f$	Ce^{4+}
55-bpy[dg]	Ce^{4+}, Co^{3+}

Table 1.2. (Continued)

---

[a] The data in the table are abstracted from reference 9 except where otherwise indicated.

[b] bpy = 2,2′-bipyridine.

[c] phen = 1,10-phenanthroline.

[d] 55-bpy = $(5,5'\text{-diester})_2(OH_2)Ru^{III}ORu^{III}(OH_2)(5,5'\text{-diester})_2$; (5,5-diester = 5,5-dicarbethoxy-2,2-bipyridine).

[e] From reference 12.

[f] From references 10 and 11.

[g] From reference 14.

been reported as active O_2 catalysts and oxidizing agents.[9] Among them, the dimeric aqua complexes of ruthenium are most intriguing. Coordinated water was thought to allow access to higher oxidation states by deprotonation of coordinated water, thus allowing concerted two- or four-electron transfer.[11] The Ru-O-Ru dinuclear center has been suggested to hold coordinated oxo groups in close proximity to promote O-O bond formation (i.e., template effect) in an oxidative elimination step, which is functionally a four-electron transfer process.

Meyer's group has devoted extensive effort to the development and characterization of a variety of catalytic ruthenyl complexes.[10,11,18-23] The group showed that bis[aqua(2,2′-bipyridine)]ruthenium(II), $Ru(bpy)_2(OH_2)^{2+}{}_2$, can undergo four sequential oxidation steps from Ru^{II} to Ru^{IV}, which are accompanied with concurrent deprotonations of the bound aqua ligands. Oxidation of Cl^- to Cl_2 in aqueous solution was catalyzed by the complex.[15] Catalytic oxidation of various organic compounds by type of complexes was also reported.[24] More recently, they reported characterizations of structure and the redox properties of the dimer, μ-oxobis[aquabis(2,2'bipyridine)ruthenium(III)] ($[(bpy)_2(H_2O)Ru{-}O{-}Ru(H_2O)(bpy)_2]^{4+}$).[11] This complex was found to be capable of catalyzing water oxidation to produce dioxygen from a solution containing Ce^{4+} ion. One fascinating feature about the dimeric system is that coupled loss of 4 electrons and 4 protons might occur, leading to structures where two oxo groups are held in close proximity, each bound to an oxidized site (Ru^{V}). The V,V dimer is unstable in water and was originally proposed to undergo decomposition to the III,III ion according to the following scheme:

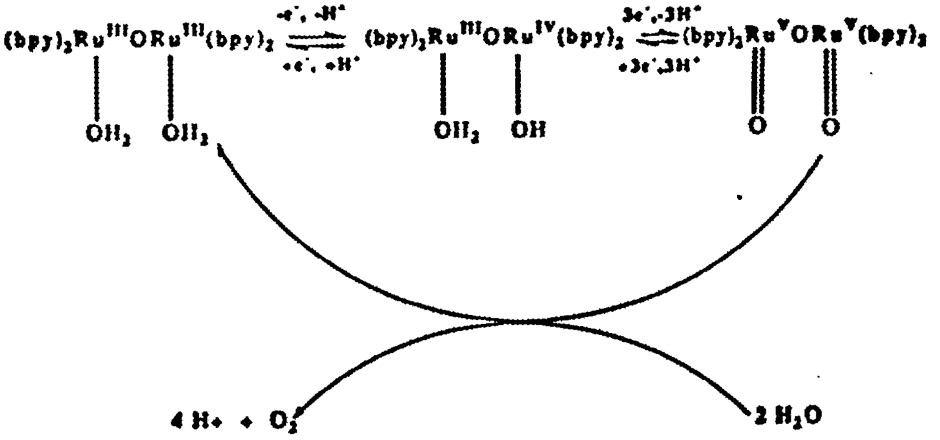

Scheme 3.

However, the mechanism or mechanisms by which water is oxidized by the μ-oxo ruthenium ion are unknown. A number of observations bearing upon this question have been made and are described below: One result[32] based on an ^{18}O labeling study at pH 1 showed that oxidation of the $H_2{}^{18}O$-labeled III,IV dimer by three equivalents of Ce^{IV} in normal water leads to isotopic distribution $^{18}O{-}^{18}O$ (6%), $^{18}O{-}^{16}O$ (63%), and $^{16}O{-}^{16}O$

(33%) in the dioxygen product. Based upon the labeling study, Meyer[32] suggested a number of competing pathways by which the dimer could oxidize water to dioxygen (see Scheme 4). Routes a and b are used to account for the appearance of $^{18}O-^{18}O$, of which route a occurs by the attack of external water molecules at the metals followed by O-O bond formation and electron release to two Ru(V) sites, and route b is a 4-electron and 4-proton intramolecular oxidative elimination process. Route c occurs by water attack at the electron deficient oxygen of the Ru^{V}-oxo site to form a bound peroxide followed by an intramolecular 2-electron step to give $^{16}O-^{18}O$. Route d is another intramolecular elimination process. In this process, an external water molecule attacks the electron-deficient oxygen of the Ru^{V}-oxo site to form a symmetrical or unsymmetrical bridging structure in which the oxygen from the external water becomes electron deficient. Then the second external water molecule attacks the oxygen and $^{16}O-^{16}O$ is released.

Subsequently, Grätzel and coworkers[14,15] studied an analogous μ-oxo ruthenium dimer containing carboxylic acids substituted on the bipyridine ring 5,5′-positions, i.e., $L_2(H_2O)Ru-O-Ru(H_2O)L_2$ (L = 5,5′-dicarboxylic acid-2,2′-bipyridine). They thought that the dimer was an even more active catalyst and suggested that the introduction of the carboxylic groups greatly enhances both the catalytic activity and durability of the dimeric complex. These improved characteristics were attributed to a combination of electronic and steric factors. The electronic effect introduced by carboxylic groups is revealed in the positive shift of redox potential and the red shift of absorption bands relative to the complex without carboxylic groups on the rings. The

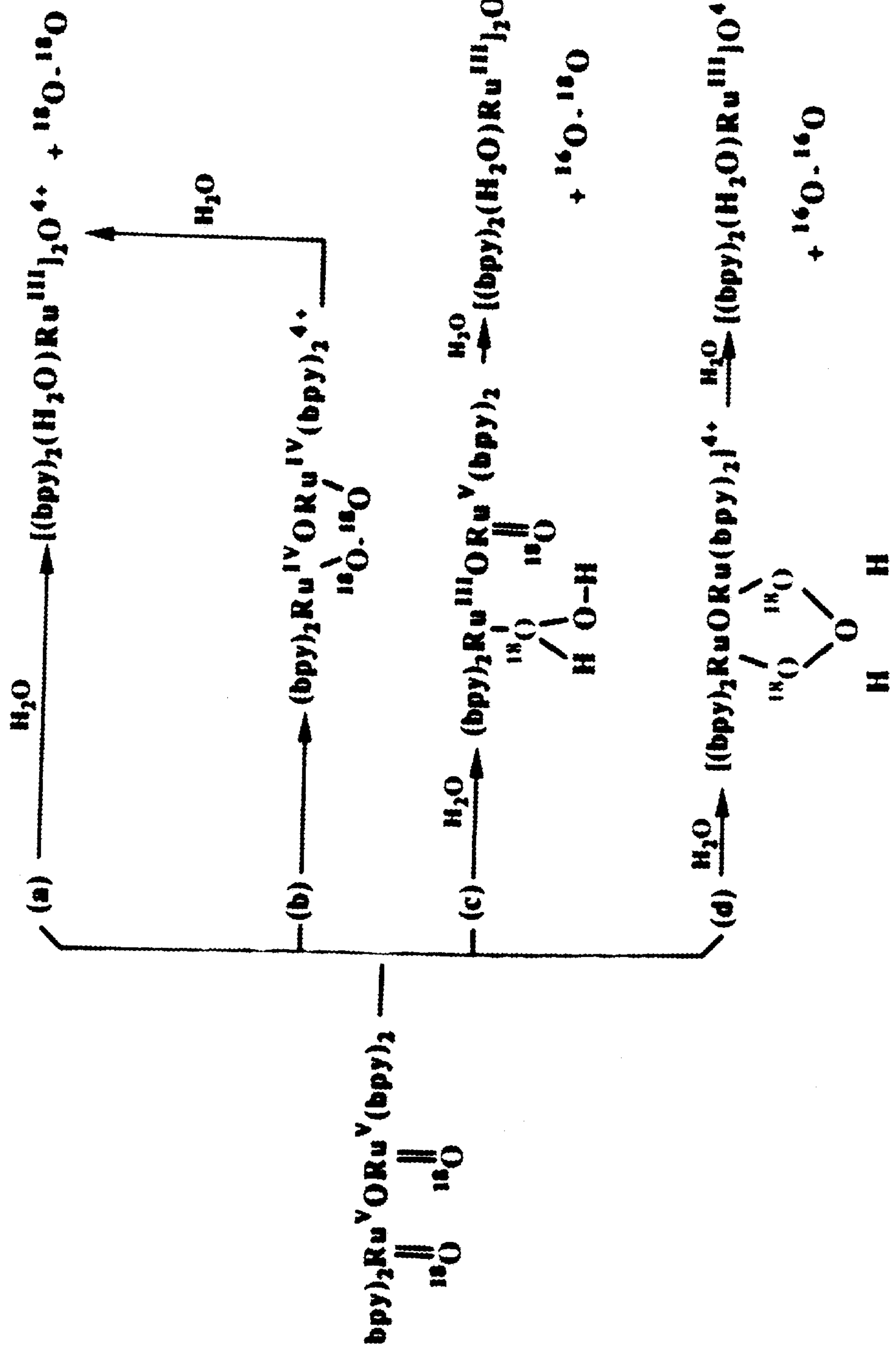

Scheme 4.

steric effect was ascribed to H-bond formation between aqua ligands and carboxylic groups on the bipyridine rings.

From the structures of the above mentioned μ-oxo ruthenium complexes, we can see that their common feature is that they possess cis-aqua ligands. Meyer[11] and Grätzel[14] and their collaborators thought that the cis-aqua ligands perform two significant functions:

1. They permit achievement of the high oxidation state, $Ru_2^{V,V}$, at reasonable potentials because progressive electron removal is accompanied by loss of protons, thereby allowing compensation for loss of electron density on Ru by increased electron donation from the ligands.

2. Because of their spatial location, they are properly disposed to undergo (as oxoyl groups) covalent bond formation leading to dioxygen formation.

Another dimeric ruthenium complex which was claimed to be able to catalytically oxidize water to dioxygen is the dimeric ruthenium edta complex ion. Studies of complexes of ruthenium with edta date from the 1960's when a series of articles appeared in the Russian literature[25-27] concerning the product of the reaction of $Ru(edta)(OH_2)$ with various chemical oxidants. At pH below 5, hydrogen peroxide reacted with the complex to produce an intensely green compound, while at pH above 7, dioxygen reacted with it to form a green compound with similar properties. The existence of a dimeric ruthenium complex was thought possible, but the description of the properties and proposed structures of the green complex varied from paper to paper. The various structures proposed are all doubly bridged, having either dihydroxo, a peroxo and a hydroxo, a dioxo and a hydroxyo, or an oxo and an aqua, as bridging groups (see Scheme 5). The oxidation states of the ruthenium atom were never clearly identified and varied depending upon the type of bridging invoked.

More recently, Ikeda and coworkers[28] reported that chlorate ion reacted with $Ru^{III}(edta)(H_2O)$ to form a green species. They obtained spectral properties similar to those of Ezerskaya, but proposed a μ-oxo-bridged dinuclear ruthenium (see Scheme 5). This kind of structure was based only on analogy with the systems characterized by Meyer for ruthenium bipyridine complexes and ruthenium amine complexes.[10,29,30] However, no direct evidence was presented to establish the μ-oxo bridged structure. In addition, based on a titrimetrically determined oxidation (one electron per two ruthenium atoms), they proposed that the dimer was a mixed-valent μ-oxo with an average oxidation state of 7/2 for each ruthenium center.

Most recently, Anson and Baar[12,13] have extensively studied this dimeric complex. They found that the proton release during oxidation with H_2O_2 and overall stoichiometry could be accommodated by equation 7 or 8.

$$2\ [(edta)Ru^{III}(H_2O)]^- + 0.5\ H_2O_2 = \{[(edta)Ru]_2O\}^{3-} + H^+ + 2H_2O \qquad (7)$$

$$2\ [(edta)Ru^{III}(H_2O)]^- + 0.5\ H_2O_2 = \{[(edta)Ru(OH)]_2\}^{3-} + H^+ + H_2O \qquad (8)$$

The implication of equations 7 and 8 was that the product of oxidation is an oxo- or a dihydroxo-bridged dimer in which the average oxidation state of the ruthenium center was 3.5. Although Anson's results have removed the possibility of peroxo-hydroxo, superoxo-

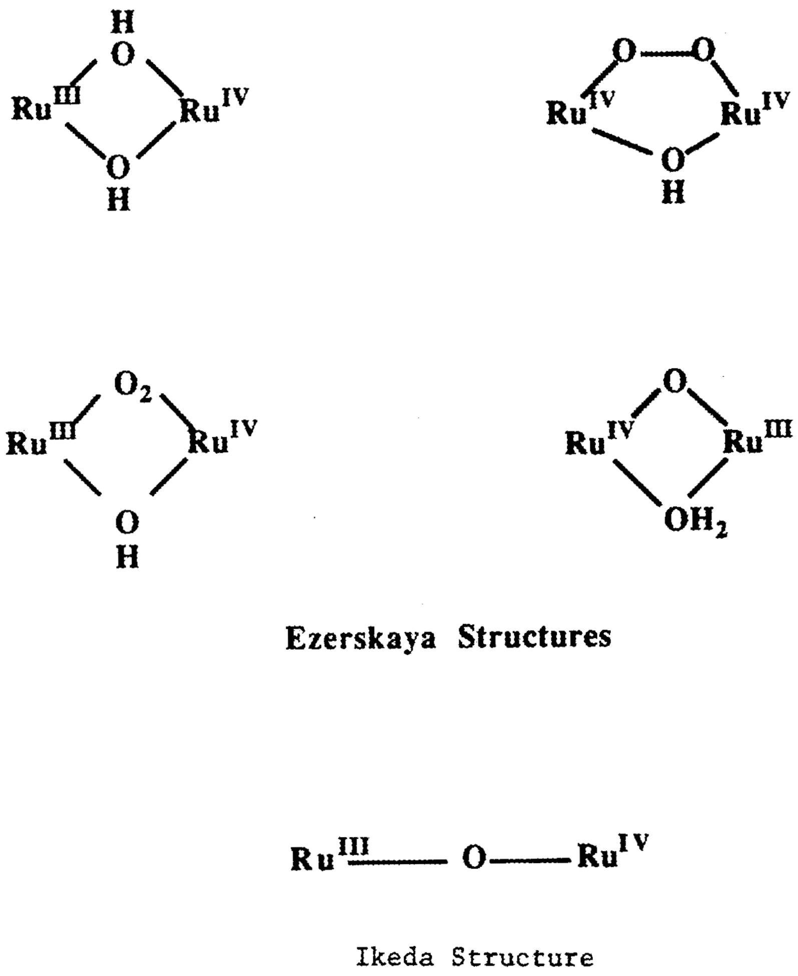

Ezerskaya Structures

Ikeda Structure

Scheme 5.

hydroxo, and aquo-oxo bridges, they still could not distinguish the μ-oxo from a dihydroxo bridge.

In addition, Anson and coworkers showed that (edta)$Ru_2^{III,IV}$ ion could be further oxidized either chemically with Ce^{4+} or electrochemically to give a spectroscopically distinct species. From a

Nernst plot of thin-layer spectroelectrochemical data, they ascertained that one-electron oxidation had occurred, yielding an $(edta)_2Ru_2^{IV,IV}$ ion. This latter species was unstable and spontaneously reverted to $(edta)_2Ru^{III}Ru^{IV}$ or a spectroscopically indistinguishable ion. Reduction of the $(edta)_2Ru_2^{IV,IV}$ was thought to occur at the expense of the solvent (water) based on observation of a positive response from a Clark polarographic electrode in the presence of Ce^{4+} ion or when the solution was poised at a potential that continuously regenerated the oxidized dimer.

Our interest in this ion was prompted by the claim that it could act as a catalyst for water oxidation. The above-mentioned μ-oxo ruthenium dimers of the general type cis,cis-$[(bpy)_2Ru(OH_2)]_2O$ have been described as being capable of catalytically oxidizing water electrochemically or in the presence of strong oxidants. As described above, the coordinated water molecules are thought to play an important role. Additionally, carboxyl group substitution at the 5,5′-position in bipyridine rings has been reported to enhance catalytic activity which is ascribed to H-bond formation with aqua ligands. Infrared and pH titrimetric studies have established a comparable structural feature in $(edta)_2Ru^{III}Ru^{IV}$, namely that edta is pentacoordinate with one carboxyl group remaining free.[13,28] However, this ion does not contain coordinated water. If the complex is a catalyst for the splitting of water into oxygen, catalysis must be accomplished through a very different mechanism from that of dimeric ruthenium complexes with bipyridine and its derivatives. Based on these considerations, we felt that a study of the comparative reactivities of bipyridine and edta-based binuclear ions might provide insight into the catalytic mechanisms for water oxidation. In addition, to understand the function of carboxylic groups on the bipyridine rings, a direct comparative study of the catalytic ability of several μ-oxo ruthenium dimers of the type of cis,cis-$[L_2Ru(OH_2]_2O$ (L = bipyridine, 5,5′-dicarboxylic acid-2,2′-bpy, 4,4′-dicarboxylic acid-2,2′-bpy) was necessary.

Given these mechanistic considerations, I undertook the tasks of establishing the structure of $(edta)_2Ru^{III}Ru^{IV}$ ion and its catalytic oxidation water mechanism and of making comparative studies of μ-oxo ruthenium dimers of the type of cis,cis-$[L_2Ru(OH_2)]_2O$. Results of these studies have served both to clarify mechanisms and provide information which should allow synthesis of superior catalysts within this series of complexes.

CHAPTER 2

EXPERIMENTAL

2.1 MATERIAL

2.1.1 Preparation of aqua(ethylenediaminetetraacetato)ruthenium(III) $[Ru^{III}(edta)(OH_2)]$

The complex ion was prepared either from $RuCl_3 \cdot 3H_2O$ via the intermediacy of Ru^{II} blue cluster complexes[31] or by ligand substitution onto the aquapentachlororuthenate(III) $[RuCl_5 \cdot OH_2{}^{2-}]$ dianion.[13]

(1) From $RuCl_3 \cdot 3H_2O$: The procedures described by Shimizu[31] were followed explicitly. Briefly, these entailed evaporation of a solution of 1.05 g $RuCl_3 \cdot 3H_2O$ in 200 mL ethanol and 150 mL 3 M HCl to dryness, redissolving the blue ruthenium crystals in a small amount of water, and adding a concentrated solution of (PTO). Because repeated recrystallization by ethanol addition to the filtrate failed to yield the expected $Ru^{III}(edta)(OH_2)$ compound, chloride ion was precipitated by adding a 5 to 10% stoichiometric excess of $AgNO_3$. AgCl was removed by centrifugation, and $Ru(Hedta)(OH_2)$ was isolated as a tan solid by adding ethanol to the supernatant. The solid product was subsequently recrystallized several times from dilute trifluoroacetic acid (HTFA)/ethanol. Infrared and optical spectra were very similar to previously reported data.[13,28] In particular, the infrared spectra in KCl exhibited strong bands at 1737 and 1656 cm^{-1} attributable to the carbonyl stretching modes of protonated and coordinated carboxyl groups, respectively, and the electronic absorption spectra comprised a broad shoulder at 360 nm and a weak maximum at 284 nm superimposed upon a background of increasing absorption at progressively shorter wavelengths. A spot test with $AgNO_3$ or KCl indicated the absence of detectable Cl^- or Ag^+ ion, respectively, in solutions prepared from the recrystallized solid. No release of Mg^{2+} from Eriochromeschwartz T could be observed spectrophotometrically when the indicator complex was added to an ammonium-buffered solution (ph 10) of $Ru(edta)(OH_2)^-$, indicating the absence of uncoordinated edta in the preparation. Control experiments established that a concentration as low as 1% edta could be detected by this method.

(2) **From $[RuCl_5OH_2^{2-}]$:** $K_2[RuCl_5 \cdot OH_2]$ (1 g) was dissolved in 50 mL HTFA, pH 2, followed by the addition of 1.05 g disodium ethylenediaminetetraacetate. The solution was heated to near boiling for one hour, then slowly evaporated at lower heat until a light yellow precipitate started to form. At this point, sufficient ethanol was added to give a copious yellow precipitate. The solid was filtered off, washed several times with ethanol, and dried in the air. After redissolving in 0.1 M HTFA, the solution was treated by adding a 5 to 10% stoichiometric excess of $AgNO_3$, and the same purification procedure was followed as described above. No free Cl^-, Ag^+, or uncoordinated edta were detected in the solution of the purified compound.

Throughout this study, experimental results using $Ru(Hedta)(OH_2)$ obtained by the two preparative methods were routinely compared without any differences being discovered.

2.1.2 Preparation of $K_3\{\mu$-oxobis[(ethylenediaminetetraacetato) ruthenium(III,IV)]\} $[(edta)_2Ru_2^{III,IV}]$

$Ru^{III}(edta)(OH_2)$ (0.86 g) was dissolved in 50 mL of water at

40°C. The acidity was adjusted to pH 5 with 1 M KOH. H_2O_2 (15 μL 30%) was added to produce a dark green solution having a pH value near 2. After one hour, the pH was adjusted to 7 with 1 M KOH, and the solution volume reduced to 10 mL in the rotoevaporator. Absolute ethanol (100 mL) was added rapidly to precipitate a fluffy green solid which was collected by filtration, washed with absolute ethanol and ether, and dried in the air. The optical absorption of the solid product gave maxima at 632 nm ($\varepsilon = 411\ M^{-1}\ cm^{-1}$) and 394 nm ($\varepsilon = 2.00 \times 10^4\ M^{-1}\ cm^{-1}$); the measured extinction coefficients were intermediate between previously reported values (2.0×10^4 at 393 nm, 4.2×10^2 at 632 nm;[12] 1.8×10^4 at 392 nm, 3.8×10^2 at 630 nm)[28].

2.1.3 Preparation of ^{18}O-labeled $(edta)_2Ru_2^{III,IV}$

The dimer was labeled in the bridging position by dissolved $Ru^{III}(edta)(OH_2)$ in isotopically enriched ^{18}O-water (85%, Monsanto or 95%, YEDA) buffered at pH 4-5 by adding anhydrous sodium acetate. Following incubation at room temperature for 15 to 30 minutes, H_2O_2 was added to form the $(edta)_2Ru_2^{III,IV}$ dimer. This period of time is sufficient to equilibrate coordinated water with solvent[33] but should not allow any significant exchange at the edta carboxyl oxygen atoms.[34]

2.1.4 Syntheses of substituted 2,2′-bipyridines

Several 4,4′- and 5,5′-disubstituted derivatives of 2,2′-bipyridine were synthesized to study the influence of electron-withdrawing and electron-donating groups on the redox and catalytic properties of the μ-oxo dimeric ruthenium bipyridyl complexes. Structures of the compounds synthesized as follows:

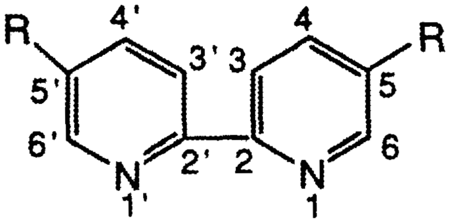

R = COOH

R= COOEt

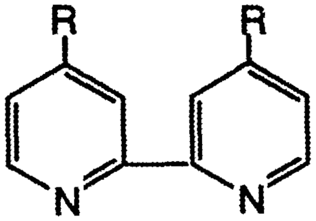

R = COOH

R = COOEt

R = OMe

Although many substituted 2,2′-bipyridines have been described,[45] those bearing 5,5′-substituents are usually less readily obtained, and few simple 5,5′-disubstituted 2,2′-bipyridines were reported before 1977.[42] Derivatives substituted in the 6- and 4-positions of pyridine rings are easily prepared from 2,2′-bpy itself. For example, 2,2′-bipyridine can be N-oxidized and nitrated to obtain intermediates from which many 4-substituted[43] and 4,4′-disubstituted derivatives[44-46] can be synthesized. Also, 6-substituted[47,48] and 6,6′-disubstituted[47,49-51] can be prepared by direct substitution on the 2,2′-bipyridine ring. However, the 5-position of 2,2′-bipyridine is unreactive toward electrophilic attack; e.g., while sulfonation[52,53] has been shown to proceed under vigorous conditions, nitration has been reported as unsuccessful.[51] Ullmann reactions with 5-substituted 2-halopyridines have been used to synthesize several 5,5′-disubstituted 2,2′-bipyridines,[54,55] but the yields are usually poor, and the 2-halopyridines are often not readily available. Fortunately, 5,5′-dialkyl-2,2′-bipyridine can be obtained in high yield by the coupling reaction of 3-alkylpyridine in the presence of a degassed Raney nickel catalyst,[56,57] and thus, 5,5'-dimethyl-2,2'-bipyridine can be prepared from the readily obtainable 3-picoline. This compound is a convenient starting material for the preparation of other 5,5'-disubstituted derivatives. In addition, 5,5'-carbethoxy-2,2'-bipyridine can be prepared by the direct coupling reaction of ethyl nicotinate in the presence of Raney nickel[56] or 10% Pd/charcoal[14] catalysts.

(1) **Preparation of 5,5'-dicarboxylic acid-2,2'-bipyridine:** We chose the following synthetic route:

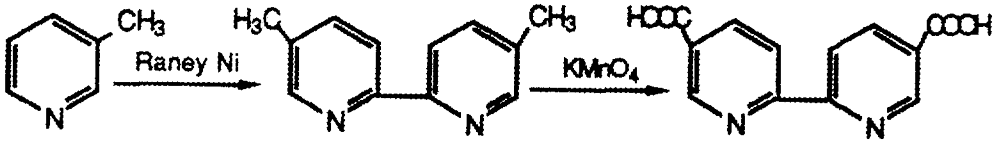

a. **Preparation of Raney nickel catalyst[58]:** A one-liter wide-mouthed Erlenmeyer flask containing 250 mL of distilled water was placed in an empty water bath and a magnetic stirrer bar put into the flask. Sodium hydroxide (52 g) was dissolved in the water while stirring. Then, 52 g of 1:1 aluminium-nickel alloy (Fluka AG) was added in portions as rapidly as possible, but at such a rate that no material was lost by frothing. When all the alloy was added, the rate of stirring was decreased, and the catalyst was washed down from the sides of flask with distilled water. As soon as the reaction had subsided, the water bath was filled with boiling water, and the catalyst was slowly stirred while the volume was maintained by occasional addition of distilled water, ensuring minimally that the catalyst remained covered. After 6 hours, stirring and heating were discontinued, and the catalyst was allowed to stand at room temperature for 12 to 15 hours. It was then washed by decantation with ten 250-mL portions of distilled water and transferred to a 500-mL round-bottomed three-necked flask by suspending it in distilled water. The total volume of the catalyst and water was adjusted to 200 mL, and the flask placed in a cold-water bath. One side arm was fitted with a 100-mL dropping funnel, and the other necks were connected to a vacuum pump. The flask was slowly evacuated and warmed in a water bath until no water was left in the flask. The temperature of the water bath was then raised to 100°C and kept at this temperature for 2 hours. After this time, the catalyst was allowed to cool to 50 to 60°C.

b. Preparation of 5,5′-dimethyl-2,2′-bipyridine by Raney nickel catalyzed dehydrogenative coupling of 3-picoline:

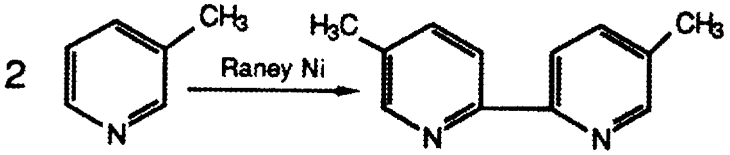

With the apparatus assembled as described above to minimize contact with air, 150 mL of 3-picoline was poured into the dropping funnel. About 80 mL of 3-picoline was run slowly onto the catalyst from the dropping funnel. The flask was shaken carefully to wet the catalyst as much as possible with 3-picoline. The other 70 mL of 3-picoline was added in the same way, and the flask was shaken again. Air was allowed to enter the flask, and the reaction mixture was refluxed for 48 hours. The flask was allowed to cool to about 60°C, and most of liquid decanted and filtered through a sintered-glass funnel. Then, 50 mL of fresh 3-picoline was added to the catalyst in the reaction flask, and the mixture was heated to reflux for 10 minutes. The flask contents were allowed to cool to about 60°C, and the 3-picoline decanted and filtered as before. This extraction was repeated two more times. The filtrates were combined and rotoevaporated under reduced pressure to remove 3-picoline. The residue from distillation was extracted with 100 mL of hot benzene. Then, most of the benzene was removed and placed in the refrigerator for 12 hours. The yellow precipitate that formed was collected by filtration. The filtrate was concentrated further and allowed to stand overnight in the refrigerator. The precipitate was again collected and combined with the first precipitate, yielding 15 g crude product.

The crude product was recrystallized twice from absolute ethanol. The solid was dissolved in 200 mL hot solvent to give a pale yellow solution, then placed in a refrigerator for 12 hours after cooling to room temperature. During this time, white crystalline needles formed, which were collected and allowed to dry in the air. A yield of 10% (12 g) of pure product was produced, which was analyzed by ^{1}H-NMR and FTIR:

^{1}H-NMR (Solvent: $CDCl_3$; ppm): 2.39 (s,$-CH_3$), 8.22 (d,H_3), 7.62 (d,H_4), 8.49 (s,H_6)

FTIR [KBr pellet; cm^{-1} (relative absorbance)]: 1598 (0.48), 1554 (0.64), 1468 (1.00), 1372 (0.60), 1244 (0.49), 1220 (0.54), 1129 (0.50), 1031 (0.65), 827 (0.83), 794 (0.47), 737 (0.62), 652 (0.59), 538 (0.42), and 467 (0.48).

c. Preparation of 5,5′-dicarboxylic acid-2,2′-bipyridine by oxidation of 5,5′-dimethoxy-2,2′-bipyridine with potassium permanganate[41]

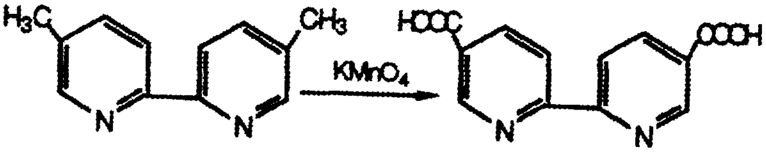

Seven g of 5,5′-dimethyl-2,2′-bipyridine was placed in 400 mL of 25% sulfuric acid. The mixture was cooled to 5°C, and 14 g of $KMnO_4$ was added while stirring. After stirring 30 minutes at 5°C, cooling was discontinued, and the temperature of the mixture rose to 35-38°C. After the evolution of heat ceased, the mixture was cooled again to 5°C, and a second portion of 14 g of $KMnO_4$ added. After a further 5 minutes, the mixture was refluxed for 16 hours. Excess potassium permanganate was reduced by addition of potassium metabisulfite (0.9 g). Upon cooling, a yellow microcrystalline powder separated and was filtered off.

To remove the monoacid, the crude product obtained above was placed in 100 mL of 1:1 sulfuric acid and refluxed for 5 hours. Upon cooling, the mixture was poured into 400 mL of water and allowed to stand overnight in the refrigerator. The yellowish precipitate obtained was isolated by filtration and dried in a vacuum. Pure product (3.8 g) was obtained and characterized by FTIR and ^{1}H-NMR. From the FTIR data given below, the band centered at 1689 cm^{-1} appeared upon oxidation of 5,5′-dimethyl-2,2′-bipyridine the corresponding diacid.

^{1}H-NMR (Solvent: $Me_2SO\text{-}d^6$; ppm): 8.45 (d,H_3), 8.58 (d,H_4), 9.20 (s,H_6).

FTIR [KBr pellet; cm^{-1} (relative absorbance)]: 2920 (0.40), 1689 (1.00), 1594 (0.78), 1427 (0.53), 1384 (0.37), 1310 (0.64), 1249 (0.32), 1143 (0.30), 1025 (0.33), 941 (0.27), 817 (0.26), 769 (0.42), 566 (0.26).

(2) Preparation of 5,5'-dicarbethoxy-2,2'-bipyridine by dehydrogenative coupling of ethyl nicotinate in the presence of 10% Pd/charcoal:

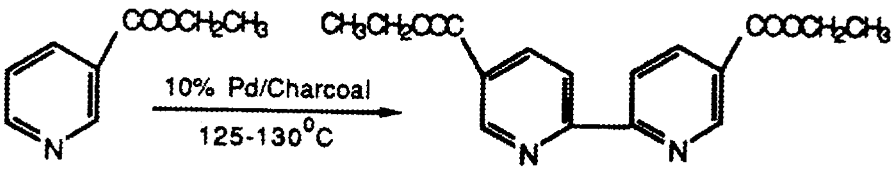

Ethyl nicotinate (85 g) and 10% Pd/charcoal (Aldrich) (25 g) were placed in a round-bottomed three-necked flask (250 mL). The reaction was initiated by heating and proceeded vigorously. After the reaction slowed, the mixture was heated and the temperature kept at 125-130°C for five days. During this period, ethyl nicotinate was occasionally added to keep the volume constant. On cooling, the catalyst was filtered off and washed with 100 mL CH_2Cl_2. The solvent was evaporated in the rotoevaporator, and the precipitate collected by filtration. The crude product was recrystallized twice in absolute ethanol. White crystalline needles (11 g) were obtained and characterized by FTIR and ^{1}H-NMR.

^{1}H-NMR (Solvent: $CDCl_3$; ppm): 4.44 (q,$-CH_2$), 1.42 (t,$-CH_3$), 8.45 (d,H_3), 8.59 (d,H_4), 9.31 (s,H_6)

FTIR [KBr pellet; cm^{-1} (relative absorbance)]: 2985 (0.41), 1722 (0.97), 1593 (0.73), 1452 (0.41), 1376 (0.45), 1282 (0.83), 1268 (0.92), 1172 (0.43), 1113 (1.00), 1023 (0.63), 855 (0.38), 765 (0.67).

(3) Preparation of 4,4'-dicarboxylic acid-2,2'-bipyridine[41]: The procedure was the same as described in Section 2.1.4(1) except that 5,5'-dimethyl-2,2'-bipyridine was replaced by 4,4'-dimethyl-2,2'-bipyridine (Fluka AG, 99%). The yield was 40%.

^{1}H-NMR (Solvent: Me_2SO-d_6; ppm): 8.85 (s,H_3), 7.91 (d,H_5), 8.93 (d,H_6).

FTIR [KBr pellet; cm^{-1} (relative absorbance)]: 3430 (0.63), 1718 (0.61), 1462 (0.48), 1366 (0.82), 1289 (1.00), 1268 (0.88), 1142 (0.47), 1071 (0.63), 1014 (0.58), 916 (0.34), 767 (0.61), 682 (0.83).

(4) Preparation of diethyl 4,4'-dicarbethoxy-2,2'-bipyridine: To a solution containing 35 mL absolute ethanol and 5 mL concentrated sulfuric acid, 1 g of 4,4'-dicarboxylic acid-2,2'-bpy was added and refluxed for 18 hours. The diacid was initially insoluble in the mixed solvent, but after a few hours it dissolved completely. The color of the solution at this point was pink, probably due to remaining traces of potassium permanganate. Upon cooling, the solution was poured into 100 mL of water, and a white precipitate immediately appeared. The mixture was placed in a refrigerator overnight. Then, the precipitate was collected by filtration and recrystallized from absolute ethanol to obtain 0.9 g. The yield was 90%.

^{1}H-NMR (Solvent: $CDCl_3$; ppm): 4.45 (q,$-CH_2$), 1.42 (t,$-CH_3$), 8.88 (s,H_3), 7.99 (d,H_5), 8.95 (d,H_6).

FTIR [KBr pellet; cm^{-1} (relative absorbance)]: 1731 (1.00), 1558 (0.40), 1364 (0.54), 1290 (0.86), 1257 (0.80), 1139 (0.53), 1020 (0.37), 761 (0.44), 691 (0.30).

(5) **Synthesis of 4,4'-dimethoxy-2,2'-bipyridine**[44-46,59]

2,2-Bipyridine was used as a starting material to synthesize the compound by a route involving the following four steps:

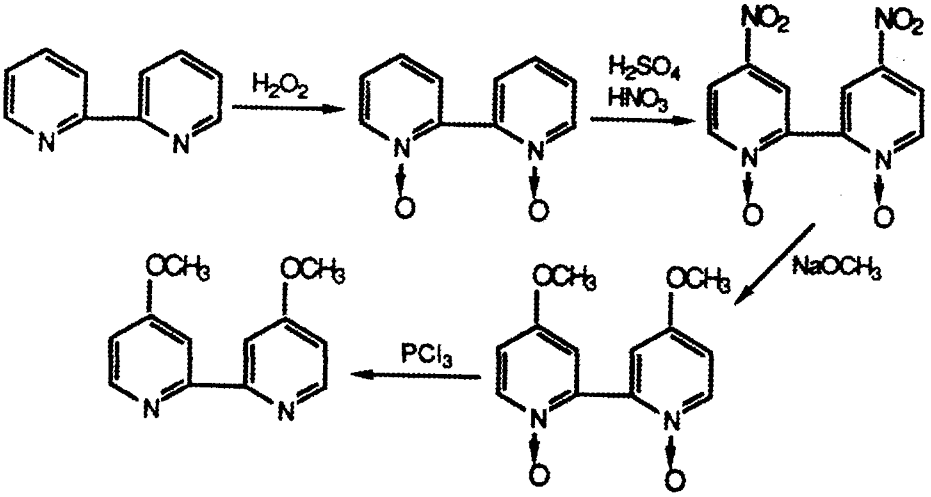

a. **Synthesis of 2,2'-bipyridine-N,N-dioxide:** To 25 mL glacial acetic acid, 2,2'-bpy and 5 mL of 30% H_2O_2 were added, which was heated on a water bath for 4 hours. Then another 5 mL 30% H_2O_2 was added and heated for another 4 hours. After cooling, solid potassium hydroxide was added while stirring to make the solution basic. During the addition of solid potassium hydroxide, pH paper was used to detect changes in the acidity of the solution. A white precipitate appeared locally and disappeared rapidly with initial addition of the base. When the solution became alkaline, a large amount of white precipitate was formed, which was subsequently collected by filtration. Purification was accomplished by dissolving the precipitate in cold water, filtering, and evaporating the filtrate by rotoevaporation under vacuum to reduce the volume. A large amount of white precipitate formed during evaporation which was filtered off and dried in vacuum, producing 4.5 g of pure product. FTIR and electronic absorption analyses were in agreement with literature values.[46]

Electronic absorption spectra in 95% ethanol [λ(nm) (ε, M^{-1} cm^{-1})]: 222 (2.1×10^4), 242 (1.5×10^4), 268 (1.6×10^4).

Literature values[46]: 221 (2.1×10^4), 238 (1.5×10^4), 267 (1.5×10^4).

FTIR [KBr pellet; cm^{-1} (relative absorbance)]: 3039 (0.69), 1479 (0.57), 1428 (0.75), 1299 (0.48), 1255 (1.00), 1147 (0.57), 1022 (0.56), 959 (0.44), 839 (0.54), 769 (0.97), 582 (0.74), 517 (0.50), 467 (0.47).

b. Synthesis of 4,4'-dinitro-2,2'-bipyridine-N,N'-dioxide[44] by nitration of 2,2'-bipyridine-N,N-dioxide: In 10 mL of 96.7% concentrated sulfuric acid, 2.5 g of 2,2'-bpy-N,N-dioxide was dissolved, and 5 mL of fuming sulfuric acid (30%) and 10 mL of fuming nitric acid (90%, specific gravity = 1.5) were added. The solution was heated on a water bath for 4 hours. During heating, brown gaseous N_2O_5 formed. The hot solution was poured onto ice, and a yellow scaly precipitate formed immediately. (If insufficient amounts of ice were used to effect rapid cooling, no precipitate formed.) The mixture was allowed to stand overnight in the refrigerator. The precipitate was collected by filtration and dried in the air, yielding 1.5 g (50%) of 4,4′-dinitro-2,2′-bpy-N,N-dioxide.

Electronic absorption spectra in 95% ethanol [λ(nm) (ε, M^{-1} cm^{-1})]: 236 (1.4 × 10^4), 330 (2.1 × 10^4).

Literature values[46]: 232 (1.5 × 10^4), 328 (2.0 × 10^4).

FTIR [KBr pellet; cm^{-1} (relative absorbance)]: 3444 (0.82), 1574 (0.53), 1518 (0.73), 1343 (1.00), 1309 (0.74), 1292 (0.89), 1115 (0.59), 929 (0.46), 749 (0.57), 677 (0.50).

c. **Synthesis of 4,4′-dimethoxy-2,2′-bipyridine-N,N-dioxide**[45]: To 120 mL methanol, 1 g of 4,4′-dinitro-2,2′-bpy-N,N-dioxide and 10 mL 25% $NaOCH_3$/methanol solution were added. The suspension was stirred for 4 hours at 30 to 35°C. During this period, the solid gradually dissolved, finally giving a clear orange-colored solution. The solution was cooled to 3°C and neutralized with concentrated sulfuric acid. The solution became light yellow, and a white precipitate appeared at the bottom of the reactor which was filtered, extracted repeatedly with methanol, and then discarded. The combined bright-yellow methanol extracts were rotoevaporated under vacuum. A yellow solid was obtained, collected by filtration, and recrystallized twice in methanol. Finally, 0.9 g (80%) of pure product was obtained. Electron absorption and FTIR spectra reported below were consistent with literature values.

Electronic absorption spectra in 95% ethanol [λ(nm) (ε, M^{-1} cm^{-1}]: 216 (2.5 × 10^4), 272 (2.1 × 10^4), 320 (3.0 × 10^4).

Literature values[46]: 216 (2.6 × 10^4), 268 (2.0 × 10^4), 320 (3.1 × 10^4).

FTIR [KBr pellet; cm^{-1} (relative absorbance)]: 3426 (1.00), 1619 (0.70), 1478 (0.74), 1428 (0.71), 1384 (0.65), 1271 (0.98), 1211 (0.78), 1018 (0.77), 778 (0.70).

d. **Synthesis of 4,4'-dimethoxy-2,2'-bipyridine:** A suspension of 1 g (0.0029 mol) 4,4'-dimethoxy-2,2'-bpy-N,N'-dioxide in 25 mL of chloroform was cooled to 0°C, and 5 mL of PCl_3 (0.05 mol) was added. After the mixture was refluxed for 1.5 hours, it was cooled and poured into a mixture of ice and water. After the phases separated, the chloroform layer was extracted several times with distilled water, and aqueous extracts were combined with the water layer from the reaction mixture. Neutralization of the aqueous solution with 25% sodium hydroxide caused formation of a voluminous white precipitate which, upon cooling the mixture, was isolated by filtration and washed thoroughly with water.

Electronic absorption spectra in 95% ethanol [λ(nm) (ε, M^{-1} cm^{-1}]: 216 (3.8×10^4), 256 (1.0×10^4), 274(sh).

Literature values: 212 (3.9×10^4), 256 (9.6×10^3), 269(sh).

^{1}H-NMR (Solvent: $CDCl_3$ (ppm)): 3.96 (s,$-OCH_3$), 8.01 (d,H_3), 6.88 (dd,H_5), 8.50 (d,H_6).

FTIR [KBr pellet; cm^{-1} (relative absorbance)]: 3472 (0.32), 2971 (0.26), 1587 (1.00), 1561 (0.67), 1460 (0.49), 1435 (0.30), 1391 (0.25), 1293 (0.85), 1232 (0.53), 1024 (0.67), 986 (0.23), 898 (0.35), 831 (0.30), 819 (0.37), 574 (0.19).

2.1.5 Syntheses of ruthenium complexes with 2,2'-bipyridine and its derivatives

(1) Synthesis of $(bpy)_2(OH_2)Ru^{III}ORu^{III}(OH_2)(bpy)_1$[1]:

$Ru(bpy)_2Cl_2 \cdot 2H_2O$ (1.1 g (2.1 mmol) was dissolved in 30 mL of water and heated to reflux with stirring for 1/2 hour. $AgNO_3$ (0.92 g, 5.4 mmol) was added, and the solution was heated at reflux for 1/2 hour. AgCl was filtered off, and the filtrate was heated at reflux for an additional 1/2 hour. Saturated $NaClO_4$ (20 mL) was added to the solution, and the volume was reduced under vacuum to 30 mL using the rotoevaporator. After standing in the refrigerator for 12 hours, the deep blue microcrystalline product was collected on a medium frit sintered glass filter and washed with 10 mL of cold 0.1 M $HClO_4$, followed by 5 mL of ice-cold water. The crude product was recrystallized by dissolving in warm water and adding saturated $NaClO_4$ solution until a precipitate just began to form. The solution was filtered and the filtrate was refrigerated overnight. The crystalline product was collected on a medium frit filter and dried in a vacuum. Pure product (0.31 g) was obtained. The yield was 24%.

(2) **Synthesis of $(bpy)_2(^{18}OH_2)Ru^{III}{}^{18}ORu^{III}(^{18}OH_2)(bpy)_2$:** The same method was used as described above except that ^{18}O-water replaced normal water as solvent. Specific procedures were altered to minimize loss of ^{18}O-solvent by evaporation and isotopic exchange with water vapor. These consisted mainly in shortening the reaction time and minimizing heating of the reaction mixture.

$Ru(bpy)_2Cl_2 \cdot 2H_2O$ (113.7 mg) and $AgClO_4$ (120.7 mg) were added to 2 mL of ^{18}O-water in a 10-mL centrifuge tube. The mouth of the tube was covered with a septum which was pierced with a hypodermic needle to allow venting. The solution was heated in a water bath for 1/2 hour. AgCl was separated by centrifugation, and the clear solution was transferred to a small beaker (5 mL). Solid sodium perchlorate was added until a precipitate just began to form, and the mixture was refrigerated overnight. The clear solution above the precipitate was carefully decanted and immediately stored to prevent exchange with water vapor. The solid precipitate was dried and stored in a vacuum desiccator. The yield was 80 mg, 80%. As described in Chapter 4, resonance Raman spectroscopy indicated that ^{18}O had been incorporated as the bridging ligand.

(3) **Synthesis of dimeric $[L_2(H_2O)Ru^{III}\text{-}O\text{-}Ru^{III}(OH_2)L_2]$ analogs of $(bpy)_2(OH_2)Ru^{III}ORu^{III}(OH_2)(bpy)_2$:**

a. **Synthesis of 5,5-dicarbethoxy derivative, i.e.:** We used $RuCl_3 \cdot 3H_2O$ as the starting material to synthesize the complex ion through the following steps.

L =

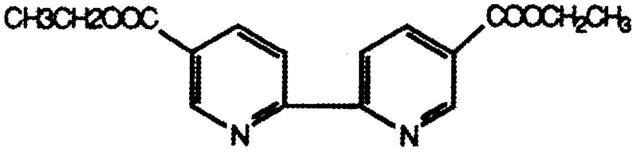

1. Synthesis of RuL_2Cl_2: $RuCl_3 \cdot 3H_2O$ (99%, 43% Ru) (386 mg) and ligand, L, (900 mg) were dissolved in absolute ethanol (100 mL), and the mixture was refluxed under an Ar atmosphere for 24 hours. After cooling, 50 mL of 1 M LiCl was added, and the ethanol was evaporated in the rotoevaporator. The crystals were isolated by filtration, washed with cold water, and air dried. The crystals were recrystallized in hot ethanol. The yield was 1.1 g, 80%.

2. Synthesis of the cis-$Ru^{II}L_2(OH_2)_2$ ion: The chloride ligand in the RuL_2Cl_2 was replaced by aqua ligands as follows: RuL_2Cl_2 (0.1 g) and $AgSO_4$ (40 mg) were added to 0.5 M sulfuric acid (35 mL). The

mixture was heated to reflux for 5 hours to precipitate the chloride as AgCl. After cooling, the white precipitate of AgCl was filtered off, and purple filtrate was kept in the refrigerator as a starting material for the next step. Light exposure was minimized during preparation and storage to avoid photoisomerization[109] of the complex to trans-isomer.

3. Electrolytic oxidative dimerization of cis-$Ru^{II}L_2(OH_2)$: Constant potential electrolysis (CPE) of the purple filtrate in 0.5 M H_2SO_4 was performed using a Princeton Applied Research Model 273 potentiostat/galvanostat connected to a standard three-electrode, two-compartment cell. The solution was electrolyzed under an argon atmosphere at 40°C and an applied potential 0.7 V vs. a $Hg/HgSO_4$ reference electrode ($E^o = 0.64$ V vs. NHE). The working and counter electrodes were Pt gauze and Pt wire, respectively. During electrolysis, optical spectra were taken periodically to detect the progress of the dimerization reaction, which was accompanied by a color change from purple to orange. Upon completion of the reaction, the dimer was isolated as follows: The solution was neutralized to pH 3.5 with 0.02 M $Ba(OH)_2$ and the $BaSO_4$ precipitate that formed was removed by filtration. The volume of the filtrate was reduced to 10 mL under vacuum in a rotoevaporator (bath temperature <50°C). $Ba(OH)_2$ (0.02 M) was re-added to adjust the pH to 3.5. The volume was reduced to 10 mL and $BaSO_4$ again removed by filtration. Then, acetone was added slowly with stirring at room temperature to induce precipitation of a blue-black solid. To minimize loss of material, the supernatant was decanted from the solid, which was washed several times with acetone and dried. The yield was 50 mg, 40%.

b. Synthesis of the 5,5'-dicarboxy derivative, i.e.:

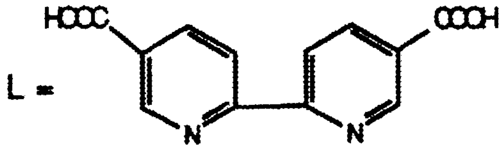

The procedure described above was followed except that ligand 5,5'-dicarboxylic acid-2,2'-bipyridine was used instead of ligand 5,5'-dicarbethoxy-2,2'-bipyridine. The yield was 0.3 g, 40%.

c. Synthesis of 4,4'-dicarbethoxy derivative, i.e.:

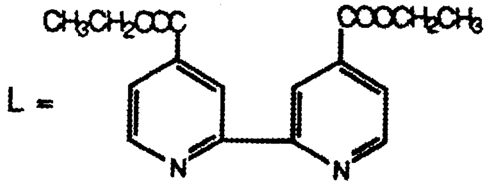

The procedure described above was followed except that ligand 4,4'-dicarbethoxy-2,2'-bipyridine was used rather than ligand 5,5'-dicarbethoxy-2,2'-bipyridine, and constant potential electrolysis was carried out at a potential of 0.8 V vs. Hg/HgSO$_4$ electrode. The yield was 0.25 g, 35%.

(4) Synthesis of [Ru(4,4'-dimethoxy-2,2'-bipyridine)$_2$(OH$_2$)]$_2$O: Ru^{II}(4,4'-dimethoxyl-2,2'-bipyridine)$_2$Cl$_2$ was synthesized following procedures described in Section 2.1.5(3). The yield was 0.4 g, 80%. Dimerization was then carried out using procedures described in Section 2.1.5(1). During preparation, the color of the solution changed from yellow to dark blue, but the solid precipitate isolated when NaClO4 was added was brown in color. The yield was 0.2 g, 65%. Optical electronic spectra and redox properties of the synthesized complexes are reported and discussed in detail in Chapter 4.

2.1.6 Preparation and purification of other reagents

(1) **Preparation of $Ru(bpy)_3^{3+}$ ion:** The $Ru(bpy)_3^{3+}$ ion is a goodoxidant in weakly acidic to alkaline solutions. $Ru(bpy)_3(ClO_4)_2$ was unacceptable as a starting material because it is sparingly soluble in aqueous solution. I therefore used $Ru(bpy)_3Cl_2$ and prepared reagent solutions free from Cl^- ion by anion exchange chromatography. The overall preparative sequence included Cl^- ion precipitation with $AgNO_3$, ion exchange to replace NO_3^- with SO_4^{2-} ion, and oxidation of $Ru(bpy)_3^{2+}$ to $Ru(bpy)_3^{3+}$ by CPE or shaking with solid PbO_2. Explicit procedures that were adopted are described below.

a. **Preparation of the anion exchange column:** Dowex (1 × 8) (chloride ion type, 100-200 mesh) was soaked in distilled water overnight, the suspension was decanted, and the beads rinsed three times in distilled water. The material was packed into a 10 × 1 cm glass column. A solution of 0.1 M sulfuric acid was passed through the column until an $AgNO_3$ test for Cl^- was negative. Finally, the column was washed with distilled water until the eluate was neutral.

b. **Removal of Cl^- ion:** $Ru(bpy)_3Cl_2 \cdot 6H_2O$ (375 mg (0.5 mmol)) was dissolved into 10 mL of water, and $AgNO_3$ (160 mg (1.0 mmol) contained in a few milliliter of water was added. The white precipitate of AgCl was removed by centrifugation. Spot tests with $AgNO_3$ or KCl indicated the absence of detectable Cl^- or Ag^+, respectively. The solution was passed several times through freshly prepared anion exchange columns to ensure removal of NO_3^- ion by exchange with SO_4^{2-} on the resin. Concentrated

H_2SO_4 was added to give a final reagent solution concentration of 0.5 M H_2SO_4. The $Ru(bpy)_3^{2+}$ ion concentration was determined by spectrophotometric analysis at 452 nm ($\varepsilon = 1.1 \times 10^4$ M^{-1} cm^{-1}).[32]

c. **Preparation of $Ru(bpy)_3^{3+}$ ion:** Either of the following procedures was used:

A given amount of solution of $Ru(bpy)_2^{2+}$ and excess solid PbO_2 were put into a plastic centrifuge tube, which was capped, and shaken vigorously by hand, during which time the color of the solution changed from orange to green. Then, the mixture was centrifuged, and the clear solution of $Ru(bpy)_3^{3+}$ was removed by pipet.

Constant potential electrolysis was carried out at potential of 0.8 V vs $Hg/HgSO_4$ electrode using Pt gauze electrode as a working electrode and Pt-wire as counter electrode in a three-compartment cell. The progress of electrolysis was detected by periodically taking optical spectra (λ_{max}: 452 nm ($Ru(bpy)_3^{2+}$); 670 nm ($Ru(bpy)_3^{3+}$)).

(2) **Preparation of Co^{3+} ion:** Co^{3+} ion is a very powerful oxidant.[36] It was prepared by CPE of 3 N $HClO_4$ solutions of $Co(ClO_4)_2$ at a potential of 1.4 V vs. the $Hg/HgSO_4$ reference electrode using the electrolytic cell described above. The progress of electrolysis was followed spectrophotometrically by monitoring the loss of absorption at 514 nm due to Co^{2+} ion. Two new peaks appeared at 402 and 604 nm and increased as electrolysis proceeded. Assuming that these absorption bands came from Co^{3+} ion, we used the following volumetric method to evaluate their apparent extinction coefficients: The oxidizing equivalents for the solutions were determined by adding excess standard $FeSO_4$ and back-titrating with standardized $KMnO_4$.[36] From the

corresponding optical spectrum of the solution, extinction coefficients were evaluated. Values obtained were 50 M^{-1} cm^{-1} at 402 nm and 43 M^{-1} cm^{-1} at 604 nm.

(3) **Purification of tetrabutylammonium hexafluorophosphate (TBAHFP):** TBAHFP is a very good general-purpose electrolyte.[62] It exhibits high solubility in a variety of solvents, is nonhygroscopic, has a wide accessible potential range, and is easy to obtain.

TBAHFP (1 g of white powder) was added to absolute ethanol (25 mL), heated until the solid dissolved, and filtered while hot. On cooling, white crystalline needles formed and were collected on a medium frit sintered glass filter. The yield was approximately 80%.

2.2 PHYSICAL METHODS

2.2.1 Optical spectroscopic measurements

Electronic absorption spectra were measured using a Perkin-Elmer Lambda 9 or a Hewlett-Packard HP-8452A spectrophotometer. Each instrument was equipped with the manufacturer's data acquisition/analysis system which was used to store, manipulate, and quantitatively analyze the data. Samples were routinely measured in 1- or 0.1-cm cells. When an inert atmosphere was required, septa-stopped deaerated cells were used.

FTIR spectra were recorded on a Perkin-Elmer Model 1800 spectrophotometer equipped with a 7500 Professional computer. Spectra were usually obtained from KBr pellets.

Resonance Raman (RR) spectra were recorded on a computer-controlled Jarrell-Ash instrument with excitation from either Spectra Physics Model 164 argon ion or Model 2025 krypton ion lasers.[122] Spectra were usually obtained from frozen solutions in capillary tubes at approximately 90 K; spectra of solids were determined by first diluting the sample by grinding with KBr and placing the material in the trough of a disk to form a ring that could be rotated in the laser beam. In both cases, back-scattered photons were collected and analyzed.

Low-temperature electron paramagnetic resonance (EPR) spectra were obtained with a Varian Model E-109 X-band instrument equipped with an Air Products LTR liquid helium cryostat. The magnetic field was calibrated using a standard 0.00033% pitch signal, for which $g = 2.0028$ was assumed.

2.2.2 Gas analyses

Gas analyses were made using a YSI 4004 polarographic electrode, a Varian Aerograph A90-P3 gas chromatograph, and a VG Analytical 11/250 mass spectrometer.

(1) The YSI 4004 Clark oxygen probe and polarographic measurements: The YSI 4004 probe is a complete polarographic system consisting of a platinum cathode, silver anode, and KCl solution held captive around the electrode by a Teflon membrane fastened with an O ring. When a polarizing voltage is applied across the Pt cathode and Ag anode, gases which can be reduced at this applied potential are reduced at the cathode, generating a current in the circuit that is detected as a probe response. Thus, the so-called "oxygen" probe can respond to other gases that can be reduced at the given polarizing potential. Here the key to selectivity is the polarizing potential. Although the manufacturer's manual states that the response of the probe to CO_2 is only 1% of that to oxygen (Table 2.1), my experiments indicate that the

Table 2.1. Response of Clark Probe to Various Gases[a]

Gas	Response
100% O_2	100% response
100% CO	less than 1%
100% CO_2[b]	around 1%
100% H_2	less than 1%
100% Cl_2	2/3 O_2 response
100% He	none
100% Nitrous Oxide	1/3 O_2 response
100% Ethylene	none

---

[a] Abstracted from the manufacturer's manual.

[b] Actually, our experiments showed that the probe had a very strong response to CO_2 at a polarizing voltage of 0.8 V and a negligible response to it at 0.6 V (see Chapter 3).

probe responds to CO_2 very strongly at a potential of 0.8 V vs. Ag/AgCl internal reference elctrode which is the recommended working potential in the manual.

Prior to use, the probe membrane was removed, and the probe was soaked in 1:1 ammonium hydroxide:water for 1.5 hours, rinsed with distilled water, and shaken to dry.

For polarographic measurements, the probe was mounted to sample headspace gases in a reaction cell (Figure 2.1) that could accept reactants and purging gases through septa-fitted openings. Response was monitored with a 1-mV time-Y recorder interfaced to the probe by the circuit shown in Figure 2.1. The instrument was calibrated by injection of a known volume of air or CO_2 just before or upon completion of the experiment.

The experiments to determine gaseous products, including CO_2 and O_2, were carried out as follows: The solutions containing metal complexes to be evaluated as catalysts for water oxidation to O_2 were placed into the reaction cell, and air was removed by purging with argon. After the pen position of the recorder reached equilibrium, the argon flow was stopped, and potential leakage of the system was checked. Argon-purged solutions of oxidants were then added to the reaction cell through one of the septa using syringe-transfer techniques to initiate the reaction. The response of the Clark probe was recorded, generally for a period from 1.5 to 4 hours.

(2) **Gas Chromatographic Analyses:** GC analysis was conducted with a Varian Aerograph A 90-P3 gas chromatograph equipped with a 72-cm glass column, 4-mm i.d., packed with a 5-Å molecular sieve and a flame

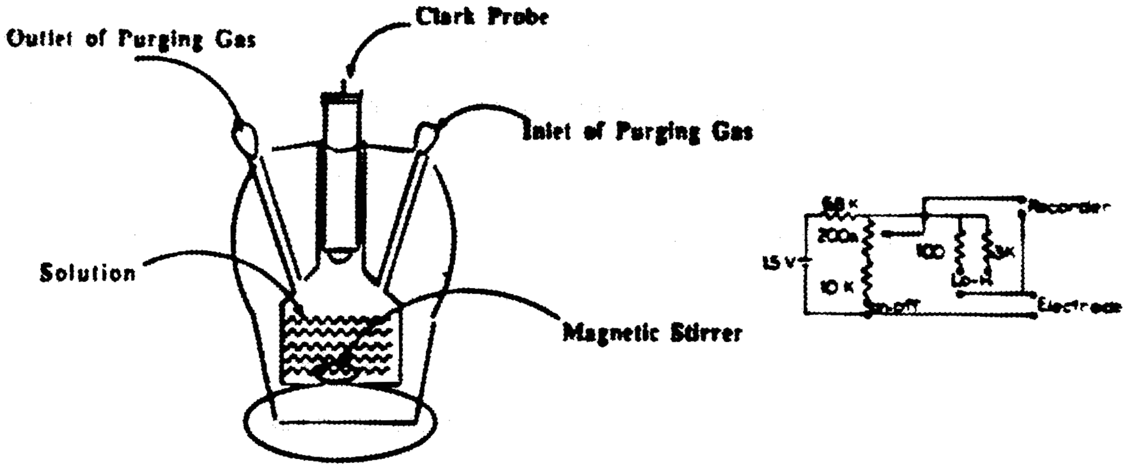

Figure 2.1. Oxygen cell and recorder interfacial circuit.

ionization detector. The instrument was calibrated by injection of a known volume of the air. Gaseous samples were prepared in the above reaction cell or small vial and removed for analysis with a Hamilton gas-tight syringe.

(3) **Mass Spectroscopy:** Because the volumes of the reaction system were generally large and only a small amount of oxygen was produced by the catalytic reaction, the air in the reaction system had to be removed as completely as possible to avoid a large background interference. To minimize atmospheric contamination, I used the following reaction apparatus (Figure 2.2): The solutions containing metal ion complex and oxidant were put into the reaction flask and sidearm, respectively. Both solutions were frozen in a dry-ice/acetone slurry. The valve was opened, and the reaction system evacuated for 15 minutes. Then the valve was closed, the dry-ice/acetone bath removed, and the flask and sidearm immersed in warm water to melt the solutions. This freeze-pump-thaw cycle was repeated until no bubbles were observed upon warming the solutions. Reaction was initiated by 180° rotation of the sidearm, which discharged the oxidant into the reaction flask containing the metal complex ion solution. Evolved gases were collected by condensation (15 minutes) under vacuum in a small tube cooled with liquid nitrogen (gaseous collector, Figure 2.2). The collector was fitted with a microstopcock and ground glass joint for direct transfer to the mass spectrometer. Spectra were routinely scanned from 20-250 or 20-100 amu. To check the system for leakage, the procedures described above were followed except that the catalyst and oxidant were absent from the solutions placed in the two reaction compartments. The mass

spectral analyses of the samples from blank experiments showed that the ratio of N_2 to O_2 was identical to that of the room air, and the amount of CO_2 was negligible, indicating no leakage of the system. Otherwise, the ratio of N_2 to O_2 and the amount of CO_2 in the blank sample should be lower and higher than those of the room air, respectively, because the boiling points of O_2 and CO_2 are higher than that of N_2 and would be condensed more easily.

2.2.3 Electrochemical Methods

(1) **Spectroelectrochemical experiment:** Development of the optically transparent thin-layer electrode (OTTLE) enabled the techniques of thin-layer electrochemistry, cyclic voltammetry, controlled potential coulometry, and spectroelectrochemistry to be performed in one unified experiment.[38-40] The experiment with OTTLE can give information on formal reduction potential (E^o), number of electrons transferred (n), mechanisms of electrode reactions, and kinetics of coupled homogeneous chemical reactions.

Cell design, construction, and assembly instructions are given in reference 37. The cell body (Figure 2.3) was machined from acrylic plastic. The actual cell was constructed on the front face of the cell body by epoxying teflon spacers and a gold minigrid over the quartz window located in the light path (Figure 2.3, G), followed by capping the cell with a quartz plate.[37] Alternatively, the gold minigrid was eliminated, and the outer quartz plate replaced by an In-doped SnO_2-coated glass plate.

Immediately before each experiment, the OTTLE was subjected to 5 minutes of cleaning with the solvent used in the experiment. The

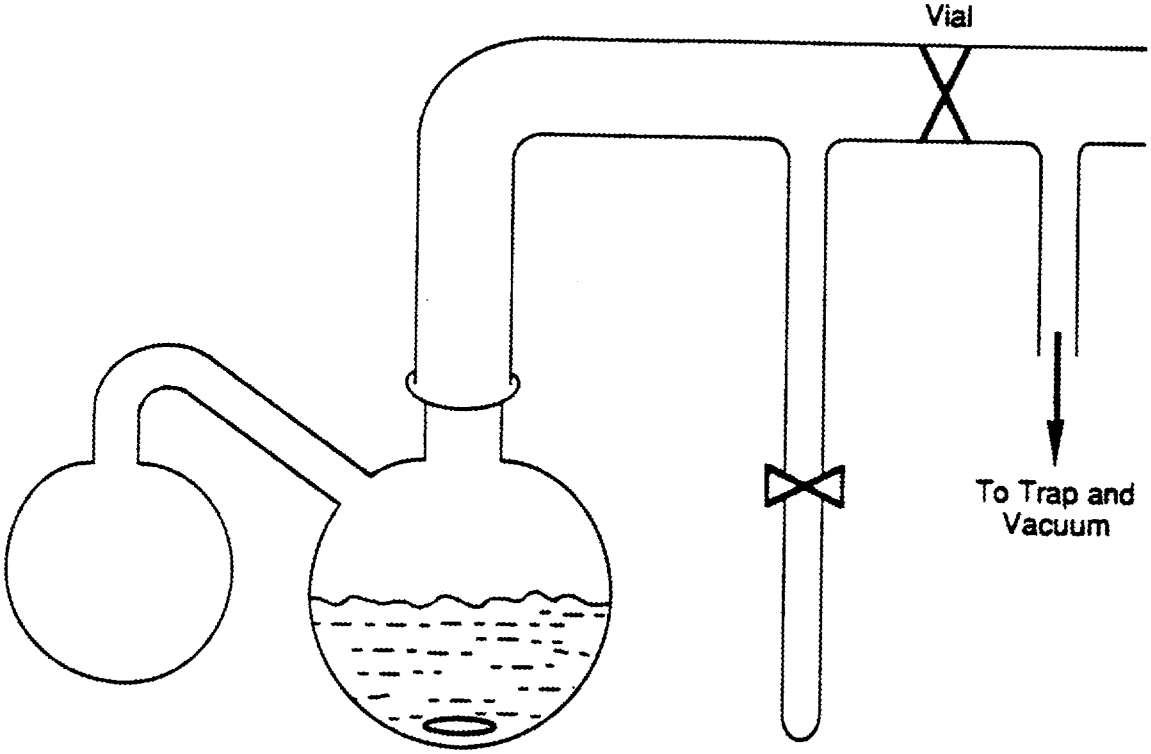

Figure 2.2 Gas collector for mass spectrum.

solution then was injected through syringe needle D until it overflowed into reference electrode compartment E. The OTTLE was positioned in the spectrophotometer sample compartment so that the optical beam passed through the center of the cell. Various potentials were applied, and the spectra were taken periodically until they no longer changed with time. The applied potential was then changed, and a new spectrum recorded. After use, the OTTLE was thoroughly rinsed by aspirating distilled water through the chamber, and the cell was filled with distilled water.

(2) **Cyclic voltammetry:** Cyclic voltammetric measurements were carried out with a computer-controlled Princeton Applied Research Model 273 potentiostat/galvanostat. The electrochemical cell used was a conventional three-electrode type with saturated calomel (SCE) or $Hg/HgSO_4$ as the reference electrode and a piece of platinum wire as an auxiliary electrode. Three types of working electrodes, including glassy carbon (GCE), platinum button (PBE), and In-doped SnO_2, were used. $E_{1/2}$ values were estimated from cyclic voltammetry as the average of oxidative- and reductive-peak potentials $(E_{p.a} + E_{p.c})/2$. All potentials reported here are vs. the saturated calomel electrode (SCE).

The following buffers were used:

For studies on the edta complexes of ruthenium: pH 0-4, trifluoroacetic acid/sodium trifluoroacetate; pH 4-5, acetic acid/sodium acetate; pH 6-12, sodium monohydrogenphosphate/sodium dihydrogenphosphate; pH 12-14, sodium hydroxide. In general, electrolyte ionic strengths were 0.1 M.

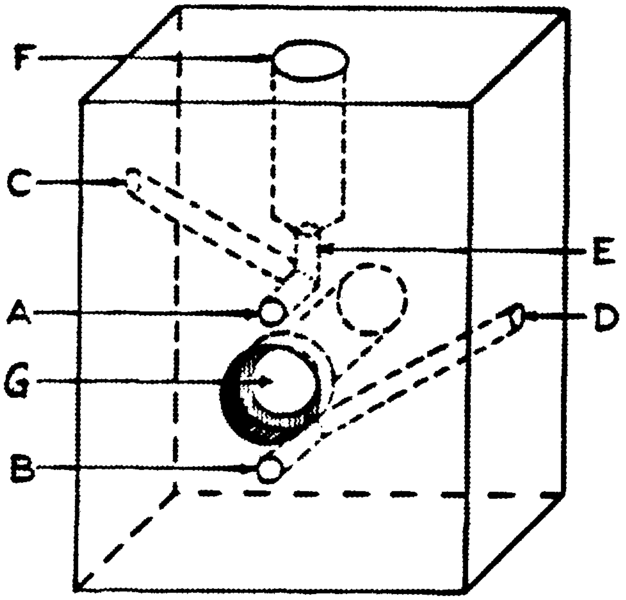

Figure 2.3. Body of OTTLE (from reference 37). A and B are the solution paths to the electrode compartment. C and D are the outlet and inlet which accept Pt (counter electrode) and normal syringe needles. E allows contact of the electrolyte to the reference electrode. F is the reference electrode hole, and G is the light path.

For the bipyridyl ruthenium complexes, sulfuric acid was used in the acidic range (pH 0-4); otherwise, the same buffers were used as with the ruthenium-edta complex.

For non-aqueous solvents, tetrabutylammonium hexafluorophophate (TBAHFP) was used as a supporting electrolyte. All solvents were spectrograde and dried overnight over a 4-Å molecular sieve prior to use. The solutions in the electrochemical cell were bubbled with argon for at least 5 minutes before cyclic voltammetric measurements to remove the dissolved oxygen and were kept under an argon atmosphere during the measurements.

(3) **Constant potential electrolysis (CPE):** CPE was carried out using the Princeton Applied Research Model 273 and a three-electrode, two-compartment cell. The working electrode was made of platinum gauze. A saturated $Na_2SO_4/Hg/HgSO_4$ reference electrode was employed to avoid chloride ion contamination. The solutions were agitated by argon bubbling or by including a magnetic stirrer bar in the sample compartment.

CHAPTER 3

STRUCTURE AND WATER-OXIDIZING CAPABILITIES OF DIMER RUTHENIUM-EDTA COMPLEX IONS

3.1 INTRODUCTION

I synthesized by two entirely separate routes monomeric $Ru^{III}(edta)(OH_2)$[10,29] and by several routes the dimeric $(edta)_2Ru_2{}^{III,IV}$ ion[10] and confirmed and extended the reported redox behavior of the dimeric ion. In examining the water oxidizing capabilities of the dimer, I observed a positive response from a Clark polarographic electrode when Ce^{4+}, $MnO_4{}^-$, and Co^{3+} ions were added in excess and the solutions were poised at a potential that allowed regeneration of the oxidized dimer. In attempting to confirm O_2 production by gas chromatography (GC) and mass spectroscopy (MS), I was unable to obtain a positive response. Instead, I consistently found a copious formation of CO_2. Since the predominant gaseous product was CO_2, not O_2, why did the Clark electrode give a positive response? (According to the manufacturer's manual, the electrode should not respond to CO_2.) To resolve this discrepancy, I examined the electrode's characteristics. I constructed a circuit whose applied potential could be varied and found that the Clark electrode responded to CO_2 at a potential of 0.8 V vs. its internal Ag/AgCl reference electrode, but gave no response at a potential of 0.6 V. However, O_2 was nearly equally responsive at both potentials. When we repeated previous experiments in which a positive response was observed from the Clark electrode at 0.8 V, no response was given at a potential of 0.6 V.

Now, all analytical tools gave us a consistent result that the gaseous product produced was CO_2, not O_2. Finally, based on the resonance Raman spectra of the complex ion and relationships between the redox potential and pH, I identified the structure of the dimer as that of a μ-oxo-bridged complex ion. The experimental data substantiating these conclusions and the prospect that this ion can act as a water-oxidation catalyst, based upon the measured electrochemical potentials, are presented in the following sections.

3.2 RESULTS AND DISCUSSION

3.2.1 Optical spectra of ruthenium-edta complexes

For the sake of later discussion, it is desirable to present the optical spectra of several ruthenium-edta complexes.

(1) Monomeric $Ru^{III}(edta)(OH_2)$

The monomer is a yellowish compound which is stable below pH 5. Under these conditions, the spectra did not change with time in an aerobic environment, but at pH >6, the compound was unstable in the presence of air and slowly changed to give the characteristic spectrum of the dimer $(edta)_2Ru_2^{III,IV}$ (Figure 3.1). Under the anaerobic conditions, however, the alkaline spectra of this compound were similar to the spectra at pH <5.

In the acidic and weak alkaline solutions, the compound had no detectable absorption band in the visible region but had a peak and two shoulders in the UV range (Figure 3.2 and Table 3.1). These bands change position and absorbance with pH. For example, at pH <5, there are two unresolved shoulders at 220 and 250 nm, a broad shoulder at 354

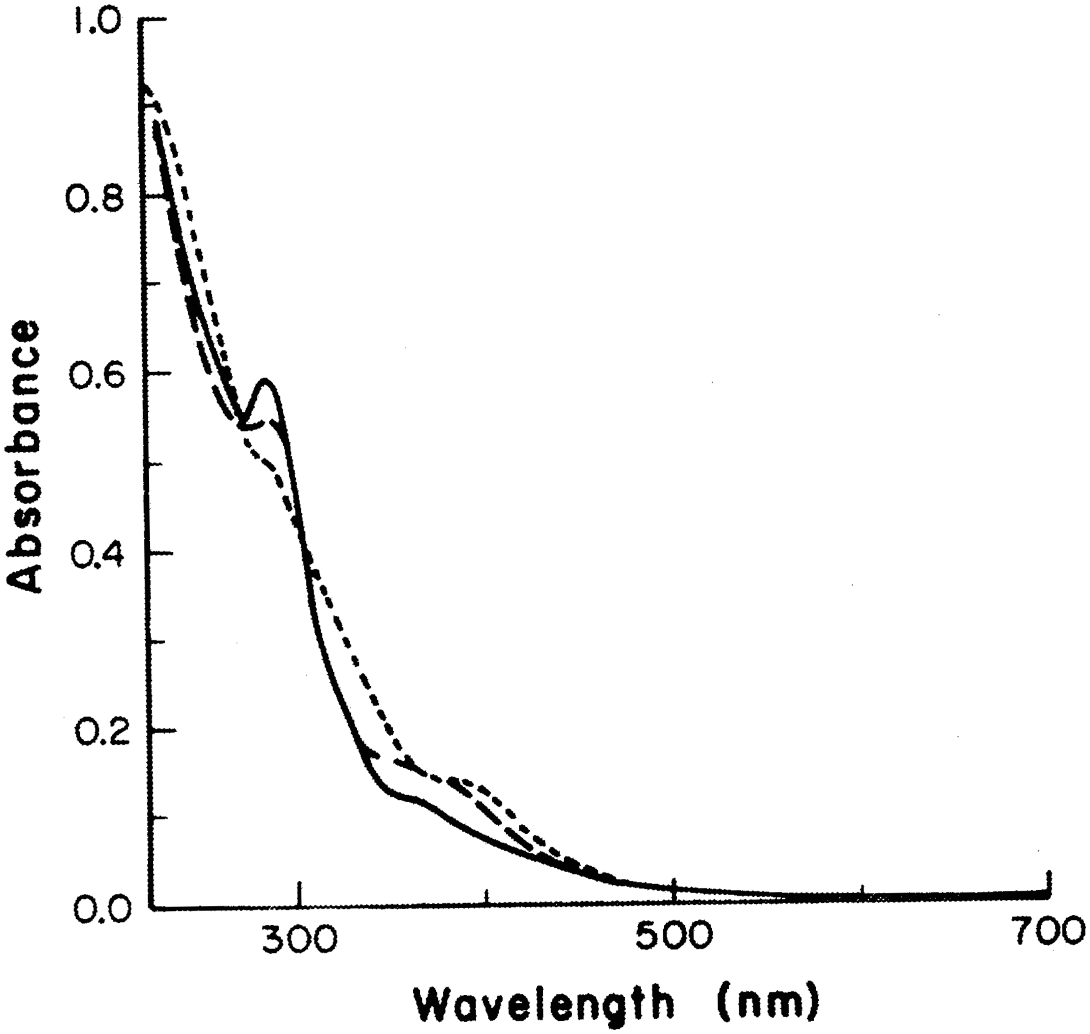

Figure 3.1. Optical spectrum of the dimeric ion, (edta)$Ru^{III}Ru^{IV}$. Conditions: 1.2 mM $(edta)_2Ru_2^{III,IV}$ in 0.1 M Ac^-/HAc, pH 5.02. Optical pathlength: 1.0 mm.

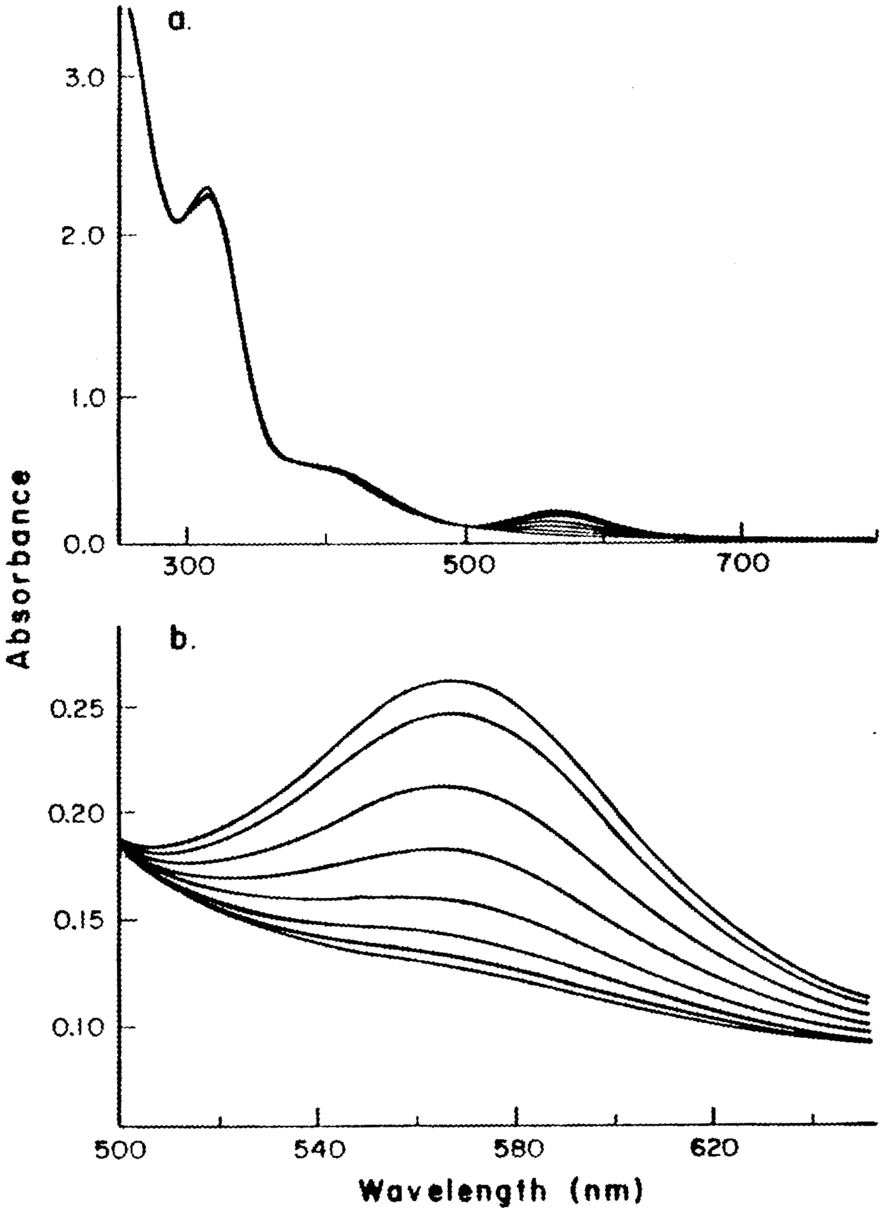

Figure 3.2. Optical spectrum of monomeric $Ru^{III}(edta)(OH_2)$ vs. pH. Conditions: 2.0 mM $Ru(edta)(OH_2)$ in aqueous solution; optical pathlength, 1 mm. Solid line: pH 1 (0.1 M CF_3COOH); dashed line: pH 5.02 (0.1 M HAc/Ac^-); dotted line: pH 8.0 (0.1 M phosphate).

Table 3.1. pH Dependence of $Ru^{III}(edta)(OH_2)$ Spectra

pH	ε (284) (M^{-1} cm^{-1})	ε (354) (M^{-1} cm^{-1})
1.05	4200	700
2.16	3800	710
3.03	3400	720
5.02	3200	740
8.0	sh	750

nm (ε = 695 M^{-1} cm^{-1}), and a weak maximum at 282 nm ($\varepsilon = 3.2 \times 10^3$ M^{-1} cm^{-1}) superimposed upon a background of increasing absorption at progressively shorter wavelengths. The extinction coefficient of the band at 282 nm decreased with decreasing acidity when pH <5. The 282-nm band became a shoulder at pH 8.

At a pH around 11.5, an interesting phenomenon was observed (Figure 3.3). When the solution was exposed to the air, the absorption spectrum comprised a broad shoulder at 400 nm and a weak maximum at 315 nm superimposed upon a background of increasing absorption at a progressively shorter wavelength, and did not change very much with time. However, when the solution was purged with argon, the weak maximum did not change, including position and intensity, but the shoulder at 400 nm gradually broadened and a new band at 566 nm appeared and its intensity increased with time. In our case, an hour was required for the 566-nm band to become evident, and several hours were

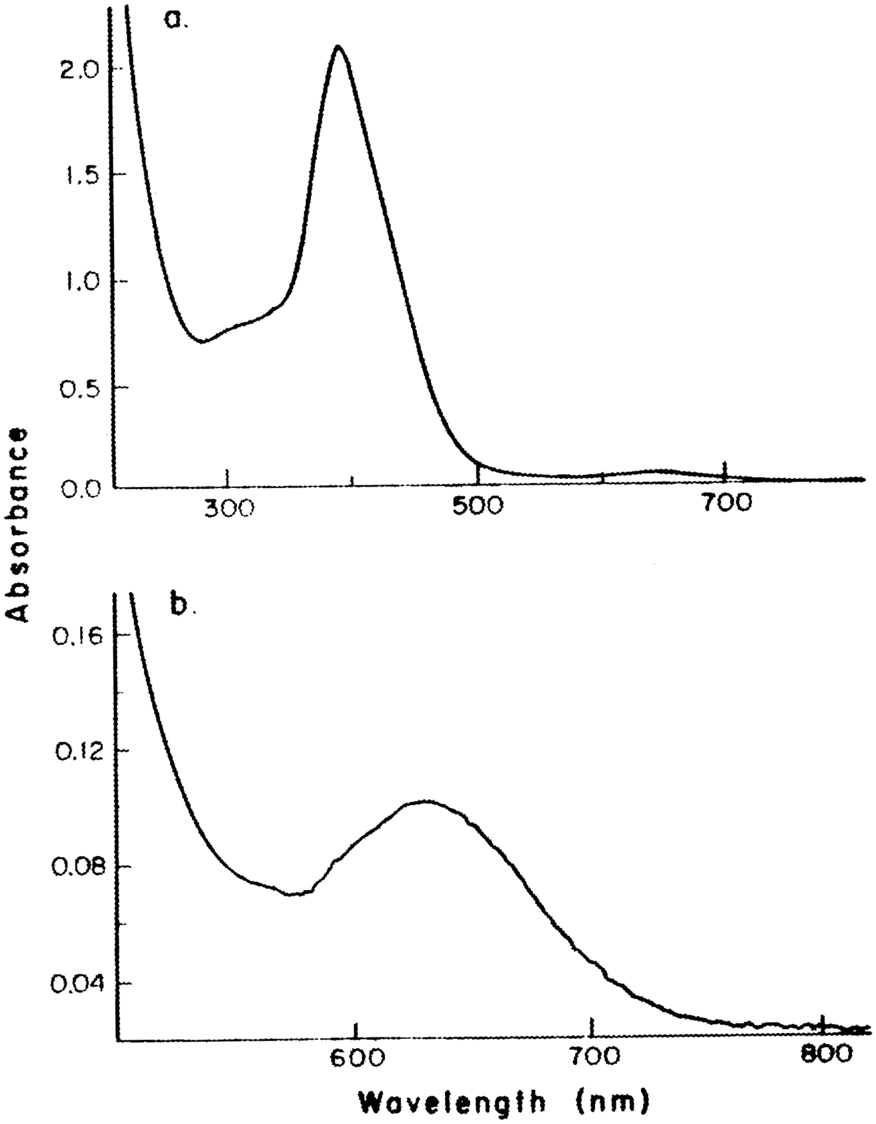

Figure 3.3. Spectral change of monomeric ion, $Ru^{III}(edta)(OH_2)$, with time. Conditions: 1.0 mM monomer $Ru(edta)(OH_2)$ in 0.1 M phosphate, pH 11.3, purged by argon; optical pathlength, 1.0 mm.

required for the band to reach equilibrium. Ni and Anson[63] also observed this phenomenon and ascribed the 566-nm band to the dimer $(edta)_2Ru_2^{III,III}$. When the solution was re-exposed to the air, the spectrum reverted to the original, i.e., before purging with argon. This behavior shows that the change is reversible.

(2) Dimeric $(edta)_2Ru_2^{III,IV}$

This ion, described as a dimeric complex containing two ruthenium ions with an average oxidation state of 3.5, is an intensely green compound. I will give evidence that the ligand bridge is a simple oxygen atom. Based upon its spectral properties, it is stable in acidic and weakly alkaline solutions (pH <10). Its spectrum (Figure 3.1) comprises two bands and a shoulder which are at 632 nm ($\varepsilon = 437\ M^{-1}\ cm^{-1}$), 394 nm ($\varepsilon = 1.8 \times 10^4\ M^{-1}\ cm^{-1}$), and 304 nm (sh, $\varepsilon = 6.7 \times 10^3\ M^{-1}\ cm^{-1}$), respectively.

In a strongly alkaline solution (pH >10), dramatic changes occurred in the spectra, with different behavior observed under aerobic and anaerobic conditions. In aerobic solutions, the dimeric complex initially exhibited bands at 324 nm ($\varepsilon = 4.1 \times 10^3\ M^{-1}\ cm^{-1}$) and 415 nm ($\varepsilon = 5.1 \times 10^3\ M^{-1}\ cm^{-1}$), and the band at 415 nm lost intensity over a period of several hours, whereas the intensity of the band at 324 nm was not significantly changed. The magnitude of the absorbance decrease at 415, which was maximally 50%, was two-fold greater at pH 12-13 than that at pH 11. However, in anaerobic solution, the peak at 324 nm gradually shifted to 314 nm, the peak at 415 nm became a shoulder and shifted to 400 nm, and a new peak at 566 nm appeared (Figure 3.4). The final spectrum at pH 11.5 under anaerobic conditions was very similar to the

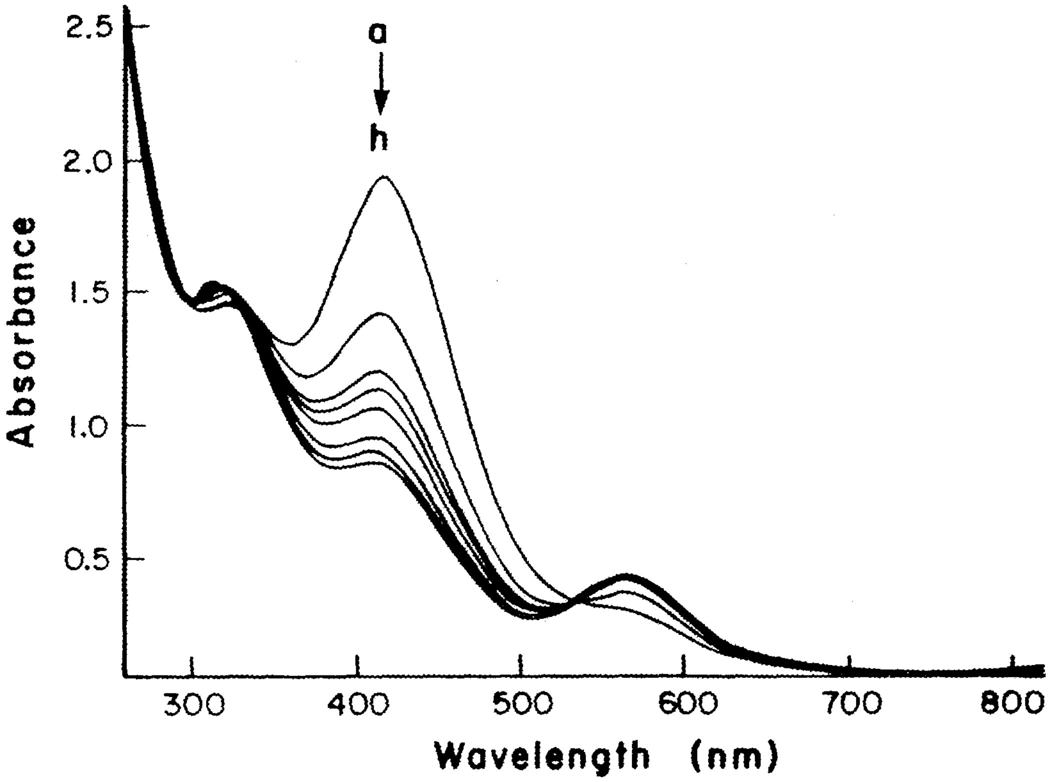

Figure 3.4. Spectral change of dimeric ion $(edta)_2Ru_2^{III,IV}$ with time. Conditions: 0.5 mM dimer $(edta)_2Ru_2^{III,IV}$, in 0.1 M phosphate, pH 12.0, purged with argon; optical pathlength, 1.0 mm. Time interval after purging with argon in minutes: (a) 0, (b) 20, (c) 110, (d) 170, (e) 230, (f) 330, (g) 400, (h) 460. Optical pathlength: 1.0 mm.

spectrum of the monomer (Figure 3.3). If Anson's assignment is correct, i.e., the 566-nm band is due to the dimer (edta)Ru_2^{III}, it is possible that the dimer $(edta)_2Ru_2^{III,IV}$ had undergone one-electron reduction to $(edta)_2Ru_2^{III}$ at pH 11-13 under anaerobic conditions. The reductant in this case may have been the ligand edta by analogy with its demonstrated reactivity under other conditions (discussed later).

(3) Dimeric $(edta)_2Ru_2^{IV}$ ion

This is an unstable compound which has been claimed to be the catalytically active state for water oxidation to oxygen.[9,10] Its spectrum is composed of a band at 428 nm and a shoulder at 312 nm (Figure 3.5). No band exists in the visible region. Because it is unstable, accurate extinction coefficients of the bands cannot be obtained, but I estimate that the absorption intensity of the band at 428 nm is equal or greater than that of the band at 393 nm of the dimer $(edta)_2Ru_2^{III,IV}$.

The $(edta)_2Ru_2^{IV}$ ion is formed by one-electron oxidation of the (edta)$Ru_2^{III,IV}$.[9] Addition of a nine-fold excess of Ce^{4+} to $(edta)_2Ru_2^{III,IV}$ in 0.1 M $HClO_4$ (or a five-fold excess in 0.2 M trifluoroacetic acid) was sufficient to cause quantitative oxidation to $[(edta)_2Ru_2^{IV}]$ ion, as was apparent from the optical absorption spectrum.

3.2.2 Vibrational spectra of Ru-edta complexes

In order to differentiate between linear or bent μ-oxo, or doubly bridged dihydroxo structures, infrared and Raman spectra were taken of the dimer and monomer salts. FTIR spectra (Figure 3.6) of the $(edta)_2Ru_2^{III,IV}$ dimeric ions taken as their sodium salts in KBr or

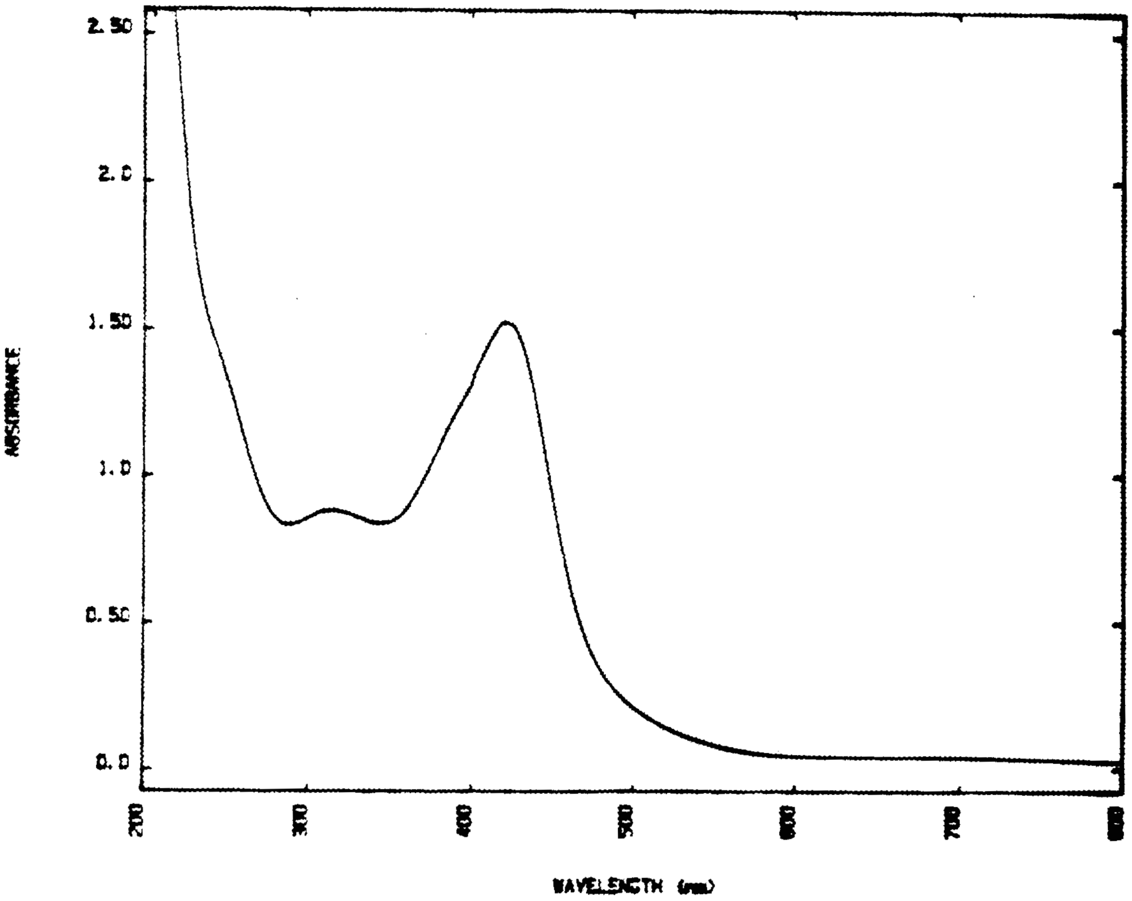

Figure 3.5. Optical spectrum of the dimeric ion $(\text{edta})_2\text{Ru}_2^{IV}$. Conditions: ~80 μM in 0.1 M CF_3COOH, prepared by a reaction of 1.5 nm $\text{Ru}^{III}(\text{edta})(OH_2)$ with ten-fold excess $KMnO_4$. Optical pathlength: 1.0 mm. The spectrum just after $KMnO_4$ was entirely consumed.

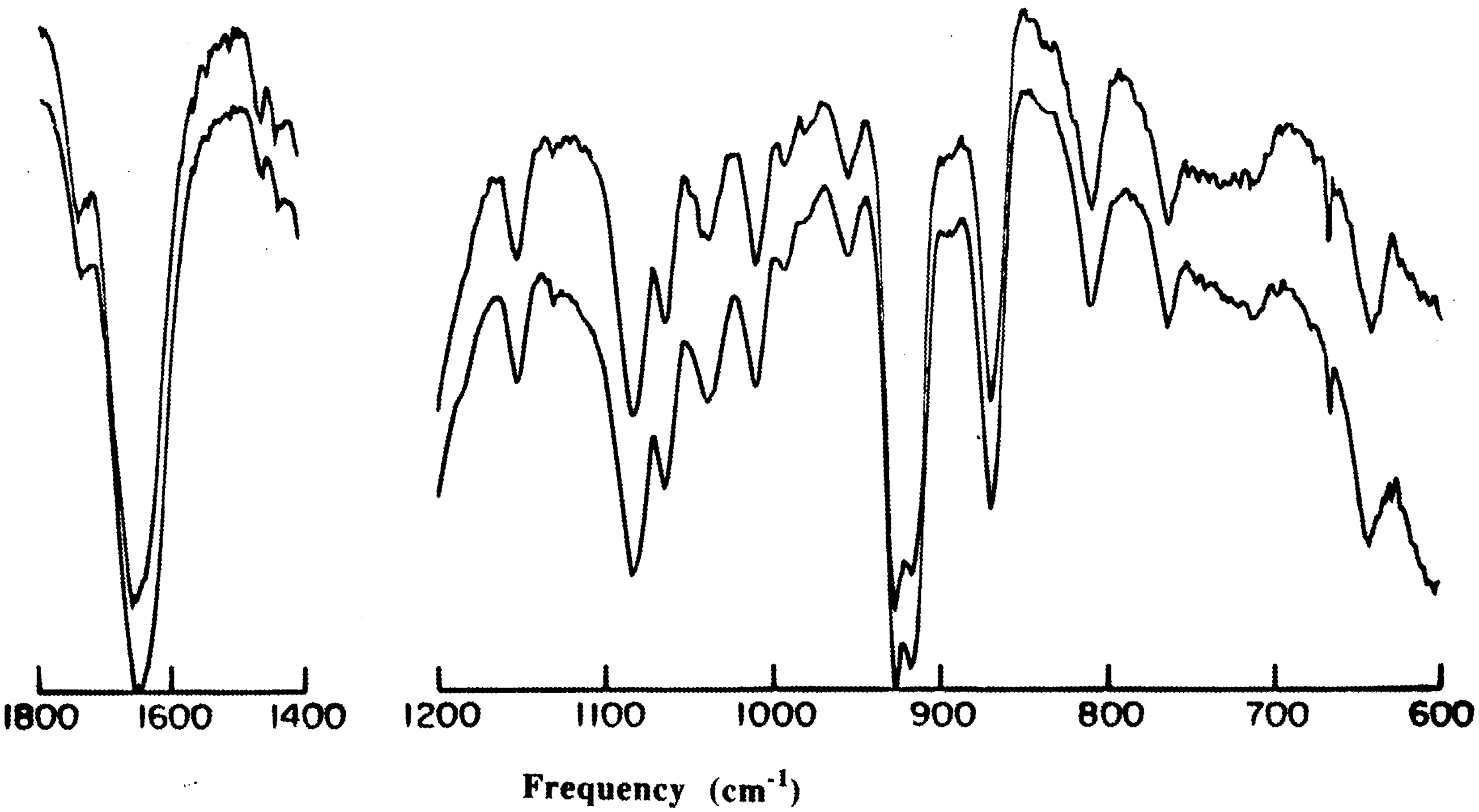

Figure 3.6. FTIR spectra of [^{16}O] (lower trace) and [^{18}O] (upper trace) [Ru(edta)(OH$_2$)]$_2$O^{III,IV} ions taken as the sodium salt in KBr. Identical results were obtained in Nujol mulls.

Nujol exhibited absorption bands attributable to carbonyl stretching modes for protonated (1734 cm^{-1}) and metal-coordinated (1653 cm^{-1}) carboxyl groups, as well as numerous medium to weak bands throughout 400 to 600 cm^{-1} which were similar to those found in the spectrum of $Ru^{III}(edta)(OH_2)$ but differed slightly in position and/or relative intensities. The largest difference observed in this range was an approximately two-fold increase in intensity in a band at 876 cm^{-1}, which also shifted to 870 cm^{-1} in the dimer. FTIR spectra of binuclear ions containing ^{16}O or ^{18}O in the ligand bridge were indistinguishable.

The dominant feature of the RR spectrum of the dimer in acidic and neutral solution is an intense symmetric band appearing at 433 cm^{-1}; additional medium-intensity bands were found at lower frequencies, but the few bands observed at higher frequencies (to 1100 cm^{-1}) were very weak (Figure 3.7). Identical spectra were obtained from samples prepared by oxidation of $Ru^{III}(edta)(OH_2)$ with H_2O_2, ClO_3^- or O_2. Spectral bandshapes were independent of exciting wavelength (456 to 674 nm), dimer concentration (1.3-40 mM) and medium acidity (pH 2-7). Spectral resolution was considerably improved by freezing the samples in a liquid N_2 cryostat; at room temperature the medium-intensity modes coalesced and appeared as a broad shoulder on the low frequency side of the intense peak. The sodium salt diluted in KBr gave a spectrum comparable to the room-temperature solution spectra. In all cases, spectra were unchanged after repetitive scanning, consistent with the absence of interfering photodegradation. However, exitation at higher energies (406 or 413 nm) caused extensive photodecomposition of both solution and solid samples.

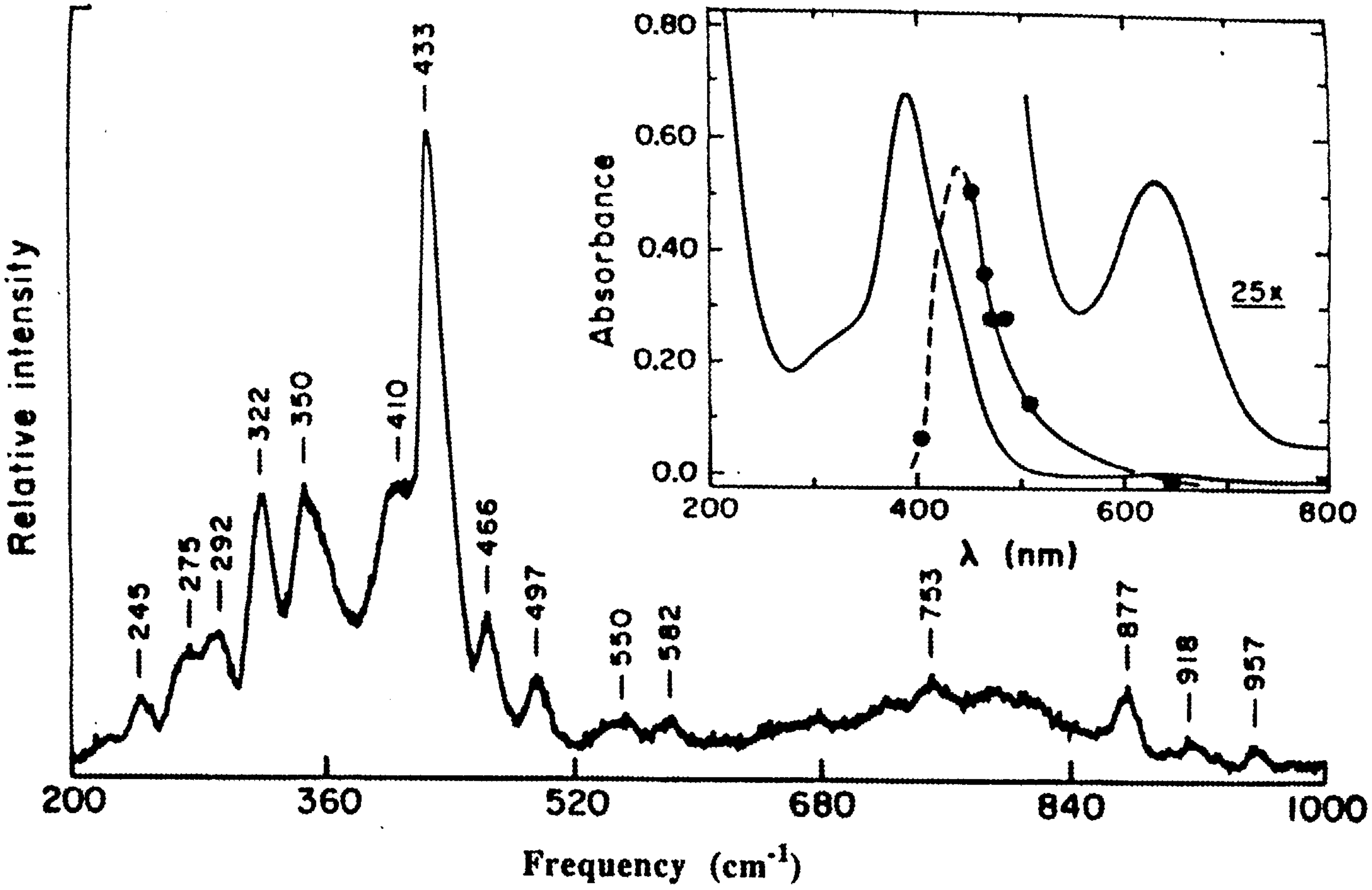

Figure 3.7. RR spectrum of 0.04 M $(edta)_2Ru_2^{III,IV}$ ion in 0.3 M acetate buffer, pH 5 with 40 mW excitation at 458 nm. Average of 11 scans taken by backscattering from a capillary tube containing the frozen sample (90 K). Inset: room temperature excitation profile scaled to 0.3 M SO_4^{2-} ion superimposed upon the electronic absorption spectrum.

Small spectral shifts to lower frequencies occurred in the 433 and 324 cm^{-1} bands when $[^{18}O]$-$Ru^{III}(edta)(OH_2)$ was used as the dimer precursor (Figure 3.8). In D_2O, the dimer from $Ru^{III}(edta)(OH_2)$ containing coordinated water of normal isotopic composition gave barely perceptible (<1 cm^{-1}) shifts of the 433 and 324 cm^{-1} bands to higher and lower frequencies, respectively, as the only spectral perturbations. Above pH 10, the dimer has been shown to undergo optical spectroscopic changes that correlate with the titrimetric uptake of OH^- ion.[9] The RR spectrum of this brown alkaline form exhibited three relatively intense bands from 337 to 414 cm^{-1} whose position and relative intensities were fairly constant over the alkaline pH region (Figure 3.9). Each of these bands shifted 2-3 cm^{-1} to lower energies when the dimer was prepared from $Ru^{III}(edta)(OH_2)$ in isotopically enriched water. Unlike the behavior of the acidic form, these bands were sensitive to deuteration, with the 337- and 372-cm^{-1} bands moving to lower energies and the 414-cm^{-1} band apparently shifting to higher energy in D_2O, although the latter effect may be a consequence of changes in relative intensities of the main peak of the high-frequency shoulder.

Excitation profiles of the acidic form of the $(edta)_2Ru_2^{III,IV}$ ion were determined by ratioing the scattering intensities of several bands in the room-temperature aqueous spectra to the symmetric breathing mode (976 cm^{-1}) of 0.3 M SO_4^- ion, which had been added in the form of its sodium salt. Results for the 433-cm^{-1} band with excitation at various wavelengths from 458 to 647 cm^{-1} are displayed in the inset to Figure 3.7. Comparable profiles were obtained for the bands centered at 350 and 272 cm^{-1}. The vibrational modes appear to be coupled to the

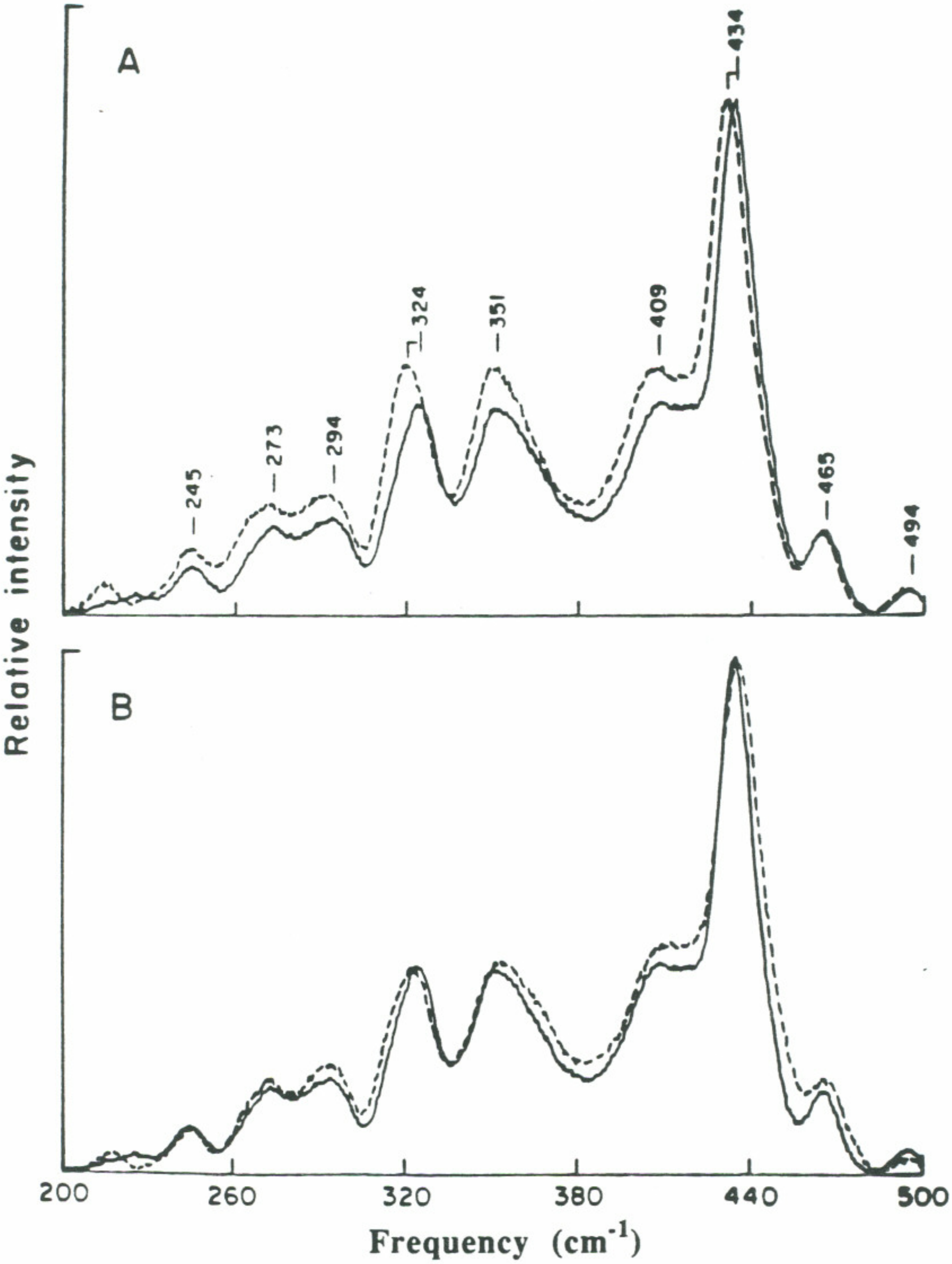

Figure 3.8. Low frequency RR spectra of 0.02 M $(edta)_2Ru_2^{III,IV}$ ion in 0.24 M acetate buffer, pH 5. Panel A: solid line, ^{16}O-bridged; dashed line, ^{18}O-bridged. Panel B: solid line, ^{16}O bridged in H_2O; dashed line, ^{16}O bridged in 98% D_2O. Experimental conditions as in Figure 3.7; average of 10 scans.

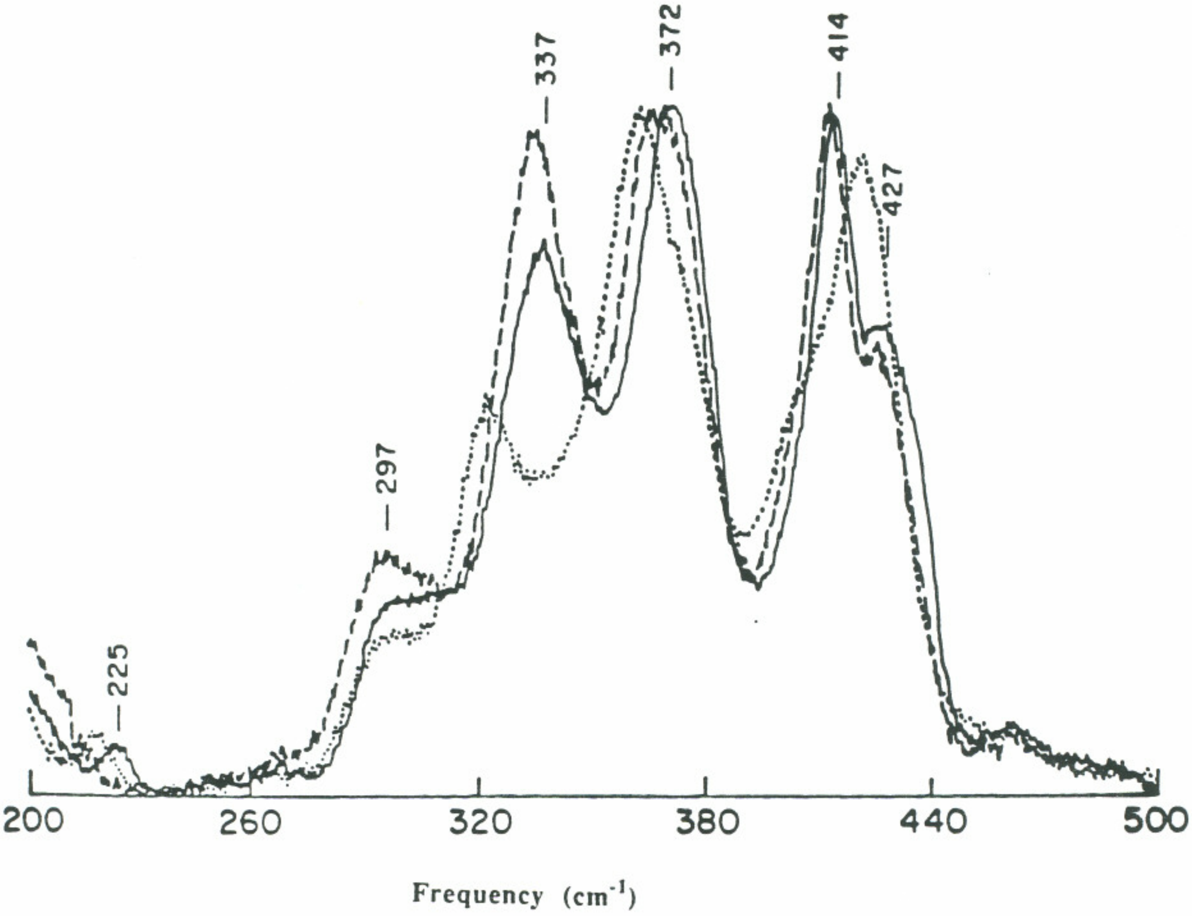

Figure 3.9. Low frequency RR spectra of 0.02 M $(edta)_2Ru_2^{III,IV}$ in 0.01 M NaOH. Solid line, ^{16}O-bridged in H_2O; dashed line, ^{18}O-bridged in 85% $[^{18}O]$-H_2O; dotted line, ^{16}O-bridged in 95% D_2O. Experimental conditions as in Figure 3.7; average of 10 scans.

electronic transition that gives the intense optical band centered at 394 nm. As mentioned above, photobleaching of the sample occurred at shorter excitation wavelengths, precluding a quantitative study of scattering intensities over this band.

One-electron oxidation to the corresponding $(edta)_2Ru_2^{IV}$ ion can be accomplished by strong oxidants such as Ce^{4+} ion. This oxidation state could be maintained indefinitely in a frozen solution below 100 K, but reverted to the (III,IV) state under these conditions upon standing at room temperature for 30 minutes. The low temperature RR spectrum of the (IV,IV) ion comprised only very broad absorption envelopes centered at 440 and 800 cm^{-1}, from which individual bands could not be resolved. The spectral intensity was maximal with 458- to 472- nm excitation, and resolution was not improved at other wavelengths. Upon warming, the RR spectrum characteristic of the $(edta)_2Ru_2^{III,IV}$ ion appeared superimposed upon this broad background and grew in intensity with time at its expense. The Ce^{4+} reagent solution did not give detectable Raman bands above 250 cm^{-1}.

3.2.3 Electron paramagnetic resonance

Electron paramagnetic resonance (EPR) spectra of $(edta)_2Ru_2^{III,IV}$ were taken to characterize its magnetic properties. In a strongly alkaline solution, pH 12-14, the low temperature EPR spectrum of the $(edta)_2Ru_2^{III,IV}$ ion gave the appearance of a composite of at least two rhombic $S = 1/2$ signals with sets of apparent g values at $g = 2.37$, 2.07, and 1.96 and $g = 2.48$, 2.07 and 1.84 (Figure 3.10). The relative intensities of the two sets varied with the sample temperature (20-100 K). The less rhombic signal became increasingly predominant at

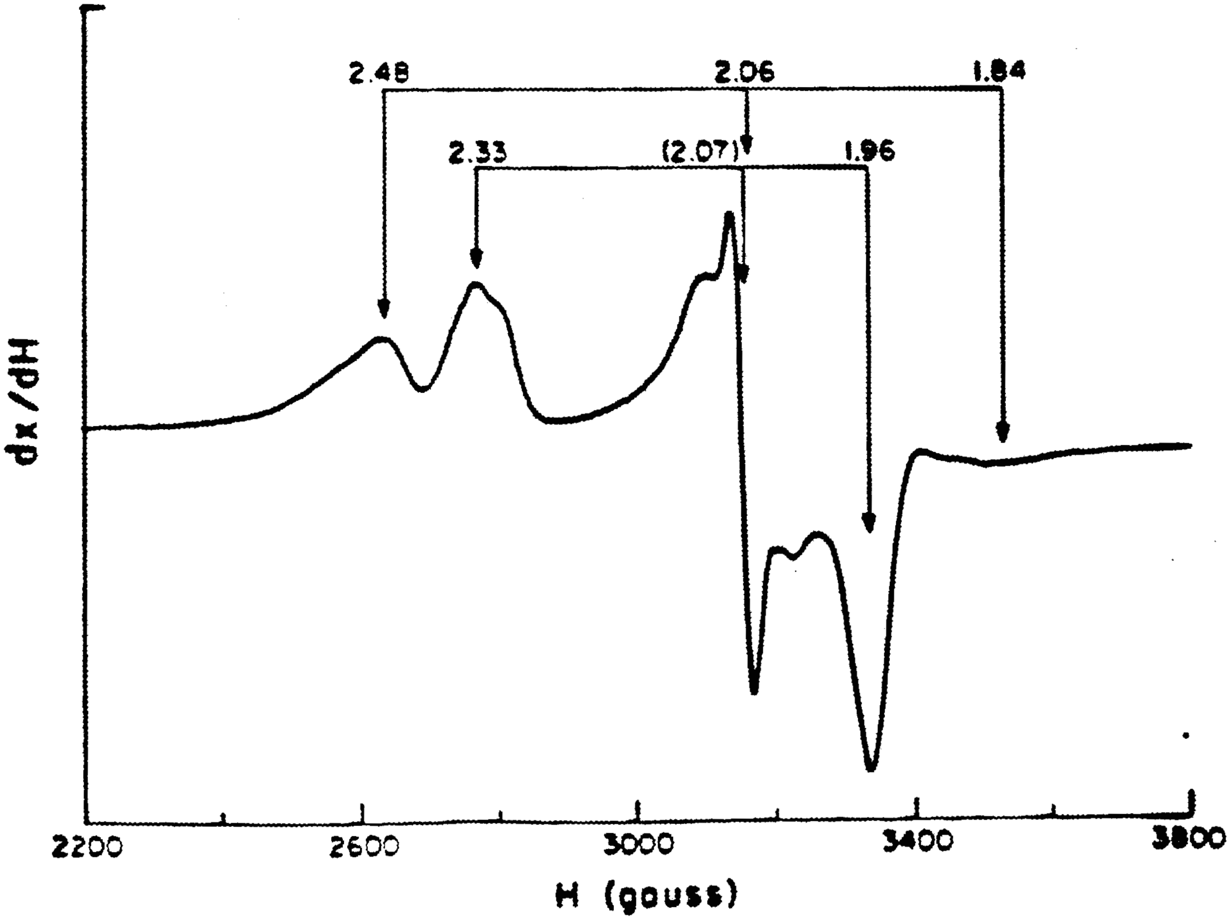

Figure 3.10. X-band EPR spectrum of $(edta)_2Ru_2^{III,IV}$ at 10 mW microwave power and 10 g modulation amplitude, in 0.01 M NaOH, 20 K. Apparent g values are indicated by the arrows.

high temperature. An aging effect was also evident, with the more asymmetric signal increasing in relative intensity with sample lifetime over a period of several hours when maintained at room temperature. In a less alkaline medium (50 mM glycine, pH 10), the EPR spectrum was even more complex and was dominated by a yet more asymmetric signal with broad bands centered at $g = 2.89$, 2.18, and 1.73 that increased in relative intensity with time. In contrast, the $(edta)_2Ru_2^{III,IV}$ ion in acidic solution gave a much more symmetric signal, which also was considerably weaker (Figure 3.11).

The EPR spectra are consistent with one unpaired spin in the dimeric complexes, and the variation in relative intensities of the rhombic set in alkaline solution with medium conditions, time and temperature indicates the simultaneous existence of several distinct dimeric species. The absence of measureable hyperfine splittings makes further structural analyses difficult.

3.2.4 Redox potentiometry

To characterize the redox behavior of the $(edta)_2Ru^{III,IV}$ ion and to probe for possible coordination of water at this oxidation level, we made an extensive study of electrochemical properties of the complex by cyclic voltammetry over the accessible acidity range (pH 1-14). I will present these results separately covering three pH regions (1-6, 7-10, 11-14) because there are distinct differences in electrochemical behavior in the different ranges.

(1) Cyclic voltammograms in the pH region 7-10

A typical cyclic voltammogram of $Ru^{III}(edta)(OH_2)$, taken at pH 7.0, is given in Figure 3.12. Eight waves are seen over the accessible

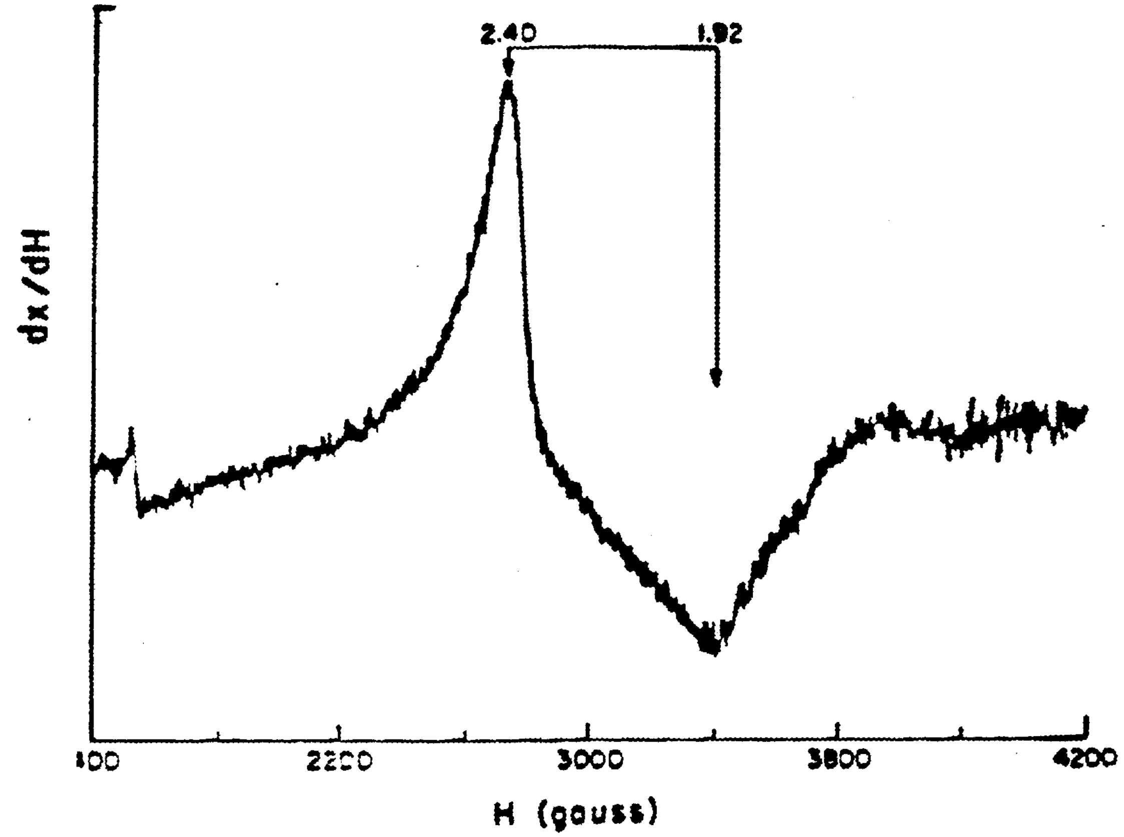

Figure 3.11. X-band EPR spectrum of (edta)$_2$Ru$_2^{III,IV}$ at 10 mW microwave power and 10 g modulation amplitude, in 0.01 M trifluoroacetic acid, 5 K. Apparent g values are indicated by the arrows.

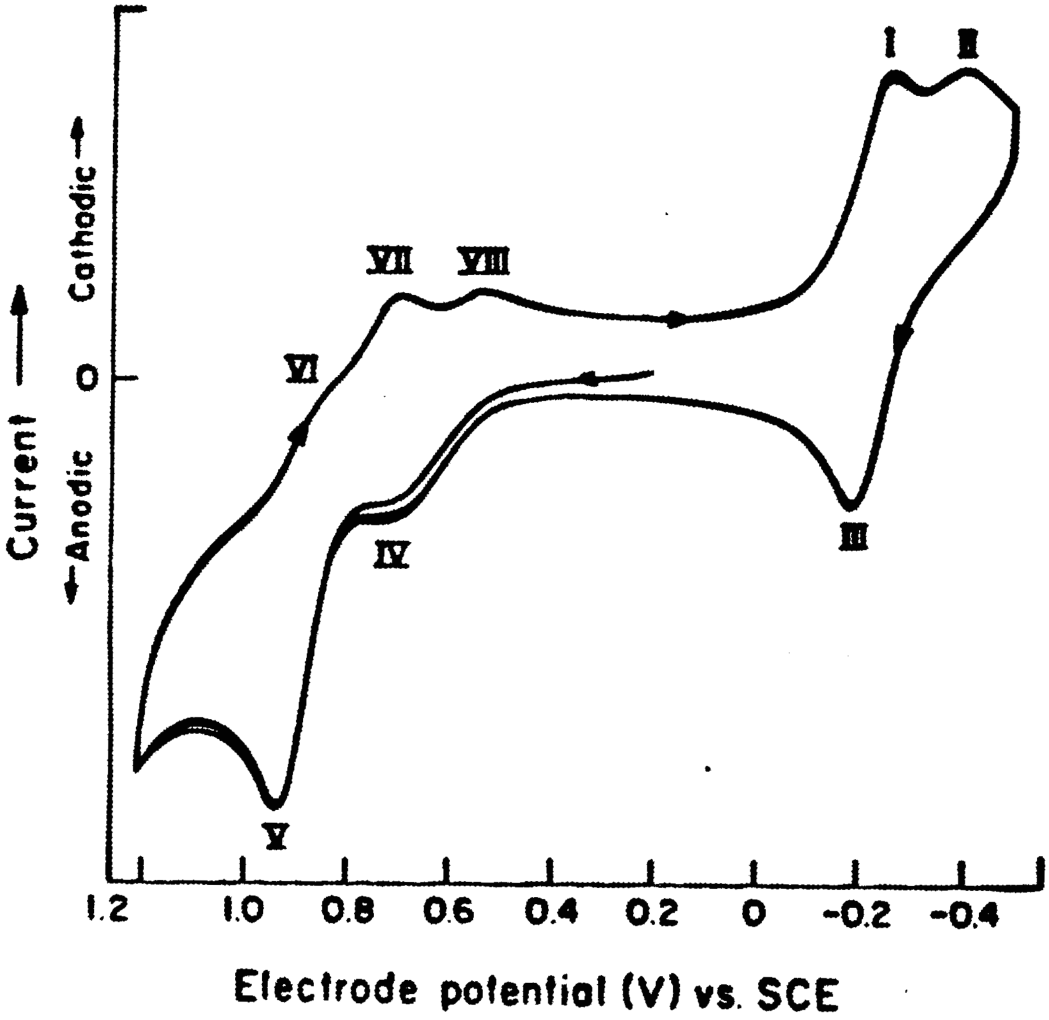

Figure 3.12. Cyclic voltammogram of 1.8 mM $Ru^{III}(edta)(OH_2)$ ion in 0.1 M phosphate, pH 7.0, glassy carbon electrode (GCE), platinum wire, and saturated calomel were used as working, counter, and reference electrodes, respectively. Scan rate = 100 mV/s; 4 cycles are displayed.

potential range. Peaks I and III, at -247 and -194 mV, correspond to reversible one-electron reduction and oxidation of $Ru^{III}(edta)(OH_2)$ and $Ru^{II}(edta)(OH_2)$, respectively,

$$Ru^{III}(edta)(OH_2) + e^- \rightleftharpoons Ru^{II}(edta)(OH_2)$$

Peak II, at -384 mV, was not observed in the initial cathodic scan nor was it observed if the anodic sweep was limited to potentials below 600 mV (see, e.g., Figure 3.14.) In acidic medium (discussed in the succeeding section), an additional peak that exhibited qualitatively the same behavior was observed at a potential that was highly pH dependent. These observations are in accord with those of Baar and Anson,[9,10] who assigned the latter peak to quasi-reversible one-electron reduction of $(edta)_2Ru_2^{III,IV}$ to $(edta)_2Ru_2^{III}$:

$$(edta)_2Ru_2^{III,IV} + e^- \rightarrow (edta)_2Ru_2^{III}$$

and peak II to irreversible two-electron reduction of the complex, $(edta)_2Ru_2^{III}$, yielding two $Ru^{II}(edta)(OH_2)$ ions:

$$(edta)_2Ru_2^{III} + 2\ e^- + 2H_2O \rightarrow 2\ Ru^{II}(edta)(OH_2)$$

Peak IV, at 715 mV in neutral solution, is associated with oxidation of $Ru^{III}(edta)(OH_2)$ to the $(edta)_2Ru_2^{III,IV}$ ion:

$$2\ Ru^{III}(edta)(OH_2) + e^- \rightarrow [(edta)_2Ru_2^{III,IV}$$

It was not observed in cyclic voltammograms (Figure 3.13) of dimeric $(edta)_2Ru_2^{III,IV}$ provided that the cathodic sweep was not carried beyond about -100 mV, the point at which reduction gives rise to the formation of monomeric complex ions. Futhermore, CPE of monomer solutions at 800 mV yielded the green $(edta)_2Ru_2^{III,IV}$ ion. Peak V, at 920 mV, has been shown by Baar and Anson[9,10] to be the one-electron oxidation of $(edta)_2Ru_2^{III,IV}$ to $(edta)_2Ru_2^{IV}$:

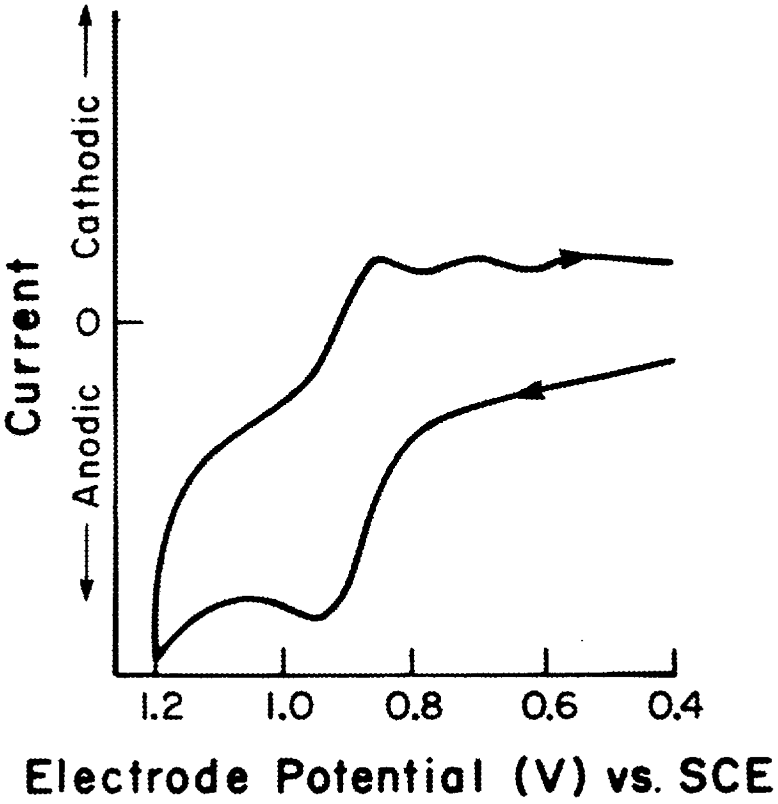

Figure 3.13. Cyclic voltammogram of 1 mM dimeric ion $(edta)_2Ru_2^{III,IV}$ in 0.1 M phosphate, pH 7.0, GCE relative to SCE. Scan rate = 500 mV/s, scan sequence: 400/1200/400.

$(edta)_2Ru_2^{III,IV} + e^- \rightarrow (edta)_2Ru_2^{IV}$

We have confirmed their spectrophotometric identification of this ion by CPE in a thin-layer cell. Specifically, electrolysis at 1.0 V vs. SCE caused the expected maximum to shift from 394 to 428 nm, with an accompanying disappearance of the 632-nm band (Figure 3.5). We assign peak VI, at 860 mV, to the coupled quasi-reversible $(edta)_2Ru_2^{IV}$ to $(edta)_2Ru_2^{III,IV}$ reduction step from the magnitude of its reduction potential. Peaks VII and VIII, at 690 and 500 mV, respectively, are also associated with oxidation to $(edta)_2Ru_2^{IV}$ level because they are not observed if the anodic sweep is reversed at a potential below 800 mV (Figure 3.14). Futhermore, the amplitudes of peak VII and VIII increased relative to peak VI with decreasing scan rate (Figure 3.15), suggesting that they represent species derived from the $(edta)_2Ru_2^{IV}$. Reversing the sweep immediately after passing cathodically through peak VII or VIII showed the presence of coupled anodic waves (VII' and VIII') for each step at -750 and -560 mV, respectively (Figure 3.16), although these waves nearly disappeared within the time required for complete cycling. The chemical nature of the species that might correspond to waves VII and VIII will be discussed in Section 3.3.

In summary, cyclic voltammograms of the $(edta)_2Ru_2^{III,IV}$ ion differ from those of $Ru^{III}(edta)(OH_2)$ in the following respects:

a. No oxidation waves were observed below 900 mV in the first scan cycle initiated in the anodic direction, but subsequent scans exhibited waves assignable to the oxidizing counterparts (waves VII' and VIII') of peaks VII and VIII if the cathodic sweep was reversed above

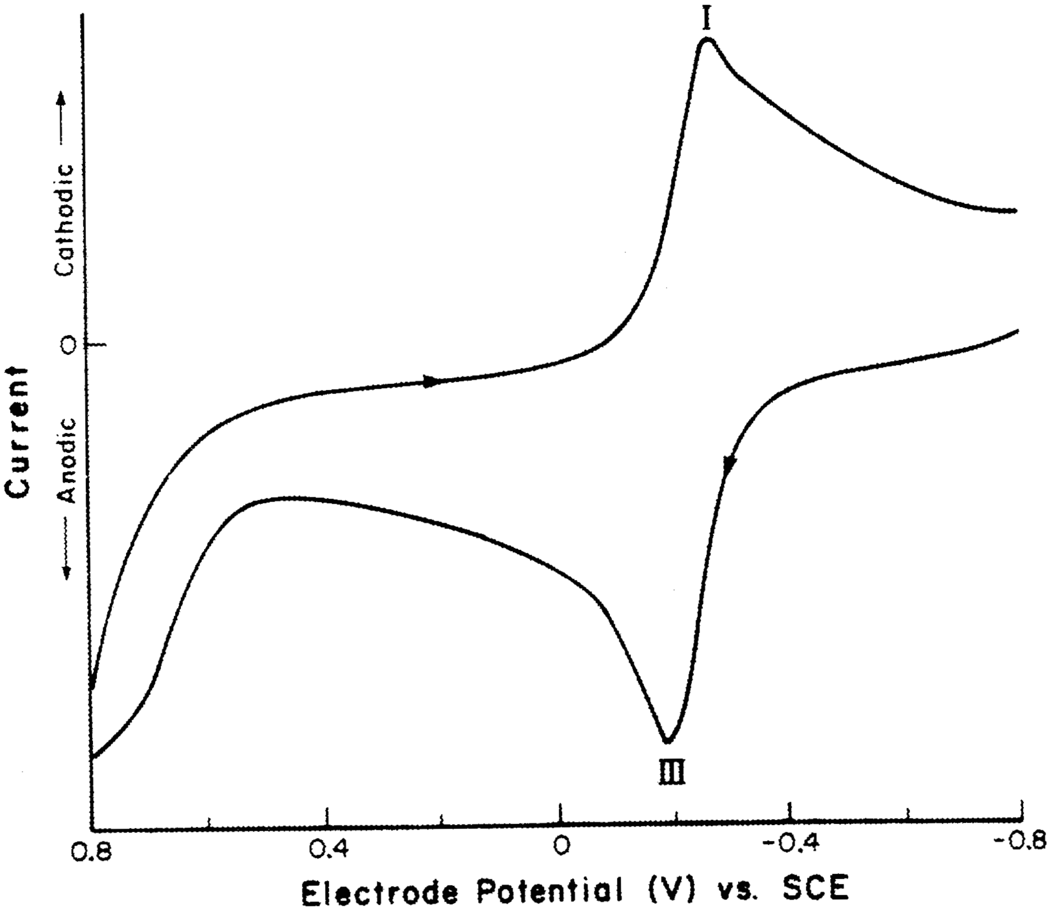

Figure 3.14. Cyclic voltammogram of 2 mM monomeric Ru(edta)(OH_2) in 0.1 M phosphate, pH 7.0, GCE relative to SCE. Scan rate = 200 mV/s. The $(edta)_2Ru_2^{III,IV}$ ion formed at 0.8 V.

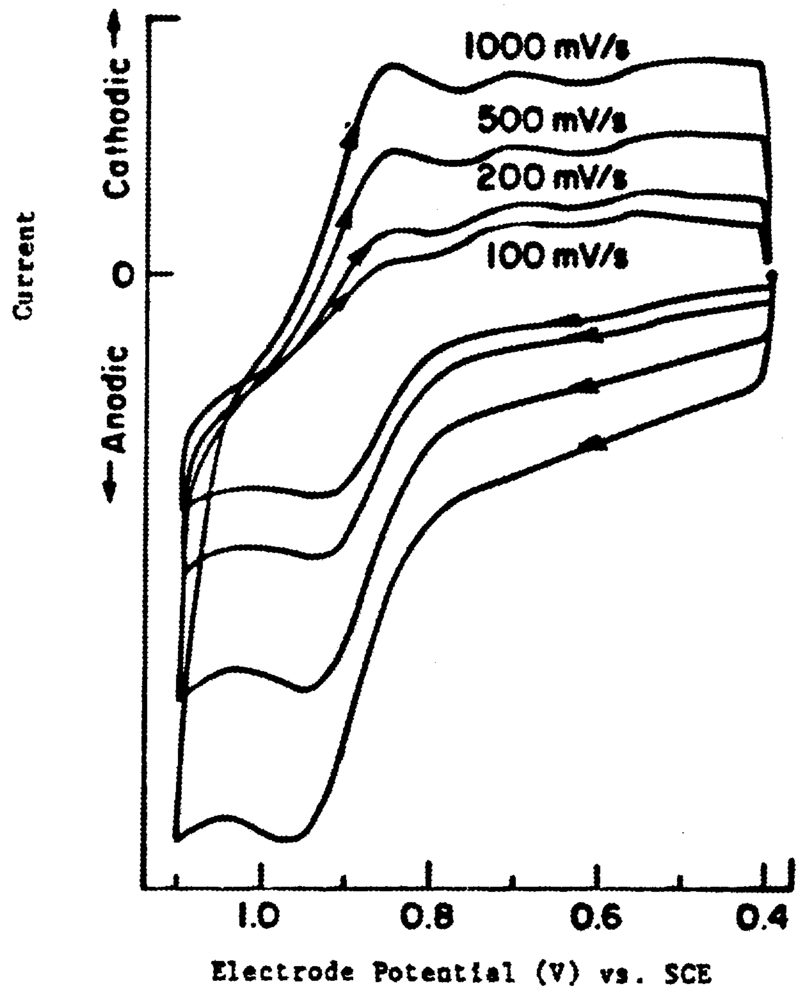

Figure 3.15. Overlay of cyclic voltammogram of dimer $(edta)_2Ru_2^{III,IV}$ at varying scan rates. Experimental conditions identical to Figure 3.12.

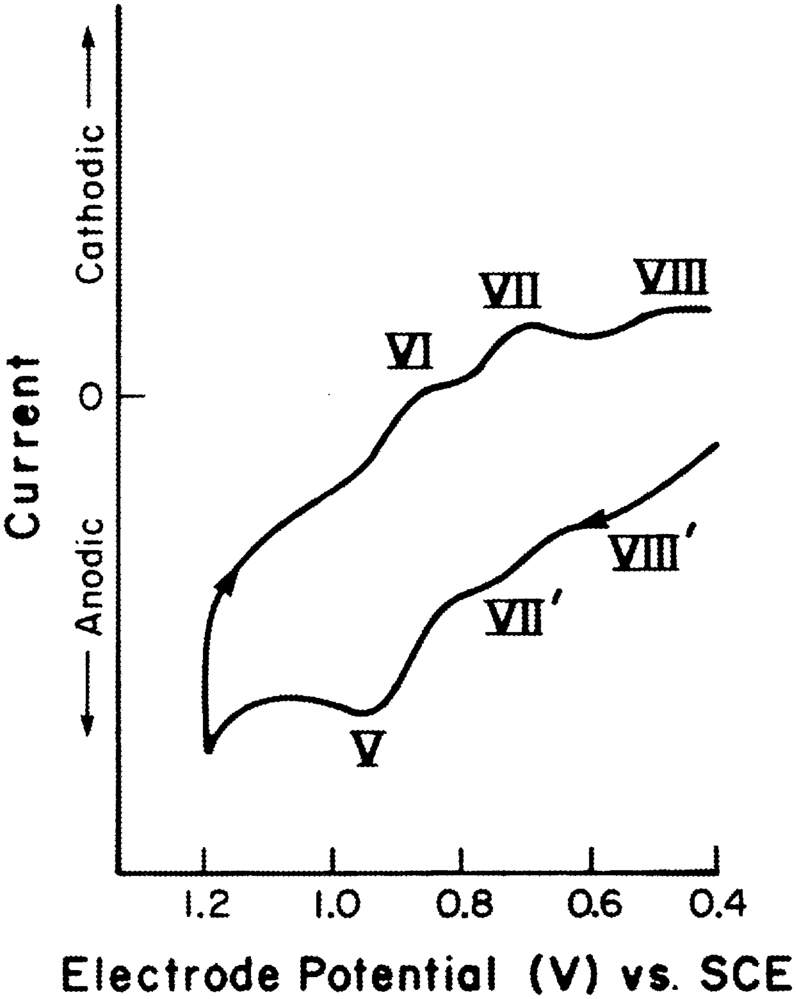

Figure 3.16. Cyclic voltammogram of 2.0 mM monomeric ion $Ru^{III}(edta)(OH_2)$ in 0.1 M phosphate, pH 7.0, GCE relative to SCE, second cycle, scan rate = 50 mV.

-100 mV (Figure 3.17) and to wave IV if the scan range was extended to -500 mV.

No oxidation wave below 900 mV was observed because the wave corresponds to oxidation of $Ru^{III}(edta)(OH_2)$ to the dimer $(edta)_2Ru_2^{III,IV}$, and no monomer exists in the solution in the first scan cycle initiated in the anodic direction. However, when the scan range was extended to -500 mV, the dimer $(edta)_2Ru_2^{III,IV}$ was reduced to the monomeric $Ru^{II}(edta)(OH_2)$, which was reoxidized upon reversing the scan to monomer $Ru^{III}(edta)(OH_2)$ so that wave IV appeared in the subsequent scans.

b. Peak I was absent from the first scan cycle initiated in the cathodic direction but was prominent in the subsequent scans. The reason for the absence of peak I is also because no monomeric $Ru^{III}(edta)(OH_2)$ ion was present in the system during the first scan, but was produced when the potential was swept through peak II (Figure 3.18). Therefore, these results are consistent with the reaction scheme and peak assignments deduced from the electrochemical behavior of the $Ru^{III}(edta)(OH_2)$ ion.

(2) Cyclic voltammograms in the range pH 1-6

A typical cyclic voltammogram of $Ru^{III}(edta)(OH_2)$ in pH 3.0 aqueous buffer is given in Figure 3.19. The potential was set at +200 mV vs. SCE, then swept to -500 mV and repetitively cycled between -500 and +1400 mV.

The initial scan yielded the expected reversible $Ru^{III}(edta)(OH_2)/Ru^{II}(edta)(OH_2)$ redox couple peaks (I and III) with $E_{1/2}$ = -199 mV. The wave V at -1000 mV had roughly the same peak

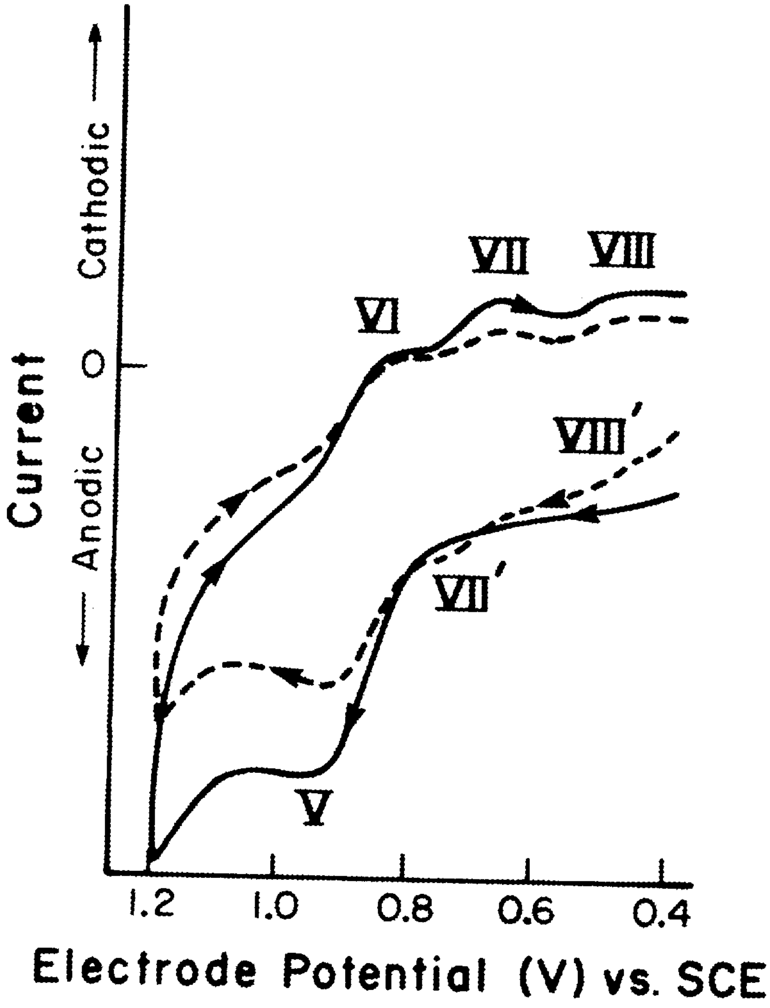

Figure 3.17. Cyclic voltammogram of 1.0 mM dimeric ion $(edta)_2Ru_2^{III,IV}$ in 0.1 M phosphate, pH 7.0, GCE relative to SCE, scan rate = 500 mV/s (Solid line is the first scan; dashed line, the second scan.)

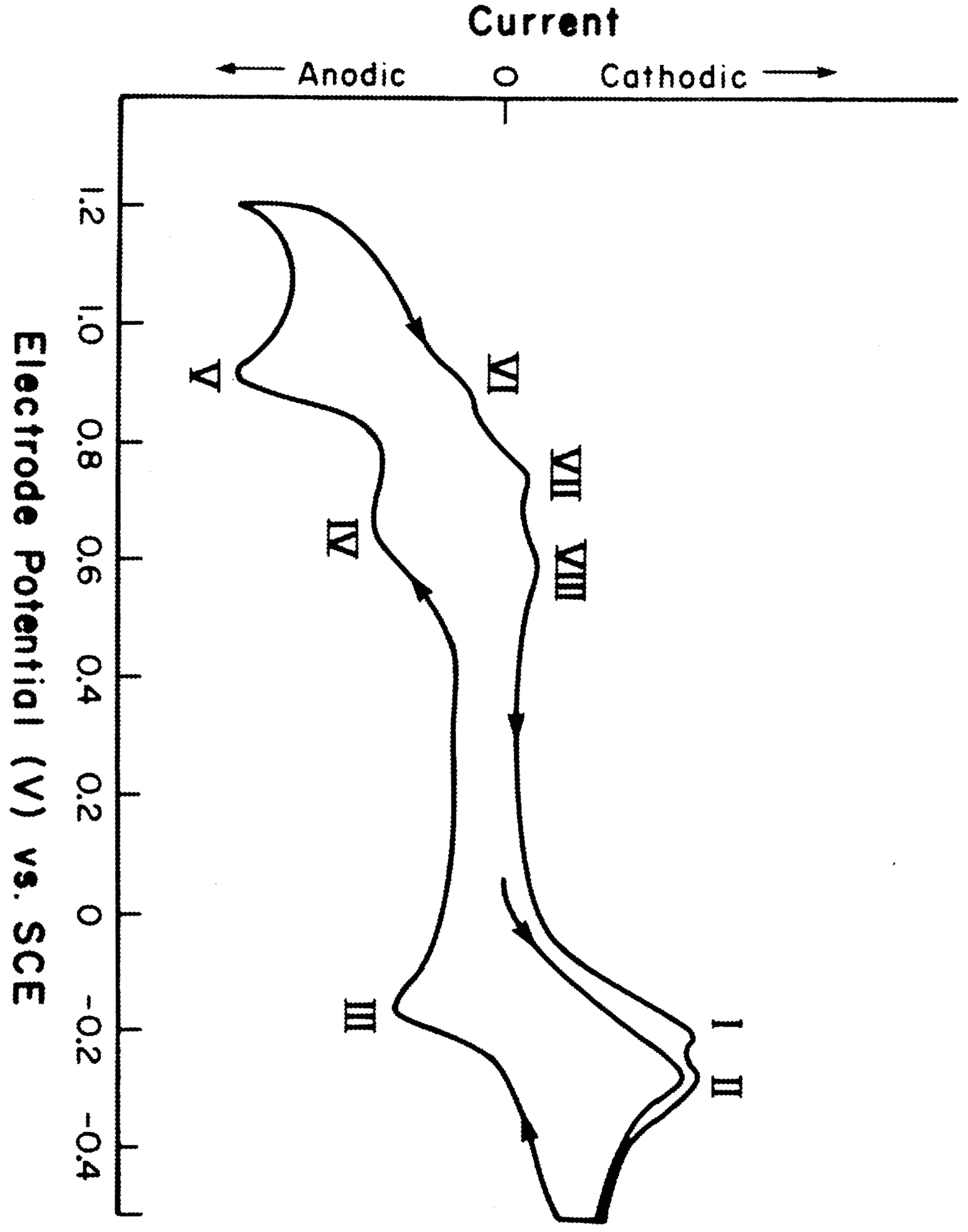

Figure 3.18. Cyclic voltammogram of 1 mM dimeric ion $(edta)_2Ru_2^{III,IV}$ in 0.1 M phosphate, pH 7.0, GCE relative to SCE, scan rate = 100 mV/s.

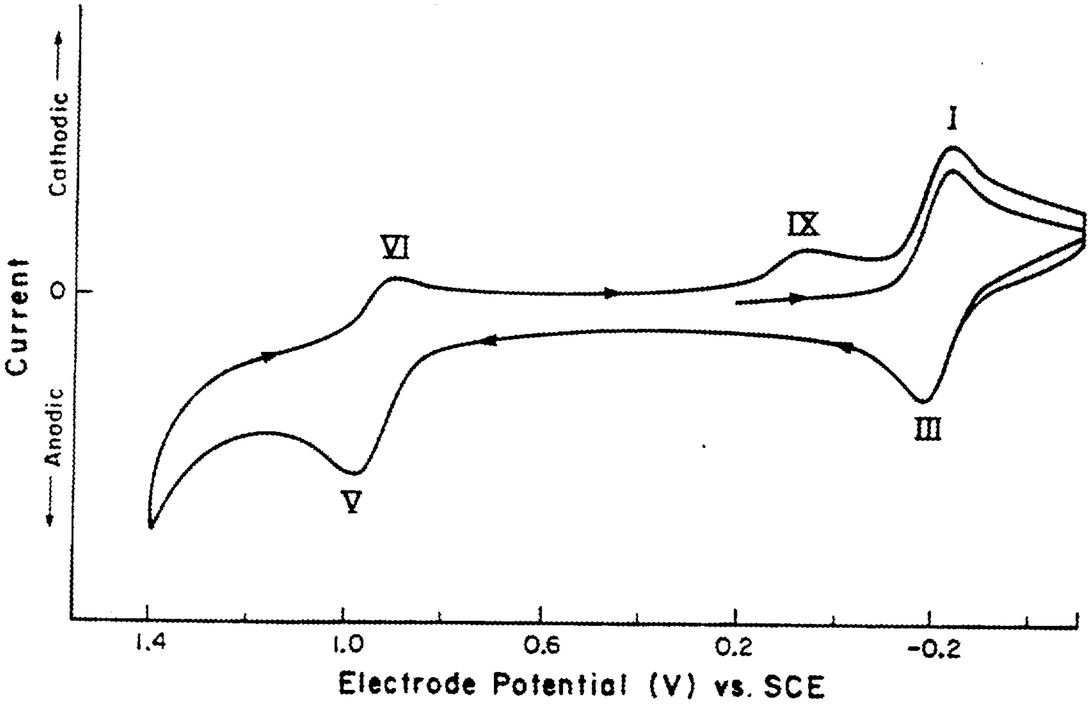

Figure 3.19. Cyclic voltammogram of 1.0 mM monomeric ion $Ru^{III}(edta)(OH_2)$ in 0.2 M CF_3COOH, pH 3.0, GCE vs. SCE, scan rate = 100 mV.

current as the Ru^{III}/Ru^{II} couple, but the return peak VI was much smaller. Peaks IV, VII, and VIII observed in the range of pH 7-10 were not seen in the more acidic solutions. When the scan continued toward more negative potential, a new wave (IX) appeared at 30 mV which was absent in the initial scan. The original peak I then appeared after scanning past IX, followed by peak III upon scan reversal. However, the cyclic voltammogram of the dimer $(edta)_2Ru_2^{III,IV}$ taken at pH 1.0 indicated that peak IX appeared within the first cycle when the potential was scanned from +600 to -500 mV (Figure 3.20) but did not appear when the scan was initiated at -500 (Figure 3.21). This meant that peak IX is related to the dimer because the dimer $(edta)_2Ru^{III,IV}$ was present when the scan was initiated at a potential of 600 mV but had been reduced to monomer $Ru^{II}(edta)(OH_2)$ when the scan was initiated at a potential of -500 mV and was not reformed if the potential was kept below 600 mV. Since this potential is less cathodic than wave I, which is assigned to the half reaction, $Ru^{III}(edta)(OH_2)/Ru^{II}(edta)(OH_2)$, wave IX probably corresponds to the reaction:

$$(edta)_2Ru_2^{III,IV}] + e^- \rightarrow (edta)_2Ru_2^{III} \text{ or } 2\ Ru^{III}(edta)(OH_2)$$

In summary, comparing Figure 3.12 with Figure 3.19, we find that cyclic voltammograms in the pH 1-6 range differ from those in pH 7-10 in the following respects:

a. The wave corresponding to peak IV in pH 7-10 is absent in the pH 1-6 range. Baar and Anson[9,10] have shown that the wave in the pH 1-6 region becomes combined with peak V.

b. Waves corresponding to peaks VII and VIII in pH 7-10 were absent in the pH 1-6 region, and the current of peak VI in the pH 1-6 range is

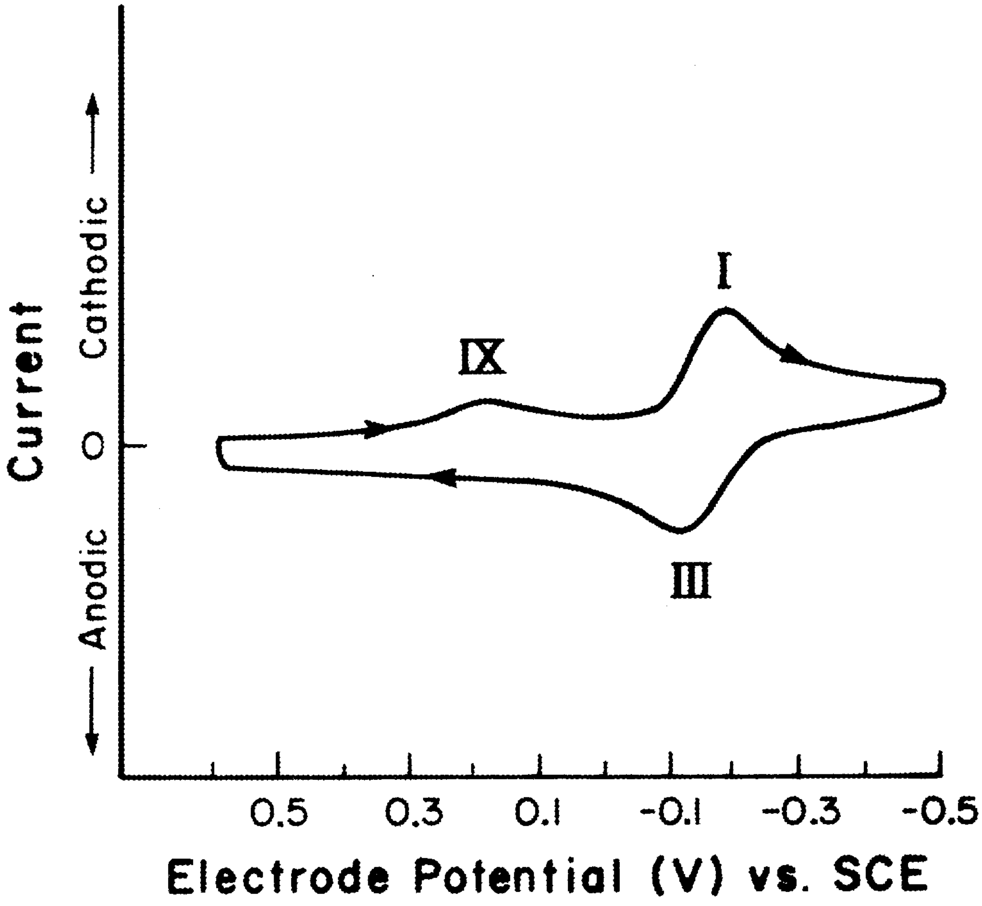

Figure 3.20. Cyclic voltammogram of 1.0 dimeric ion $(edta)_2Ru_2^{III,IV}$ in 0.2 M CF_3COOH, pH 1.0, GCE vs. SCE, scan rate = 100 mV/s, scan sequence: 600/-500/600 mV.

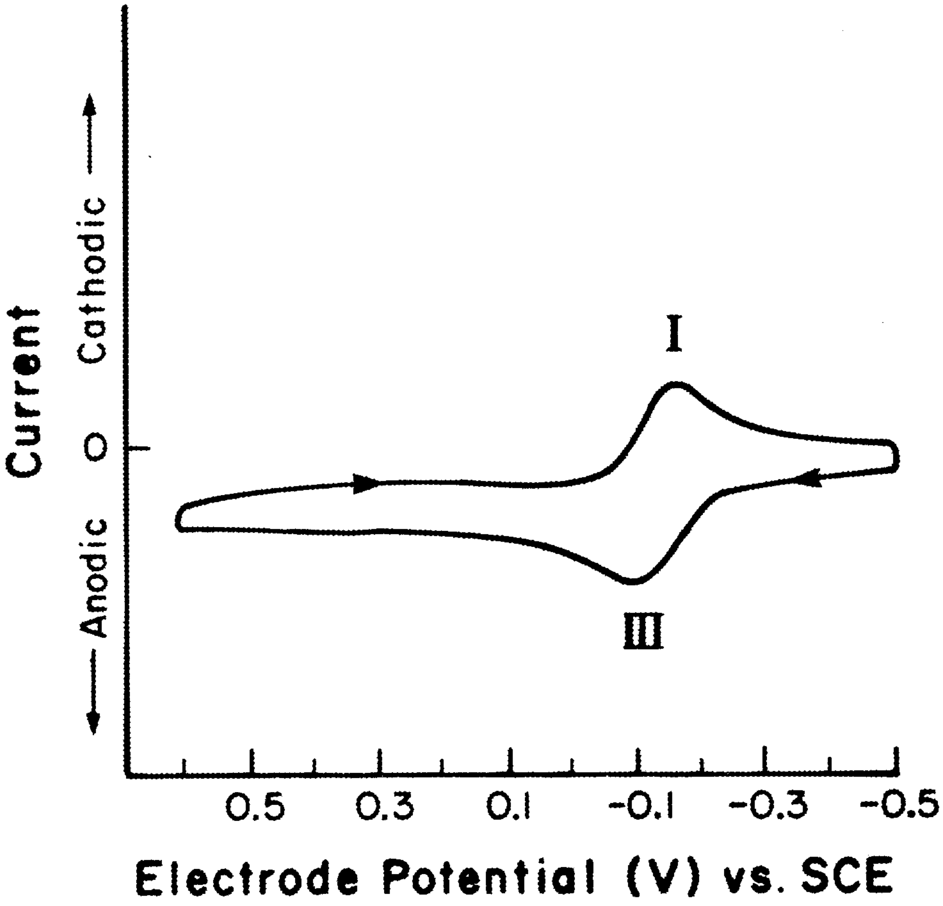

Figure 3.21. Cyclic voltammogram of 1 mM dimeric ion $(edta)_2Ru_2^{III,IV}$ in 0.2 M CF_3COOH, pH 1.0, GCE vs. SCE, scan rate = 100 mV/s, scan sequence: -500/600/-500 mV.

higher than that in the pH 7 to 10. These results will be discussed in succeeding sections.

(3) Cyclic voltammogram in the pH range 11–14

In this range the cyclic voltammograms become very complicated. Two sharp peaks appear below 400 mV, and two symmetric sharp peaks appear above 400 mV, which had characteristics of adsorption peaks, i.e.:

a. The peak intensities increased with the number of scan repetitions, suggesting the amount of electroactive material adsorbed on the electrode increased with time.

b. After several cycles, the working electrode was removed from the solution containing the compound, rinsed thoroughly with distilled water, then placed in the electrolyte solution which contained no complex ion. The sharp peaks were still observed upon sweeping the potential, indicating their origin was strongly adsorbed material.

Similar results were obtained using various working electrodes, including glassy carbon, platinum, and In-doped SnO_2.

(4) pH Dependence of midpoint reduction $E_{1/2}$ and peak potentials

Figure 3.22 gives the pH dependence of $E_{1/2}$(V/VI) for the couple $(edta)_2Ru_2^{III,IV}/(edta)_2Ru_2^{IV}$, $E_{1/2}$(I/III), for the couple $Ru^{II}(edta)(OH_2)/Ru^{III}(edta)(OH_2)$, and potentials for peaks II, IV, VII, and VIII. From Figure 3.22, it can be seen that the curves for peaks IV, VII, and VIII and $E_{1/2}$(V/VI) are pH independent over the accessible range, except for the small change at pH <3.5 that can be assigned to protonation of two uncoordinated carboxylato groups of edta ($pK_a \approx 2.5$)[9] for the curve $E_{1/2}$(V/VI). This virtual pH independence means that there is no change in proton content of the dimers upon one-electron oxidation/reduction. Since Ikeda et al.[26] have shown that the dimer $(edta)_2Ru_2^{III,IV}$ has no aqua ligand based upon pH titrimetric data, we can conclude from the electrochemical behavior that the dimeric $(edta)_2Ru_2^{IV}$ also has no aqua ligands.

The potential for the oxidation of the monomeric $Ru(edta)(OH_2)$ ion to the $(edta)_2Ru_2^{III,IV}$ dimer (peak IV) is pH independent in the pH 7-10 range. The pK_a of solvent coordinated to $Ru^{III}(edta)(OH_2)$ is reported to be 7.6.[31] Therefore, above pH 7.6 the monomer exists in the form of $Ru^{III}(edta)(OH)$ so that the half reaction can be assigned to

$$2Ru^{III}(edta)(OH) \rightarrow (edta)Ru^{III}\text{-}O\text{-}Ru^{IV}(edta) + e^- + H_2O.$$

This assignment can explain why the potential of wave IV is not dependent upon pH in alkaline media. However, in the acidic range, the monomer exists in the form of $Ru^{III}(edta)(OH_2)$. Apparently, its oxidation becomes more difficult than in the pH 7-10 region because the monomer would be more easily oxidized with removal of a proton from coordinated H_2O; i.e., the more strongly σ-donating OH^- is formed, stabilizing the higher oxidation state. The oxidative wave should therefore be shifted to a less positive potential. This may be why peak IV overlaps peak V in the acidic range.

The slope of line displaying pH dependence of peak IX is -110 mV per pH unit, which is very close to 120 mV/pH required by a $1e^-/2H^+$ reaction. This wave was assigned to the reaction $(edta)_2Ru_2^{III,IV} \rightarrow (edta)_2Ru_2^{III}$ or $Ru^{III}(edta)(OH_2)$. Because the dimer $(edta)_2Ru_2^{III,IV}$ has no aqua ligand, and the monomer exists in the form of $Ru^{III}(edta)(OH_2)$ in the acidic range, we can write the following

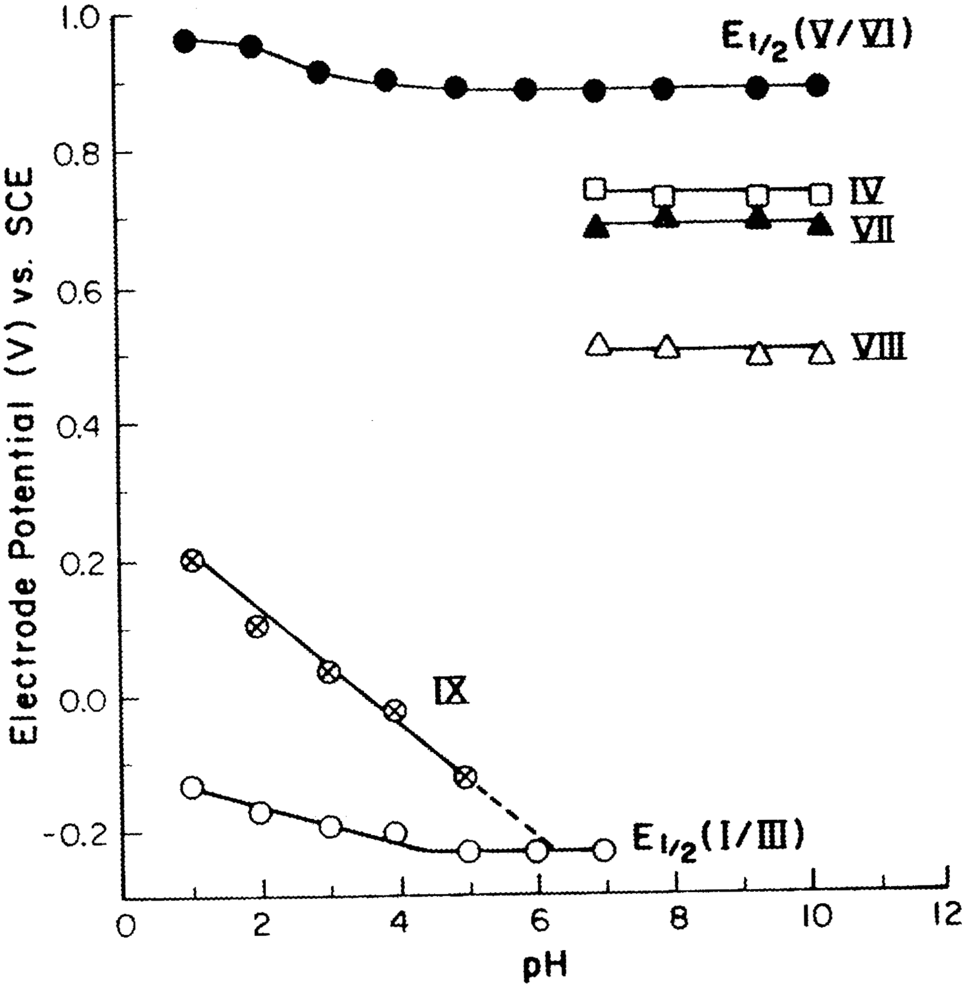

Figure 3.22. Relationship between peak or midpoint reduction potentials and pH; the lines are marked by the corresponding peak numbers.

to explain the relation between potential and pH. At pH 5, peak IX has shifted to the point where it appears as a weak shoulder superimposed upon a background of increasing charge. When pH = 6, the peak overlaps peak I. From pH 1 to 4, the small change in potentials with acidity observed for the $Ru^{III}(edta)(OH_2)/Ru^{II}(edta)(OH_2)$ couple can be assigned to gradual deprotonation of the single uncoordinated carboxylate group of the edta ligand. From pH 4 to 7, the potentials do not change with pH, and the half reaction can be assigned to

$$Ru^{III}(edta)(OH_2) + e^- \rightarrow Ru^{II}(edta)(OH_2)$$

3.2.5 Decomposion of the dimeric complex ion $(edta)_2Ru_2^{IV}$

(1) Decay of $(edta)_2Ru_2^{IV}$

Addition of a stoichiometric excess of strong oxidant, i.e., with $E^o > 1.0$ V vs. SCE, caused immediate conversion from $Ru^{III}(edta)(OH_2)$ or $(edta)_2Ru_2^{III,IV}$ ions to the dimer $(edta)_2Ru_2^{IV}$, which was identified by its characteristic absorption band at 428 nm. Upon standing, the excess oxidant was consumed, and the original spectrum of the $(edta)_2Ru_2^{III,IV}$ reappeared as identified by its characteristic absorption band at 393 nm. A typical spectral change with time is given in Figure 3.23. In the figure, the intensity of the absorption band at 428 nm decreases and eventually disappears while the intensity of the band at 393 nm increases with time.

Chemical oxidants used in this study included Ce^{4+}, Co^{3+}, and MnO_4^-. For all three oxidants, we obtained results very similar to those displayed in Figure 3.23 so long as oxidant was used in large excess. The ratio of oxidant to monomer $Ru^{III}(edta)(OH_2)$ or the dimer $(edta)_2Ru_2^{III,IV}$ required for detection of the absorption band at 428 nm

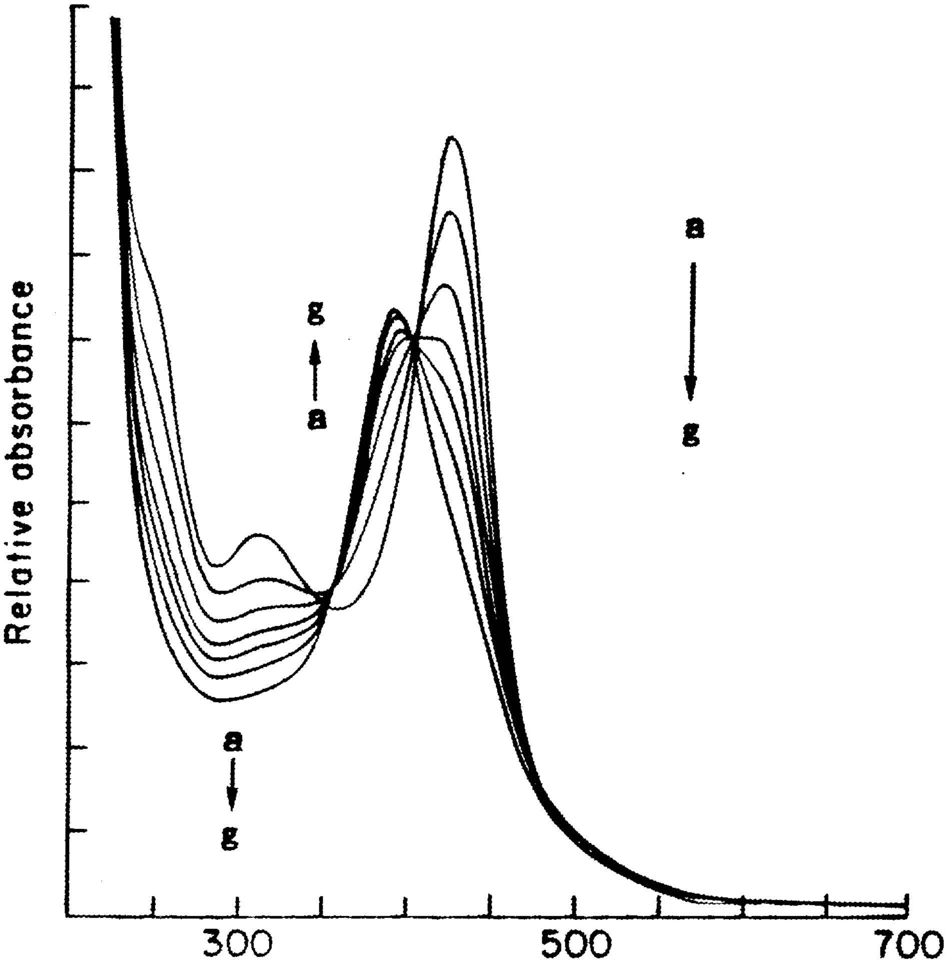

Figure 3.23. Decay of $(edta)_2Ru_2^{IV}$ ion following Co^{3+} oxidation of $(edta)_2Ru_2^{III,IV}$ ion. Conditions: Co^{3+}, 1.5 mM; $(edta)_2Ru_2^{III,IV}$, 0.25 mM; 0.34 M $HClO_4$; ambient temperature. Time interval after oxidation (a) 20 sec, (b) 3 min, (c) 6 min, (d) 9 min, (e) 12 min, (f) 15 min, (g) 21 min.

of the dimer $(edta)_2Ru_2^{IV}$ became larger as the solution pH increased. For example, using $KMnO_4$ as the oxidant, the absorption band at 428 nm could be observed at the oxidant/complex ratio of 4/1 when pH = 0, but the band could not be seen even at a ratio of 8/1 when pH = 3. For Ce^{4+}, we never detected the band at 428 nm at pH 5 (even in the ratio 50/1). Baar[10] reported that he obtained the result similar to the one depicted in Figure 3.23 at pH 5 with Ce^{4+} as the oxidant, although some uncertainty arose regarding actual conditions because the figure caption illustrating the effect in his thesis indicated that the solution was acidic (pH 1).

Whether or not the dimer $(edta)_2Ru_2^{IV}$ can be observed probably depends upon its relative formation and decay rates. Because the ratio of oxidants to the monomer at which $(edta)_2Ru_2^{IV}$ can be observed becomes increasingly larger with increasing pH, the ratio of the decay rate to the formation rate must increase. The redox potential or oxidizing ability of $KMnO_4$ decreases with increasing pH because H^+ ion appears as a reactant in the stoichiometric equation,

$$MnO_4^- + 5\ (edta)_2Ru_2^{III,IV} + 8\ H^+ = 5\ (edta)_2Ru_2^{IV} + Mn^{2+} + 4\ H_2O$$

We anticipate, therefore, that the $(edta)_2Ru_2^{IV}$ formation rate will decrease with increasing pH. Although the Ce^{4+} ion redox potential is nominally pH-independent, it is extensively hydrolyzed at higher pH in the absence of complexing agents. In acetate buffer at pH 5, we did not observe formation of hydrous oxide of Ce^{4+}. The ion may, therefore, have been extensively complexed to acetate. In either event, either deprotonation of coordinated H_2O or carboxylate ligation would be expected to lower the reduction potential of the Ce^{4+} ion and, therefore, to reduce its capacity to oxidize the $(edta)_2Ru_2{}^{III,IV}$ ion at pH 5.

Two possible explanations exist for the apparent reversion of $(edta)Ru_2{}^{IV}$ to the spectrum of the $(edta)_2Ru_2{}^{III,IV}$. One originally proposed by Baar and Anson[9,10] is that $(edta)_2Ru_2{}^{IV}$ oxidized solvent, H_2O. They argued that since the spectrum of $(edta)_2Ru^{III,IV}$ reappeared after all of the oxidant was consumed, there must have been some species in the solution that was oxidized. The added Ce^{4+} did not appear to destroy the edta complex to any great extent, so the only remaining oxidizable species was water. They further investigated the possibility of oxidation of water to dioxygen using a Clark oxygen probe as a detector and observed a positive response upon addition of Ce^{4+}. Therefore it was understandable that they concluded that the dimer $(edta)_2Ru_2{}^{IV}$ or the complex in a more highly oxidized state was able to catalyze water oxidation. An alternative explanation is that the dimer, $(edta)_2Ru_2{}^{IV}$ is unstable and oxidizes its ligand, edta, within the complex. This explanation requires that the product ion have an absorption spectrum similar to that of $(edta)_2Ru_2{}^{III,IV}$.

Upon careful analysis, it became evident that the apparent reversion to $(edta)_2Ru_2{}^{III,IV}$ was not quantitative; i.e., some bleaching was found, which was particularly evident at longer electrolysis times or when large concentration excesses of oxidant were used. Semiquantitative estimates of the bleaching stoichiometry were made by sequentially adding five-fold concentration excesses of Ce^{4+} ion, with sufficient time being given between additions for the equilibration of system. After the first addition, the final spectrum gave an absorbance at 394 nm that was identical with the value expected for the simple dilution of the $(edta)_2Ru_2^{III,IV}$ ion, but deviations from quantitative recovery appeared and became progressively greater with subsequent additions, so that by the fourth cycle, 22% of the complex absorption intensity had been lost. At this point, the apparent redox stoichiometry corresponded to 91 Ce^{4+} ions reduced/dimer bleached.

(2) Identification of gaseous products of reactions of the complex ions $(edta)_2Ru_2^{III,IV}$ or $Ru^{III}(edta)(OH_2)$ in the presence of excess oxidant or during constant potential electrolysis (CPE)

These alternative interpretations regarding catalytic capabilities of the $(edta)_2Ru_2^{IV}$ ion can be easily distinguished by positive identification of gases formed in the reaction. If the complex ion is a catalyst for water oxidation, O_2 will form; if the complex ion is decomposing, CO_2 is expected to be formed among the gases.[72]

The gaseous products formed upon reduction of the $(edta)_2Ru_2^{IV}$ ion were analyzed by several techniques, including the Clark oxygen electrode, gas chromatography, and mass spectroscopy.

According to the manufacturer's manual, the Clark probe responds only to oxygen, chlorine, nitrous oxide, and nitric oxide (see Table 2.1). The response to CO_2 is reported to be 1% that of O_2. When the polarization potential (PP) vs. internal reference Ag/AgCl electrode is -0.8 V, from our own data (Figure 3.24) we can see that the response of the probe to O_2 is almost independent of applied potential over the range of -0.6 to -0.8 V and the response to CO_2 is very weak at PP > -0.7 V but rises abruptly beyond -0.7 V and is comparable to the response to the air at PP -0.8 V. Therefore, at PP ≈ -0.8 V, the Clark

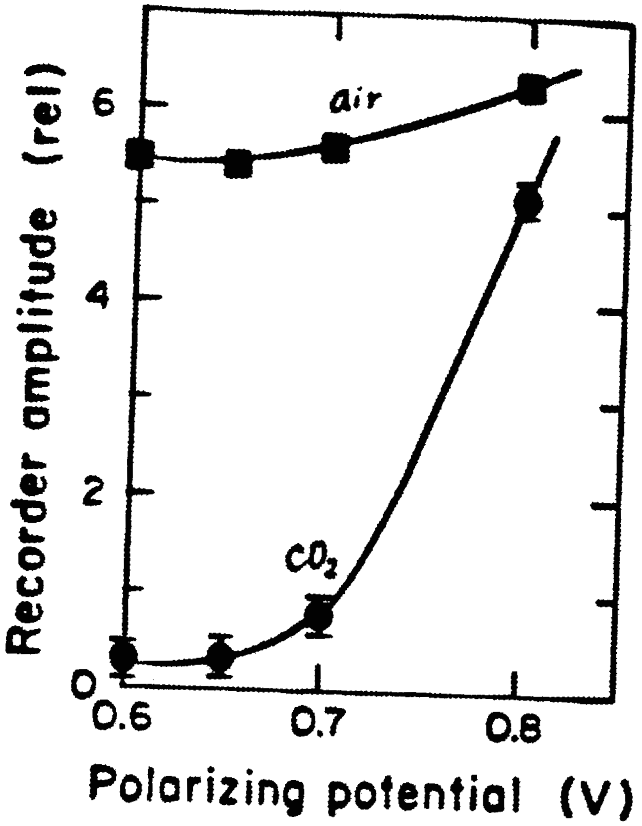

Figure 3.24. Response of Clark electrode to air and CO_2 at various potentials. Gas (1 mL) was injected into 10 mL headspace over 10 mL H_2O in a sealed vial. Comparable effects were observed when the gas was injected into a dry vial.

probe has a response to both CO_2 and O_2; at PP = -0.65 V, the probe only responds to O_2, not to CO_2. One possible reaction of CO_2 at the Clark electrode is:

$$CO_2 + 2\ e^- + 2\ H^+ \rightarrow CO + H_2O$$

The standard electrode potential for this reaction is -0.1 V vs. NHE (normal hydrogen electrode), while at pH 7 the potential becomes -0.52 V.[125] However, direct electroreduction of CO_2 has been reported to require at least -2 V vs. SCE.[126] Obviously, this reaction cannot occur at the Clark electrode poised at -0.8 V vs. Ag/AgCl internal reference electrode. Another possible reaction is:

$$2\ H^+ + 2\ e^- \rightarrow H_2$$

The H^+ ion arises from the dissolving of CO_2 in the electrolyte solution (assuming the pH = 5 or 6) in the Clark electrode. The standard electrode potential of H^+/H_2 couple is 0 V, while at pH 5-6, the potential becomes -0.30 to -0.36 V vs. NHE (-0.50 to -0.56 V vs. Ag/AgCl electrode). If the hydrogen ion reduction at the Pt electrode in the Clark electrode is associated with a 100-200 mV overpotential, the observation is understandable that the Clark electrode responds to CO_2 at a poised potential of -0.8 V vs. Ag/AgCl electrode, but not at -0.65 V vs. Ag/AgCl.

Adding any of the oxidants, including Ce^{4+}, Co^{3+}, and MnO_4^-, in the acidic solution containing the monomer $Ru^{III}(edta)(OH_2)$ or the dimer $(edta)_2Ru_2^{III,IV}$ gave an immediate response from the probe located in the headspace of the reaction cell when poised at PP 0.8 V vs. its internal Ag/AgCl reference electrode (Figure 3.25). The reducible gas accumulated approximately in parallel with solution optical change, and

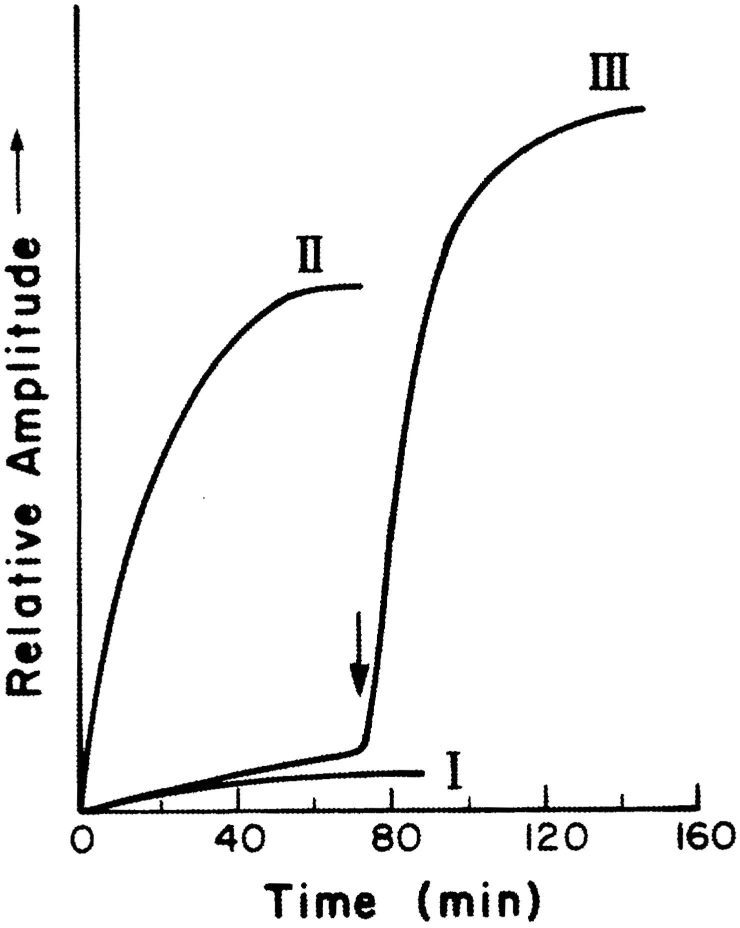

Figure 3.25. Clark Electrode response. Curve I: 7.0 μM monomeric ion, RuIII(edta)(OH_2), in 4 ml 0.2 M CF_3COOH/Na, pH 1.0, adding 70 μM $KMnO_4$, PP = 0.6 V. Curve II: The same conditions as curve I except PP = 0.8 V. Curve III: CPE curve. Conditions: 4 μM dimeric ion $(edta)_2Ru_2^{III,IV}$ in 25 ml 0.1 M phosphate, pH 12.0, applied potential 1.2 V vs. SCE, PP 0.8 V. The arrow indicates the point of acidification with $HClO_4$.

its evolution ceased when the $(edta)_2Ru_2^{IV}$ ion was depleted. No response was observed when the $(edta)_2Ru_2^{III,IV}$ was oxidized chemically or electrochemically in alkaline solution or under any conditions when the electrode was poised at PP 0.6 V (Figure 3.25). However, acidifying the alkaline solution following oxidation-reduction cycling, i.e., after the redox processes were completed, gave immediate response from the electrode (Figure 3.25) if poised at PP 0.8 V, but no response at PP 0.6 V. Since the electrode responds to both O_2 and CO_2 when poised at PP 0.8 V, but only to O_2 at PP 0.6 V, the results obtained indicate that the gaseous product cannot be O_2, but is most likely CO_2.

To further identify the gaseous product, headspace gases from spent reactions were analyzed with a gas chromatograph. In all cases examined, including both acidic and basic media, O_2 could not be detected beyond small amounts attributable to contamination with air during injection, i.e., appearing in a N_2/O_2 ratio of 4/1. These results infer that CO_2, rather than O_2, was the gas formed during $(edta)_2Ru_2^{IV}$ ion reduction.

This suggestion was confirmed for the acidic reactions with strong oxidants by collection and mass spectrometric analysis of condensable product gases (Figure 3.26). The strong peak at 44 amu originates from CO_2. The small amount of O_2 detected in the mass spectrum is attributable to the N_2/O_2 ratio to background air in the instrument.

The amount of CO_2 formed by the $(edta)_2Ru_2^{III,IV}$ reaction with various oxidants and by reaction at a platinum anode under diverse experimental conditions was determined with the Clark electrode using calibration curves constructed by injecting known amounts of CO_2 under

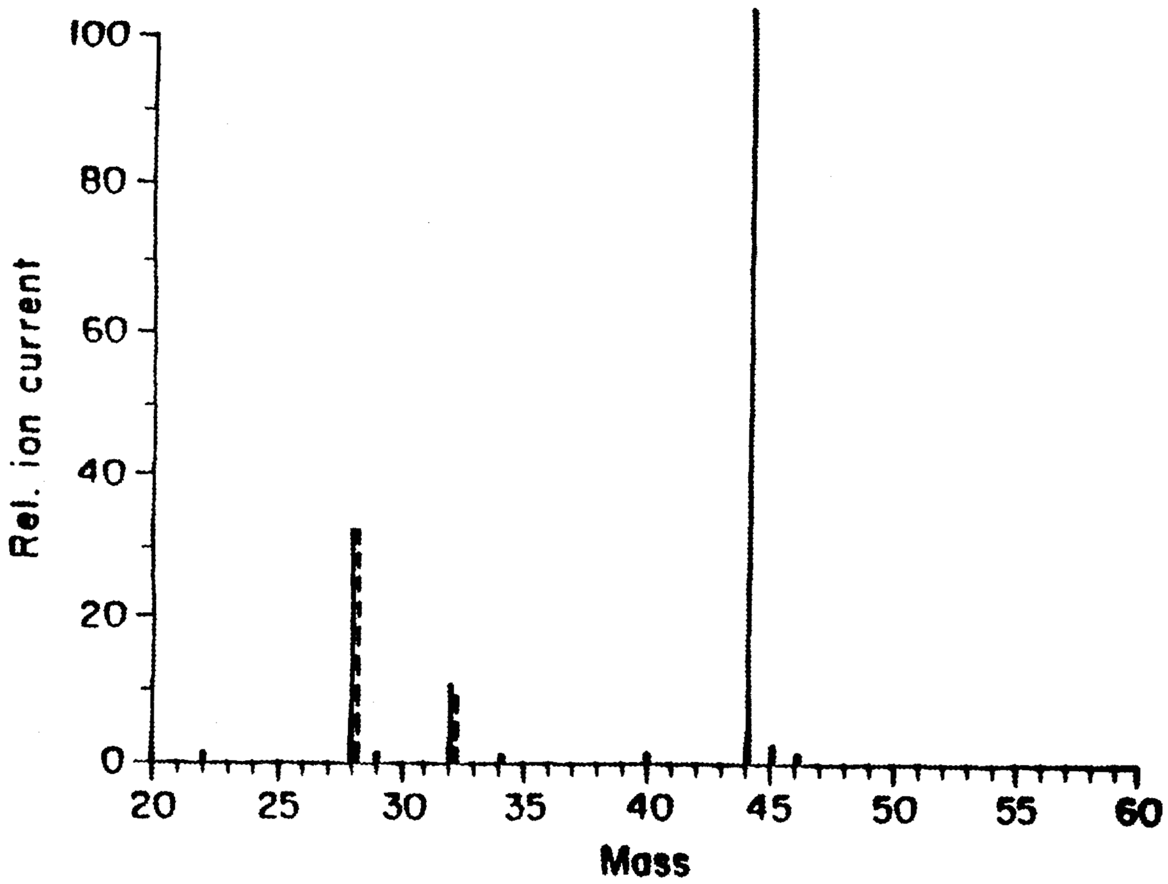

Figure 3.26. Mass spectra of headspace gases following MnO_4^- oxidation of $(edta)_2Ru_2^{III,IV}$. Conditions: $[MnO_4^-] = 13$ mM; $[(edta)_2Ru_2^{III,IV}] =$ 0.5 mM, pH 1 ($HClO_4$). Dashed line gives relative intensities of background scaled to N_2.

equivalent experimental conditions. The results are summarized in the Table 3.2. Evidence for O_2 formation was sought under all experimental conditions for which data are reported by using the Clark probe poised at 0.6 V. However, a positive response beyond the small deflection attributable to CO_2 was never observed at this potential, however.

3.2.6 Nature of the ligand bridge

Molecular vibrational spectroscopy, including infrared and Raman spectroscopies, is well established as a technique of general usefulness in structural investigations of oxometal complexes.[110,114-117,127,128] Earlier articles have discussed two kinds of bonding schemes, mono- and di-oxo bridging systems, and the effects they should have on the infrared and Raman spectra.[116-118] For mono-oxo bridged metal dimers, the group M-O-M is generally treated as a three-body system.[116,118] Such a system should have three normal modes, including asymmetric, ν_{as}(M-O-M), and symmetric, ν_s(M-O-M), stretching modes and a bending, δ(M-O-M), mode. In general, only the first two modes are treated by theory so that such a system can be characterized by a two-constant force field, i.e., the metal-oxygen stretch, k, and the cross-oxygen (M-O-M) stretch-stretch interaction, k_i. We list symmetry class, vibration class, spectral activity, and secular equations in Table 3.3.

As seen in the table, for a linear system the symmetric mode is Raman active, whereas the asymmetric mode is infrared active. For bent systems both modes are infrared and Raman active. The asymmetric M-O-M stretching vibration must have a higher frequency than the symmetric one in both the linear and bent systems for any reasonable values of k and k_i. Even if k and k_i are the same in a bent system as in a linear one,

Table 3.2. CO_2 Yields From reactions of $[Ru(Hedta)]_2O$ With Strong Oxidants[a]

Oxidant (μeq)	Dimer (μmol)	pH[b]	CO_2 (μmol)	Oxidant/CO_2
Ce^{4+}, 8-25	1.0	1.0	4-10	2.1-2.5[c]
Ce^{4+}, 50	1.0	1.0	10	5.0
MnO_4^-, 45-80	2.0	1.0	16-21	5.0
Co^{3+}, 16-51	0.3-1.8	0.4 ($HClO_4$)	7-26	2.0-3.2
$Ru(bpy)_3^{3+}$, 12	1.2	4.4 (1 M acetate)	4.5	2.7
Pt anode,[d] 5.5-46	5.0	7-11 (0.1 M PO_4)[e]	3-22	2-9[f]

---

[a] Excepting CPE experiments, reaction was initiated by anaerobic addition of oxidant to the dimer in 4 mL total volume at ambient temperature.

[b] Trifluoracetic acid, unless otherwise indicated

[c] Ratios increased monotonically with increasing oxidant concentration

[d] Poised at 0.45 V vs. $Hg/HgSO_4$ (0.85 V vs. SCE)

[e] At pH 13, copious evolution of CO_2 occurred, but solvent oxidation may have caused a large overestimate of current passed.

[f] Ratio increased with decreasing pH.

Table 3.3. Symmetry Analysis and Secular Equations of Metal-Oxygen Stretching Modes in the μ-oxo Dimeric Complexes[a]

M-O-M Geometry	M-O-M Skeletal Symmetry	Symmetry Species	Activity[b]	Secular Equations[c]
Linear	$D\ \infty$		R	$\lambda = \mu_M(k + k_i)$
			IR	$\lambda = (\mu_M + 2\mu_O)(k - k_i)$
Bent	C_{2v}	A_1	IR, R	$\lambda = [\mu_M + \mu_O(1 + \cos \phi)](k + k_i)$
	B_1	IR, R		$\lambda = [\mu_M + \mu_O(1 - \cos \phi)](k - k_i)$

[a] Abstracted from reference 116.

[b] R = Raman active; IR = infrared active.

[c] $\lambda = (5.889 \times 10^{-7})\nu^2$, where ν is the frequency in wavenumbers, μ_M and μ_O are reciprocals of the masses of the metal atom and the oxygen atom, respectively, in amu, k and k_i are force constants in mdynes/Å, and ϕ is the M-O-M angle.

the antisymmetric mode would have a higher frequency, by a factor of approximately $[(1-\cos \phi)/2]^{1/2}$ (ϕ is the M-O-M angle), in the bent system. Moreover, the extensive metal-oxygen bonding which is possible in a linear system[118] must be less extensive in the bent system, i.e., k(bent system) < k(linear system). This is an additional reason to expect that the antisymmetric mode of a linear system will occur at a higher frequency than any other of the M-O stretching modes in either type of the M-O-M groups. On the other hand, the symmetric mode for the linear system has lower frequency than that for the bent system. Wing and Callahan[116] calculated the change in vibrational frequency of bridge modes as a function of M-O-M angle (Figure 3.27). For the calculations the mass of the metal was taken as that of molybdenum, M-O stretching force constant was set at 3.8 mdyn/Å, and interaction constant was assumed to be 0.2 mdyn/Å.

For linear M-O-M species, the asymmetric stretch mode is found in the range of 800 to 900 cm^{-1}, and the symmetric stretch around 300 cm^{-1}.[115] Bending of the M-O-M linkage results in a lowering of the antisymmetric stretching frequencies to the 700- to 800-cm^{-1} range, and an increase of symmetric stretching frequencies to the 350- to 550-cm^{-1} range.[127,128]

To fit these data, the δ(M-O-M) mode is calculated to lie below 200 cm^{-1}; however, a vibrational band that is sensitive to isotopic substitution in the bridge is often observed at frequencies close to 300 cm^{-1}. For this reason, it has been suggested[124] that the δ(M-O-M) mode is coupled to other ligand vibrations in the molecule, most prominent is the stretching motion of ligand atom trans to the μ-oxo bridge.

Recent studies[9,10] have eliminated from consideration many of the diverse types of ligand bridge proposed earlier for the $(edta)_2Ru_2^{III,IV}$ ion; these data are consistent with only formulations of μ-oxo or dihydroxy-bridged structures. Our RR results now establish that the bridge is a μ-oxo ion.

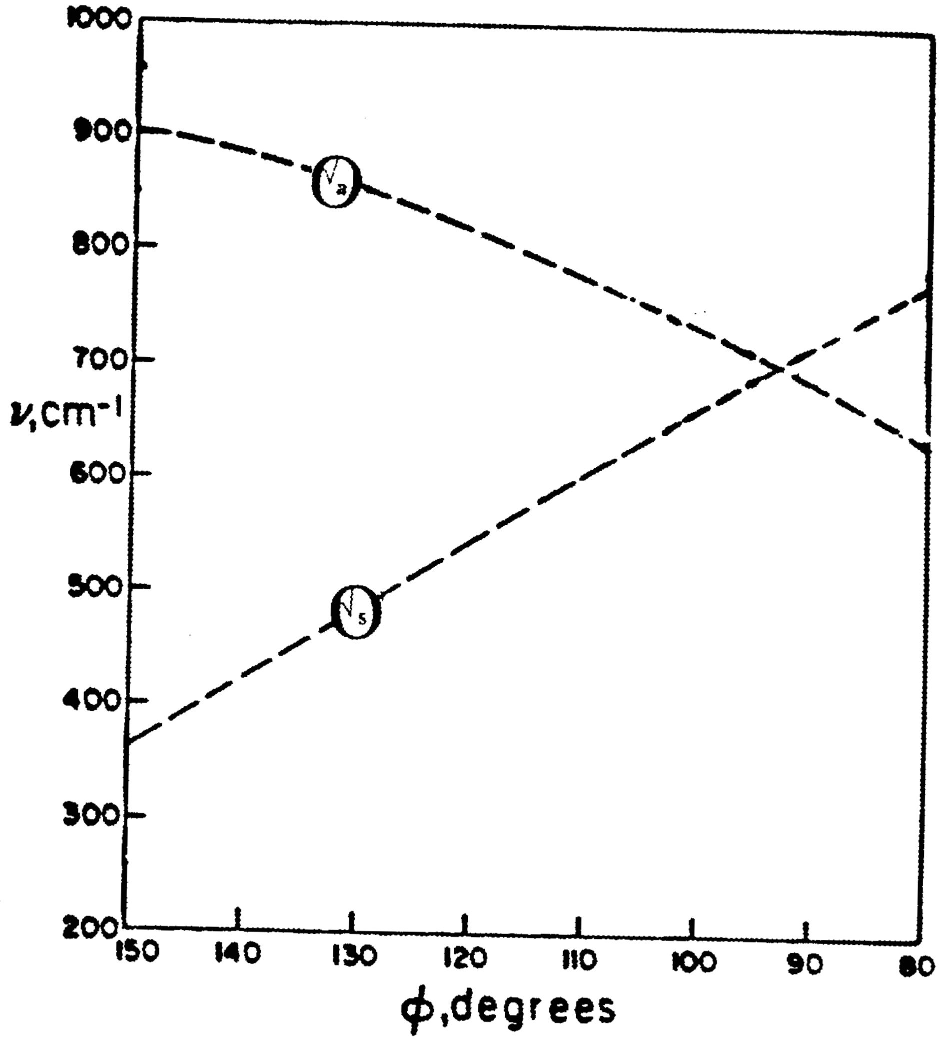

Figure 3.27. Variation in metal-oxygen bridge vibrations as a function of the M-O-M angle. When M = Mo, k_b = 3.8 mdyn/Å, k_i = 0.2 mdyn/Å.; ν_s and ν_a are symmetric and asymmetric stretching vibration frequencies (abstracted from reference 116).

The $(edta)_2Ru_2^{III,IV}$ ion in acidic and weak alkaline media displays two RR bands, at 434 and 324 cm^{-1} (Figure 3.8), that are sensitive to ^{18}O substitution in the bridge; their positions and relative intensities are analogous to results from model studies, which support their assignment to the ν_s(Ru-O-Ru) and ligand-mixed δ(Ru-O-Ru) modes, respectively. The ν_{as}(Ru-O-Ru) mode was not observed. The small magnitude of the isotopic shifts, $\Delta\nu = 1\text{-}2\ cm^{-1}$, and the virtual absence of a deuterium isotope effect (Figure 3.8) establish that the bands at 434 and 324 cm^{-1} are not attributable to metal-aquo ligand stretching motions and that the bridging oxo atom is deprotonated. The barely detectable shift to higher frequencies of ν_s in D_2O may be attributable to H-bonding to solvent; very similar effects observed in metalloproteins containing binuclear Fe-O-Fe centers have been attributed to internal hydrogen bonding to the μ-oxo atom.[124] Therefore, the cumulative data from this and earlier studies are consistent only with a simple μ-oxo monobridged structure. From the magnitude of the ^{18}O-induced shift in ν_s, a Ru-O-Ru angle of 165° is estimated for the $(edta)_2Ru_2^{III,IV}$ μ-oxo dimer using the following method:[116]

for a bent M-O-M segment the secular equations (Table 3.3) for symmetric and asymmetric stretching vibrational modes are:

$$\lambda = [\mu_M + \mu_O(1 + \cos\phi)](k + k_i) \text{ and}$$

$$\lambda = [\mu_M + \mu_O(1 - \cos\phi)](k - k_i)$$

We also know:

$$\lambda = (5.889 \times 10^{-7})\nu^2$$

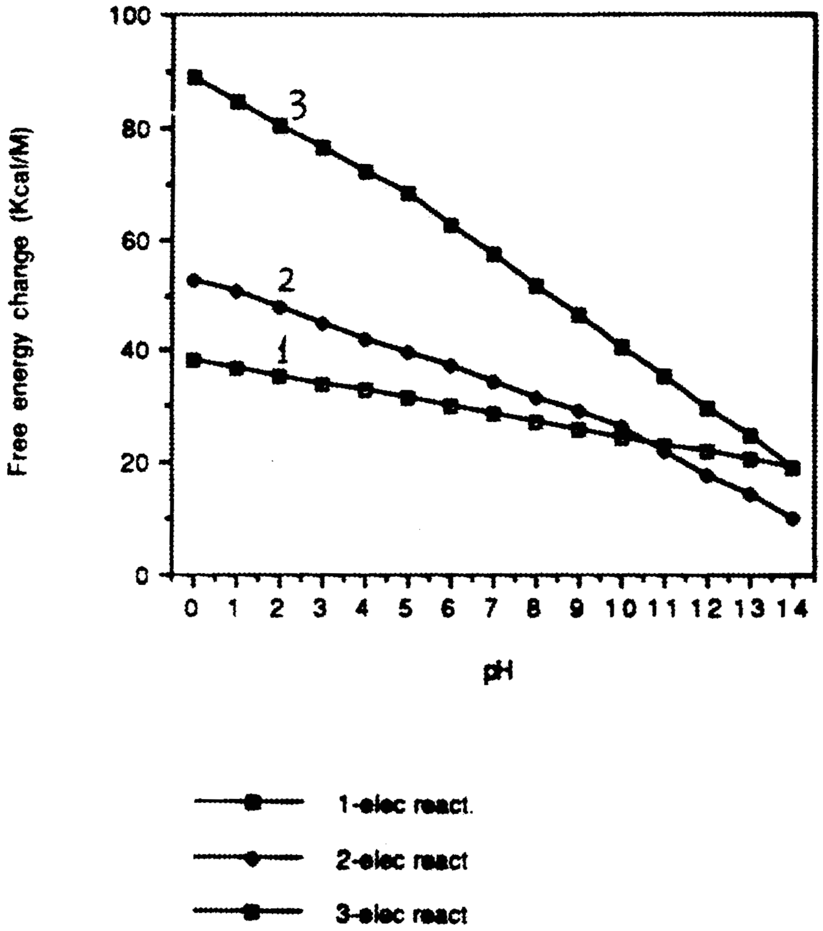

Figure 3.28. Relationship between pH and standard free-energy changes of 1-, 2-, and 3-electron oxidation of H_2O by $(edta)_2Ru_2^{IV}$ ion. Line 1, 1-electron reaction: $(edta)_2Ru_2^{IV} = H_2O \rightleftharpoons (edta)_2Ru_2^{III,IV} + OH + H^+$; line 2 (break point corresponds to pK_a of H_2O_2), 2-electron reaction: $(edta)_2Ru_2^{IV} + 2H_2O \rightleftharpoons (edta)_2Ru_2^{III} + H_2O_2 + 2H^+$; line 3 (break point corresponds to pK_a of HO_2), 3-electron reaction: $(edta)_2Ru_2^{IV} + 2H_2O \rightleftharpoons (edta)_2Ru_2^{III,II} + HO_2 + 3H^+$.

So, we obtain the following equations

for symmetric mode

$$\cos \phi = \frac{(\nu_s^{2} - \nu_s^{*2})\, \mu_M}{\nu_s^{*2} \mu_O - \nu_s^{2} \mu_O^{*}} - 1$$

for asymmetric mode

$$\cos \phi = 1 - \frac{(\nu_{as}^{2} - \nu_{as}^{*2})\, \mu_M}{\nu_{as}^{*2} \mu_O - \nu_{as}^{2} \mu_O^{*}}$$

where ν_s and ν_s^* are symmetric vibration frequencies for ^{16}O and ^{18}O as bridging ligands, respectively; μ_M, μ_O and μ_O* are reciprocals of the masses of the metal atom, ^{16}O and ^{18}O, respectively. Substituting these known values into either equation, we can obtain the angle ϕ.

3.2.7 Other ligands

None of the bands in the RR spectrum of the $(edta)_2Ru_2^{III,IV}$ μ-oxo ion are attributable to coordinated water. The difference in the zero-point vibrational energies upon substitution of ^2H and ^{18}O would lower the energies of simple R-O stretching motions by 9 and 17 cm^{-1}, respectively, which is far greater than any observed isotope-induced shift (Figure 3.8). We were also unable to identify by this method the Ru-O stretching vibration of H_2O in $(bpy)_2(OH_2)Ru^{III}ORu^{III}(OH_2)(bpy)_2$ (Chapter 4), a μ-oxo ion whose structure has been established by X-ray crystallography.[8] Therefore, one can draw no conclusions from these measurements concerning the presence or absence of coordinated water in the $(edta)_2Ru_2^{III,IV}$ μ-oxo ion. However, pH measurements[26] have indicated the absence of titratable protons in the pH 2-10 region for the dimer, whereas $Ru^{III}(edta)(OH_2)$ exhibits a loss of a single proton with $pK_a = 7.6$.[31] Thus, although not definitive, the RR results are consistent with titrimetric data. On the basis of these observations, the dimeric ion can be identified as $[\mathrm{Ru(edta)}]_2\mathrm{O}^{-1}$ (in an acidic solution), with the ligand environment of each ruthenium presumably including pentacoordinate edta and the μ-oxo atom.

Apart from a small increase above pH 2 attributable to protonation of pendant carboxylate groups,[31] the half-wave potential for one-electron oxidation is pH independent over the range pH 1-10 (Figure 3.22). This result indicates that the initially formed $(\mathrm{edta})_2\mathrm{Ru}_2{}^{\mathrm{IV}}$ μ-oxo ion also possesses no bound H_2O, since coordination would undoubtedly occur with the release of protons in this pH region, e.g.,

$$2\mathrm{H_2O} + [\mathrm{Ru(edta)}]_2\mathrm{O}^{2-} \rightleftharpoons [\mathrm{Ru(edta)(OH)}]_2\mathrm{O}^{4-} + 2\mathrm{H}^+$$

Primary-sphere solvation should therefore give rise to half-wave potentials that increase with solution pH, contrary to the observed pH-independent behavior. The additional reduction waves at 712 and 539 mV in the cyclic voltammograms above pH 6 have several possible origins. They were attributed to electrode adsorption phenomena,[9,10] but have anodic half-waves that suggest quasi-reversible processes. Alternatively, they might represent species that have undergone aquation at one or more edta ligation sites. This notion is consistent with their lower reduction potentials since hydroxo ligands formed by deprotonation should preferentially stabilize the higher oxidation state.[119] A third possibility is that these species are products of $(\mathrm{edta})_2\mathrm{Ru}_2{}^{\mathrm{IV}}$ ion decomposition since it is apparent that the complex in the (IV,IV) oxidation state is unstable with respect to CO_2 evolution (Table 3.2). This latter circumstance does not exclude aquation since degradation of the ligand will ultimately be accompanied by loss of edta binding sites. The short lives of these intermediary ions, which are less than the voltammetric sweep times, compromise attempts to identify them.

In alkaline solution, pH >11, the RR spectrum of the $(\mathrm{edta})_2\mathrm{Ru}_2{}^{\mathrm{III,IV}}$ μ-oxo ion becomes more complex and is dominated by three bands in the low frequency region, each of which undergoes small shifts to lower energies when $[^{18}\mathrm{O}]$-$\mathrm{H}_2\mathrm{O}$ is coordinated in the precursor $\mathrm{Ru}^{\mathrm{III}}(\mathrm{edta})(\mathrm{OH}_2)$ ion (Figure 3.9). If ligation were restricted solely to edta and the μ-oxo atom, this result would imply the existence of at least two discrete species. However, more dramatic frequency shifts are found in $\mathrm{D}_2\mathrm{O}$ (Figure 3.9). The magnitudes of shifts in the 372- and 337-cm^{-1} bands, $\Delta\nu$ = 10-14 cm^{-1}, are sufficiently large that these bands might be assigned to Ru-O stretching motions of coordinated hydroxide ion, were it not for much smaller shifts accompanying substitution of the heavier oxygen isotope. (Since the isotopically substituted dimers were prepared in the $\mathrm{H}_2{}^{18}\mathrm{O}$-enriched solvent, hydroxide substitution upon alkalinization would lead to incorporation of $^{18}\mathrm{O}$ in these position as well.) On the basis of spectroscopic and titrimetric data indicating reversible uptake of one OH^- per dimer, Baar and Anson[9] have proposed formation of a mixed-dibridged structure comprising one oxo and one hydroxo ligand which is governed by an equilibrium $\mathrm{p}K_a$ of 10.3. It is not apparent that the vibrational properties of this ion can solve the dilemma posed by larger isotope shifts arising from deuterium than from $^{18}\mathrm{O}$ substitution. Several additional observations suggest that the structural properties of the dimeric ion in the alkaline solution are more complicated. These include the differential temperature dependence for rhombic EPR signals of the alkaline ions and temporal changes in both their EPR and optical properties described in section 3.2. It should also be noted that our alkaline EPR spectra are very similar to spectra previously reported by Baar,[10] although major differences exist in the reported EPR spectra of the μ-oxo dimer under more acidic conditions. From these data, it appears that multiple dimeric species can exist in alkaline solution, and the prospect exists that some of these might be formed by solvent substitution at edta-binding sites.

3.2.8 Catalysis vs. ligand decomposition

The one-electron reduction potential of the $(edta)Ru_2^{IV}$, approximately 0.9 mV, is clearly insufficient to drive one-electron oxidation of water, for which $E_7^{o\prime}(OH/)H_2O) = 2.16$ V relative to SCE.[66] The potentials for two- or three-electron reduction to $(edta)_2Ru_2^{III,III}$ and $(edta)_2Ru_2^{III,II}$, respectively, can be estimated from the midpoint potentials determined by Baar and Anson[9,10] as follows:

From their potentials, i.e.,

$$(edta)_2Ru_2^{IV} + e^- \rightarrow (edta)_2Ru_2^{III,IV} \qquad E_m = 0.89\ V^{9}$$

$$(edta)_2Ru_2^{III,IV} + e^- \rightarrow (edta)_2Ru_2^{III} \qquad E_m = -0.13\ V^{9,10}$$

$$(edta)_2Ru_2^{III} + e^- \rightarrow (edta)_2Ru_2^{III,II} \qquad E_m = -0.33\ V^{10}$$

the values for the couple, $(edta)_2Ru_2^{IV}/(edta)_2Ru_2^{III}$, are $E_7^{o\prime} = (0.89 - 0.13)/2 = 0.38$ V, and for the couple, $(edta)Ru_2^{IV}/(edta)_2Ru_2^{III,II}$, $E_7^{o\prime} = (0.89 - 0.13 - 0.33)/3 = 0.14$ V.

The latter value is relatively uncertain because the $(edta)_2Ru_2^{III}$ ion is highly unstable and correspondence of its reduction wave to a one-electron process has not been firmly established. Nonetheless, the formal potentials[66] for two- and three-electron reduction of H_2O_2 and O_2^- are $E_7^{o\prime}(H_2O_2/H_2O) = 1.08$ V and $E_7^{o\prime}(O^-/H_2O) = 0.96$ V, again indicating energetically highly unfavorable water oxidation pathways. The driving force for four-electron oxidation cannot be calculated because the $[(edta)_2Ru_2^{III,II}]/[(edta)_2Ru_2^{II,II}]$ potential is unknown, but even with the $(edta)_2Ru_2^{III,III}/(edta)_2Ru_2^{III,II}$ potential taken as an upper limit, it is still unfavorable by 0.5 V. The stoichiometric equations for water oxidation by the dimer generally involve proton release; consequently, the energetics for these reactions become more favorable in alkaline solution. Nonetheless, even at pH 12, the thermodynamic barrier remains greater than 0.4 V for each of these reactions. It is clear, then, that the $(edta)_2Ru_2^{IV}$ ion is thermodynamically incapable of oxidizing water. To further show that the complex cannot be a catalyst for water oxidation, I calculate the standard free energy changes, ΔG^o, for the following 1-, 2-, and 3-electron reactions:

$$(edta)_2Ru_2^{IV} + H_2O \rightarrow (edta)_2Ru_2^{III,IV} + OH + H^+ \qquad \Delta G_1^o$$

$$(edta)_2Ru_2^{IV} + 2H_2O \rightarrow (edta)_2Ru_2^{III,III} + H_2O_2 + 2\,H^+ \qquad \Delta G_2^o$$

When pH >10, the reaction becomes

$$(edta)_2Ru_2^{IV} + 2H_2O \rightarrow (edta)_2Ru_2^{III,III} + HO_2^- + 3H^+$$

because the pK_a of H_2O_2 is ~10.

$$(edta)_2Ru_2^{IV} + 2H_2O \rightarrow (edta)_2Ru_2^{III,II} + HO_2 + 3H^+ \qquad \Delta G_3^o$$

When pH >5, the reaction becomes

$$(edta)_2Ru_2^{IV} + 2H_2O \rightarrow (edta)_2Ru_2^{III,II} + O_2^- + 4H^+$$

because the pK_a of HO_2 is ~5 based upon the equation

$$G^o = -nF\ \Delta E$$

where n = the number of electrons of the redox reaction, F = Faraday constant and ΔE = the potential difference between two corresponding half reactions. The ΔG^o obtained are plotted as a function of pH (Figure 3.28). From the figure we can see that all ΔG^o are positive, which indicates that all the above reactions are not spontaneous thermodynamically. Break points of lines 2 and 3 correspond to pK_a's of H_2O_2 and HO_2.

Baar and Anson have suggested that O_2 formation might occur by disproportionation of $(edta)_2Ru_2^{IV}$ ion to give a more highly oxidized and reactive complex in low yield.[9] One possible mechanism for rendering accessible high oxidation states of the dimer is partial aquation of the initially formed $(edta)_2Ru_2^{IV}$. Aquation might also introduce new catalytic pathways by allowing coordinative stabilization of intermediary species formed upon oxidation of ligated water. These possibilities cannot be assessed because relevant thermodynamic data are unavailable. This discussion is hypothetical, however, since we have been unable to detect O_2 formation, even in a highly alkaline media where OH^- ligation and energetics of water oxidation are less demanding. In fact, in CPE experiments, CO_2 evolution rates were greater under more alkaline conditions.

Edta itself is susceptible to oxidation by strong oxidants,[34] and coordination complexes containing certain redox metal ions undergo photodegradation upon illumination of their CT bands to yield CO_2.[67,68] In addition, there are a few examples in which edta acts a chemical reductant. For example, the Mn^{III}(edta) complex can be prepared by reacting MnO_2 with excess edta.[69,70] The edta oxidation products in this reaction were not characterized. Ogino and coworkers[71] have reported that the Mn^{III}(edta) complex decomposes to Mn^{II}, ethylenediamine-N,N',N'-triacetic acid, and ethylenediamine-N,N'-diacetic acid. Very recently, Easom and Bose[72] have studied the reaction of bis-(2-hydroxy-2-ethylbutyrato)oxochromate(V) with edta. They found that the reaction products were CO_2, Cr^{III}(edta), and Cr^{III}(edtri) (edtri = ethylenediamine N,N,N'-triacetic acid) and proposed the following stoichiometric redox equation based on the quantitation relation of the products:

$$3\ Cr^{V} + \text{edta} = 3\ Cr^{III} + \text{edtri} + 2\ CO_2 \qquad (3.1)$$

The mechanism proposed based upon a kinetic study was slow substitution of edta upon Cr^{V} followed by rapid intramolecular electron transfer to form the Cr^{III} complexes. From Table 3.4, it can be seen that CR^{III} complexes with aminopolyacetic acid ligands of similar structure possess very similar absorption properties, including both absorption maxima (nm) and extinction coefficients.

Under the experimental conditions of this study, rapid evolution of CO_2 occurs upon addition of chemical oxidants to edta-containing solutions. The reaction stoichiometry for complete oxidation of edta can be written as

$$\begin{aligned} &34\ Ce^{4+} + 12\ H_2O + C_{10}H_{16}N_2O_8 = \\ &\quad 34\ Ce^{3+} + 10\ CO_2 + 2\ NH_4^{+} + 32\ H^{+} \end{aligned}$$

Therefore, up to 68 Ce^{4+}/dimer may be required for oxidative bleaching of the complex, assuming there is no change in the metal oxidation state.

Table 3.4. Absorption Maxima (nm) and Extinction Coefficients (M^{-1} cm^{-1}) for (Aminopolycarboxylato)chromium(III) Complexes in Aqueous Solution

Complex	$\lambda_1(\varepsilon)$	$\lambda_2(\varepsilon)$	Ref
Cr(edta)(H_2O)	534 (213)	392 (114)	73
	545 (200)	395 (104)	74
Cr(edtri)(H_2O)[a]	540 (133)	386 (105)	74
Cr(edda)($H_2O)_2$[b]	529 (77)	401 (47)	70
	527 (119)	392 (72)	70
Cr(edda)(acac)[b]	532 (65)	380 (168)	76
Cr(Hedta)[c]	538 (85)	387 (253)	76

[a] edtri = ethelenediamine-N,N,N'-triacetic acid.

[b] acac = 2,4-pentanedione; edda = ethylenediamine-N,N'-diacetic acid.

[c] Hedta = N-(hydroxyethyl)-ethylenediamine-N,N',N'-triacetic acid.

From the above discussion it is probable that acetoxy substituents are susceptible to oxidation. As previously described, addition of several-fold excess Ce^{4+} ion gave initially imperceptible net spectral changes following exhaustion of the oxidant, although CO_2 was evolved (as measured with the Clark electrode). Thus, the immediate reaction product gave an absorption spectrum very similar to the reactant $(edta)_2Ru_2^{III,IV}$ ion. This behavior is reminiscent of reaction 3.1 and suggests that the initial reaction involves preferential oxidation of the pendant carboxyl group. By analogy with reaction 3.1, the immediate reaction products would include CO_2 and ligated ethylenediaminetriacetate or N-methylethylenediaminetriacetate.[68] Because, in this instance, the initial product is still probably pentacoordinated through an N_2O_3 ligand set, its absorption spectrum, including absorption maxima and extinction coefficients, should be very similar to that of the reactant (see Table 3.4). If the two pendant acetoxy groups are initially oxidized, the initial products probably remain pentacoordinated through two N_2O_3 ligand sets and retain similar absorption spectra until twelve equivalents of Ce^{4+} are consumed. This behavior is in semiquantitative agreement with experimental results. Subsequent addition of Ce^{4+} ion may lead to the loss of ligand and spectral change, which would account for both the absence of spectroscopically detectable intermediates and decreasing Ce^{4+}/dimer bleaching stoichiometry that accompanies progressive oxidation of the complex. The theoretical limit (Table 3.2) for complete edta oxidation, i.e., oxidizing equivalents/dimer = 68, is probably not achievable because other fragmentary oxidation products, e.g., formic acid,[67] are resistant to further oxidation. In our experiments, the oxidant was always the limiting reagent. Under these conditions, the oxidant/CO_2 (Table 3.2) ratio was generally less than the value for complete edta oxidation, which is 3.4, which also supports the idea that CO_2 is first formed from more highly oxidized, i.e., carboxylate, ligand carbon atoms. Edta oxidation involves proton release so that the energetics for this reaction become increasingly favorable as pH increases. This might be the reason why the oxidant/CO_2 ratio decreases with increasing pH.

To summarize, the $(edta)_2Ru_2^{IV}$ ion appears incapable on thermodynamic grounds of catalyzing water oxidation, and other potentially catalytic complexes that might be derived from it are too unstable with respect to ligand oxidation to function effectively in this capacity.

CHAPTER 4

RUTHENIUM COMPLEXES WITH BIPYRIDINE AND ITS DERIVATIVES

4.1 INTRODUCTION

To search for the better catalysts for oxidizing water to oxygen, I synthesized the ligands 4,4′-dicarboxylic acid-2,2′-bipyridine, 4,4′-dicarbethoxy-2,2′-bipyridine, 4,4′-dimethoxy-2,2′-bipyridine, 5,5′-dicarboxylic acid-2,2′-bipyridine, and 5,5′-dicarbethoxy-2,2′-bipyridine and their monomeric and dimeric complexes of ruthenium; studied electron absorption spectra, vibrational spectra, and redox properties of these complexes; and performed a direct comparative study of their catalytic capabilities. Based upon these results, I will discuss possible mechanisms by which water is catalytically oxidized to oxygen.

4.2 RESULTS AND DISCUSSION

4.2.1 NMR spectra of bipyridine and its derivatives

The chemical shifts of bipyridine (bpy) and its derivatives are given in Table 4.1. My assignment of ^{1}H chemical shifts of 5,5′-dicarbethoxy-2,2′-bipyridine (5,5′-diester) differs somewhat from the previous assignment made by Grätzel and coworkers.[14] The structural formula of the compound is

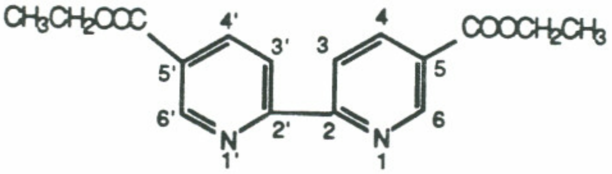

in which there are five kinds of protons, comprising H^3, H^4, H^6 pyridyl ring protons and the methyl and methylene protons of the ethyl ester group. There should be five corresponding bands in ^{1}H-NMR. From

Table 4.1. ^{1}H-NMR Chemical Shifts of Bipyridine and Its Derivatives

Group	$-CH_2$	$-CH_3$	H^3	H^4	H^5	H^6
H	–	–	8.41	7.82	7.32	8.69
4,4′-CH_3	–	2.44	8.22	–	7.14	8.54
5,5′-CH_3	–	2.39	8.22	7.62	–	8.49
4,4′-COOH	–	–	8.85	–	7.91	8.93
5,5′-COOH	–	–	8.45	8.58	–	9.20
4,4′-COOEt	4.45	1.42	8.88	–	7.99	8.95
5,5′-COOEt	4.44	1.42	8.45	8.59	–	9.31
4,4′-OCH_3	–	3.96	8.01	–	6.88	8.50

Figure 4.1, we can see that there are five peaks at 1.42, 4.44, 8.45, 8.59, and 9.31 ppm, respectively. The peaks at 1.42 and 4.44 ppm are triplet and quadruplet, respectively, which are easily assigned to $-CH_3$ and $-CH_2$ according to multiplicities and positions. The 9.31-ppm peak is only a singlet and at the lowest field so that it can be assigned to H^6. These are consistent with Grätzel's assignment. However, I believe that the peak at 8.45 should belong to H^3, whereas 8.59 is H^4, which is the opposite of the Grätzel's assignment. The proton at the 4-position is ortho to a carboxylate group which is very strong electron-withdrawing and para to the nitrogen atom which is also electron-withdrawing (see Figure 4.1), whereas the proton at the 3-position is meta to both the carboxylate group and nitrogen atom. So, the electron density of the proton at the 4-position should be lower than that of the

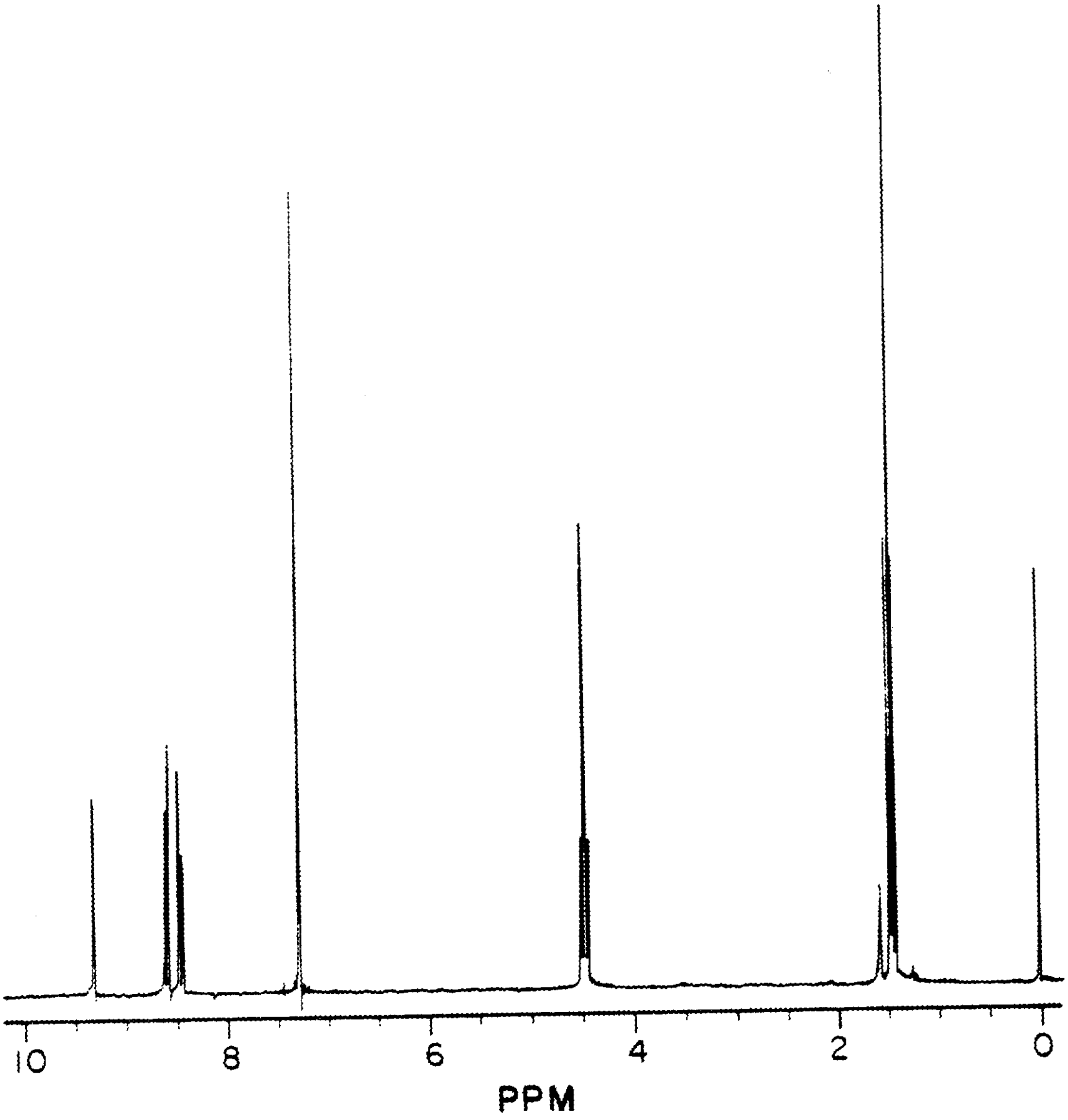

Figure 4.1. ^{1}H-NMR spectrum of 5,5′-dicarbethoxy-2,2′-bipyridine, $CDCl_3$ as solvent, Me_4Si as internal standard.

proton at the 3-position, and the chemical shift due to the 4-proton should be correspondingly shifted to lower fied.

The chemical shift (2.44 ppm) of methyl protons 4,4'-dimethyl-2,2'-bipyridine is shifted to slightly low field than the corresponding methyl proton (2.39 ppm) of 5,5'-methyl-2,2'-bipyridine. This effect can be explained by hyperconjugation. The six-membered heterocycle of pyridine has the same six-electron bonding pattern as benzene and its delocalization and aromaticity are essentially the same as that of benzene. However, because the nitrogen atom in pyridine is more electronegative than the carbon atom, dipolar resonance structures of the type given below are more important, and the molecule has a dipole moment with its negative pole at nitrogen.

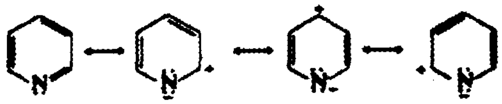

The electron densities at para and ortho carbon atoms are, therefore, lower than that of meta carbon atoms. Bipyridine has very similar dipolar resonance structures. Since the electron density on the 4-carbon is lower, the methyl proton is less shielded, and the resonance position is shifted to lower field.

The substituents on the bipyridine rings cause a regular progression of change in chemical shifts of ring protons. In general, electron-withdrawing groups such as -COOH and -COOEt cause the resonance positions to shift to slightly lower fields, whereas electron-donating groups such as $-CH_3$ and $-OCH_3$ shift the positions to higher fields. The Hammet constants, σ, of aromatic ring substituents have been used to correlate to enormous amounts of data, including equilibrium and rate constants as well as many physical properties.[64] Plotting chemical shifts, δ, of corresponding protons as a function of σ for the different substituents gives a linear relationship (Figure 4.2). This relationship can be understood qualitatively because σ provides a substituted bipyridine.

4.2.2 Infrared spectra of bipyridine and its derivatives

The infrared spectrum of bipyridine is given in Figure 4.3. Small bands around 3000 cm^{-1} are generally assigned to C-H stretching vibrations, the strongest band at 758 cm^{-1} to the C-H out-of-plane bending vibration, the several medium-intensity bands between 1250 and 1000 cm^{-1} to C-H in-plane bending vibrations, and several strong bands in the range of 1400-1600 cm^{-1} to aromatic C=C and C=N stretching vibrations.[120,121]

When bipyridine was oxidized by H_2O_2 to form 2,2'-bipyridine-N,N'-dioxide, the strengths of all bands decreased relative to a new strong band which appeared at 1255 cm^{-1} (Figure 4.4). This band is assignable to the N-O stretching vibration.[120,121] Nitration at the 4,4' ring positions of 2,2'-bipyridine-N,N'-dioxide caused two new strong bands to appear at 1518 and 1343 cm^{-1} (Figure 4.5); these bands are attributable to $-NO_2$ asymmetric and symmetric stretching vibrations, respectively. They disappeared when $-NO_2$ was replaced by $-OCH_3$ (Figure 4.6). The strongest band in this spectrum at 1271 cm^{-1} is due to the N-O group.

Band positions of ester and acid carbonyl stretching frequencies for the 4,4'- and 5,5'-derivatives of bipyridine are compared in Table 4.2. When 4,4'- or 5,5'-dimethyl-2,2'-bipyridine was oxidized by $KMnO_4$ to form 4,4'- or 5,5'-dicarboxylic acid-2,2'-bipyridine, typical

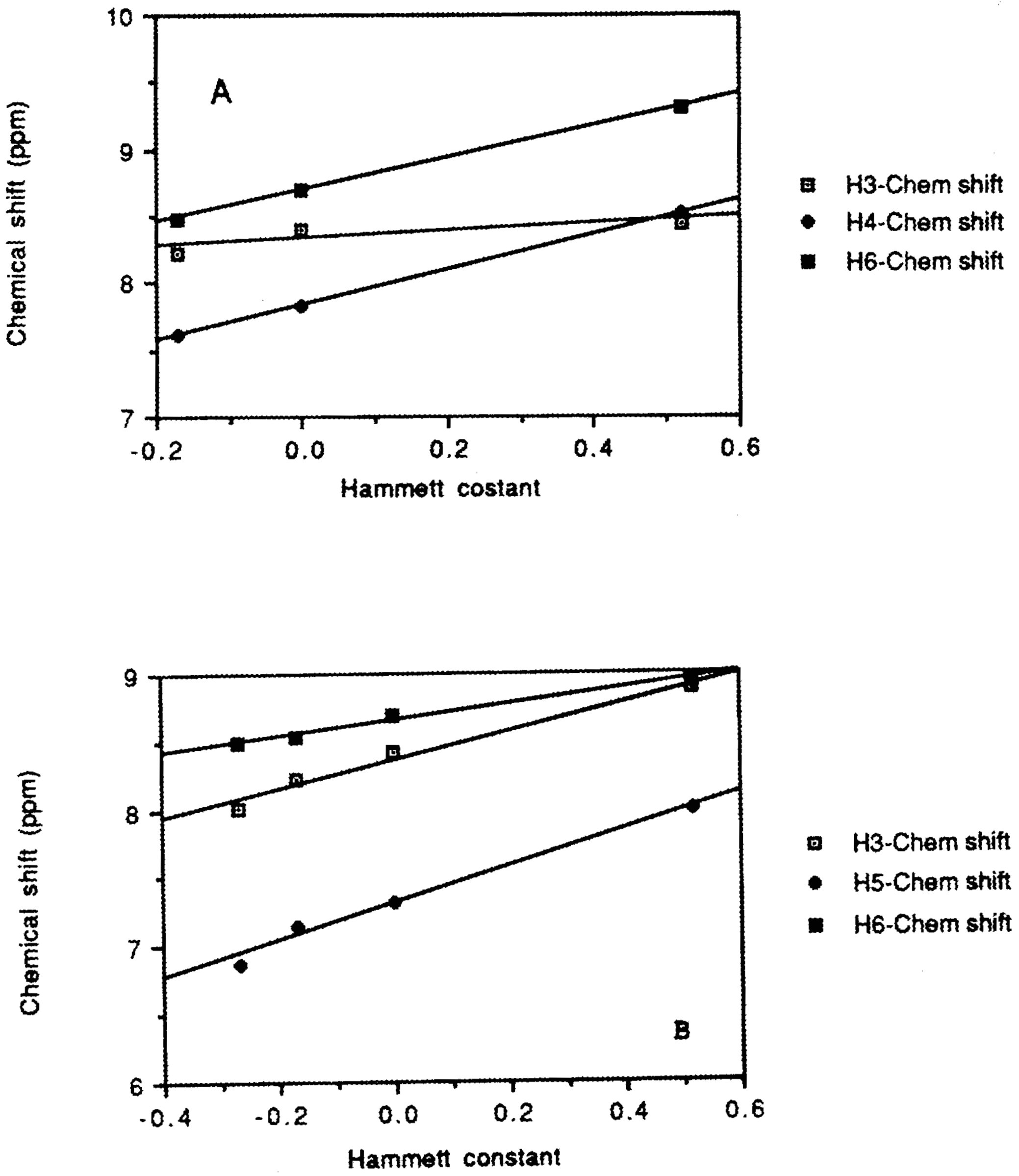

Figure 4.2. Relationship between chemical shifts of protons and the substituent Hammett constant. Hammett constants: $-OCH_3$, -0.27; $-CH_3$, -0.17; -H, 0; -COOEt, 0.52. A: 5,5'-substituted bipyridine B: 4,4'-measure of the relative electron-donating or -withdrawing capacity of the substituent group.

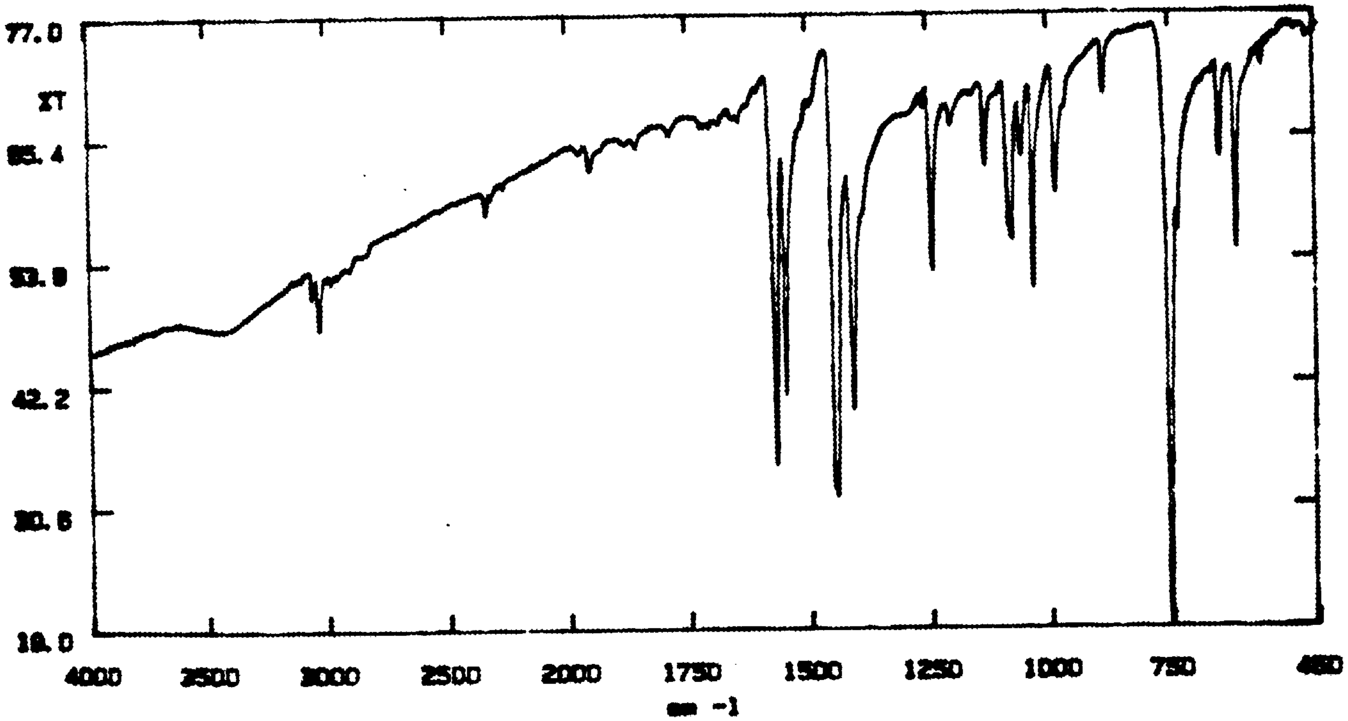

Figure 4.3. FTIR spectrum of 2,2'-bipyridine taken in KBr pellet.

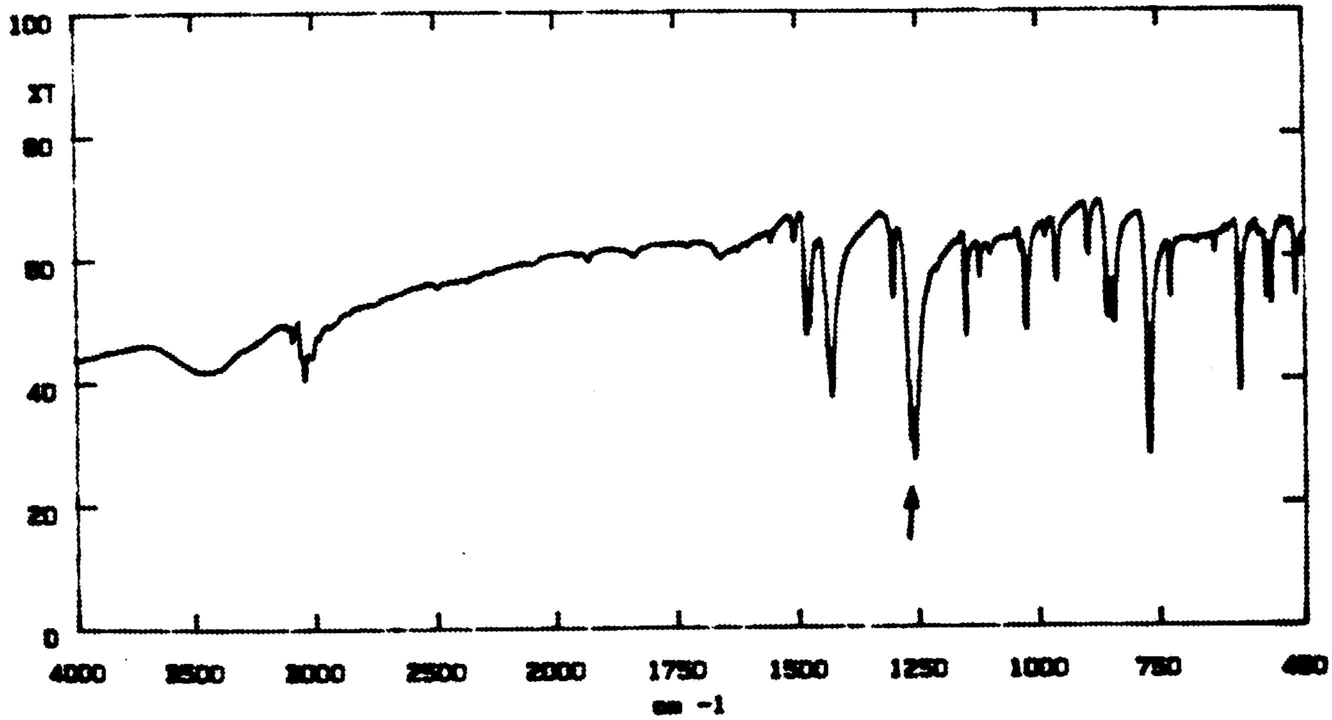

Figure 4.4. FTIR spectrum of 2,2'-bipyridine-N,N'-dioxide taken in KBr pellet; the arrow indicates the position of N-O stretching vibration band.

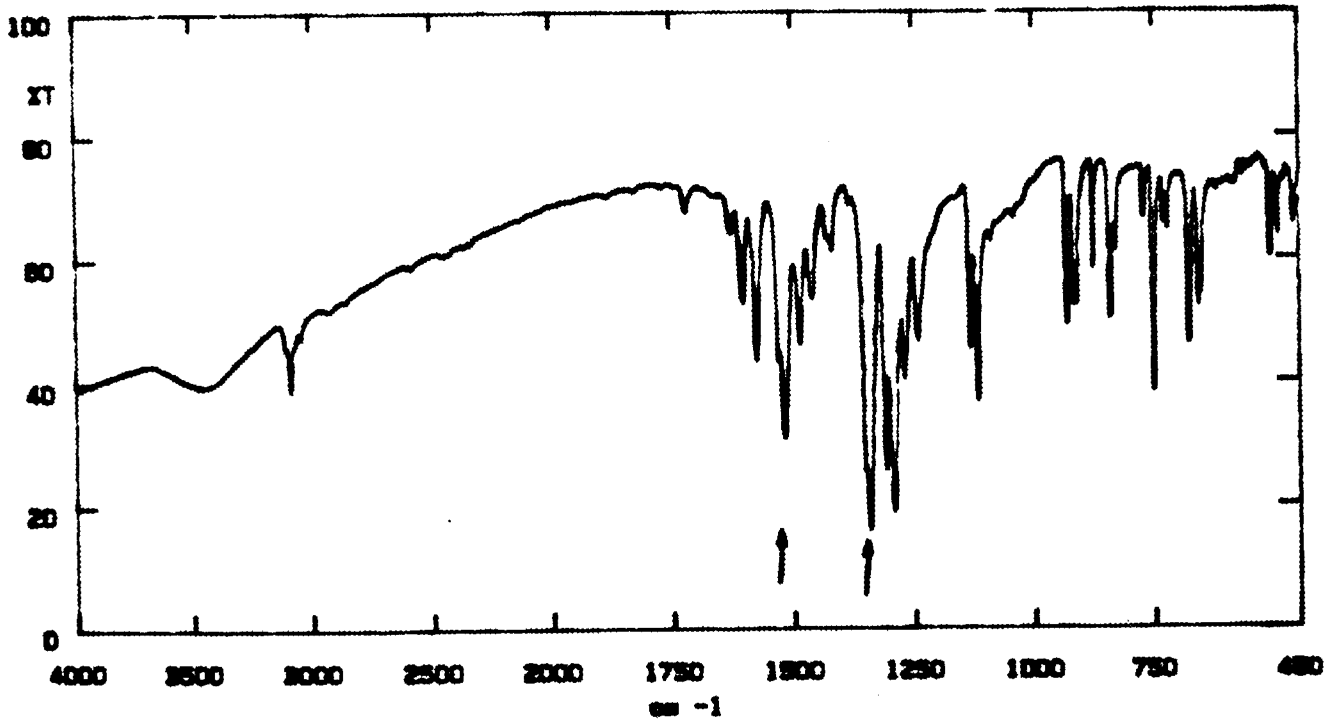

Figure 4.5. FTIR spectrum of 4,4'-dinitro-2,2'-bipyridine-N,N'-dioxide taken in KBr pellet; arrows indicate the positions of asymmetric and symmetric stretching vibration bands of $-NO_2$.

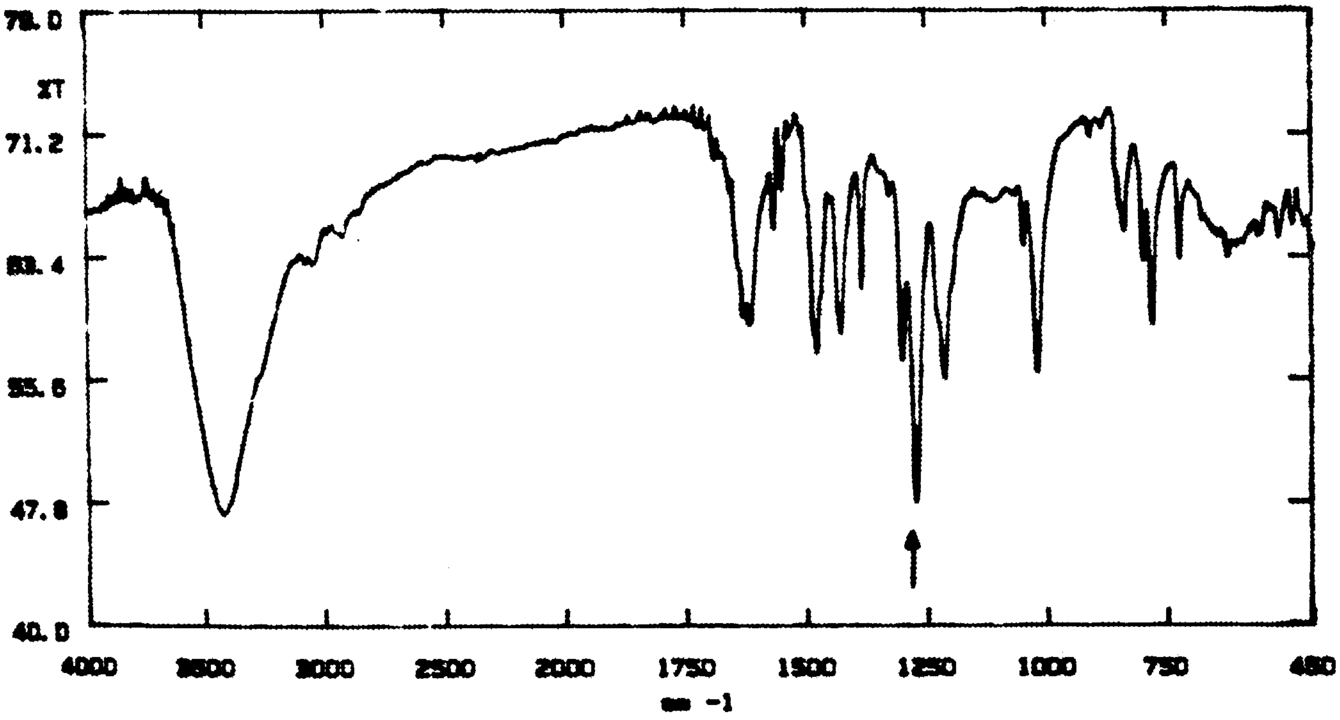

Figure 4.6. FTIR spectrum of 4,4′-dimethoxy-2,2′-bipyridine-N,N′-dioxide taken in KBr pellet; the arrow indicates the postion of N–O stretching vibration band.

carbonyl bands appeared at 1718 (or 1689 cm^{-1}) (Figures 4.7, 4.8, respectively). However, when the carbonyl protons were replaced by ethyl groups, the bands were shifted from 1718 and 1689 cm^{-1} to 1731 and 1722 cm^{-1}, respectively (Figures 4.9, 4.10). The band positions of these compounds are tabulated in Table 4.2.

The carbonyl bands at the 4,4'-positions are blue shifted relative to those of carbonyl at 5,5'-positions, and the carbonyl bands from carboxylate ethyl esters are also blue shifted relative to those of the carboxylic acid. In general, the typical C=O position of the dimeric solid Ar(CO)OH compounds is 1690 cm^{-1}.[120,121] From Table 4.2, the value of 5,5-diacid (1689 cm^{-1}) is in agreement with this typical value, while the value of 4,4'-diacid is a little higher in frequency (1718 cm^{-1}). As described in the preceding section, the electron densities at ring carbon atoms <u>para</u> and <u>ortho</u> to the nitrogen atom on the rings are lower than those at the <u>meta</u> carbon atoms. The C=O band position varies with the double bond character of the carbonyl group.
When <u>para</u> to N, tautomeric forms such as

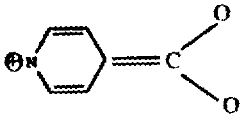

contribute less than when -COOH is <u>meta</u> to N, i.e.,

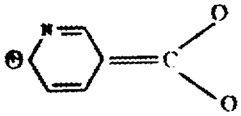

because N is more electronegative than C. Hence, there is a greater amount of single-bond character in C-O when <u>meta</u> to nitrogen on the ring.

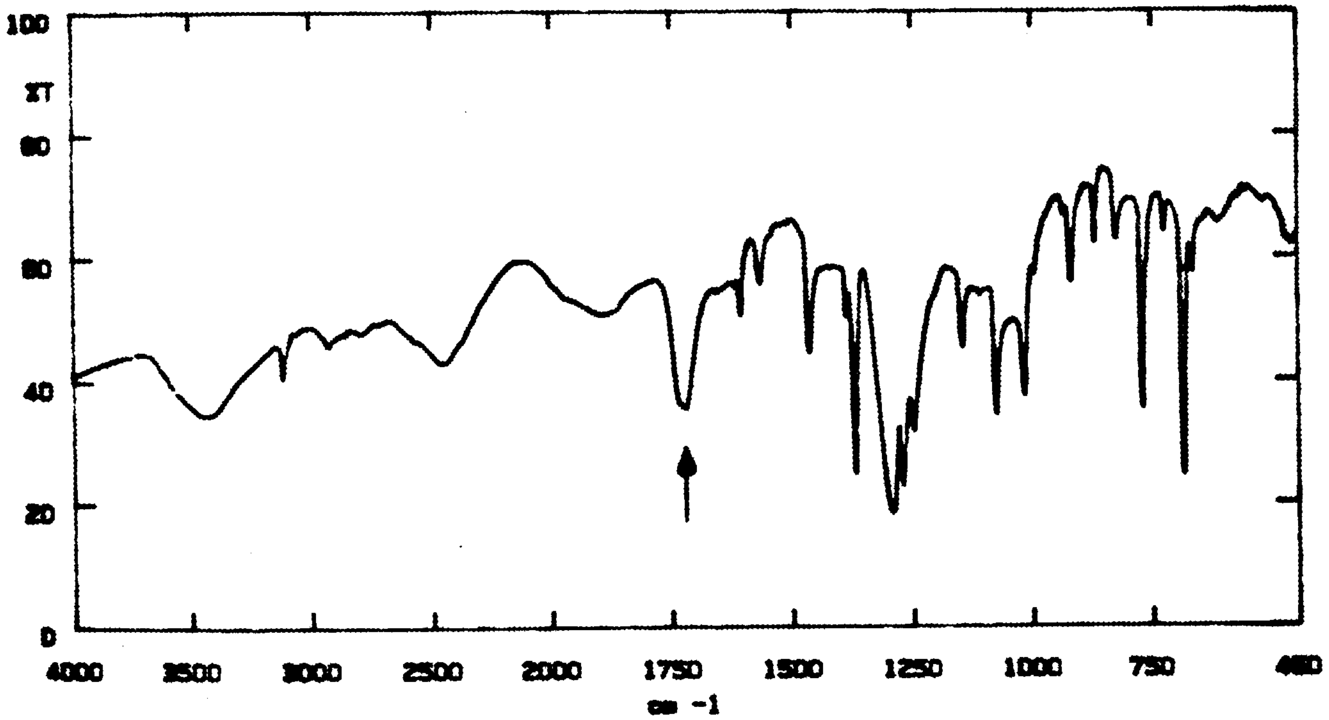

Figure 4.7. FTIR spectrum of 4,4′-dicarboxylic acid-2,2′-bipyridine taken in KBr pellet; the arrow indicates the position of the carbonyl stretching vibration.

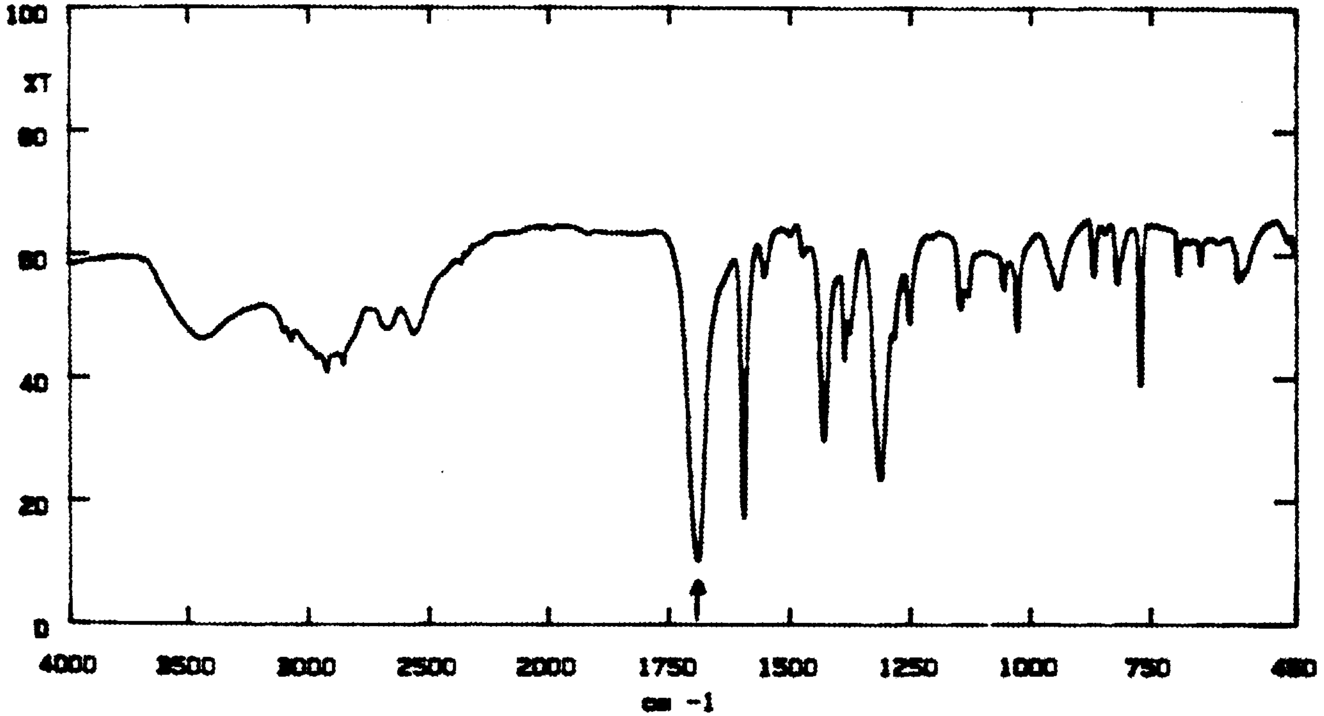

Figure 4.8. FTIR spectrum of 5,5′-dicarboxylic acid-2,2′-bipyridine taken in KBr pellet; the arrow indicates the position of the carbonyl stretching vibration.

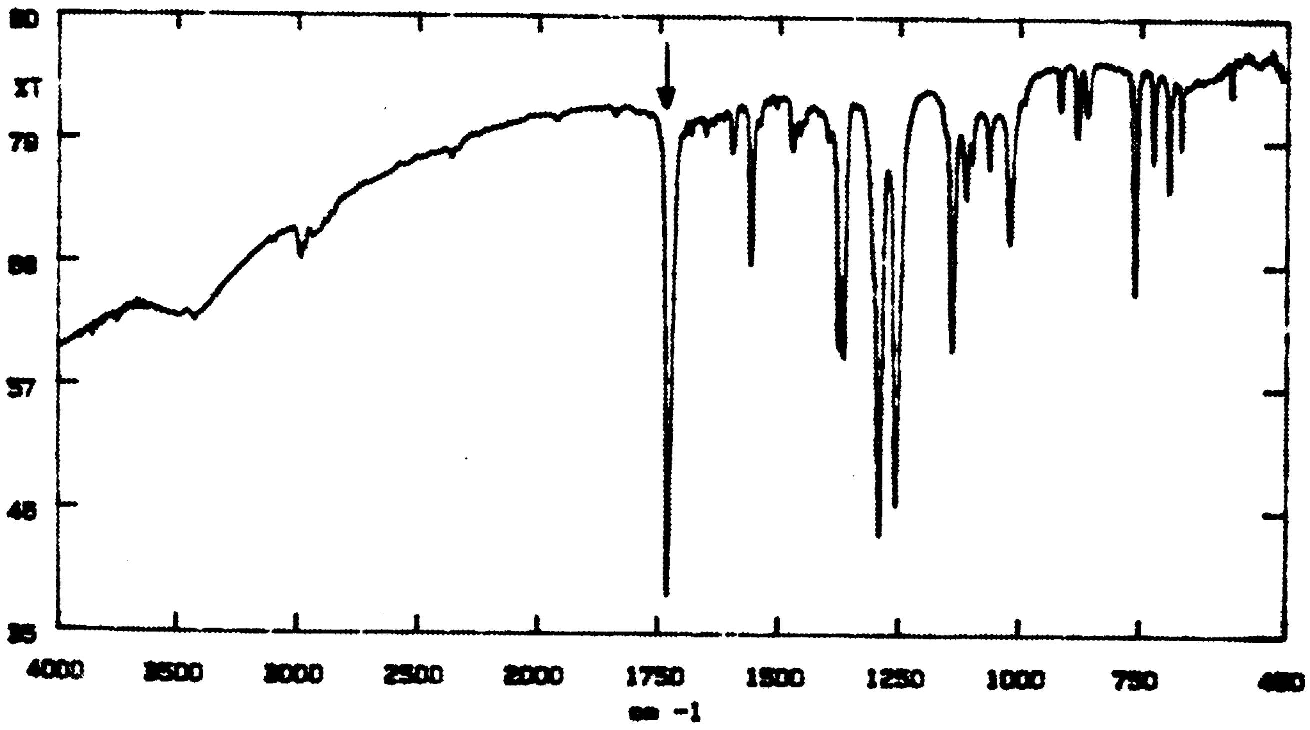

Figure 4.9. FTIR spectrum of 4,4′-dicarbethoxy-2,2′-bipyridine taken in KBr pellet; the arrow indicates the position of the carbonyl stretching vibration.

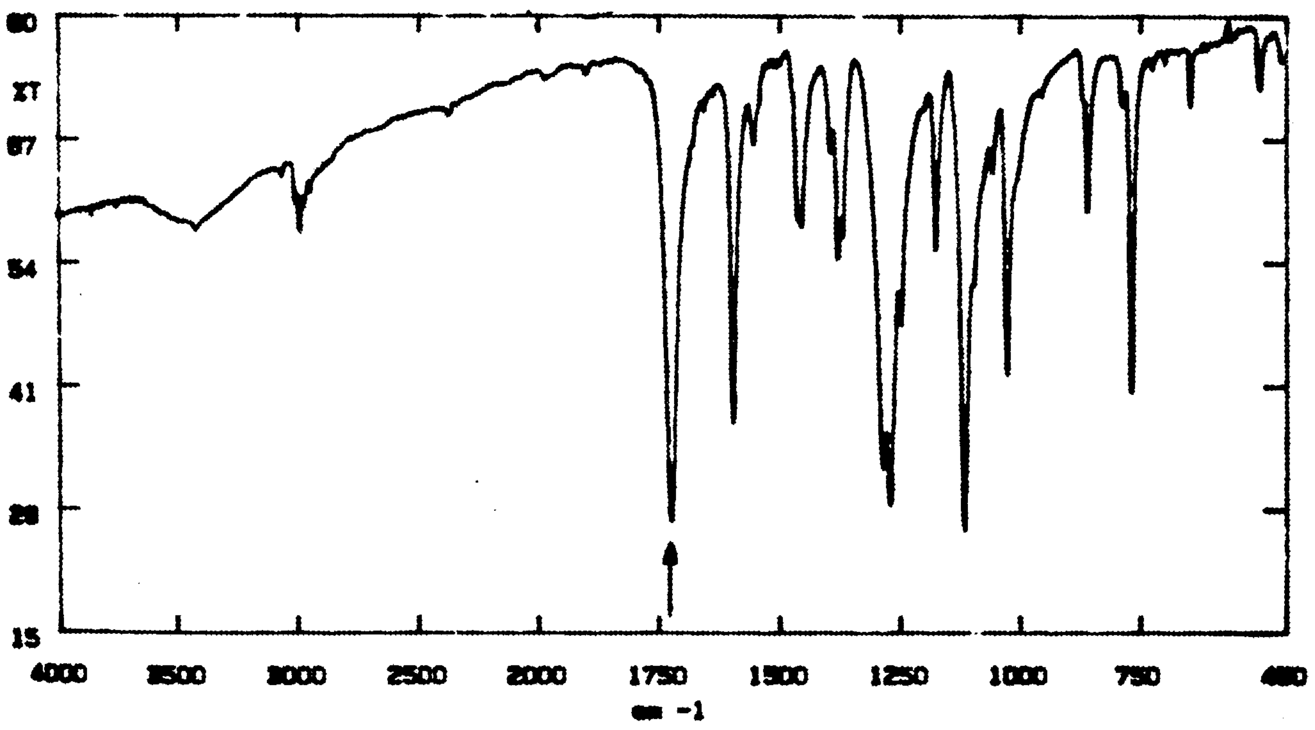

Figure 4.10. FTIR spectrum of 5,5′-dicarbethoxy-2,2′-bipyridine taken in KBr pellet; the arrow indicates the position of the carbonyl stretching vibration.

Table 4.2. The band positions of carbonyl stretching vibrations of carboxy-substituted 2,2′-bipyridine

Compound	Frequency (cm^{-1})
4,4′-dicarboxylic acid-2,2′-bpy	1718
5,5′-dicarboxylic acid-2,2′-bpy	1689
4,4′-dicarbethoxy-2,2′-bpy	1731
5,5′-dicarbethoxy-2,2′-bpy	1722

The fact that the vibrational frequency of ester carbonyls is higher than that of acid carbonyls may be explained as follows: when the carbonyl group is hydrogen bonded to a hydroxylic substance, the carbonyl stretching absorption is displaced to lower frequencies because association of a hydrogen with a carbonyl group decreases the double-bond character of the carbonyl bond, i.e.,

$$C{-}O\cdots H{-}O$$

The typical free carboxylic acid carbonyl stretching frequencies appear near 1760 cm^{-1}. However, in the liquid or solid states most acids exhibit a strong carbonyl absorption in the 1700-cm^{-1} region, which is due to dimerization of acid molecules, i.e.,

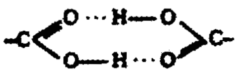

This dimerization is probably the major factor contributing to the lower carbonyl stretching frequencies for the carboxybipyridines relative to their ethyl esters (Table 4.2). Another factor is that the electron donation from the alkyl group of ester increases electron density on the carbonyl carbon, hence strengthens the -C=O bond and increases the carbonyl-stretching frequencies.

4.2.3 Optical absorption properties of complexes

(1) Spectra of $RuL_2(OH_2)_2$ ions

The absorption spectra of each of the cis-diaquabis-bipyridylruthenium(II) ions can be divided into two sets (see Table 4.3), one of which is very similar to the spectra of the corresponding free bipyridine ligands. For $[Ru^{II}(5,5'\text{-diester})_2(OH_2)_2]^{2+}$, the latter set is composed of three bands at 302, 260, and 253 nm. For $[Ru^{II}(4,4'\text{-diester})(OH_2)_2]^{2+}$ and $[Ru^{II}(bpy)_2(OH_2)_2]^{2+}$, this set is composed of two bands at 314 and 250 nm and 290 and 245 nm, respectively. Compared to the absorption bands of the free ligands, all bands in the coordination complexes are somewhat red shifted with larger extinction coefficients. The other set in the visible and near-UV range which has no analogy in the free ligand spectra is composed of two bands. These bands are at 545 and 365 nm for $[Ru^{II}(5,5'\text{-ester})_2(OH_2)_2]^{2+}$, 512 and 384 nm for $[Ru^{II}(4,4'\text{-ester})_2(OH_2)_2]^{2+}$, and 480 and 335 nm for $[Ru^{II}(bpy)_2(OH_2)_2]^{2+}$. The near-UV bands are progressingly red shifted in the sequence $[Ru^{II}(bpy)_2(OH_2)_2]^{2+} < [Ru^{II}(5,5'\text{-diester})(OH_2)_2]^{2+} < [Ru^{II}(4,4'\text{-diester})_2(OH_2)_2]^{2+}$ while the visible bands are red shifted in the order $[Ru^{II}(bpy)(OH_2)]^{2+} < [Ru^{II}(4,4'\text{-diester})_2(OH_2)_2]^{2+} < [Ru^{II}(5,5'\text{-diester})_2(OH_2)_2]^{2+}$.

All the six-coordinate complexes studied here do not have strict octahedral symmetry, but C_2 symmetry. Therefore it is not strictly

Table 4.3 Electronic Absorption Band Maximum and Extinction Coefficients of Monomeric Complexes and Free Ligands[a,b]

Compound	Band maximum (nm)	Extinction Coefficient (M^{-1} cm^{-1})
$Ru^{II}(5,5'\text{-diester})_2(OH_2)_2^{2+}$	545	5.8×10^3
	365	sh
	302 (297)	7.4×10^4 (3.0×10^4)
	260 (255)	2.1×10^4 (1.6×10^4)
	253 (249)	2.2×10^4 (1.7×10^4)
$Ru^{II}(4,4'\text{-diester})_2(OH_2)_2^{2+}$	512	1.0×10^4
	384	9.0×10^3
	314 (298)	3.6×10^4 (1.2×10^4)
	250 (250)	(sh) (1.1×10^4)
$Ru^{II}(bpy)_2(OH_2)_2^{2+}$	480	8.5×10^3
	335	7.7×10^3
	290 (278)	5.0×10^4 (9.1×10^3)
	245 (238)	2.4×10^4 (7.8×10^3)

[a] Complexes in 0.5 M H_2SO_4, bipyridine and substituted bipyridine in CH_3CN. Numbers in parentheses are corresponding values for the free ligands.

[b] Data for $Ru^{II}(bpy)_2(OH_2)$ are from reference 108.

correct to consider the metal d-orbitals as t_{2g} and e_g because of the reduced symmetry. However, to simplify the discussion we will use labels, t_2 and e, for the metal d-orbitals, d_{xy}, d_{yz}, d_{zx}, and $d_{x^2-y^2}$, d_{z^2}, respectively (a procedure recommended by Bryant et al.).[79,80]

A simplified energy-level diagram (Figure 4.11)[82] used for hexacyano complexes of the iron group will be used here as a basis for general introduction to the electronic spectra of coordination complexes. As we know, molecular orbitals, $e(\sigma^*)$ and $t_{2g}(\pi)$, are located mainly on the metal atom while those π and π^* are located on the ligand molecules (Figure 4.11). Possible excitations would be $t_2(\pi) \rightarrow e_g^*(\sigma)$, $t_2 \rightarrow \pi^*$, $\pi \rightarrow e^*(\sigma)$, $\pi \rightarrow \pi^*$. Based on these general considerations, the low-lying absorption bands of the transition metal ion complexes may be classified into three types: ligand-field (LF), charge-transfer (CT) (including metal-ligand charge transfer (MLCT) and ligand-metal charge transfer (LMCT)), and intra-ligand transitions (IL). LF transitions take place between the d shell electrons of the central metal ion. As a consequence of excitation, an electron is promoted from t_2 orbitals to the e orbitals giving rise to weak Laporte-forbidden absorption bands with extinction coefficients below 100. MLCT transitions correspond to the transfer of charge from the central metal ion to the ligand moiety. These transitions usually have a greater intensity (extinction coefficients = 2000 to 25000)[83] than LF transitions since the Laporte rule no longer applies. When present, bands make it very difficult to locate and identify LF transitions. these intense LMCT transition involves electron transition from ligand to metal ion. For the metal ions of low oxidation states such as Ru^{II}

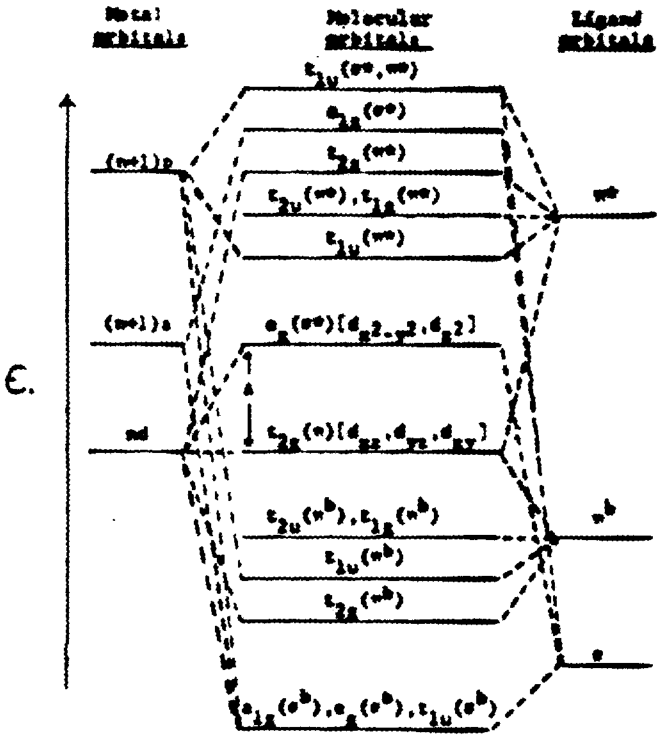

Figure 4.11. Molecular orbital energy level diagram for metal hexacyanides and hexacarbonyl (from reference 82).

studied here, such transitions would occur at a higher energy than the visible or near ultraviolet region and are correspondingly difficult to identify.[84] IL transitions arise from the excitation of a molecule to a $\pi^b \rightarrow \pi^*$ excited configuration achieved by promotion of an electron from a π-bonding orbital to an empty π-antibonding orbital within the ligand aromatic system. These bands can be identified by their similarity to bands observed in the free ligand spectra.[84] Normally, ligand bands are very intense, having molar extinction coefficients of 25000 or higher, and usually appear in the UV region.

Based upon these general considerations, the two bands of the complexes observed in the visible and near UV region are assigned to CT transitions ($t_2 \rightarrow \pi_1^*$ and $t_2 \rightarrow \pi_2^*$) because their extinction coefficients are too great to be associated with LF transitions. In addition, the fact that electron withdrawing substituents such as 4,4'-COOEt and 5,5'-COOEt on the bipyridine rings cause substantial bathochromic shifts in the band maximum is consistent with the expected behavior of an electron transfer from ruthenium(II) center to unoccupied orbitals of the ligands. This effect can be understood from the standpoint of electrostatics, where electron withdrawal from the ring causes lowering of the ligand π^* orbitals, i.e., the energy of the electron transfer required decreases, so the absorption bands are red shifted. Ohsawa et al.[85] performed MNDO molecular orbital calculations on bipyridine and its 4,4'-COOH and 5,5'-COOH derivatives, and found that the π_1^*-π_4^* levels of the substituted bipyridine are lower relative to bipyridine. This lowering has been ascribed to the inductive effect of -COOH. The conjugative effect of -COOH was found to preferentially lower π_1^* and π_4^* levels in 5,5′-COOH but to lower the π_2^* and π_3^* levels in 4,4′-COOH (Figure 4.12)[85]. Since π^* orbitals of substituted bipyridine are lower than corresponding orbitals of bpy, it is reasonable that CT absorption bands are red shifted. (Of course, the effect of the substituents to the metal ion t_2 orbital energies should also be considered because the position of absorption maximum depends upon energy difference between orbitals. However, I assume that the effect of substituents on the bpy rings on t_2 orbitals on the metal ion is smaller than that of the orbitals on the ligands themselves.) According to Figure 4.12, the level of the lowest-lying orbital, π_1^*, of 5,5′-diacid is lower than that of 4,4′-diacid while the second lowest lying orbital, π_2^*, of 5,5′-diacid is higher than that of 4,4′-diacid. These relative orderings are consistent with the positions of CT absorption bands of corresponding complexes; i.e., the lowest-energy absorption bands of a complex with 5,5′-diacid and 4,4′-diacid are 545 and 512 nm, respectively, whereas the second-lowest absorption bands are 365 and 384 nm, respectively.

Based on the similarities of the UV bands of complexes and corresponding free ligands, I assign these bands to IL transitions. The fact that all these bands are red shifted relative to those of corresponding free ligands can be ascribed to the electrostatic effect of the positive charge of metal ion on the energy levels of the ligands.[87]

(2) Solvent effect on the optical absorption spectra of RuL_2Cl_2 complexes

Many transition-metal complexes display solvatochromic behavior.

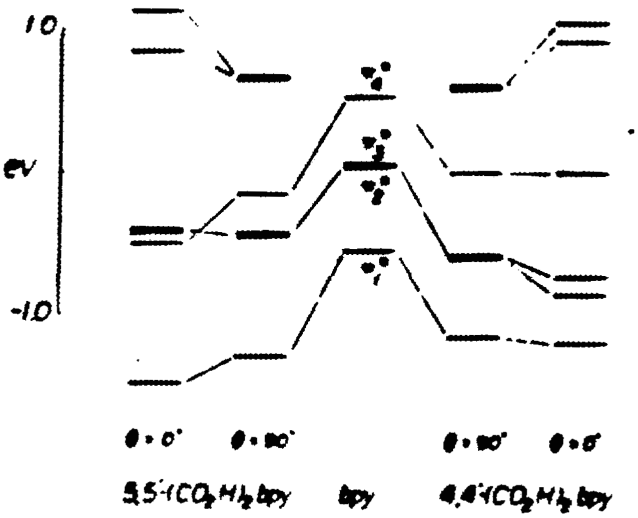

Figure 4.12. Low lying unoccupied levels of bpy, 4,4'-diacid and 5,5'-diacid obtained from MNDO calculations, where θ refers to the dihedral angle beween COOH and bpy units. θ is defined such that COOH and bpy units are coplanar at 0° (from reference 85).

Although solvent effects on the d-d transition of various Co(III) and Cr(III) complexes were found as early as 1956 by Bjerrum et al.,[88] the majority of known cases involve transitions which are largely charge transfer in character. For example, Miller and Dance[89] have noted strong solvent effects on the interligand charge-transfer transitions in some mixed-ligand dithiolene complexes and have found that the observed solvatochromic shifts correlate with the gas-phase dipole moments of the various solvents employed. Burgess[90] and Gidney et al.[93] have found that the charge-transfer band maximum for the metal to bpy ligand transition $d\pi \rightarrow \pi^*$(bpy) in such complexes as $Fe^{II}(bpy)_2(CN)_2$ and $M(bpy)(CO)_4$ (M = W, Mo) and square-planar d^8 complexes $M^{II}(bpy)_2X_2$ (M = Pt, Pd; X = Cl, Br, I) is influenced strongly by solvent and correlates with the ET solvent scale[91] and Z scale.[92] The striking solvent sensitivity of $Ru(NH_3)_5L^{2+}$ series was noted by Ford et al.,[86] but attempts to correlate the shifts of band maxima with known solvent parameters such as dielectric constant and Z scale did not succeed.[86] Recently, many authors[94-99] have used Gutmann donor number (DN)[93] to correlate with solvatochromic shifts.

We studied the effect of solvent upon optical absorption spectra of several monomeric ruthenium complexes with bipyridine and its derivatives, $Ru^{II}L_2Cl_2$ (L = bpy, 4,4'-diester, and 5,5'-diester) and $Ru^{II}(bpy)_3Cl_2$. Their absorption band maxima and extinction coefficients are given in Table 4.4.

In Figures 4.13 and 4.14, plots are shown for the several complexes of wave number vs. the donor number (DN) and acceptor number (AN) defined by Gutmann.[94] The DN of a solvent (S) is defined as the

Table 4.4. Electronic Absorption Data for RuL_2Cl_2 in Different Non-aqueous Solvents[a]

	Absorption Maximum (nm)			
Solvent(DN)	$Ru(bpy)_2$	$Ru(bpy)_3$	Ru(55 ester)	Ru(44 ester)
DMSO(29.8)	558 (2.0×10^3)	453 (1.4×10^4)	658 (6.5×10^3)	588 (2.2×10^4)
	358 (2.0×10^3)	290 (6.6×10^4)	398 (8.1×10^3)	432 (2.0×10^4)
	302 (1.0×10^4)	—	312 (5.3×10^4)	322 (5.3×10^4)
DMF(26.6)	562 (870)	454 (1.2×10^4)	666 (7.1×10^3)	590 (2.3×10^4)
	382 (800)	288 (5.7×10^4)	396 (9.1×10^3)	434 (2.1×10^4)
	300 (4.2×10^3)	—	312 (5.9×10^4)	520 (5.4×10^4)
PC(15.1)	554 (644)	452 (1.3×10^4)	656 (6.7×10^3)	582 (1.4×10^4)
	380 (620)	288 (7.0×10^4)	394 (8.4×10^3)	428 (1.3×10^4)
	298 (3.4×10^3)	242 (2.3×10^4)	310 (5.7×10^4)	320 (4.0×10^4)
	242 (2.1×10^3)	210 (3.8×10^4)	254 (2.3×10^4)	246 (3.0×10^4)
MeCN(14.1)	550 (890)	451 (1.4×10^4)	648 (5.4×10^3)	580 (2.3×10^4)
	378 (870)	289 (8.8×10^4)	392 (6.9×10^3)	426 (2.2×10^4)
	298 (4.8×10^3)	242 (2.2×10^4)	310 (5.0×10^4)	318 (6.6×10^4)
	242 (2.1×10^3)	—	254 (1.9×10^4)	244 (5.3×10^4)
NM(2.7)	548 (2.9×10^3)	451 (1.5×10^4)	640 (6.5×10^3)	580 (2.6×10^4)
	378 (3.8×10^3)	—	388 (8.0×10^3)	426 (2.5×10^4)

[a] $Ru(bpy)_2$ = $Ru^{II}(bpy)_2Cl_2$; $Ru(bpy)_3$ = $Ru^{II}(bpy)_3Cl_2$; Ru(55 ester) = $Ru^{II}(5,5'\text{-diester})_2Cl_2$; Ru(44 ester) = $Ru^{II}(4,4'\text{-diester})_2Cl_2$. DMSO = dimethyl sulfoxide; DMF = dimethylformamide; PC = propylene carbonate; MeCN = acetonitrile; NM = nitromethane.

negative enthalpy change at 25°C for the reaction

$SbCl_5 + S = Cl_5SbS$

in 1,2-dichloroethane with $[SbCl_5] = 10^{-3}$ M. As such, it presumably measures largely the electron-pair donor ability or "donicity" of S relative to 1,2-dichloroethane, whose interaction with $SbCl_5$ is assumed to be nearly zero. The acceptor number (AN) is defined as a dimensionless number related to chemical shift, δ, of ^{31}P in Et_3PO in the particular solvent, with hexane as a reference solvent on the one hand, and Et_3PO-$SbCl_5$ in 1,2-dichroloethane on the other hand, to which the acceptor numbers of 0 and 100 have been assigned, respectively:

$$AN = \frac{\delta_{corr} \times 100}{\delta_{corr(Et3PO\ SbCl5)}} = 2.348\delta_{corr}$$

where δ_{corr} is the δ value extrapolated to infinite dilution and corrected for the difference in volume susceptibilities between hexane and the respective solvents.

It is clear from the Figures 4.13 and 4.14 that correlations can be made with DN and AN values. It is notable that for the MLCT bands t_2-π_1^*, shown in Figure 4.13, the plots of ν and DN have negative slopes, indicating that the energy of optical transition decreases as the electron-donating ability of the solvent increases. Also, as shown in Figure 4.14, the plots of ν and AN have positive slopes, indicating that the energy of the optical transition increases as the electron-acceptor ability of the solvent increases. Careful inspection of the figures show that the slopes of the plots are almost the same for complexes $Ru^{II}(bpy)_2Cl_2$, Ru^{II}(5,5'-diester)Cl_2, and Ru^{II}(4,4'-

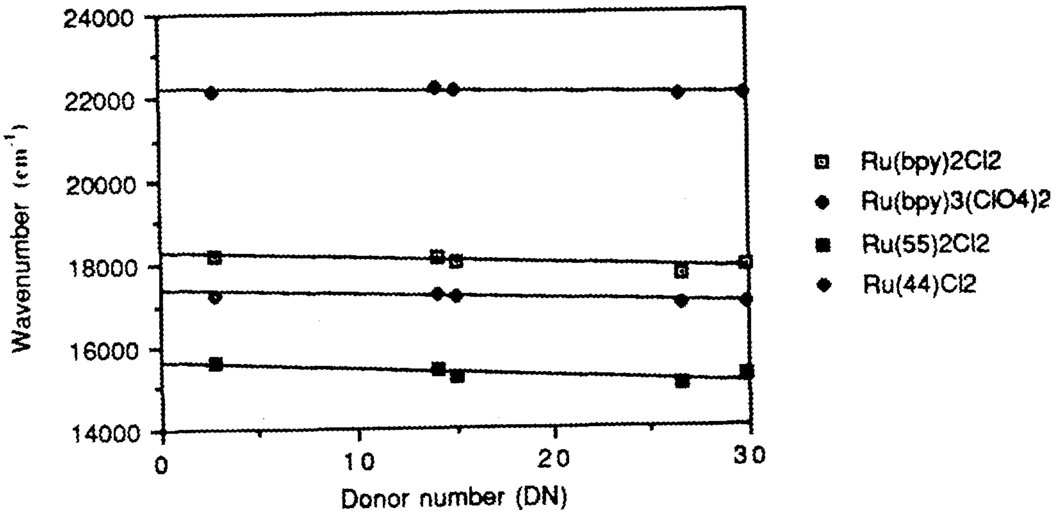

Figure 4.13. Relationship between electron absorption frequencies (visible region) of RuL_2Cl_2 complexes in various solvents and DN of corresponding solvents.

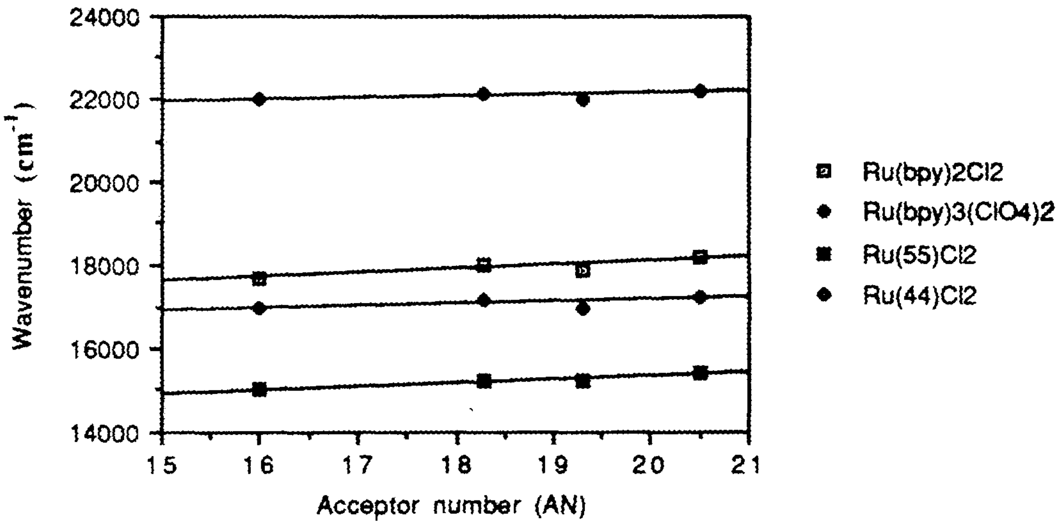

Figure 4.14. Relationship between electron absorption frequencies (visible region) of RuL_2Cl_2 complexes in various solvents and AN of corresponding solvents.

diester$)_2Cl_2$, which indicates that the sensitivity of the optical transition to solvents is nearly independent of the identity of substituents on the bpy rings. However, for the complex $Ru^{II}(bpy)_3^{2+}$, the solvent effect is almost negligible. These data suggest that the solvent effect arises primarily from interaction between the chloro ligands and solvent molecules.

The position of the absorption band maximum depends upon the difference of energy levels between the ground and excited states. If the excited state is stabilized by solvation relative to the ground state, a red shift occurs; if the ground state is stabilized relative to the excited state, a blue shift occurs. According to the preceding discussion, MLCT excitation transfers an electron localized mainly on the metal ion t_2 orbital to π^* on the bpy ligand. Ground and excited states can be represented by the schematic diagrams:

bpy-Ru^{II}-Cl:S	bpy-Ru^{III}-Cl:S
Ground State	Excited State

The electron density on Cl within the excited state decreases, so the stabilizing effect of the electron-pair donation from solvent will be greater for the excited state than for the ground state, and the effect will increase as DN increases. Stabilization of the excited state with regard to the ground state means that the absorption band maxima are increasingly red shifted as the DN of solvent increases. From the standpoint of solvent acceptor properties, the extent of Cl solvation will reflect the electron density on the Cl ligand. Because the electron density on the Cl is smaller in the excited state than in the ground state, the extent of solvent interaction decreases. The greater the solvent AN, the larger will be the excited-state destabilization relative to the ground state and, therefore, the greater the blue shift.

(3) UV/visible spectra of μ-oxo-bridged dimeric ions

The electronic absorption spectra of the μ-oxo-bridged ruthenium complexes show several interesting features. Table 4.5 lists absorption maxima and extinction coefficients for each of the complexes. The high intensity, low-energy band at about 650 nm is characteristic of the Ru^{III}-O-Ru^{III} μ-oxo bridged dimers and gives them their intense blue or blue-green color. The CT absorption bands which are characteristic of monomeric complexes are not now present. This indicates that the origin of this absorption band and the bonding mode in the μ-oxo-bridged dimers is totally different from those of monomers.

The ultraviolet spectra are still similar to those of monomers, which are characteristic of the various bipyridyl ligands. As in the case of monomers, these absorption bands are somewhat red shifted relative to corresponding free ligands.

When the μ-oxo bridged dimers are oxidized to corresponding III,IV ions, the high intensity, low-energy bands at around 650 nm disappear when the ligands are 2,2'-bipyridine or its 4,4'-diester and 5,5'-diester derivatives or decrease in intensity when the ligand is 4,4'-dimethoxy derivative, and a new band appears in the region of 450-500 nm. The ultraviolet bands for all complexes undergo a slight red shift.

Substituents on the bipyridine rings have a marked effect on the position of the low energy band around 650 nm. Carboxylate groups at 5,5'-positions and 4,4'-positions red shift the band from 637 nm, the position of the band in the underivatized complex, to 648 and 680 nm,

Table 4.5. Electronic Absorption Data

for Several μ-Oxo-Bridged Dimeric Complexes[a]

Complexes	Absorption Maximum (ε)	Ref. Value
$(bpy)_2(OH_2)Ru^{III}$-O-$Ru^{III}(OH_2)(bpy)_2$	639(1.7x10^4)	637(2.1x10^4)[b]
	283(4.5x10^4)	280(5.0x10^4)
	243(3.5x10^4)	242(4.0x10^4)
$(bpy)_2(OH_2)Ru^{IV}ORu^{III}(OH_2)(bpy)_2$	446(1.9x10^4)	444(2.2x10^4)[b]
	302(6.5x10^4)	304(6.6x10^4)
	246(5.7x10^4)	246(5.9x10^4)
(5,5′-diester)$_2(OH_2)Ru^{III}$-O-$Ru^{III}(OH_2)$	648(1.6x10^4)	654(1.8x10^4)[c]
(5,5′-diester)$_2$	298(6.7x10^4)	296(7.0x10^4)
	257(4.2x10^4)	257(5.5x10^4)
(5,5′-diester)$_2(OH_2)Ru^{III}$-O-$Ru^{IV}(OH_2)$	498(1.6x10^4)	500(1.7x10^4)[c]
(5,5′-diester)$_2$	325(9.8x10^4)	325(9.5x10^4)
	312(9.9x10^4)	313(1x10^5)
	256(8.0x10^4)	258(8.5x^{1}0^4)
(4,4′-diester)$_2(OH_2)Ru^{III}$-O-$Ru^{III}(OH_2)$	680(2.4x10^4)	678(2.1x10^4)[d]
(4,4′-diester)$_2$	304(5.7x10^4)	304(4.9x10^4)

Table 4.5. (Continued)

Complexes	Absorption Maximum (ε)	Ref. Value
$(4,4'\text{-diester})_2(OH_2)Ru^{III}\text{-O-}Ru^{IV}(OH_2)$	$494(1.7\times10^4)$	$500(1.8\times10^4)^d$
$(4,4'\text{-diester})_2$	332(sh)	
	$316(4.6\times10^4)$	
	286(1.9x104)	
$(4,4'\text{-methoxy})_2(OH_2)Ru^{III}\text{-O-}Ru^{III}(OH_2)$	$658(1.9\times10^4)$	
$(4,4'\text{-methoxy})_2$	$330(1.2\times10^4)$	
	$264(4.7\times10^4)$	
	$222(1.1\times10^5)$	

[a] Medium is 0.5 M H_2SO_4.

[b] From reference 11.

[c] From reference 14.

[d] From reference 118.

respectively. Thus, the effect is position sensitive. The methoxy group causes a shift to 658 nm.

In addition, pH also influences the position of this band. In Figure 4.15 the results are shown for $(bpy)_2(OH_2)Ru^{III}\text{-O-}Ru^{III}(OH_2)(bpy)_2$. Between pH 0 and 5 the absorption maximum position remains around 639 nm, but at pH 6 it changes to 643 nm where it remains until pH 8. Then it begins to decrease, reaching 626 nm at pH 11.

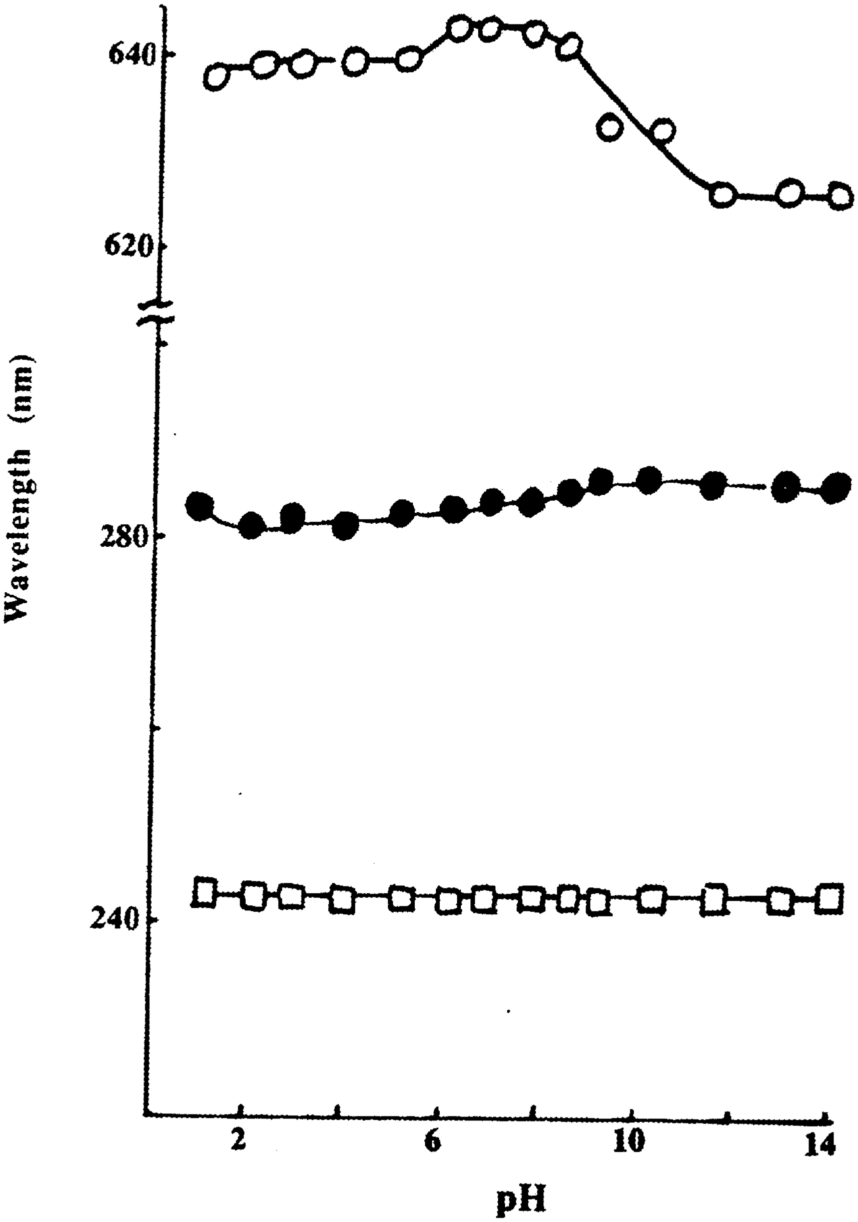

Figure 4.15. Relationship between pH and band maximum positions of $(bpy)_2(OH_2)Ru^{III}ORu^{III}(OH_2)(bpy)_2$ ion. ○, 639-nm band (0.5 M H_2SO_4); ●, 283 nm-band (0.5 M H_2SO_4); □, 243 nm-band (0.5 M H_2SO_4).

Apart from displacement of the maximum position, there is significant broadening of the absorption band in the alkaline region. These spectral changes arise from the various acid-base equilibria involving the two aqua ligands. The two pK_a values have been determined as 5.9 and 8.38. The spectral changes match these pK_a values. The pH does not affect the positions of band maxima in the UV region (Figure 4.15).

The origin of the transitions is readily accounted for by using the model developed by Dunitz and Orgel[100] for the linear ion, $[Cl_5Ru\text{-}O\text{-}RuCl_5]^{4-}$. Based upon the symmetry (C_{4v}) of this complex anion, they obtained the following frontier molecular orbital energy level diagram for the Ru-O-Ru segment:

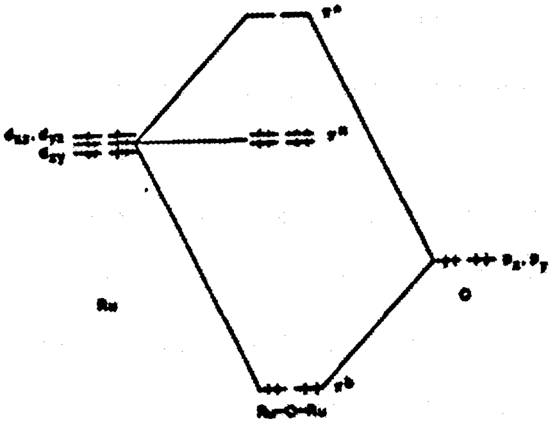

Many chemists have subsequently utilized this scheme to explain the UV/visible[101-104] and Raman[105] spectral properties of μ-oxo-bridged dimeric complexes, as well as trimers.[106,107]

In our case, because the complexes have bent geometry (for example, the angle of the bridging Ru-O-Ru in the complex $(bpy)_2(OH_2)Ru\text{-}O\text{-}Ru(OH_2)(bpy)_2$ is 165°),[11] all dimeric complexes have at most C_{2v} symmetry if the two aqua ligands are located in a cis-cis configuration. So the degeneracy of the molecular orbitals is lifted further (Figure 4.16). For the segment Ru^{III}–O–Ru^{III}, which has 14 electrons in the Ru–O–Ru orbital set (five from each ruthenium atom and four from the oxygen atom), the electron configuration of the complex ion is expected to be:

$(a_1)^2(b_1)^2(b_1)^2(a_2)^2(a_2)^2(b_2)^2(a_1)^2(b_1)^0$

The electronic transitions of this ion, therefore, involve excitation of electrons in the low-energy orbitals to the b_1^*, viz.,

(1) $a_1^*(e_u) \rightarrow b_1^*(e_u)$ $(b_1 \times a_1 = b_1)$ allowed in x polarization
(2) $b_2(e_g) \rightarrow b_1^*(e_u)(b_1 \times b_2 = a_2)$ forbidden
(3) $a_2(e_g) \rightarrow b_1^*(e_u)(b_1 \times a_2 = b_2)$ allowed in y polarization
(4) $a_2(b_{1u}) \rightarrow b_1^*(e_u)$ $(b_1 \times a_2 = b_2)$ allowed in y polarization
(5) $b_1(b_{2g}) \rightarrow b_1^*(e_u)$ $(b_1 \times b_1 = a_1)$ allowed in z polarization

So, we can assign the the highly intense, low energy bands at around 650 nm to the transitions, $a_2(b_{1u}) \rightarrow b_1^*(e_u)$, $a_2(e_g) \rightarrow b_1^*(e_u)$, and $b_1(b_{2g}) \rightarrow b_1^*(e_u)$. Because all of these transitions are allowed and their energies do not differ much, this might be why we observed a highly intense, broad visible band with some structure. We refer to this band as π^n--π^* because all occupied orbitals involved are non-bonding ones. (The $a_1(e_u)$ is very close in energy to the unoccupied $b_1(e_u)$ orbital, so that its absorption band would be in the infrared region.)

The bands in the ultraviolet region can be assigned to intraligand transitions for the following reasons: a) Their extinction coefficients are very large ($> 5 \times 10^4$) while the frontier orbital transitions described above in the ultraviolet range are not so intense (for instance, $\varepsilon = 5.4 \times 10^3$ M^{-1} cm^{-1} for the band at 386 nm for

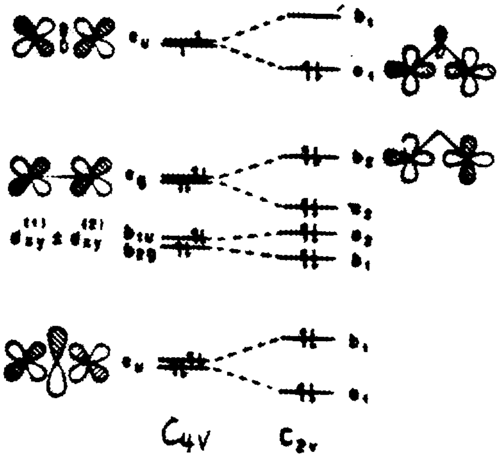

Figure 4.16 Frontier molecular orbitals originating from the Ru-O-Ru segment (from reference 104).

$\{[\mathrm{Ru(NH_3)_5}]_2\mathrm{O}\}^{4+}$; 2.1 × 10^3 M^{-1} cm^{-1} for the band at 255 nm for $\{[\mathrm{Ru(NH_3)_5}]_2\mathrm{O}\}^{5+}$).[104] b) The bands are very sharp without structure, while CT bands are usually broad with some structure. c) The formal charge on the central ruthenium ions does not influence much of the band positions (for example, 298 and 257 nm for $\mathrm{Ru^{III}}$-O-$\mathrm{Ru^{III}}$(5,5′-diester) as compared to 316 and 257 nm for $\mathrm{Ru^{III}}$-O-$\mathrm{Ru^{IV}}$(5,5′-diester)). In general, CT bands are very sensitive to the formal charge on the central metal ion. d) The band positions are very close to those of the corresponding free ligand. In general, the ultraviolet CT bands arising from the Ru-O-Ru segment are probably obscured by the overlapping more intense IL bands. The high intensity, low energy bands shifted to around 500 nm upon one-electron oxidation to the $\mathrm{Ru^{III}}$-O-$\mathrm{Ru^{IV}}$ state, but their intensities did not change much. Because the charge of the segment increases, the energy levels of all orbitals are expected to decrease.[107] The fact that the absorption bands are blue shifted indicates that the lowest unoccupied molecular orbital decrease is less than the highest occupied molecular orbital involved in the low-energy excitation.

The other coordinated ligands also influence the absorption spectra. For example, the bipyridine ring substituents cause shifts in the low-energy bands. This is probably because the orbitals of these ligands influence d orbitals of the metal ions, thereby affecting the levels of frontier orbitals. Similarly, replacement of H_2O by OH^- affects the ruthenium d orbital energies. However, only the low-energy band in the visible region is affected, which further confirms that the origin of the UV bands is different from that of the low energy bands in the visible range.

4.2.4. Vibrational spectra of $(bpy)_2(OH_2)Ru^{III}$-O-$Ru^{III}(OH_2)(bpy)_2$

FTIR spectra of the perchlorate salt of the $[(bpy)_2(OH_2)Ru^{III}]_2O$ ion were taken as KBr pellets (Figure 4.17). For comparison, the FTIR spectrum of the monomeric complex $Ru^{II}(bpy)_2Cl_2$ is also given (Figure 4.18).

As mentioned in Chapter III, for bent M-O-M species both symmetric and asymmetric modes are infrared active, and these modes are usually found in the ranges of 350-500 and 750-900 cm^{-1}, respectively. For 2,2'-bipyridine, the 800- to 900-cm^{-1} region is free of vibrational bands (Figure 4.3). No new bands with significant intensities were found in this region for the μ-oxo bridged dimer. Below 800 cm^{-1}, there are three strong vibrational bands centered at 768, 727, and 626 cm^{-1} for the dimer, but in this range, the free ligand also has three bands centered at 761, 654, and 620 cm^{-1}, and the monomer possesses three bands at 761, 725, and 657 cm^{-1}. This makes identification of any bands which are due to Ru-O-Ru in this region difficult. The dimer has also a set of very strong vibrational bands in the region of 1050-1150 cm^{-1}, which are absent in the spectra of both the monomer and the free ligand. FTIR spectra of the dimers containing ^{16}O and ^{18}O in the ligand bridge were indistinguishable (Figure 4.19).

The dominant feature of the RR spectrum of the $(bpy)_2(OH_2)Ru^{IV}ORu^{III}(OH_2)(bpy)_2$ ion in acidic solution (0.5 M H_2SO_4) is an intense band appearing at 403 cm^{-1} (Figure 4.20); additional medium-intensity bands were found at lower frequencies (244, 272, 311, and 350

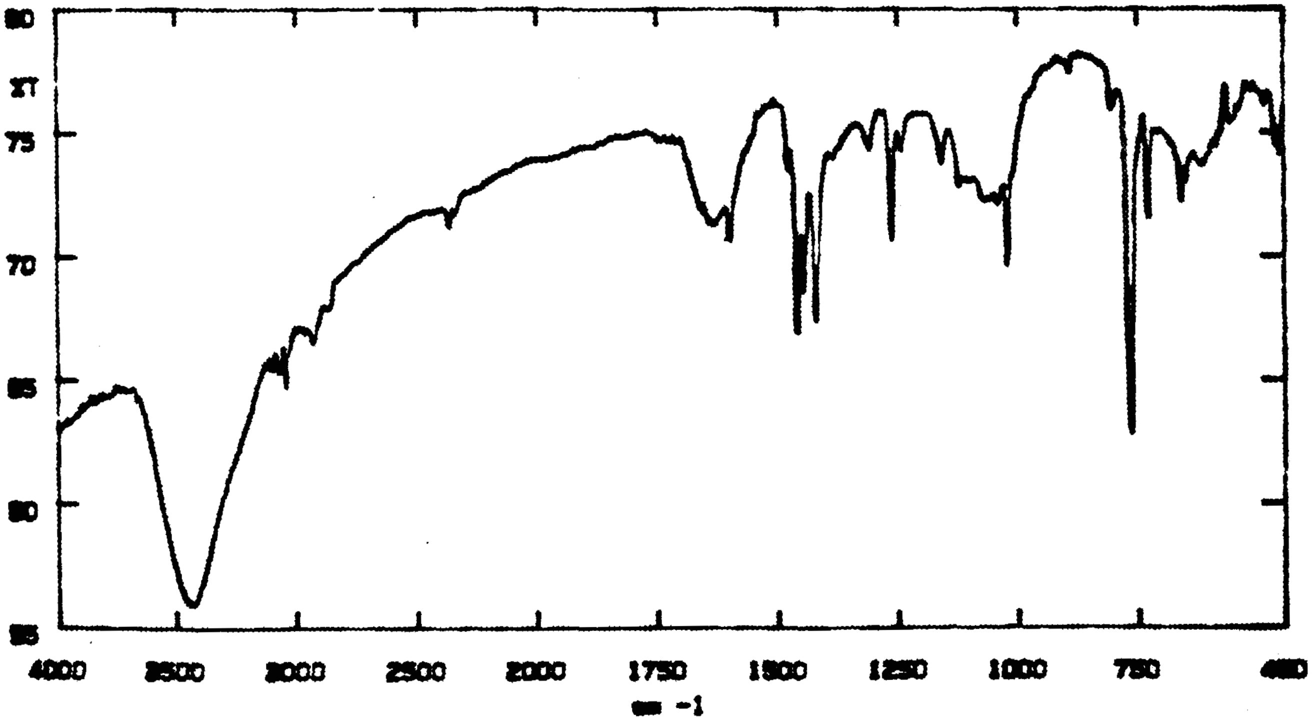

Figure 4.17. FTIR spectrum of $[(bpy)_2(OH_2)Ru^{III}ORu^{III}(OH_2)(bpy)_2](ClO_4)_4$ in KBr pellet.

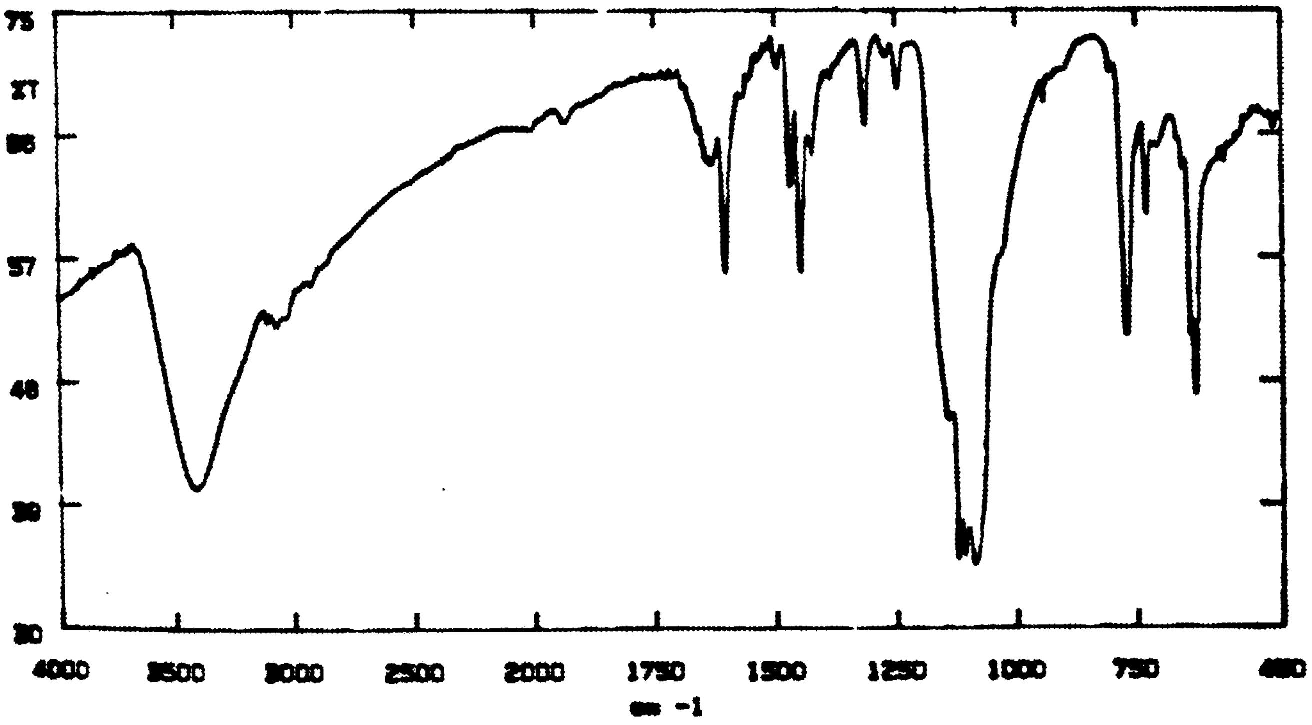

Figure 4.18. FTIR spectrum of $[(bpy)_2(OH_2)Ru^{III}ORu^{III}(OH_2)(bpy)_2](ClO_4)_4$ in KBR pellet.

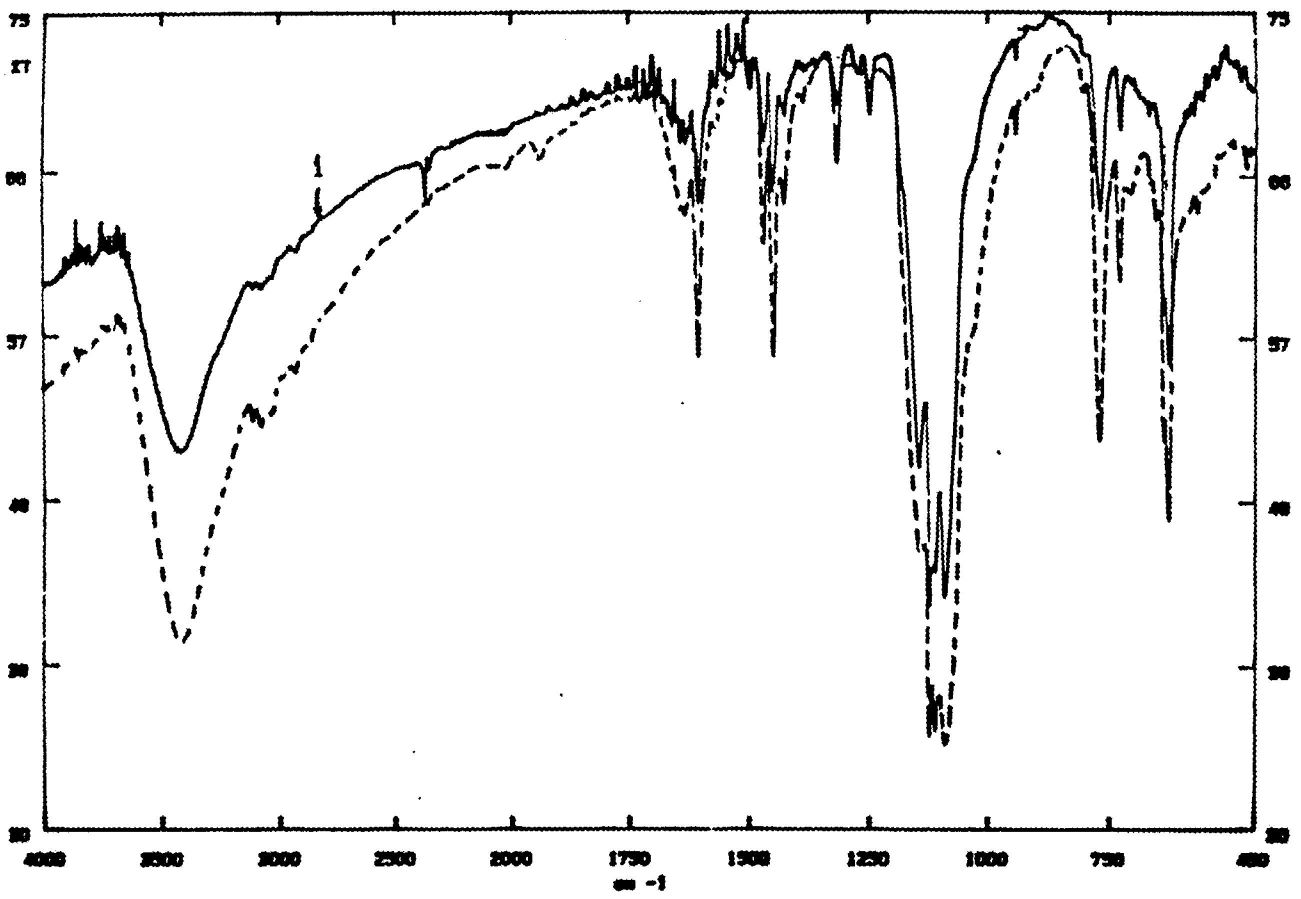

Figure 4.19. FTIR spectra of $[(bpy)_2(OH_2)Ru^{III}ORu^{III}(OH_2)(bpy)_2](ClO_4)_4$ in KBr pellet; solid line, -^{18}O; dashed line, -^{16}O.

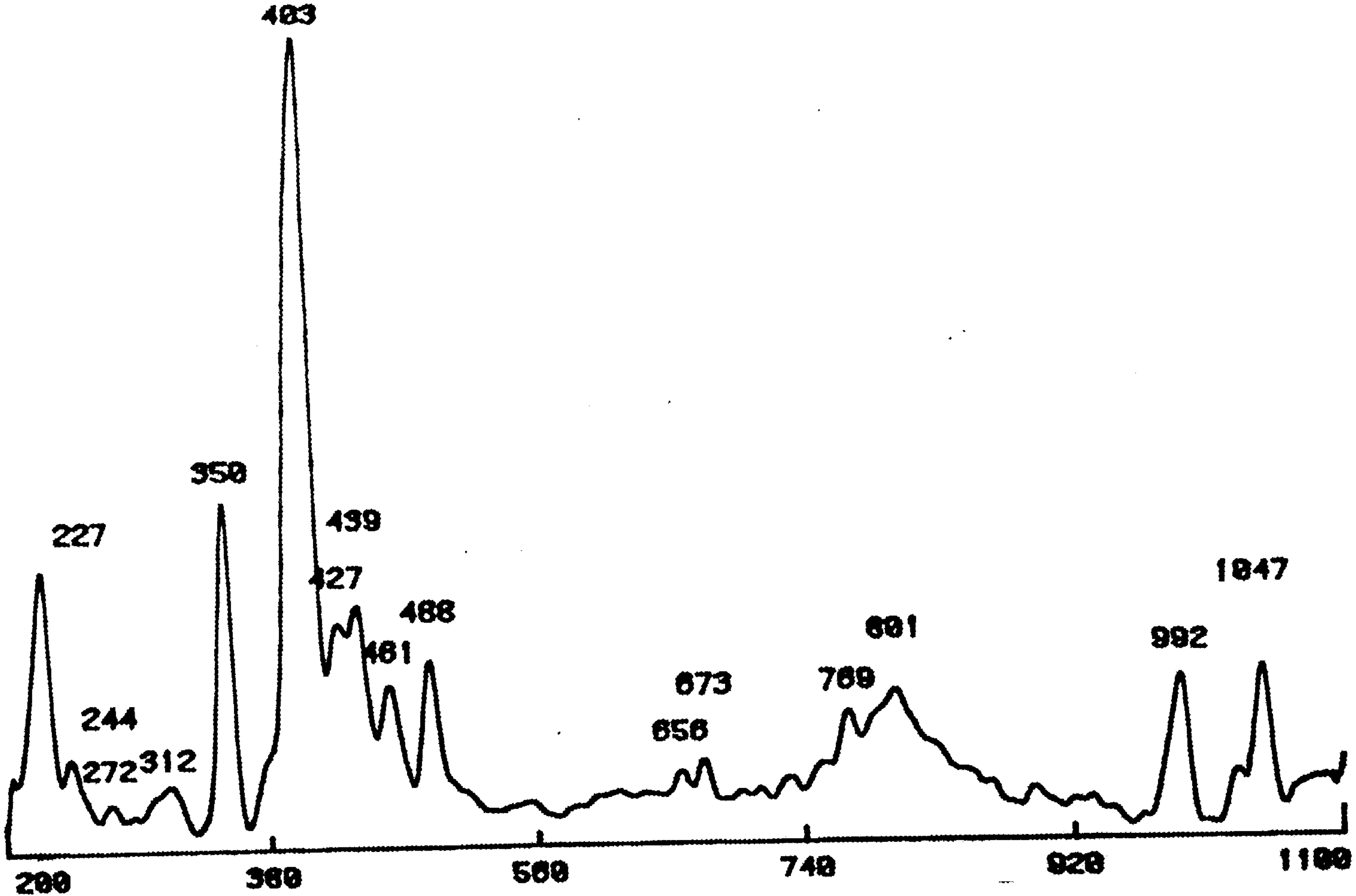

Figure 4.20. RR spectrum of 1 mM $(bpy)_2(OH_2)Ru^{IV}ORu^{III}(OH_2)(bpy)_2$ ion in 0.5 M H_2SO_4, with 50-mW excitation at 514 nm; average of 16 scans that was taken by backscattering from a capillary tube containing the frozen sample (90 K).

cm^{-1}), but a few medium and weak bands were observed at higher frequencies (441, 461, 488, 769, 801, 993, and 1046 cm^{-1}). Identical spectra were obtained in 1 M $HClO_4$ solution except that the band centered at 993 cm^{-1} (in 0.5 M H_2SO_4, oxidant $Ce(SO_4)_2$) was replaced by the band at 933 cm^{-1} (in 1 M $HClO_4$; oxidant $(NH_4)_2Ce(NO_3)_6$). The bands centered at 403, 801, and 311 cm^{-1} are interesting because they shifted to 394, 787, and 299 cm^{-1} when the dimer was prepared in ^{18}O-water (Figure 4.21). The spectral position of the dominant band was pH-sensitive and shifted progressively from 403 cm^{-1} at pH 0 to 392 cm^{-1} at pH 6. At pH 6, substitution of D_2O for normal water also caused small shifts in several bands including the dominant band which shifted from 392 to 387 cm^{-1} (Figure 4.22). To clarify whether or not exchange takes place between coordinated H_2O and solvent molecules in aqueous solution, spectra of $(bpy)_2(^{18}OH_2)Ru^{IV}(^{18}O)\ Ru^{III}(OH_2)(bpy)_2$ in normal water were determined during different times. It was found that the spectra were unchanged within 1 to 2 hours after oxidizing $(bpy)_2(^{18}OH_2)Ru^{III}(^{18}O)Ru^{III}(^{18}OH_2)(bpy)_2$ to $(bpy)_2(^{18}OH_2)Ru^{III}(^{18}O)Ru^{IV}(^{18}OH_2)(bpy)_2$ by three-fold excess Co^{3+} ion in normal water (Figure 4.23), but the spectra changed around 400 cm^{-1} when the sample was aged for 12 hours at room temperature (Figure 4.24) or heated at 70°C for 16 hours (Figure 4.25). From the difference spectra (Figure 4.26), we can see a minimum centered at 402 cm^{-1} and a maximum centered at 420 cm^{-1}, which account for these spectral changes. We ascribed this change to the replacement of the ^{18}O-water ligand by normal water. If this assignment is correct, this observation shows

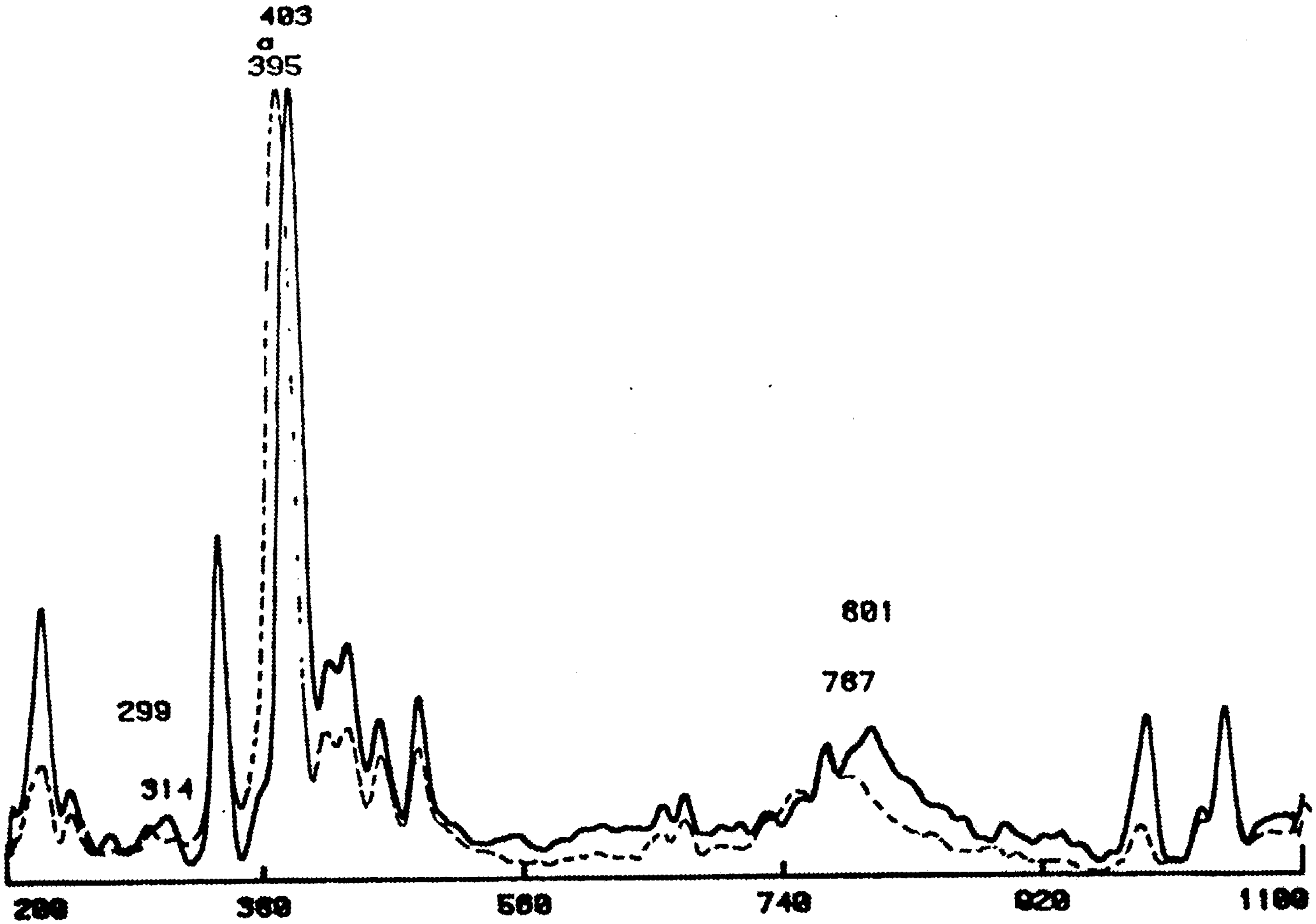

Figure 4.21. RR spectrum of 1 mM $(bpy)_2(OH_2)Ru^{IV}ORu^{III}(OH_2)(bpy)_2$, conditions as in Figure 4.20. Solid line, ^{16}O bridged; dashed line, ^{18}O bridged.

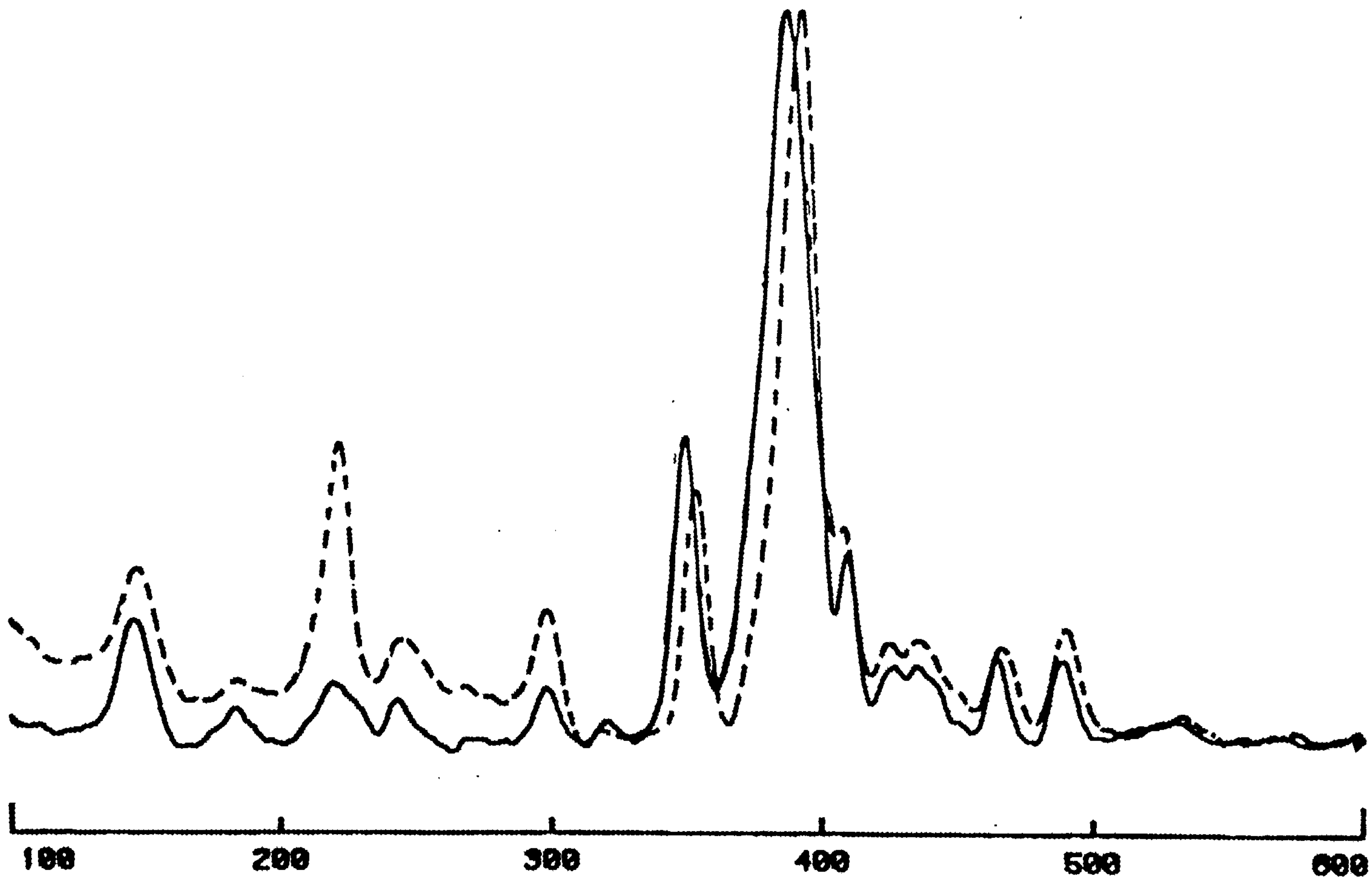

Figure 4.22. RR spectra of 1 mM $(bpy)_2(OH_2)Ru^{IV}ORu^{III}(OH_2)(bpy)_2$ prepared by CPE at 0.7 V vs. SCE in pH = 6 0.1 M phosphate solution; other conditions as in Figure 4.20. Solid line, D_2O as solvent; dashed line, H_2O as solvent.

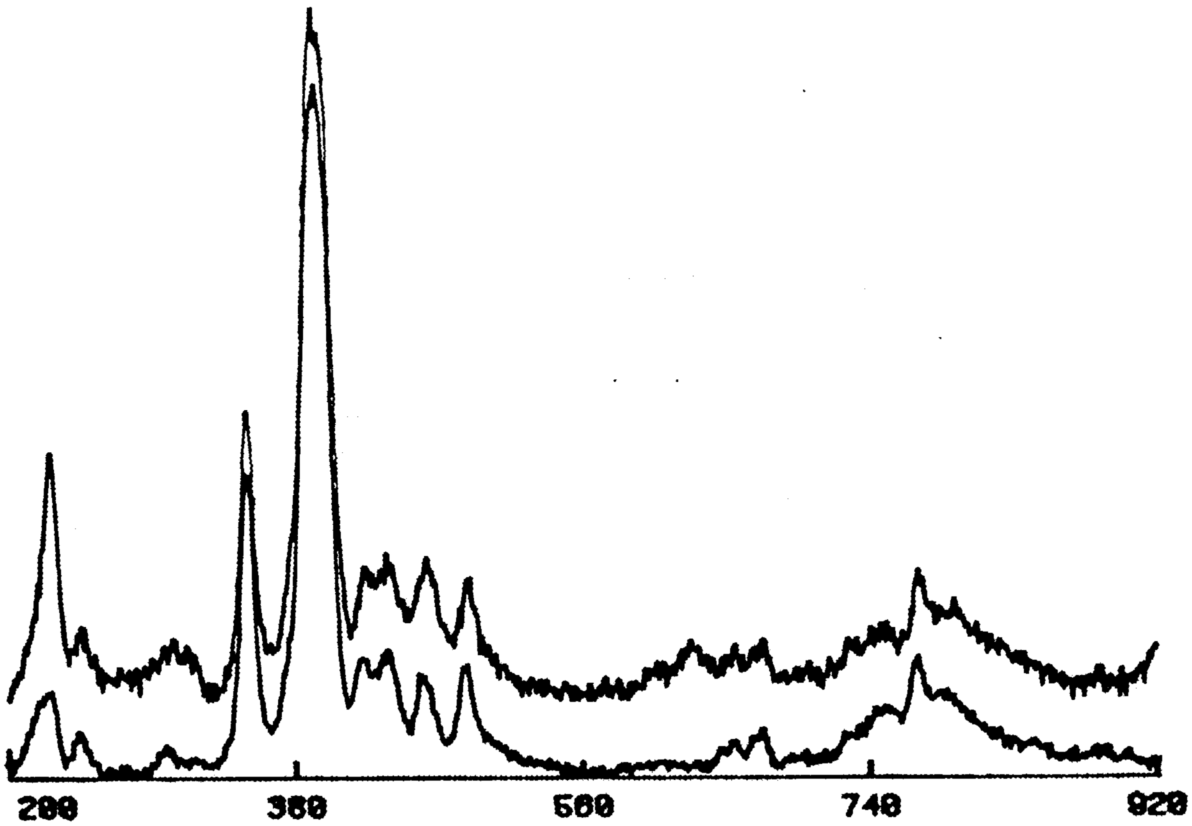

Figure 4.23. RR spectra of the samples that were prepared by adding three-fold excess Co^{3+} to 1 mM ^{18}O-labeled $(bpy)_2(OH_2)Ru^{III}ORu^{III}(OH_2)(bpy)_2$ in 0.5 M H_2SO_4; other conditions as in Figure 4.20. Upper trace: spectrum measured immediately after preparation; lower trace: two hours after preparation.

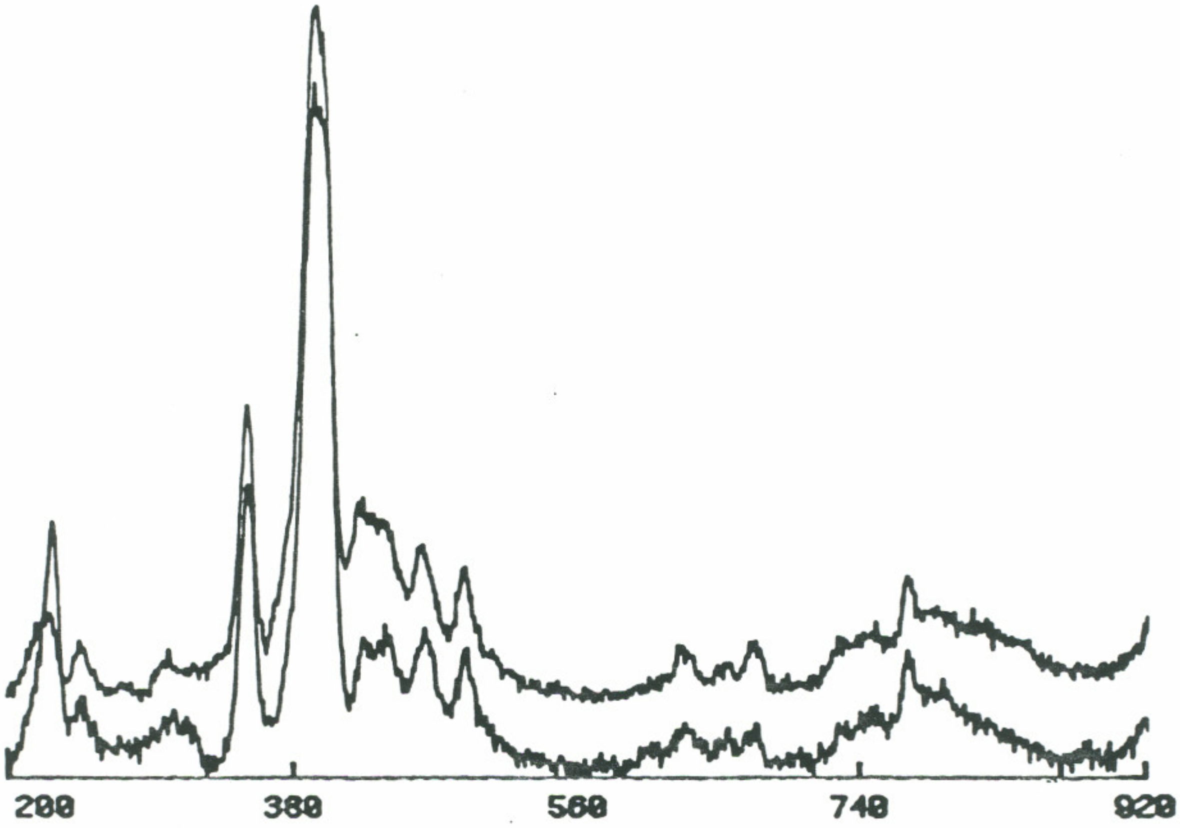

Figure 4.24. RR spectra of the samples that were prepared by adding three-fold excess Co^{3+} to 1 mM ^{18}O-labeled $(bpy)_2(OH_2)Ru^{III}ORu^{III}(OH_2)(bpy)_2$ in 0.5 M H_2SO_4; other conditions as in Figure 4.20. Upper trace: at room temperature 12 hours after preparation; lower trace: 2 hours after preparation.

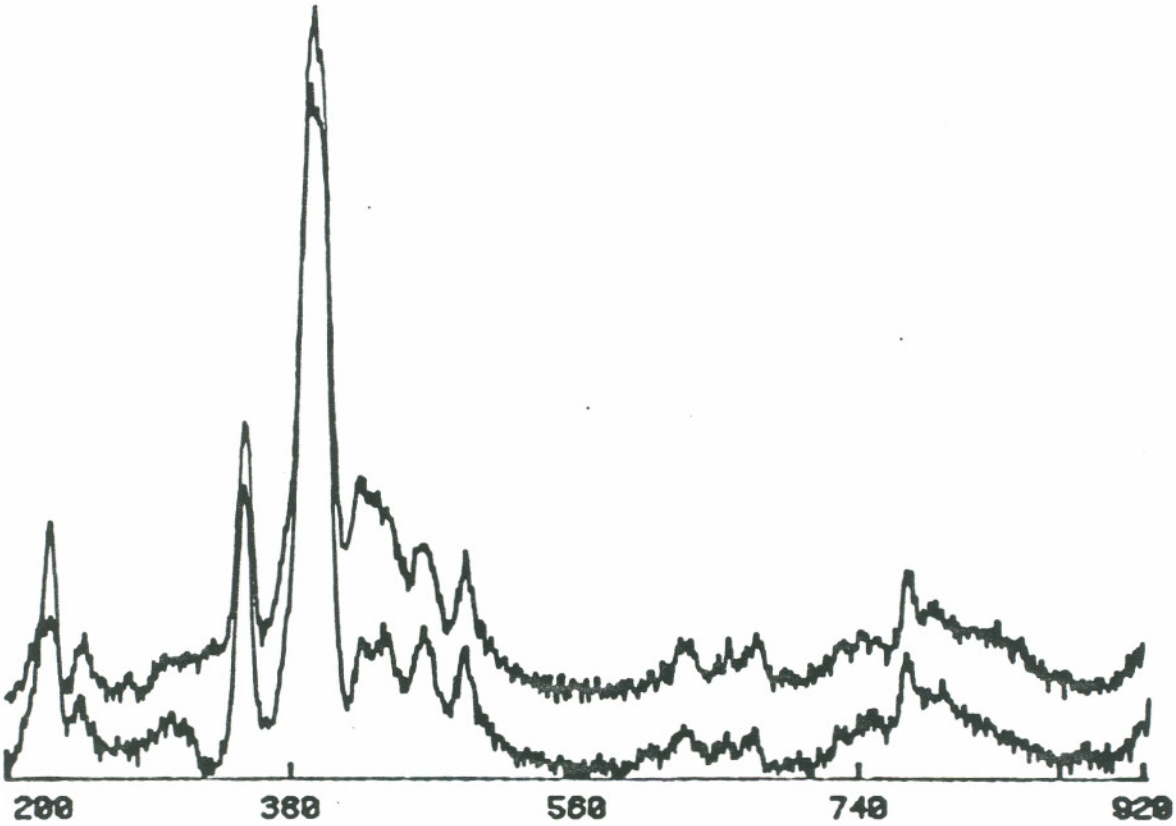

Figure 4.25. RR spectra, conditions are as in Figure 4.24. Upper trace: heated at 70°C 16 hours after preparation; lower trace: 2 hours after preparation.

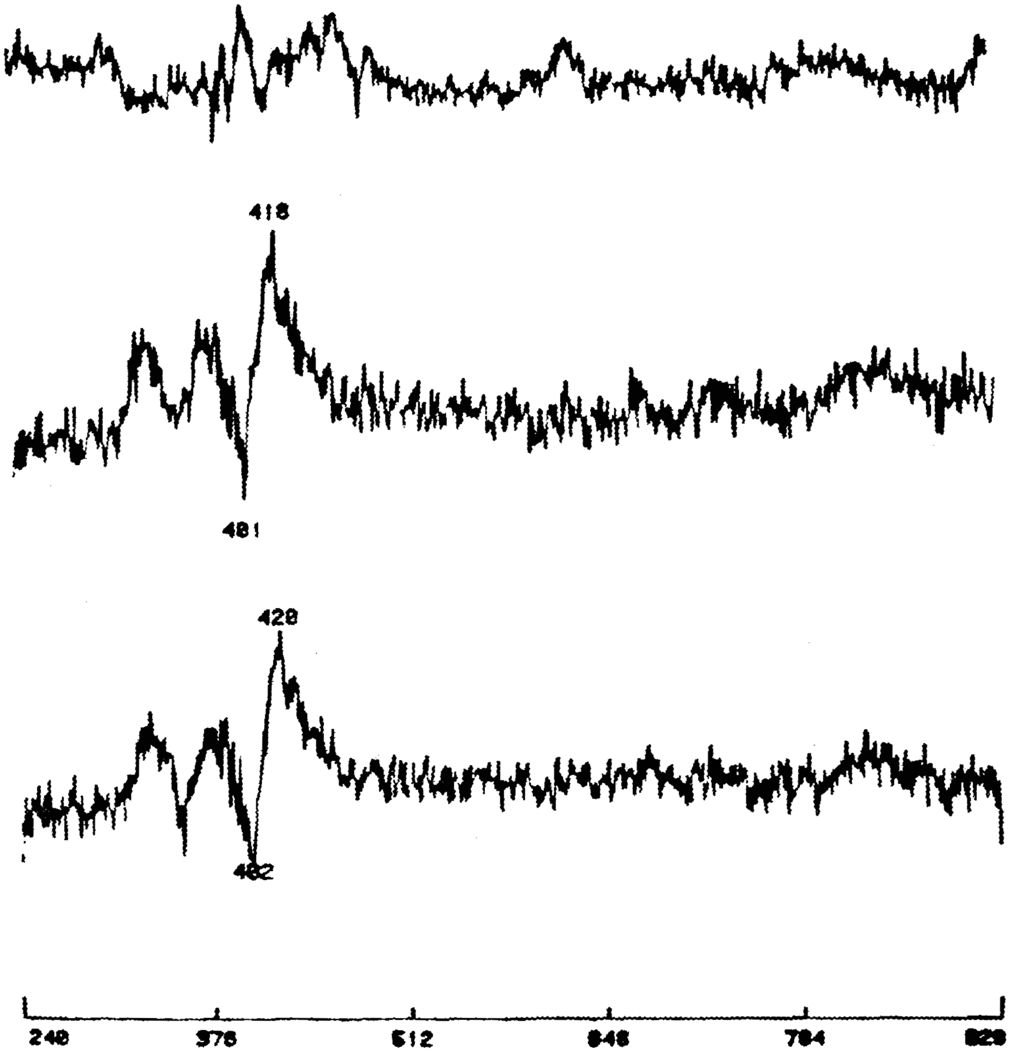

Figure 4.26. RR difference spectra 1 mM $(bpy)_2(OH_2)Ru^{III}$–O–$Ru^{IV}(OH_2)(bpy)_2$ ion in 0.5 M H_2SO_4 from single turnover experiments Minus: upper trace, the spectrum of a reference sample taken 2 hours after preparation; middle trace, 12 hours after preparation; lower trace, heated at 70°C for 16 hours ater preparation. Conditions as in Figure 4.20.

that no exchange between aqua ligands of the ion and water molecules of the solvent occurs within a few hours and that carrying the $(bpy)_2(OH_2)Ru^{III}ORu^{III}(OH_2)(bpy)_2$ ion through its catalytic cycle also does not promote exchange of coordinated H_2O with solvent.

The spectra entirely changed after heating at 70°C for 40 hrs (Figure 4.27). The dominant band centered at 394 cm^{-1} shifted to 389 cm^{-1}, and the relative intensity decreased substantially as three new intense bands appeared in the range of 800-850 cm^{-1}.

The dominant feature of the RR spectra of the $(bpy)_2(OH_2)Ru^{III}ORu^{III}(OH_2)(bpy)_2$ ion in acidic and neutral media is an intense band centered at 377 cm^{-1} which appears as a doublet that probably arises from an overlapping small peak at 367 cm^{-1} (Figure 4.28); additional medium and weak bands were found at lower and higher frequencies. When ^{16}O was replaced by ^{18}O in the ligand bridge, the band at 377 cm^{-1} was shifted to 367 cm^{-1}; whereas a small peak remained at 377 cm^{-1} (Figure 4.29). The difference spectrum (Figure 4.30) shows that the shift is due to a single band. Another band which was sensitive to isotope substitution in the ligand bridge was centered at 746 cm^{-1}. When ^{16}O was replaced by ^{18}O in the ligand bridge, the band shifted to 736 cm^{-1}. The lower-frequency isotope-sensitive band existing in the $(bpy)_2(OH_2)Ru^{IV}ORu^{III}(OH_2)(bpy)_2$ ion at around 300 cm^{-1} was not observed in the $(bpy)_2(OH_2)RuI^{II}ORu^{III}(OH_2)(bpy)_2$ ion. When the pH was increased to 8, the band at 378 cm^{-1} shifted to 375 cm^{-1}, and the small peak at 367 cm^{-1} disappeared. Increasing the pH to 10 caused no further changes in the RR spectrum. In D_2O, the relative heights of the two peaks at 367 and 377 cm^{-1} inverted from the order seen in normal

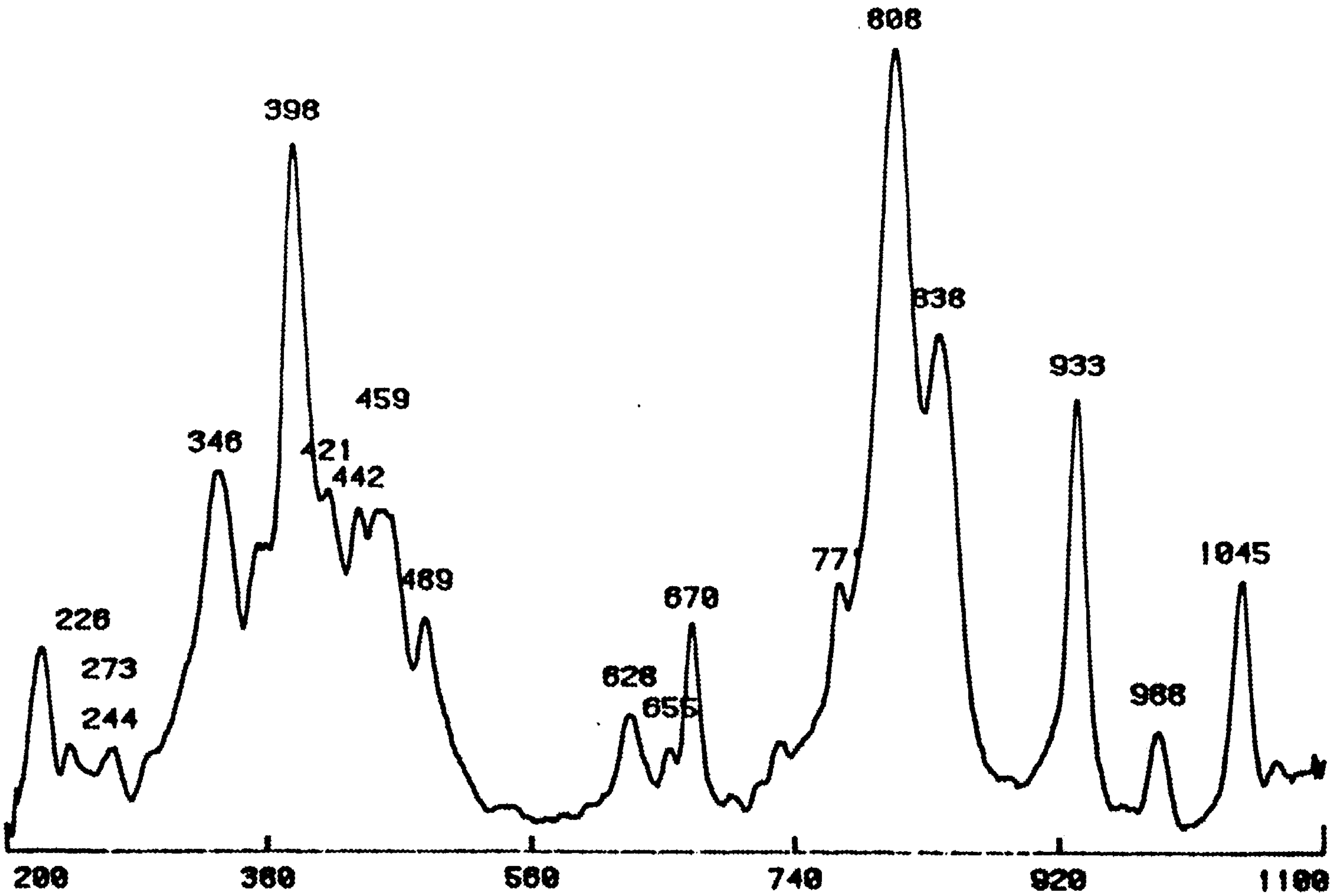

Figure 4.27. RR spectrum of the sample that was prepared by adding five-fold excess Co^{3+} to 1 mM $(bpy)_2(OH_2)Ru^{III}ORu^{III}(OH_2)(bpy)_2$ and heated 40 hours at 70° C; other conditions as in Figure 4.20.

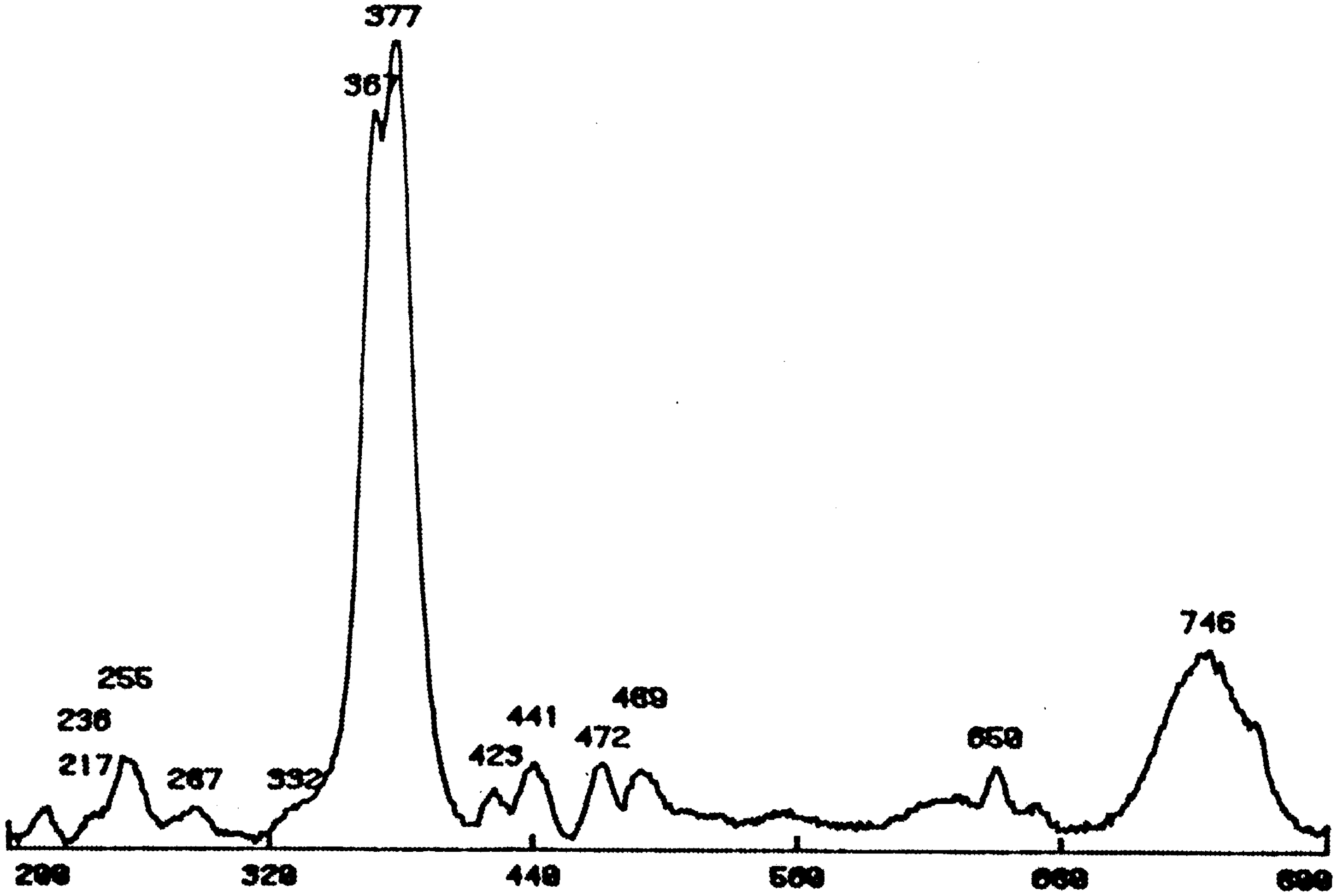

Figure 4.28. RR spectrum of 1.0 mM $(bpy)_2(OH_2)Ru^{III}ORu^{III}(OH_2)(bpy)_2$ ion in pH 6, 20 mM phosphate solution, with 60-mW excitation at 647 nm; other conditions as in Figure 4.24.

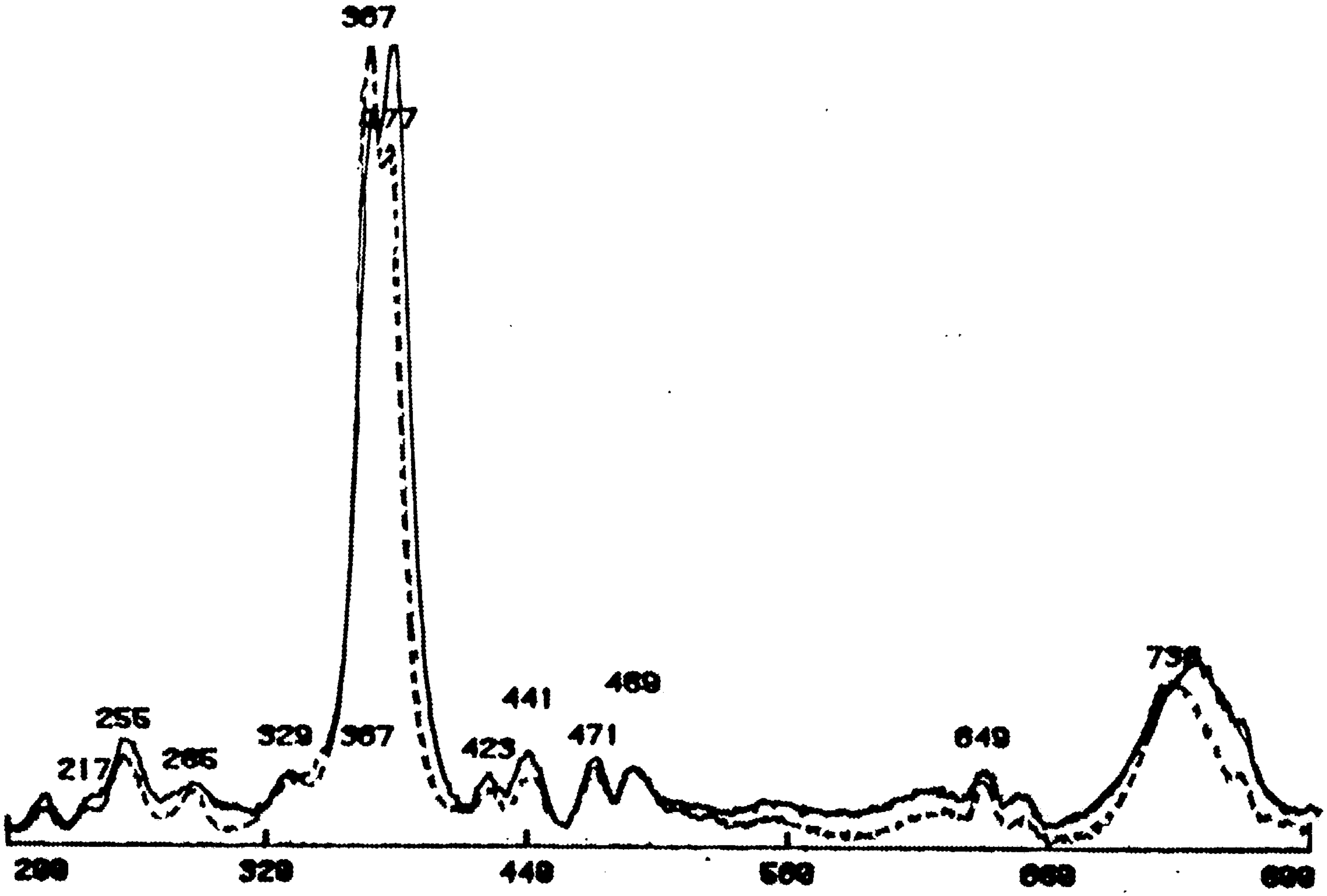

Figure 4.29. RR spectra of 1 mM $(bpy)_2(OH_2)Ru^{III}ORu^{III}(OH_2)(bpy)_2$; conditions as in Figure 4.28. Solid line, ^{16}O bridged; dashed line, ^{18}O bridged.

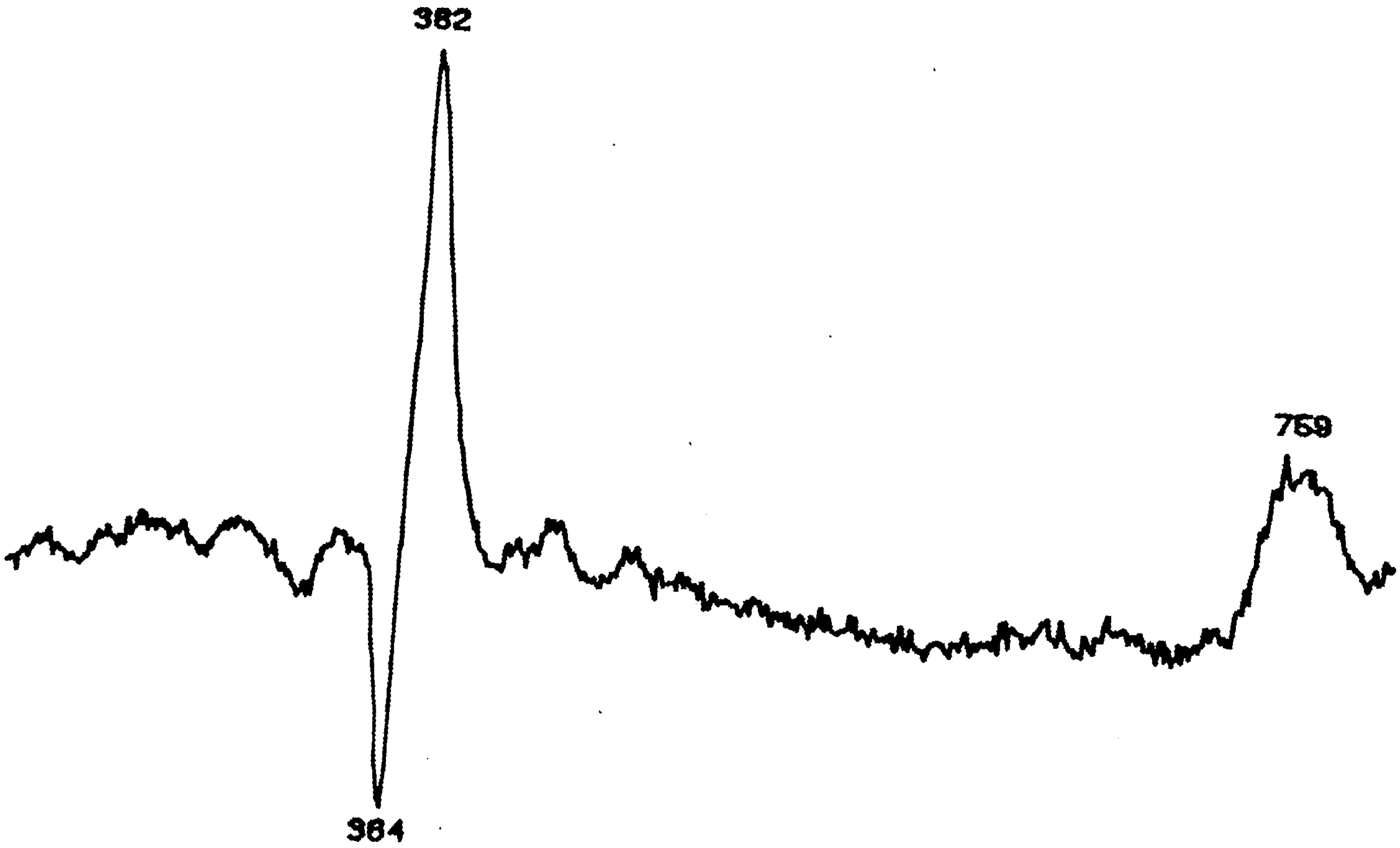

Figure 4.30. RR difference spectrum. Conditions are as in Figure 4.29, ^{16}O minus ^{18}O.

water, i.e., in normal water the peak at 367 cm^{-1} was higher than the peak at 377 cm^{-1}, but in D_2O the peak at 377 cm^{-1} was higher than the peak at 367 cm^{-1} (Figure 4.31). This effect is attributable to the shifting of a single band within the intense envelope, most likely the dominant band of the cluster, suggested by the D_2O minus H_2O difference spectrum (Figure 4.32).

The band in the $(bpy)_2(OH_2)RuI^{II}ORu^{IV}(OH_2)(bpy)_2$ ion centered at 403 cm^{-1} can be assigned to the symmetric stretching vibration mode. When ^{16}O was replaced by ^{18}O in the ligand bridge, the band shifted from 403 to 394 cm^{-1}, confirming this assignment. In addition, a weak band centered at 801 cm^{-1} which is sensitive to isotope substitution in the ligand bridge can be assigned to the asymmetric vibration stretching mode or possibly an overtone of the 403 cm^{-1} band. The other isotope-sensitive band centered at 311 cm^{-1} can be assigned to the bending vibration mode coupled to other ligand vibrations in the complex, most likely the stretching motion of the ligand atom trans to the μ-oxo bridge. By analogy, the band centered at 377 cm^{-1} in the $(bpy)_2(OH_2)Ru^{III}ORu^{III}(OH_2)(bpy)_2$ ion can be assigned to symmetric stretching vibration mode, whereas the band centered at 746 cm^{-1} can be assigned to the asymmetric band or first overtone of the band at 377 cm^{-1}.

The D_2O-induced shift in ν_s for $(bpy)_2(OH_2)Ru^{IV}ORu^{III}(OH_2)(bpy)_2$ ion is thought to arise from hydrogen bonding between an oxygen atom in the ligand bridge and the solvent.[122]

A possible explanation for the shift in ν_s from 403 to 377 cm^{-1} upon one-electron reduction of the $(bpy)_2(OH_2)Ru^{III}ORu^{IV}(OH_2)(bpy)_2$ ion

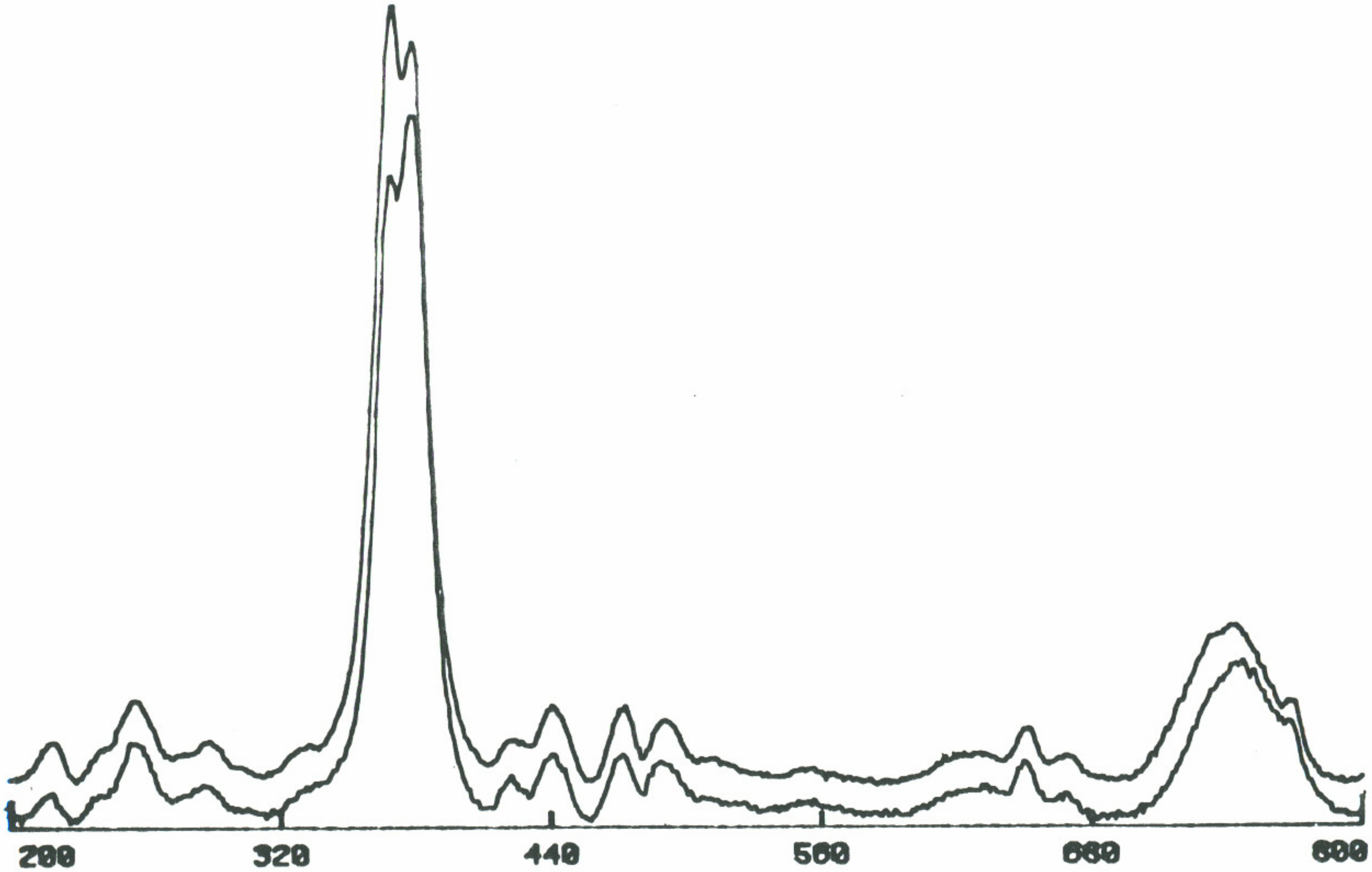

Figure 4.31. RR spectra of 1 mM $(bpy)_2(OH_2)Ru^{III}ORu^{III}(OH_2)(bpy)_2$ ion in 20 mM PO_4^{3-} (pH 6). Conditions are as in Figure 4.20. Upper trace: solvent was D_2O; lower trace: solvent was normal water.

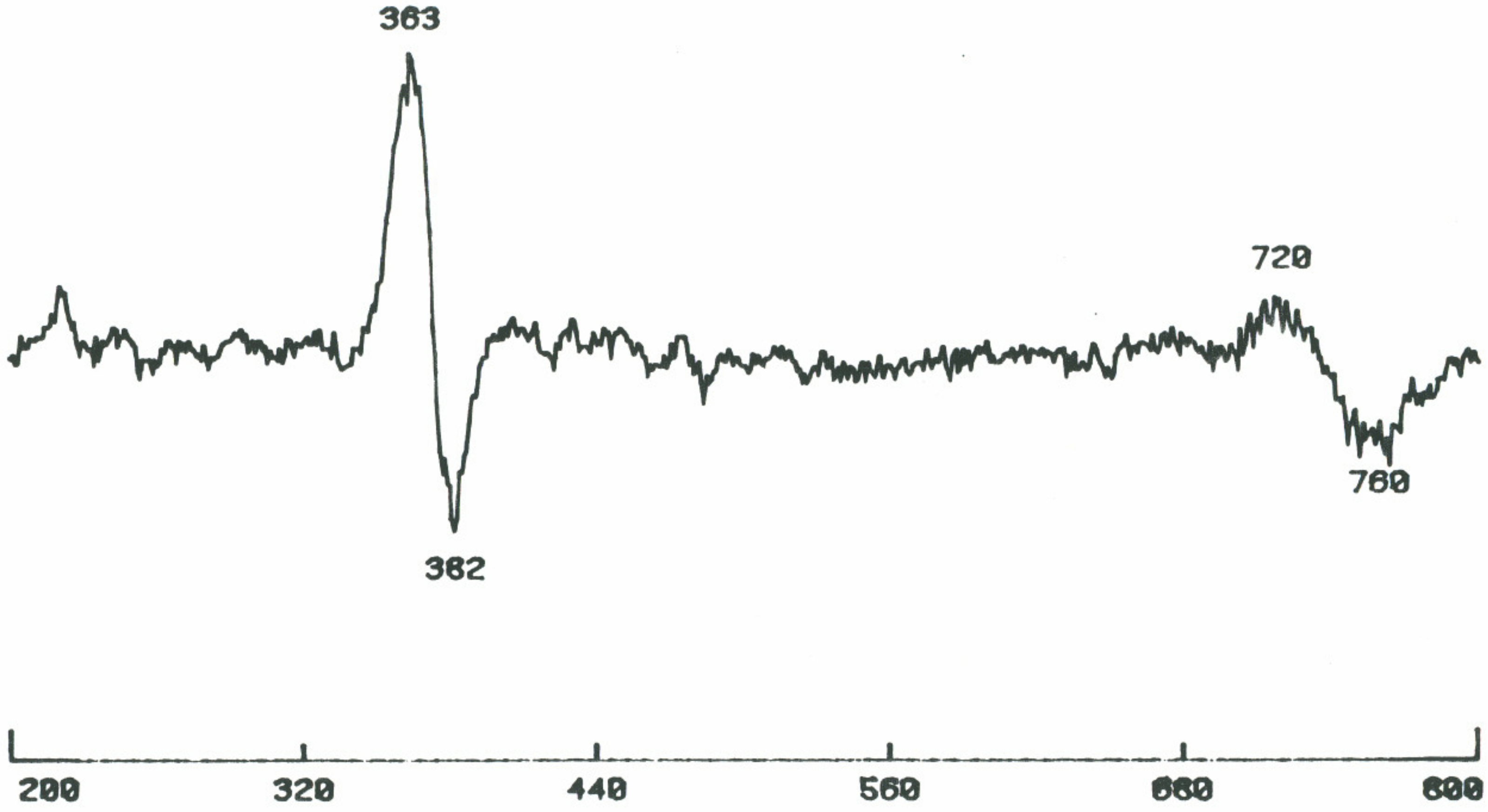

Figure 4.32. RR difference spectrum, D_2O minus H_2O. Conditions are as in Figure 31.

to $(bpy)_2(OH_2)Ru^{III}ORu^{III}(OH_2)(bpy)_2$ ion can be found by consideration of the Dunitz-Orgel bonding mode (Figure 4.16). One of thirteen valence electrons (four from oxygen and nine from two ruthenium atoms) of the complex $(bpy)_2(OH_2)Ru^{IV}ORu^{III}(OH_2)(bpy)_2$ is in the antibonding orbital while the others are in non-bonding or bonding orbitals. For the complex ion $(bpy)_2(OH_2)Ru^{III}ORu^{III}(OH_2)(bpy)_2$, an extra electron must be put into the antibonding orbital. Since the extra electron in $(bpy)_2(OH_2)Ru^{III}ORu^{III}(OH_2)(bpy)_2$ ion goes into antibonding orbital, the bond strength between oxygen and ruthenium atoms in the segment Ru-O-Ru decreases. This argument assumes equal Ru-O-Ru bond angles in the $(bpy)_2(OH_2)Ru^{III}ORu^{III}(OH_2)(bpy)_2$ and $(bpy)_2(OH_2)Ru^{III}ORu^{IV}(OH_2)(bpy)_2$ ions. Actually, based upon their isotopic shifts ($403 - 394 = 9\ cm^{-1}$) for $(bpy)_2(OH_2)Ru^{III}ORu^{IV}(OH_2)(bpy)_2$ and ($377 - 367 = 10\ cm^{-1}$) for $(bpy)_2(OH_2)Ru^{III}ORu^{III}(OH_2)(bpy)_2$), the Ru-O-Ru angles in both ions are estimated to be about 150°.[115,125]

We have found that the frequencies of the symmetric stretching vibration bands for the $(bpy)_2(OH_2)Ru^{IV}ORu^{III}(OH_2)(bpy)_2$ ion shifted from 404 to 401 to 392 cm^{-1} as pH varies from 0 to 2 to 6; and its pK_{a1} and pK_{a2} are 0.4 and 3.3, respectively,[11] corresponding to deprotonation of one and both aqua ligands at pH 2 and 6, respectively. The stronger σ-donation by OH^- increases the electron density of the antibonding orbital, thus weakening the bonding interaction in the μ-oxo bridge and shifting ν_s to lower values.

4.2.5 Redox Potentiometry

Cyclic voltammetry was performed in order to understand the effect of substituents and solvents on the redox properties of the monomeric and μ-oxo dimeric complexes.

(1) Cyclic voltammetry of $RuL_2(OH_2)_2$ monomeric complexes in aqueous solution

Figure 4.33 shows a typical cyclic voltammogram of $Ru^{II}(5,5'\text{-diester})_2(OH_2)_2{}^{2+}$ in deaerated 0.5 M H_2SO_4 solution. The current-voltage curve displays oxidative and reductive peak potentials at 805 and 746 mV vs. SCE, respectively. The 59-mV peak separation indicates a reversible one-electron oxidation of the ion to the corresponding Ru^{III} complex:

$$Ru^{II}(5,5'\text{-diester})_2(OH_2)_2{}^{2+} \rightleftharpoons Ru^{III}(5,5'\text{-diester})_2(OH_2)_2{}^{3+} + e^-$$

The halfwave redox potential, $E_{1/2}$, derived from Figure 4.33, is 776 mV vs. SCE. Figure 4.34 shows a cyclic voltammogram of $Ru^{II}(4,4'\text{-diester})_2(OH_2)_2{}^{2+}$ in 0.5 M H_2SO_4 solution. Oxidative and reductive waves are at 880 and 771 mV vs. SCE, respectively, indicating quasi-reversible behavior. The midpoint potential is 826 mV vs. SCE.

In Table 4.6, we compare half-wave potentials of three monomeric complexes, $Ru^{II}(bpy)_2(OH_2)_2{}^{2+}$, $Ru^{II}(5,5'\text{-diester})_2(OH_2)_2{}^{2+}$, and $Ru^{II}(4,4'\text{-diester})_2(OH_2)_2{}^{2+}$. $Ru^{II}(bpy)_2(OH_2)_2{}^{2+}$ exhibits the lowest redox potential followed by $Ru^{II}(5,5'\text{-diester})_2(OH_2)_2{}^{2+}$ and $Ru^{II}(4,4'\text{-diester})_2(OH_2)_2{}^{2+}$. This clearly indicates that the electron-withdrawing groups shift the reduction potential to higher values, stabilizing the lower oxidation state.

This behavior is consistent with the spectral red shifts discussed above. However, interpretation of the results in terms of changes in

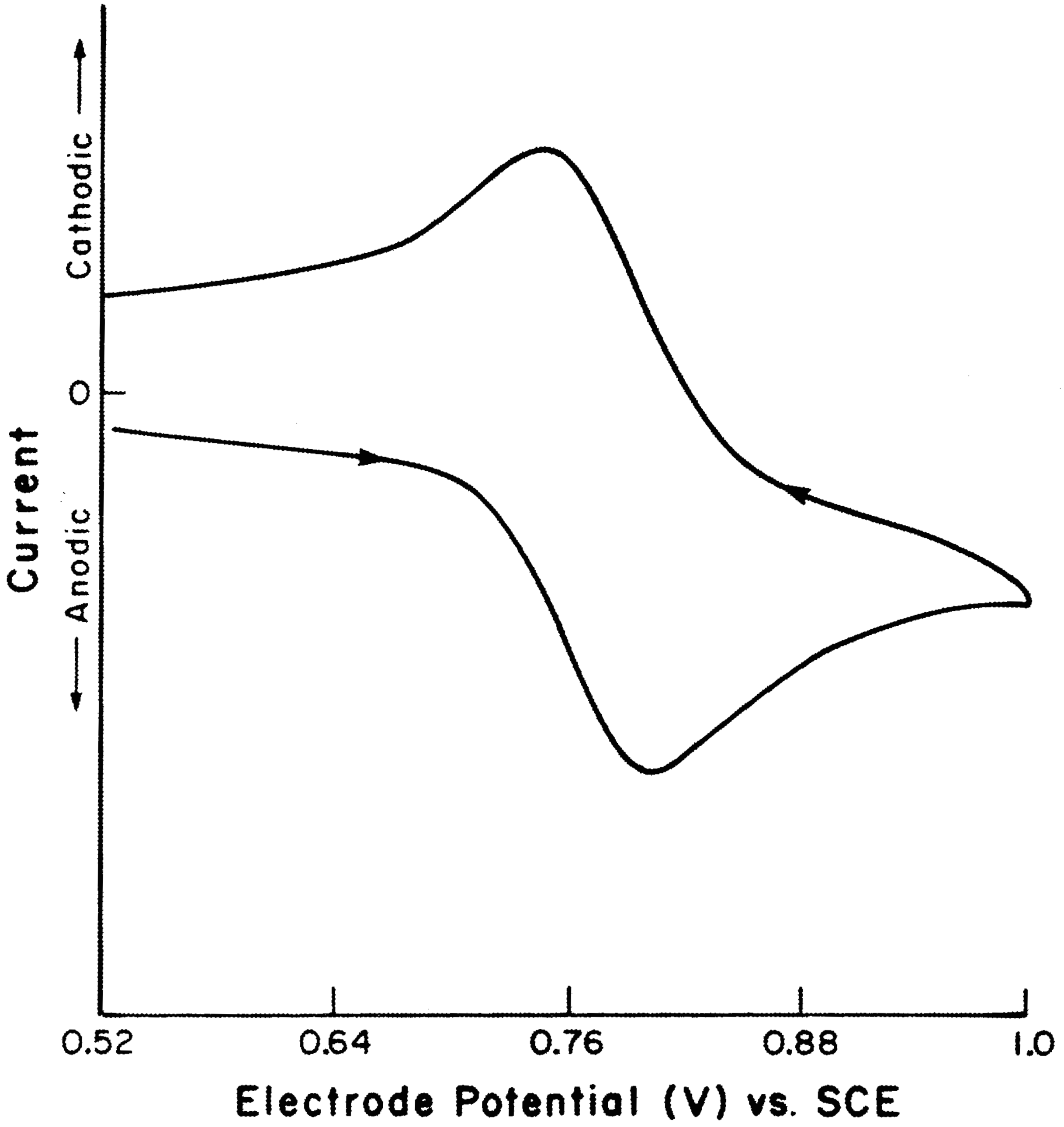

Figure 4.33. Cyclic voltammogram of 1 mM Ru(5,5'-diester)$_2$(OH$_2$)$_2$ ion in 0.5 M H_2SO_4. Glassy carbon, saturated calomel, and Pt wire are the working, reference, and counter electrodes, respectively. Scan rate = 50 mV/sec.

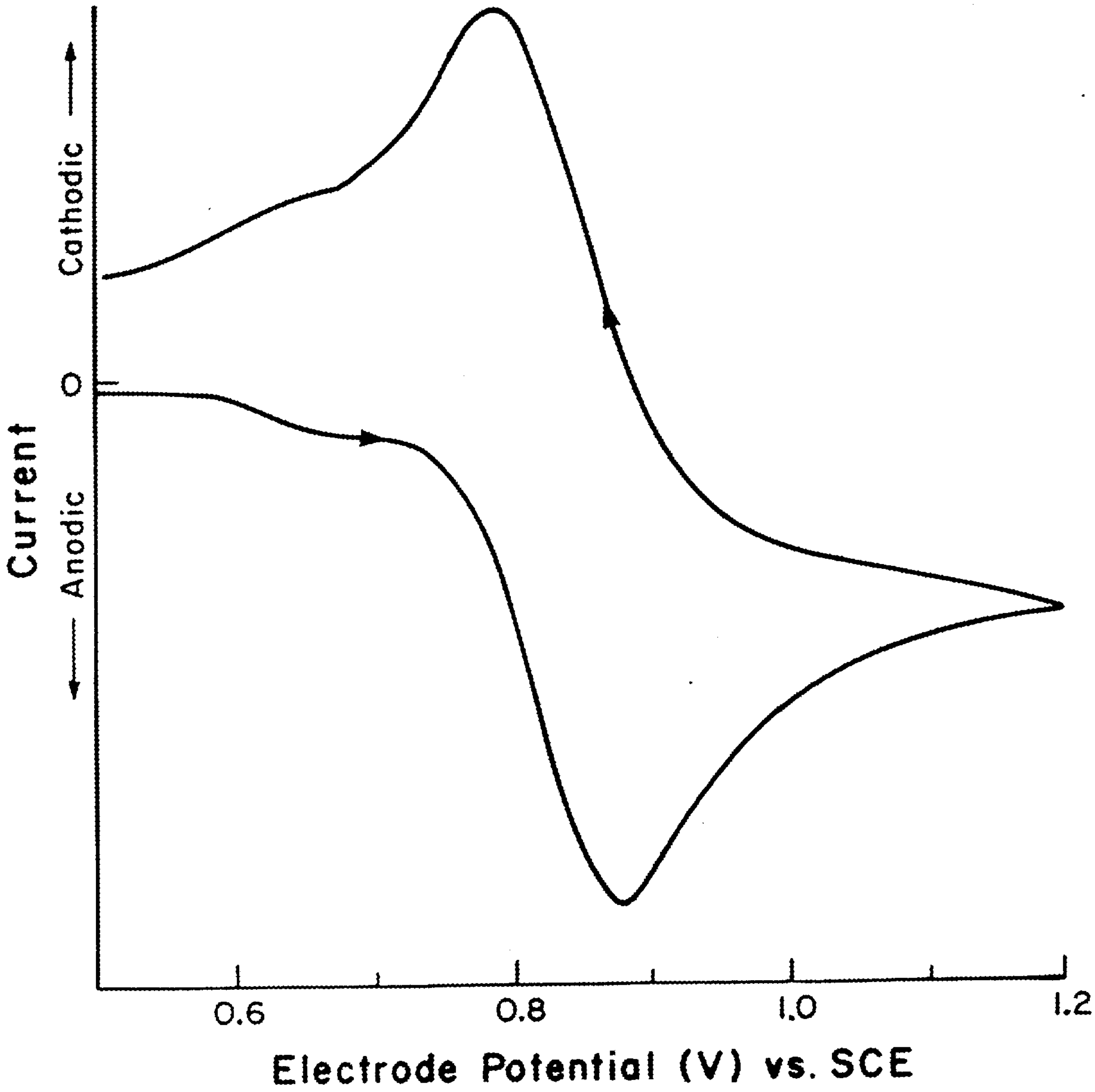

Figure 4.34. Cyclic voltammogram of 1 mM Ru(4,4′-diester)$_2$(OH$_2$)$_2$ ion in 0.5 M H_2SO_4. In-doped SnO_2, working electrode; scan rate = 50 mV/sec.

Table 4.6. Redox Potentials of Three Monomeric Complexes

Complex	Medium	$E_{1/2}$ (mV)
$Ru^{II}(bpy)_2(OH_2)_2{}^{2+}$	1 M CF_3COOH	630[a]
$Ru^{II}(5,5'\text{-diester})_2(OH_2)_2{}^{2+}$	0.5 M H_2SO_4	776
$Ru^{II}(4,4'\text{-diester})_2(OH_2)_2{}^{2+}$	0.5 M H_2SO_4	826

[a] From reference 109.

ground-state energies is more straightforward in redox potentiometry because the reference state is the free electron in vacuum. A positive shift in the redox potential can be interpreted as a decrease in the ground-state energy level, provided that the solvation energies of oxidized and reduced states do not differ much in the ions being compared. The observation that the electron-withdrawing groups positively shift the reduction potential indicates that the reduced-state energy decreases relative to the oxidized state.

From the standpoint of electrostatics, it is understandable that the electron-withdrawing groups on the bpy rings make the reduced state more stable relative to the oxidized state than unsubstituted bpy. In addition, the greater effect at the ring 4,4'-positions in comparision to the ring 5,5'-positions on the redox potential (Table 4.6) can be understood in terms of the greater electron density at positions that are ortho and para to the substituents than at meta positions. Thus, the 4,4'-COOEt substituents which are para to the ligating N-atom are in a position to promote metal t_2 orbital-ligand backbonding by conjugative effects, whereas 5,5'-COOEt substituents can only influence the electronic distribution through inductive withdrawal of electron density.

(2) Solvent effect on the redox potentials of several monomeric complexes.

Half-wave reduction potentials, $E_{1/2}$ ($Ru^{III/II}$), of several monomeric complexes, $Ru^{II}(bpy)_2Cl_2$, $Ru^{II}(4,4\text{-diester})_2Cl_2$, $Ru^{II}(4,4'\text{-dimethoxy})_2Cl_2$, $Ru^{II}(5,5'\text{-diester})_2Cl_2$, and $Ru^{II}(bpy)_3Cl_2$, taken in various solvents are given in Table 4.7. From the table, we can see that the solvents have considerable influence on the $E_{1/2}$, but we cannot directly compare these $E_{1/2}$ in the different solvents because they are referred to as different standard states. To compare the $E_{1/2}$ of a solute in different solvents, we must refer to the same original point, i.e, zero potential. At present, the $E_{1/2}$ of ferricinium-ferrocene ($Fe(C_5H_5)_2^{+/o}$) couple is extensively used as zero potential,[96,97,111] i.e., the $E_{1/2}(Fc^{+/o})$ of this pair is considered as solvent independent. So we can simply regard the $E_{1/2}$ in all solvents as zero.

The $E_{1/2}(Fc^{+/o})$ is used to correct the $E_{1/2}$ of all monomeric complexes in different solvents as follows: subtract $E_{1/2}(Fc^{+/o})$ from $E_{1/2}$ of the monomeric complexes in the same solvent and call the difference the corrected $E_{1/2}$. The corrected $E_{1/2}$ of the monomeric complexes in different solvents is plotted as a function of DN of the corresponding solvents (Figure 4.35). A series of linear relationships is obtained, one for each complex ion. From Figure 4.35, we find that the $E_{1/2}$ of a given complex decreases with increasing DN of the solvent.

We use the following thermodynamic cycle to discuss the solvent effect:

Table 4.7. Half-wave Potentials for Several Monomers in Different Non-Aqueous Solutions[a]

	Half-wave Potential (V) vs. SCE					
Solvent(AN)	$Ru(bpy)_2$	$Ru(bpy)_3$	Ru(55ester)	Ru(44ester)	Ru(44me)	Fc^+/Fc[b]
DMSO(19.3)	.366	1.24	.592	.626	.148	.439
DMF(16.0)	.345	1.29	.588	.607	.130	.493
PC(18.3)	.310	1.21	.533	.564	.111	.328
MeCN(19.3)	.286	1.26	.519	.548	.028	.342
NM(20.5)	.275	1.28	.606	.539	.067	.147

[a] $Ru(bpy)_2$ = $Ru^{II}(bpy)_2Cl_2$; $Ru(bpy)_3$ = $Ru^{II}(bpy)_3(ClO_4)_2$;

Ru(55ester) = Ru^{II}(5,5'-diester)$_2Cl_2$;

Ru(44ester) = Ru^{II}(5,5'-diester)$_2Cl_2$;

Ru(44me) = Ru^{II}(4,4'-dimethoxy)$_2Cl_2$;

Fc^+/Fc = ferricinium/ferrocene couple

DMSO = dimethylsulfoxide; DMF = dimethylformamide;

MeCN = acetonitrile;

PC = propylene carbonate; NM = nitromethane.

Supporting electrolyte: 0.1 M tetrabutylammonium hexafluorophosphate.

[b] From reference 111.

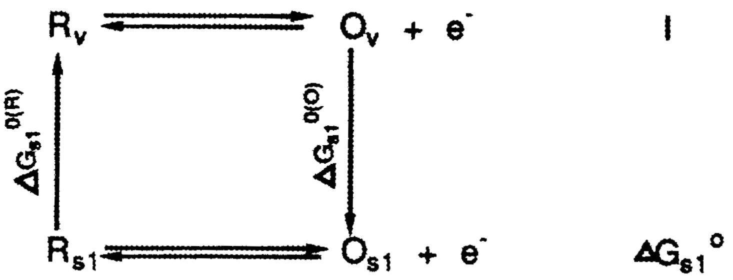

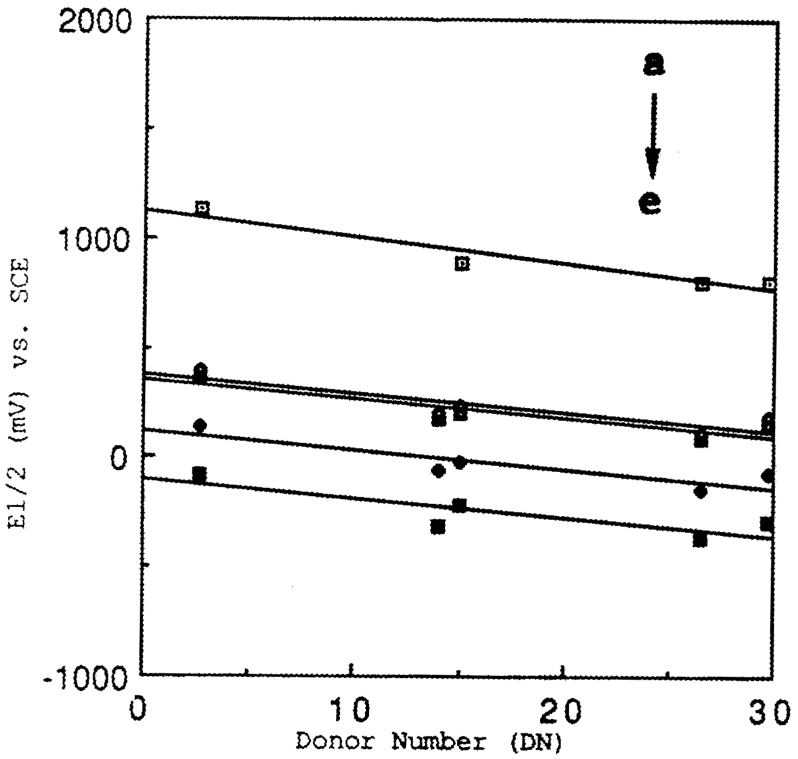

Figure 4.35. **Relationship between reduction potentials of RuL_2Cl_2** complexes in various solvents and corresponding solvent DN.

a. $Ru(bpy)_3Cl_2$; b. $Ru(4,4'\text{-diester})_2Cl_2$; c. $Ru(5,5'\text{-diester})_2Cl_2$; d. $Ru(bpy)_2Cl_2$; e. $Ru(4,4'\text{-dimethoxy})_2Cl_2$.

where R and O are reduced and oxidized states, subscripts S_1 and v are solvent and vacuum, I is ionization potential, $\Delta G_{s1}{}^{o}(O)$ and $\Delta G_{s1}{}^{o}(R)$ are solvation energies of the oxidized and reduced states in the solvent S_1 and $\Delta G_{s1}{}^{o}$ is standard free energy of the redox reaction in the solvent. From the cycle, we get

$$\Delta G_{s1}{}^{o} = I - \Delta G_{s1}{}^{o}(R) + \Delta G_{s1}{}^{o}(O) \tag{4.1}$$

Similarly, for solvent S_2, we obtain an analogous equation

$$\Delta G_{s2}{}^{o} = I - \Delta G_{s2}{}^{o}(R) + \Delta G_{s2}(O) \tag{4.2}$$

Here we do not consider the electron because its energy is independent of the solvent.[112] According to the thermodynamic formula

$$\Delta G^{o} = -nFE^{o}$$

where n, F, and E^{o} are the number of electrons of the redox reaction, Faraday constant, and standard electrode potential, respectively. Therefore, we have

$$\begin{aligned} E_{s2}{}^{o} - E_{s1}{}^{o} = 1/nF[(\Delta G_{s2}{}^{o}(O) - \Delta G_{s2}{}^{o}(R)) \\ - (\Delta G_{s1}{}^{o}(O) - \Delta G_{s1}{}^{o}(R))] \end{aligned} \tag{4.3}$$

From equation 4.3, if the solvent S_2 stabilizes the oxidized state relative to the reduced state more than solvent S_1, the first term in the brackets will be more negative than the second term. (Note that all G_s are negative.) So the difference, $E_2{}^{o} - E_1{}^{o}$, will be negative, indicating that E^{o} decreases as the relative capability of solvent to stabilize the oxidized-state increases. Qualitatively, this result is understandable because the species is more easily oxidized as the oxidized state is stabilized relative to the reduced state.

The solvent donor number (DN) is a parameter that reflects the electron-donating capability of solvent. The expectation is that solvents with higher DN will preferentially stabilize the oxidized state and thereby lower the midpoint potential, $E_{1/2}$. This expectation is met by the experimental results displayed in Figure 4.35.

(3) Cyclic voltammetry of the μ-oxo bridged dimers

The cyclic voltammographic behavior of the $(5,5'\text{-diester})_2(OH_2)Ru^{III}\text{-O-}Ru^{III}(OH_2)(5,5'\text{-diester})_2$ ion was studied in detail to provide comparison with the well-studied underivatized analogy.[11] Two waves (I and III) were observed at potentials 850 and 750 mV upon scanning from 0.5 to 1.5 V vs. SCE (Figure 4.36), which corresponded to the one-electron oxidation/reduction step:

$$(5,5'\text{-diester})_2(OH_2)Ru^{III}\text{-O-}Ru^{III}(OH_2)(5,5'\text{-diester})_2 \rightarrow$$
$$(5,5'\text{-diester})_2(OH_2)Ru^{III}\text{-O-}Ru^{IV}(OH_2)(5,5'\text{-diester})_2 + e^-$$

The other wave (II) at 1300 mV is irreversible and has almost no coupled wave in the return cathodic scan. This wave corresponds to the oxidation of the mixed-valence dimer to a higher valence state. From the relative amplitudes of waves, the step appears to be a one-electron oxidation. Possible reasons why the wave does not have a coupled reduction wave may be that the higher oxidation state dimer catalytically oxidizes the ligand and/or water to dioxygen. The amplitudes of the quasi-reversible oxidative and reductive waves (I, II) are nearly identical, suggesting that oxidative degradation of the dimer in its higher oxidation state is minimal.

The relationships between the $Ru_2^{III,III/III,IV}$ midpoint reduction potentials and pH for the underivatized and 5,5'-diester derivatized μ-oxo ions are shown in Figure 4.37. They are very similar except that the curve for the diester derivative complex is shifted to higher

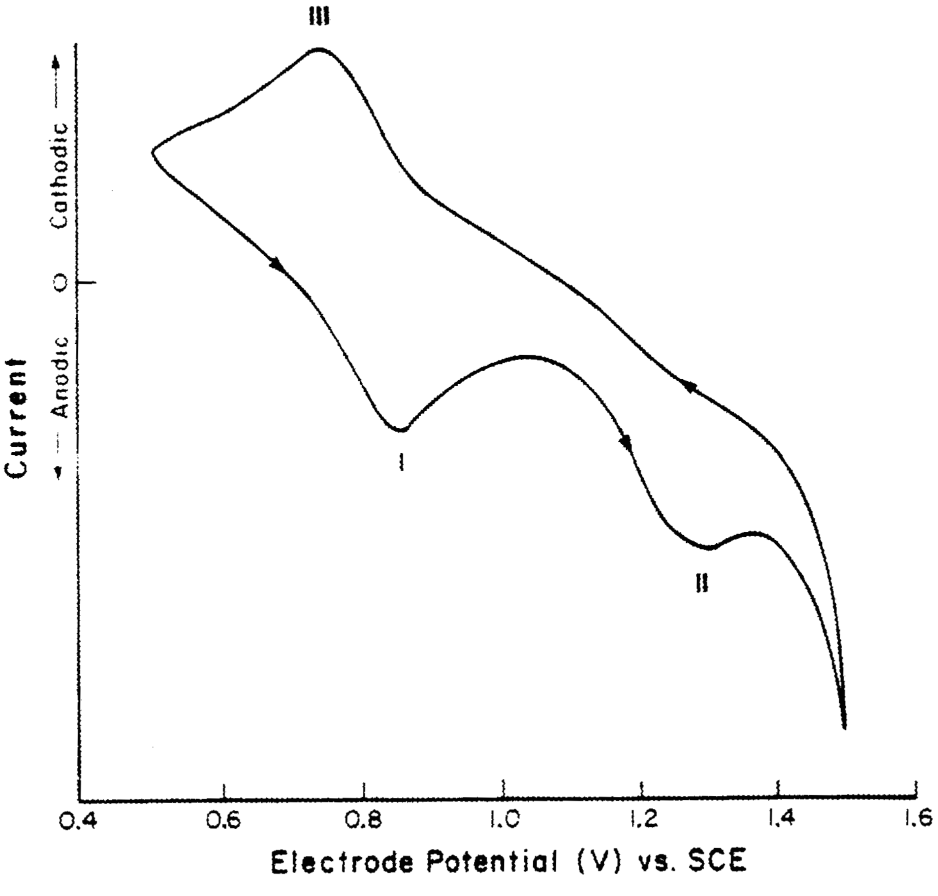

Figure 4.36. Cyclic voltammogram of 1.0 mM (5,5′-diester)$_2$(OH$_2$)Ru^{III}-O-Ru^{III}(OH$_2$)(5,5′-diester)$_2$ ion in 0.1 N HSO$_4^-$/SO$_4^{2-}$, pH 3.02; other conditions as in Figure 4.34.

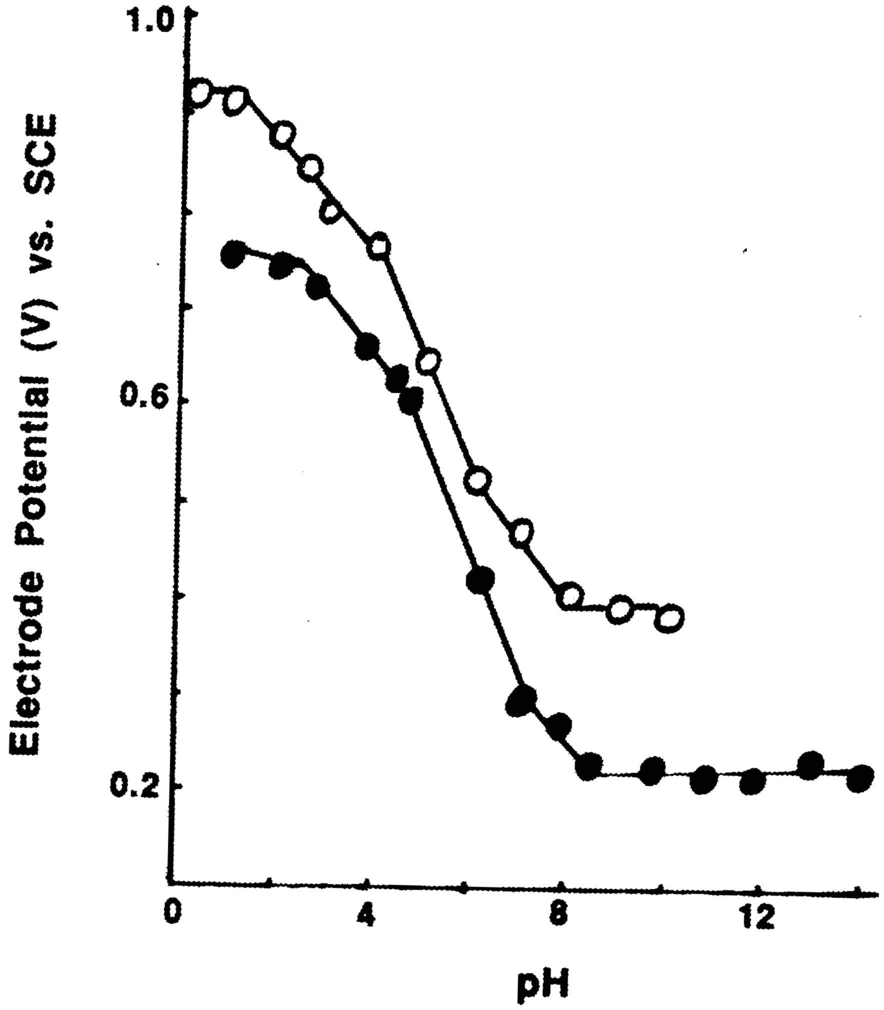

Figure 4.37. Relationship between reduction potential and pH. o: (5,5'-diester)$_2$(OH$_2$)Ru^{III}-O-Ru^{III}(OH$_2$)(5,5'-diester)$_2$. ●: (bpy)$_2$(OH$_2$)Ru^{III}ORu^{III}(OH$_2$)(bpy)$_2$.

potentials with corresponding changes in slopes apprearing at more For the (III,III)/(III,IV) couple, there are five distinctly acidic acidic values. This behavior is consistent with expectations based upon adding electron-withdrawing substituents to the rings.

For the (III,III)/(III,IV) couple, there are five distinctly different regions of pH behavior as shown in Figure 4.37. When pH <1.0, $E_{1/2}$ for the couple is pH-independent. This shows that there is no change in proton content of the dimer upon one-electron oxidation, and the oxidative process is as shown in reaction 4.11:

$$(5,5'\text{-diester})_2(OH_2)Ru^{III}\text{-O-}Ru^{III}(OH_2)(5,5'\text{-diester})_2 \rightarrow$$
$$(5,5'\text{-diester})_2(OH_2)Ru^{III}\text{-O-}Ru^{IV}(OH_2)(5,5'\text{-diester})_2 + e^- \quad (4.11)$$

From pH 1 to 4, $E_{1/2}$ decreases by 60 mV per pH unit, consistent with the loss of one proton upon oxidation, reaction 4.12:

$$(5,5'\text{-diester})_2(OH_2)Ru^{III}\text{-O-}Ru^{III}(OH_2)(5,5'\text{-diester})_2 \rightarrow$$
$$(5,5'\text{-diester})_2(OH_2)Ru^{III}\text{-O-}Ru^{IV}(OH)\ (5,5'\text{-diester})_2 +$$
$$H^+ + e^- \quad (4.12)$$

In the pH range of 4.0 to 6.0, $E_{1/2}$ decreases by 120 mV per pH unit, consistent with the loss of two protons upon oxidation, reaction 4.13:

$$(5,5'\text{-diester})_2(OH_2)Ru^{III}\text{-O-}Ru^{III}(OH_2)(5,5'\text{-diester})_2 \rightarrow$$
$$(5,5'\text{-diester})_2(OH)Ru^{III}\text{-O-}Ru^{IV}(OH)\ (5,5'\text{-diester})_2 +$$
$$2H^+ + e^- \quad (4.13)$$

In the pH 6.0 to 8.0, $E_{1/2}$ decreases by 60 mV per pH unit, indicating the existence of a second one-electron, one-proton region, equation (4.14):

(5,5′-diester)$_2$(OH)Ru^{III}–O–Ru^{III}(OH$_2$)(5,5′-diester)$_2$ →
(5,5′-diester)$_2$(OH)Ru^{III}–O–Ru^{IV}(OH) (5,5′-diester)$_2$ +
H$^+$ + e$^-$ (4.14)

Above pH 8, $E_{1/2}$ is once again independent of pH, and the oxidation process is shown in equation (4.15):(5,5′-diester)$_2$(OH)Ru^{III}–O–Ru^{III}(OH)(5,5′-diester)$_2$ →
(5,5′-diester)$_2$(OH)Ru^{III}–O–Ru^{IV}(OH) (5,5′-diester)$_2$ + e$^-$ (4.15)

From the first and second break points of the $E_{1/2}$ vs. pH line, pK_{a1} and pK_{a2} for (5,5′-diester)$_2$(OH$_2$)Ru^{III}–O–Ru^{IV}(OH$_2$)(5,5′-diester)$_2$ ion are estimated to be < 1 and 3.2, respectively. From the third and fourth break points, pK_{a1} and pK_{a2} for (5,5′-diester)$_2$(OH$_2$)Ru^{III}–O–Ru^{III}(OH$_2$)(5,5′-diester)$_2$ are estimated to be 5.5 and 7.5, respectively. The corresponding values for the unsubstituted ions are reported[11] to be pK_{a1} = 5.9 and pK_{a2} = 8.3 for (bpy)$_2$(OH$_2$)]$_2$Ru^{III}ORu^{III}(OH$_2$)(bpy); pK_{a1} = 0.4 and pK_{a2} = 3.2 for (bpy)$_2$(OH$_2$)Ru^{III}ORu^{IV}(OH$_2$)(bpy)$_2$. The shift of pK_a to lower values is understandable because the presence of strong electron-withdrawing groups on the bipyridine rings removes electron density from the central ruthenium ion, strengthening the H$_2$O coordinate bond and making deprotonation of aqua ligands easier.

4.2.6 μ-Oxo bridged dimer catalysis of the oxidation of water by Co^{3+} ion.

Earlier work had shown that μ-oxo bridged dimeric complexes, L$_2$(OH$_2$)Ru^{III}–O–Ru^{III}(OH$_2$)L (L = bpy,[10,11] 4,4-diacid′′,[118] and 5,5′-diacid[14] derivatives), can catalytically oxidize water to dioxygen in the presence of strong oxidants, Co^{3+} and Ce^{4+}. Although it has been suggested that the dicarboxy derivatives are catalytically more active than the underivatized dimer, direct comparison has not heretofore been made. Therefore, I undertook a study of the comparative behavior of the diester and dimethoxy derivatives with the underivatized compound under identical experimental conditions.

(1) Direct comparative study of catalytic activity of several μ-oxo-bridged dimeric complexes

The dimer-catalyzed Co^{3+} oxidation of water to dioxygen was investigated by adding Co^{3+} in excess to 0.5 M H_2SO_4 solutions of dimers, $L_2(OH_2)Ru^{III}$-O-$Ru^{III}(OH_2)L_2$ (L = bpy, 4,4'-diester, 5,5'-diester, and 4,4'-dimethoxy), in a closed, degassed vessel (Figure 2.1), using the Clark oxygen electrode polarized at a potential of 0.6 V vs. internal Ag/AgCl electrode as a detector. Under these conditions the electrode is unresponsive to CO_2 but is sensitive to O_2. When a deoxygenated Co^{3+} solution was added to solutions of the dimers, an immediate response was observed from the polarographic electrode. The response curves of Clark electrode with these complexes as catalysts at identical concentrations are shown in Figure 4.38. Based upon initial rates, the sequence of catalyzing abilities of these complexes is:

$(bpy)_2(OH_2)Ru^{III}$-O-$Ru^{III}(OH_2)(bpy)_2$ =
4,4'-dimethoxy > 5,5'-diester > 4,4-diester

The reaction calalyzed by the underivatized compound was complete under the experimental conditions within three hours, yielding a stoichiometric amount of O_2 (0.25 equivalents of the added Co^{3+}). For the diester derivatives, reaction was incomplete even after four hours, although a near-stoichiometric amount of O_2 had formed in the case of the 5,5'-diester derivative. Catalysis by the 4,4'-dimethoxy derivative

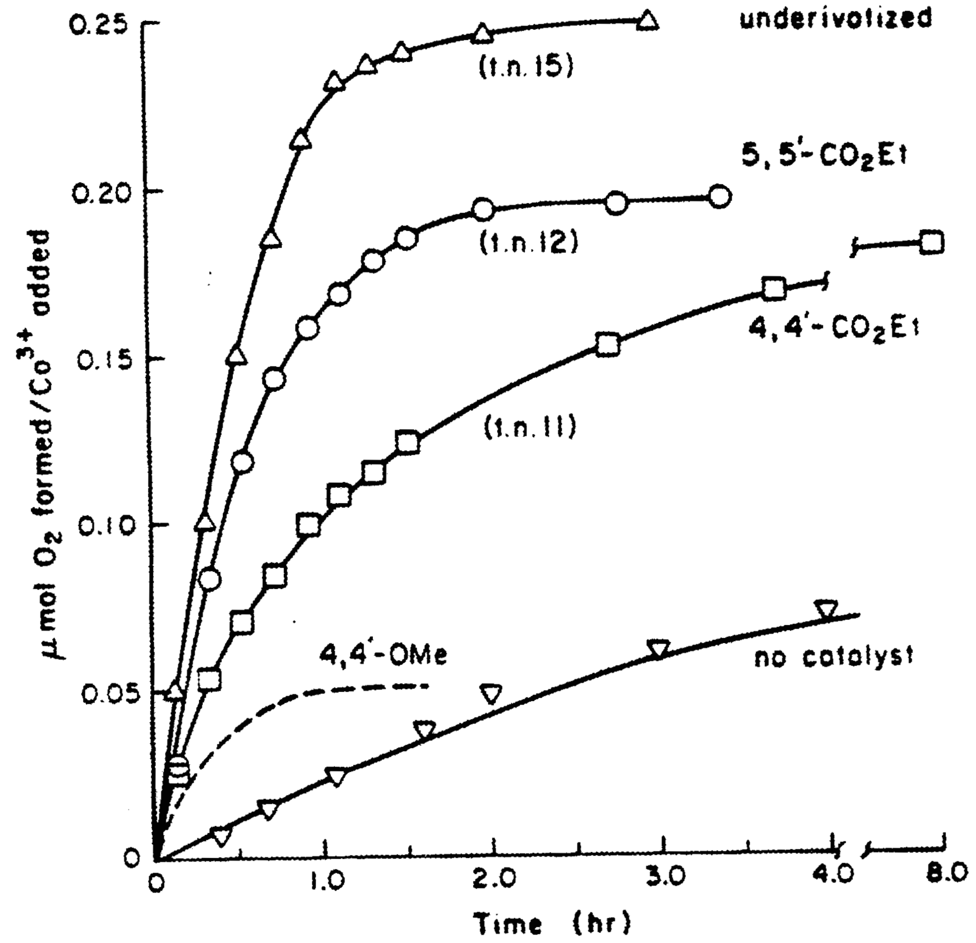

Figure 4.38. Comparison of catalytic capabilities of underivatized and derivatized μ-oxo dimeric complexes: t.n. is turnover. Underivatized: $(bpy)_2(OH_2)Ru^{III}ORu^{III}(OH_2)(bpy)_2$; 5,5'-COOEt: $(5,5'\text{-diester})_2(OH_2)Ru^{III}\text{-}O\text{-}Ru^{III}(OH_2)(5,5'\text{-diester})_2$; 4,4'-COOEt: $(4,4'\text{-diester})_2(OH_2)Ru^{III}\text{-}O\text{-}Ru^{III}(OH_2)(4,4'\text{-diester})_2$; 4,4'-OMe: $(4,4'\text{-methoxy})_2(OH_2)Ru^{III}\text{-}O\text{-}Ru^{III}(OH_2)(4,4'\text{-methoxy})_2$

during the first 10 minutes was higher than 5,5′-diester and 4,4′-diester derivatives and comparable to that of the underivatized complex, but the reaction stopped after 40 minutes. With the exception of the 4,4′-dimethoxy derivative, which was extensively bleached, the optical spectra of product solutions gave no evidence for degradation of the complexes, which exhibited bands for the III,IV ions at the original concentration levels.

The sequence of the catalytic ability can be explained as follows: Reduction potentials of 5,5′-diester and 4,4′-diester derivatives are shifted to higher values relative to underivatized complex because of the electron-withdrawing effect of the substituents. Therefore, the thermodynamic barrier to form the catalytically active species (IV,IV; IV,V; or V,V) increases. Thus, the rate of the oxidation reaction becomes slower and steady-state levels of the catalytically active species decrease. For the 4,4′-dimethoxy derivative, the catalytic oxidation state(s) should be more accessible, and the reaction comparatively accelerated. This effect might account for the observation that the catalytic activity of this complex reaches the level of the underivatized complex during the first 10 minutes of reaction. However, electron donation to the ring decreases its stability toward oxidative degradation, so that ligand decomposition becomes competitive with water oxidation. This might be the reason that the curve for 4,4′-dimethoxy derivative rapidly becomes flat.

It should be emphasized that Figure 4.38 has only semiquantitative significance with an experimental error of 20-25%. The uncertainty arises from the several sources, including standardization of Co^{3+}

(2-3%), adding Co^{3+} solution to the reactor with syringe (4-5%), response of Clark oxygen eletrode (4-5%), calibration of Clark oxygen electrode (4-5%) and leakage of the reaction system (4-5%).

From the results obtained, I reach the following conclusion: Since the underivatized complex ion, $(bpy)_2(OH_2)Ru^{III}ORu^{III})(OH_2)(bpy)$, has sufficient reduction potential in its higher oxidation states to catalytically oxidize water to oxygen, it is not neccessary to add the electron-withdrawing groups to the ligand to increase its reduction potential. Practically, adding the electron-withdrawing substituent not only does not improve capability of the catalyst but causes an adverse effect. On the contrary, to decrease the catalyst oxidation reaction barrier and accelerate the catalytic reaction, electron-donating substituents should be added to the ligand to decrease its reduction potential, at least to the extent that the reduction potential is still high enough to oxidize water to oxygen. The fact that the initial catalytic activity of the 4,4'-dimethoxy derivative is comparable to that of the underivatized complex confirms this point. Unfortunately, the electron-donating capability of methoxy is too strong to stabilize the ligand toward oxidation. If the moderate electron-donating substituents such as $-CH_3$ are added to the bipyridine rings, we might obtain the better catalysts.

(2) ^{18}O-Labeling study

To investigate the mechanism or mechanisms by which water is catalytically oxidized to dioxygen by μ-oxo ion, we also performed ^{18}O labeling studies. The ^{18}O-labeled μ-oxo bridged dimeric complex ion $(bpy)_2(^{18}OH_2)Ru^{III}(^{18}O)Ru^{III}(^{18}OH_2)(bpy)_2$ was used as the catalyst, and the gas product collection and analysis were performed according to the methods described in Chapter 2. The isotopic distribution obtained is given in Table 4.8. From the Table, the yield of $^{16}O-^{18}O$ does not exceed 20%, whereas $^{18}O-^{18}O$ is at most 1%. This indicates that the oxygen atoms forming O_2 are either derived primarily from solvent H_2O or that ligand aquation occurred rapidly during turnover. If ligand aquation is negligible during reaction, this result is inconsistent with earlier proposed intramolecular mechanisms for μ-oxo-ion-catalyzed oxidation of water to oxygen because according to the intramolecular mechanism the $^{18}O-^{18}O$ distribution should be much higher than the value obtained here. The resonance Raman results from single turnover experiments described earlier (see Figures 4.23-4.26) were interpreted to indicate that exchange of coordinated water did not occur during catalyzed water oxidation. Therefore, it appears that the intramolecular mechanisms can be excluded from consideration.

Table 4.8. Isotopic Distribution of

$bpy)_2(^{18}OH_2)Ru^{III18}ORu^{III}(^{18}H_2)(bpy)_2$-catalyzed $H_2{}^{16}O$ Oxidation[a]

$[Co^{3+}]/[Ru_2O]$	$^{34}O_2/^{32}O_2$	$^{36}O_2/^{32}O_2$
2.5/1	0.10	0.002
3.5/1	0.11	0.01
5/1	0.18	0.002

[a] Medium is 0.5 M H_2SO_4.

Actually, in terms of distance between the aqua ligands within the μ-oxo ion, it is also unlikely that two oxygen atoms that finally produce the dioxygen molecule are the result of a bimolecular reaction between water molecules bound to each ruthenium atom. The distance between two bound water molecules in (III,III) has been shown by crystal structure studies to be approximately 3.6 Å, and the Ru-O-Ru angle was found to be 165°. The Ru-O-Ru bond distance would not be expected to shorten to such an extent so that the two coordinated water molecules come close enough to react with each other upon oxidation to a (III,IV) or higher oxidation state. The Ru-O bond length in the Ru-O-Ru segment cannot be shorter than Ru=O double bond length (1.74 Å).[100] From RR results, we know that the Ru-O-Ru angle is 150° in III,IV and III,III oxidation states. If assuming that the Ru-O-Ru angle in the active form of the catalyst remains 150°, we can obtain a separation distance between the two coordinated water molecules equal to 2.46 Å. We know that single-bond covalent radius of oxygen is 0.60 Å[119] so that oxygen single-bond distance is 1.2 Å. (Double-bond distance is even shorter.) Obviously, the two coordinated water molecules are not close enough to react with each other. Thus, it seems that the function of the aqua ligands is only to permit achievement of high oxidation states within the catalyst at a reasonable potential by progressive loss of protons; whereas the oxidized dimer acts as an electron sink to remove several electrons from the bound water molecule, which then reacts with unbound water molecules to form peroxide or similar species that undergo further reaction with solvent. Based upon the above discussion, I propose a scheme (see next page) to describe the experimental observation.

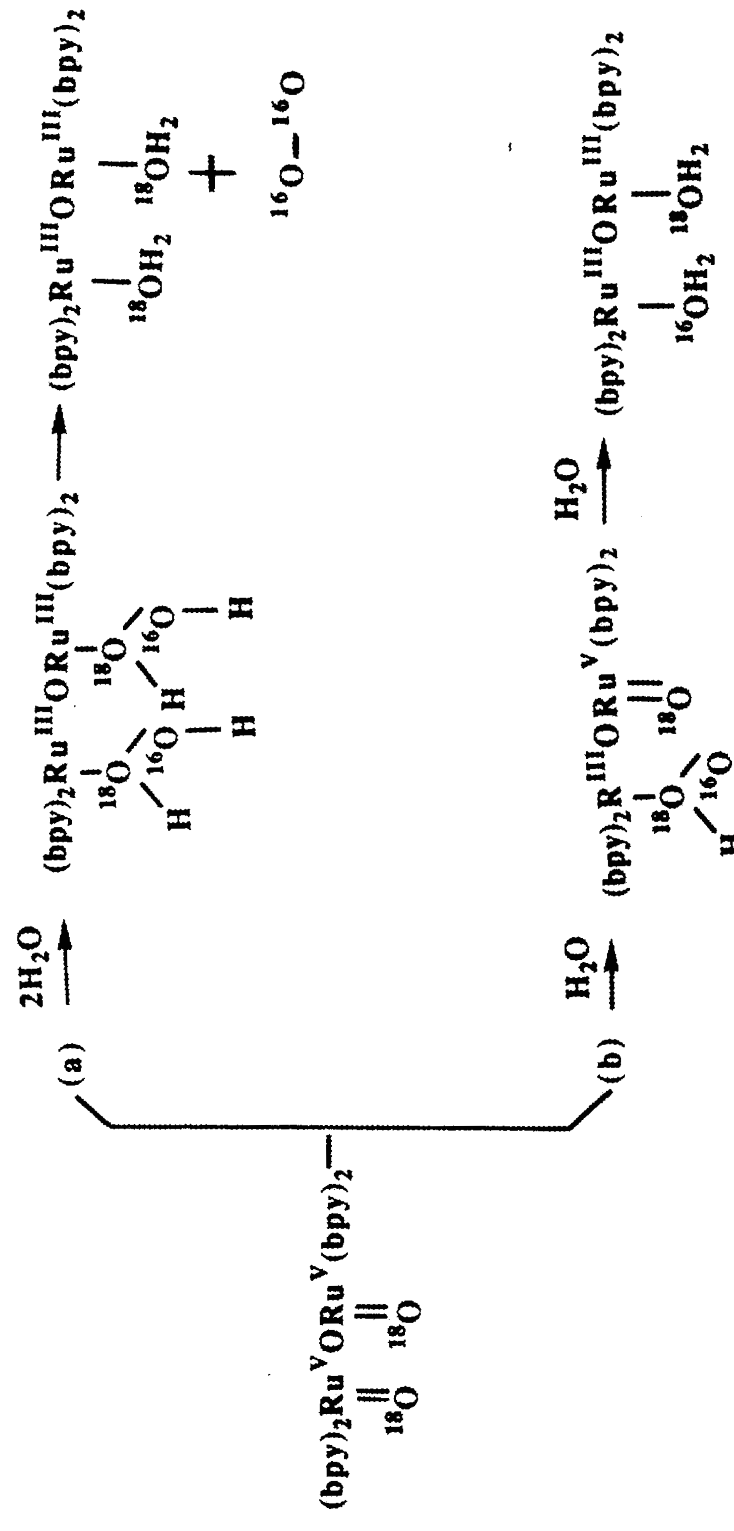

Scheme 6.

In route (a), two external water molecules attack the oxygen atoms of each electron deficient Ru^{V}-oxo site to give two bound peroxides followed by O-O bond formation and a release of $^{16}O-^{16}O$ as the observed major product. This route can overcome the difficulty of too great a distance between two aqua ligands to allow their direct reaction and still has the advantage of a 4-electron process which is favorable thermodynamically. Route (b) is the same as the mechanism (c) (Chapter I) proposed by Meyer.[20] It involves the formation of bound peroxide followed by a second intramolecular 2-electron step to form the $^{16}O-^{18}O$ product. As for formation of trace amounts of $^{18}O-^{18}O$, that can be explained by the route (a) (Chapter I) proposed by Meyer[20], i.e., the process is a synchronous 4-electron transfer which consists of an attack of external molecules at the metal atoms, O-O bond formation, and electron release to the two Ru^{V} sites.

CHAPTER V

SUMMARY AND CONCLUSION

Monomeric $Ru^{III}(edta)(OH_2)$ and dimeric $(edta)_2Ru_2^{III,IV}$ complexes were synthesized. $Ru^{III}(edta)(OH_2)$ was stable at pH <5, but at pH >5 it slowly oxidized in air to give the dimer $(edta)_2Ru_2^{III,IV}$. The $(edta)_2Ru_2^{III,IV}$ was a green, stable compound at pH <10 which had two characteristic bands at 632 and 394 nm, respectively, and a shoulder at 304 nm. These two compounds changed to a spectroscopically indistinguishable species in a strong alkaline solution (pH ~11) under anaerobic conditions, which was assigned[65] as $(edta)_2Ru_2^{III,III}$ from its characteristic band at 566 nm. The dimeric $(edta)_2Ru_2^{IV,IV}$ formed upon one-electron oxidation of $(edta)_2Ru_2^{III,IV}$ was unstable and spontaneously reverted to a species with an optical spectrum very similar to that of $(edta)_2Ru_2^{III,IV}$. The gaseous products formed during $(edta)_2Ru_2^{IV,IV}$ reduction were analyzed by several techniques. Adding oxidants such as MnO_4^-, Ce^{4+}, and Co^{3+} in acidic media gave an immediate response from a Clark electrode poised at −0.8 V vs. internal Ag/AgCl reference electrode. No response was observed when the $(edta)_2Ru_2^{III,IV}$ ion was oxidized chemically or electrochemically in alkaline solution or under any conditions when the Clark electrode was poised at −0.6 V vs. its internal reference electrode. However, acidifying alkaline solutions gave immediate response from the electrode if poised at −0.8 V vs. Ag/AgCl after the redox processes were completed. These results indicated that the predominant gaseous product was CO_2. Mass spectrometry and gas chromatographic analyses confirmed this result.

The source of CO_2 was coordinated edta. These results rule out the possibility that the dimeric ion is a water oxidation catalyst, as initially claimed by Baar and Anson.[12]

Several spectroscopic techniques were used to identify the bridging ligand in the dimer. EPR results indicated that the dimeric $(edta)_2Ru_2^{III,IV}$ had an unpaired spin and existed as a mixture of several distinct species in alkaline solutions, although it was apparently only a single ion in neutral and acidic media. FTIR spectra exhibited absorption bands attributable to the carbonyl stretching mode for protonated (1734 cm^{-1}) and metal-coordinated (1652 cm^{-1}) carbonyl groups that were very similar to spectra of monomeric $Ru^{III}(edta)(OH_2)$. Complex ions prepared from ^{18}O-H_2O were indistinguishable from those prepared in H_2O of normal isotopic composition. Therefore, it was not possible to identify the bridging ligand by FTIR spectroscopy. The RR spectra of the $(edta)_2Ru_2^{III,IV}$ in acidic and neutral solutions exhibited an intense symmetric band at 433 cm^{-1} which shifted to 431 cm^{-1} when the dimer was prepared in ^{18}O-water and was assigned to the symmetric-stretching vibrational mode of the μ-oxo dimer. A second band at 324 cm^{-1} underwent a comparable isotope-dependent shift to lower energies. The RR spectra were insensitive to deuterium substitution. These features indicated that the dimer was a μ-oxo ion; from the magnitude of the isotope shift, the Ru-O-Ru angle was estimated to be 165°.

Redox properties of the monomeric $Ru^{III}(edta)(OH_2)$ were studied by cyclic voltammetry over a wide pH range. To test several wave assignments, the dimeric $(edta)_2Ru_2^{III,IV}$ was also studied by cyclic volammetry. The reduction potential for the $(edta)_2Ru_2^{III,IV}/(edta)_2Ru_2^{IV}$ couple was acid insensitive over the pH range 2-10, suggesting that the dimer did not contain coordinated water in either oxidation state. (The absence of coordinated water in the $(edta)_2Ru_2^{III,IV}$ had been previously established from its pH titrimetric behavior.) Furthermore, the half-wave potential for the couple was 0.9 V vs. SCE, indicating that the $(edta)_2Ru_2^{IV}$ could not be a four-equivalent water oxidation catalyst. Calculations showed that the $(edta)_2Ru_2^{IV}$ could not be a catalyst for two- or three-electron water oxidation processes, either. Thus, the $(edta)_2Ru_2^{III,IV}$ ion appeared incapable of catalyzing water oxidation on thermodynamic grounds, and higher oxidation states of the complex were too unstable with respect to ligand oxidation to function effectively in this capacity.

To search for better water oxidation catalysts, a series of μ-oxo dimeric ruthenium complexes containing derivatized bipyridyl ligands were synthesized. The derivative included 4,4'-dicarbethoxy, 5,5-dicarbethoxy and 4,4'-dimethoxy compounds. ^{1}H-NMR and FTIR spectra were used to confirm structures of the ligands and their complexes. The μ-oxo dimers had several accessible oxidation states. The (III,III) dimers were dark-blue or blue-green compounds with a low-energy, highly intense optical band at 637-680 nm. Upon one-electron oxidation to the (III,IV) dimer, the band around 650 nm disappeared (for 4,4-diester and 5,5'-diester complexes) or decreased in intensity (for 4,4'-dimethoxy), and a new band appeared at around 500 nm. Spectral properties were interpretable in terms of a nonlinear three-center Ru-O-Ru bonding model. The solution pH had influence on the position of this band that was attributable to the various acid-base equilibria involving the two H_2O ligands. The electronic absorption spectra and cyclic voltammetric behavior of the monomers, RuL_2Cl_2 (L = 4,4'-diester, 5,5'-diester, 4,4'-dimethoxy), were studied in various non-aqueous solvents. The solvent effect on the spectral maximum position and half-wave potential was quantitatively discussed within the framework of the concept of solvent donor number (DN). The RR spectra of the $(bpy)_2(OH_2)Ru^{IV}ORu^{III}(OH_2)(bpy)_2$ ion exhibited an intense band at 403 cm^{-1} which shifted to 395 cm^{-1} upon substitution of ^{18}O in the ligand bridge. Two other bands, at 801 and 314 cm^{-1}, also underwent an isotope-dependent shift to lower energies. These three bands were assigned to symmetric stretching, asymmetric stretching, and bending vibration modes, respectively. From the magnitude of isotopic shifts, the Ru-O-Ru angle in the dimeric $(bpy)_2(OH_2)Ru^{III}ORu^{IV}(OH_2)(bpy)_2$ ion was estimated to be 150°. The pH effect on the position of the band at 403 cm^{-1} was also observed which was ascribed to stronger σ-donicity of OH^- than H_2O. In addition to these bands, a weak band underlying the symmetric stretching mode appeared to shift ~15 cm^{-1} to higher energies, based upon difference spectral shifts, when the ^{18}O-H_2O-containing (III,IV) ion was incubated in normal isotopic water. On this basis, the band was assigned to the $Ru-OH_2$ stretching mode of coordinated H_2O. The results were also interpreted to indicate that the exchange with solvent water is slow and does not occur at this site during the catalyzed water oxidation cycle.

Direct comparative studies indicated that the relative catalytic capacities of several μ-oxo dimeric ions were:

$(bpy)_2(OH_2)Ru^{III}ORu^{III}(OH_2)(bpy)_2$ ≈
(4,4'-dimethoxy)$_2(OH_2)Ru^{III}ORu^{III}(OH_2)$(4,4-dimethoxy)$_2$ >
(5,5'-diester)$_2(OH_2)Ru^{III}ORu^{III}(OH_2)$(5,5'-diester)$_2$ >
(4,4'-diester)$_2(OH_2)Ru^{III}ORu^{III}(OH_2)$(4,4'-diester)$_2$

However, the 4,4'-dimethoxy derivative was too unstable to oxidation and was rapidly destroyed in the presence of the oxidant Co^{3+} ion. The study suggested that better catalysts might be obtained if bipyridine derivatives which contained moderate electron-donating substituents such as CH_3 groups were used as ligands. Finally, based upon the oxygen isotope distribution of O_2 in single-turnover experiments, intramolecular oxidative elimination mechanisms for catalytic water oxidation were ruled out and alternative mechanisms were proposed that were consistent with the experimental observations.

REFERENCES

1. Zamaraev, K. I.; Parmon, V. N.; "Development of Molecular Photocatalytic Systems for Solar-Energy Conversion: Catalysts for Oxygen and Hydrogen Evolution from Water," In Energy Resources through Photochemistry and Catalysis, (1983) Chap. 5, pp 123-162, Grätzel, M., Ed., Academic Press, New York.
2. Fujishima, A.; Honda, K.; Nature (London) (1972) 238, 37.
3. Grätzel, M.; Acc. Chem. Res. (1981) 14, 376.
4. Grätzel, M.; Discuss. Faraday Soc. (1981) 70, 359.
5. Nozik, A.; Discuss. Faraday Soc. (1981) 70, 7.
6. Bard, A. J.; Science (1980) 207, 139.
7. Bolton, J. R.; Science (1978) 202, 705.
8. Kiwi, J.; Grätzel, M.; Angew. Chem. Int. Ed. Engl. (1978) 17, 11.
9. Mills, A.; Chem. Soc. Rev. (1989) 18, 285.
10. Gersten, S. W.; Samuels, G. J.; Meyer, T. J.; J. Am. Chem. Soc. (1982) 104, 4029.
11. Gilbert, J. A.; Eggleston, D. S.; Murphy, W. R.; Geselowitz, D. A.; Gersten, S. W.; Hodgson, D. J.; Meyer, T. J.; J. Am. Chem. Soc. (1985) 107, 3855.
12. Baar, R. B.; Anson, F. C.; J. Electroanal. Chem. (1985) 187, 265.
13. Baar, R. B.; Ph.D. Dissertation, California Institute of Technology (1985).
14. Rotzinger, F. P.; Munavalli, S.; Comte, P.; Hurst, J. K.; Grätzel, M.; Pern, F.-J.; Frank, A. J.; J. Am. Chem. Soc. (1987) 109, 6919.
15. Nazeeruddin, M. K.; Rotzinger, F. P.; Comte, P.; Grätzel, M.; J. Chem. Soc. Chem. Commun. (1988) 872.

16. Ramaraj, R. K.; Kaneko, M.; Angew. Chem. Int. Ed. Engl. (1986) 25, 825.

17. Ramaraj, R. K.; Kanako, M.; Chem. Lett. (1987) 261.

18. Ellis, C. D.; Gilbert, J. A.; Murphy, W. A.; Meyer, T. J.; J. Am. Chem. Soc. (1983) 105, 4842.

19. Tokeuchi, K. J.; Samuels, G. J.; Gersten, S. W.; Gilbert, J. A.; Meyer, T. J.; Inorg. Chem. (1983) 22, 1407.

20. Meyer, T. J.; J. Electrochem. Soc. (1984) 131, 221c.

21. Tokeuchi, K. J.; Thompson, M. S.; Pips, D. W.; Meyer, T. J.; Inorg. Chem. (1984) 23, 1845.

22. Raven, S. J.; Meyer, T. J.; Inorg. Chem. (1988) 27, 4478.

23. Llobet, A.; Curry, M. E.; Evans, H. T.; Meyer, T. J.; Inorg. Chem. (1989) 28, 3131.

24. Thompson, M. B. A.; Meyer, T. J.; J. Am. Chem. Soc. (1980) 102, 2310.

25. Ezerskaya, N. A.; Solovykh, T. P.; Russ. J.; Inorg. Chem. (1966) 11, 991.

26. Ezerskaya, N. A.; Solovykh, T. P.; Russ. J.; Inorg. Chem. (1966) 11, 1168.

27. Ezerskaya, N. A.; Solovykh, T. P.; Russ. J.; Inorg. Chem. (1968) 13, 96.

28. Ikada, M.; Shimizu, K.; Sato, G. P.; Bull. Chem. Soc. Jpn. (1982) 55, 797.

29. Weaver, T. R.; Meyer, T. J.; Adeyami, S. A.; Brown, G. M.; Eckberg, R. P.; Hatfield, W. E.; Johnson, E. C.; Murray, R. W.; Untereker, D.; J. Am. Chem. Soc. (1975) 97, 3039.

30. Bauman, J. A.; Meyer, T. J.; Inorg. Chem. (1983) 19, 345.

31. Shimizu, K.; Bull. Chem. Soc. Jpn. (1977) 50, 2921.

32. Ghosh, P.; Brunschwig, B. S.; Creutz, C.; Sutin, N.; J. Am. Chem. Soc. (1984) 106, 4772.

33. Matsubara, T.; Creutz, C.; Inorg. Chem. (1979) 18, 1956.

34. Andrade, C.; Jordan, R. B.; Taube, H.; Inorg. Chem. (1970) 9, 711.

35. Warngvist, B.; Inorg. Chem. (1970) 9, 682.

36. Skoog, D. A.; West, D. M.; Fundamentals of Analytical Chemistry, (1969) 2nd ed., pp 421-423, Holt, Rinehart and Winston, Inc., New York.

37. Anderson, C. W.; Halsall, H. B.; Heineman, W. R.; Anal. Biochem. (1979) 93, 366.

38. DeAngells, T. P.; Heineman, W. R.; J. Chem. Ed. (1976) 53, 594.

39. Kuwana, T.; Heineman, W. R.; Acc. Chem. Res. (1976) 9, 241.

40. Heineman, W. R.; Anal. Chem. (1978) 50, 390A.

41. Launikonis, A.; Lay, P. A.; Mau, A. W.-H.; Sargeson, A. M.; Sasse, W. H. F.; Aust. J. Chem. (1986) 39, 1053.

42. Whittle, C. P.; J. Heterocycl. Chem. (1977) 14, 191.

43. Jones, R. A.; Roney, B. D.; Sasse, W. H. F.; Wade, K. O.; J. Chem. Soc. B (1967) 106.

44. Haginirva, J.; J. Pharm. Soc. Jpn. (1955) 75, 731.

45. Maeker, G.; Case, F. H.; J. Am. Chem. Soc. (1958) 80, 2745.

46. Wenkert, D.; Woodward, R. B.; J. Org. Chem. (1983) 48, 283.

47. Burstall, F. H.; J. Chem. Soc. (1938) 1662.

48. Case, F. H.; J. Org. Chem. (1966) 31, 2398.

49. Geissman, T. A.; Schatter, M. J.; Webb, I. D.; Robert, J. D.; J. Org. Chem. (1946) 11, 741.

50. Murase, I.; Nippon Kagaku Zasshi (1956) 77, 682.

51. Willink, H. D. T.; Wibant, J. P.; Rec. Trav. Chim. (1935) 54, 275.

52. Anderson, S.; Constable, E. C.; Seddon, K. R.; Turp, J. E.; J. Chem. Soc. Dalton Trans. (1985) 2247.

53. Pirzard, N. H.; Pojer, P. M.; Summers, L. A.; Z. Naturforsch (1976) 316, 115.

54. Case, F. H.; J. Am. Chem. Soc. (1946) 68, 2574.

55. Kurita, K.; Williams, R. L.; J. Polym. Soc. Polym. Chem. Ed. (1973), 11, 3125.

56. Badge, G. M.; Sasse, W. H. F.; J. Chem. Soc. (1956) 616.

57. Sasse, W. H. F.; J. Chem. Soc. (1961) 1347.

58. Sasse, W. H. F.; Org. Synth. (1973) 5, 102.

59. Ochiai, E.; J. Org. Chem. (1953) 18, 543.

60. Byrd, L.; Miller, L. L.; Pletcher, D.; Tetrahedron Lett. (1972) 2419.

61. Miller, L. L.; Mayeda, E. A.; J. Am. Chem. Soc. (1970) 92, 5818.

62. Kissinger, P. T.; Heineman, W. R.; "Solvents and Supporting Electrolytes," In Laboratory Techniques in Electroanalytical Chemistry, (1984) Chap. 13, pp 367-382, Kissinger, P. T. Heineman, W. R., Eds., Marcer Dekker Inc. New York.

63. Hendrickson, J. B.; Cram, D. J.; Hammond, G. S.: "Organic Chemistry," (1970) Chap. 24, McGraw-Hill Book Company, New York.

64. March, J.; Advanced Organic Chemistry, (1977) Chap. 9, McGraw-Hill Book Company, New York.

65. Ni, C. L.; Anson, F. C.; J. Electroanal. Chem. (1986) 202, 101.

66. Bajaj, H. C.; van Eldik, R.; Inorg. Chem. (1988) 27, 4052.

67. Koppenol, W. H.; Butler, J.; Adv. Free Radical Biol. Med. (1985) 1, 91.

68. Carey, J. H.; Langford, C. H.; Can. J. Chem. (1973) 51, 3665.

69. Natarajan, P.; Endicott, J. F.; J. Phys. Chem. (1973) 77, 2049.

70. Yoshino, Y.; Ouchi, A.; Tsunoda, Y.; Kojima, M.; Can. J. Chem. (1962) 40, 775.

71. Hamm, R. E.; Suwyn, M. A.; Inorg. Chem. (1967) 6, 139.

72. Shirakashi, T.; Ogino, H.; Tanaka, N.; Nippon Kagaku Kaishi (1972) 1658.

73. Easom, K. A.; Bose, R. N.; Inorg. Chem. (1988) 27, 2331.

74. Hamm, R. E.; J. Am. Chem. Soc. (1953) 75, 5670.

75. Ogino, H.; Watanabe, T.; Nobuyuki, T.; Inorg. Chem. (1975) 9, 2093.

76. Weyh, J. A.; Pierce, R. L.; Inorg. Chem. (1971) 10, 858.

77. Guardalabene, J.; Gulnak, S.; Keder, N.; Shepherd, R. E.; Inorg. Chem. (1979) 18, 22.

78. Roecker, L.; Kutner, W.; Gilbert, J. A.; Simmons, M.; Murray, R. W.; Meyer, T. J.; Inorg. Chem. (1985) 24, 3784.

79. Bryant, G. M.; Fergusson, J. E.; Powell, H. K. J.; Aust. J. Chem. (1971) 24, 257.

80. Bryant, G. M.; Fergusson, J. E.; Aust. J. Chem. (1971) 24, 275.

81. Orgel, L. E.; J. Chem. Soc. (1961) 3683.

82. Gray, H. B.; BEACH, N. A.; J. Am. Chem. Soc. (1963) 82, 2922.

83. Jorgenson, C. K.; "Absorption Spectra and Chemical Bonding in Complexes," (1962) Pergamon Press, Ltd, Oxford.

84. Klassen, D. M.; Crosby, G. A.; J. Chem. Phys. (1968), 48, 1853.

85. Ohsawa, Y.; Whangbo, M. H.; Hanck, K. W.; Dearmond, M. K.; Inorg. Chem. (1984), 23, 3426.

86. Ford, P.; Rudd, D. P.; Gaunder, R.; Taube, H.; J. Am. Chem. Soc. (1968) 90, 1187.

87. Hanazak,I.; Nagakura, S.; Inorg. Chem. (1969) 8, 648.

88. Bjerrum, J.; Adamson, A. W.; Bostrup, O.; Acta Chem. Scand. (1956) 10, 329.

89. Miller, T. R.; Dance, I. R.; J. Am. Chem. Soc. (1973) 95, 6970.

90. Burgess, J.; Spectrochim. Acta, Part A (1970), A26, 139; 1957.

91. Reichardt, C.; Angew. Chem. Int. Ed. Engl. (1965) 4, 29.

92. Kosower, E. M.; J. Am. Chem. Soc. (1958) 80, 3253.

93. Gidney, P. M.; Gillard, R. D.; Heaton, B. T.; J. Chem. Soc., Dalton Trans. (1973) 132.

94. Gutman, V.; "The Donor-Acceptor Approach to Molecular Interaction," (1978) Chap. II, Plenum Press, New York.

95. Curtis, J. C.; Sullivan, B. P.; Meyer, T. J.; Inorg. Chem. (1983) 22, 224.

96. Chang, J. P.; Fung, E. Y.; Curtis, J. C.; Inorg. Chem. (1986) 25, 4233.

97. Creutz, C.; Chou, M. H.; Inorg. Chem. (1987) 26, 2995.

98. Fung, E. Y.; Chua, A. C. M.; Curtis, J. C.; Inorg. Chem. (1988) 27, 1294.

99. Kilamura, N.; Sato, M.; Kim, H. B.; Obata, R.; Tazuke, S.; Inorg. Chem. (1988) 27, 651.

100. Dunitz, J. D.; Orgel, L. E.; J. Chem. Soc. (1953) 2594.

101. Weaver, T. R.; Meyer, T. J.; J. Am. Chem. Soc. (1975) 97, 3039.

102. Baumann, J. A.; Meyer, T. J.; Inorg. Chem. (1980) 19, 345.

103. Raven, S. J.; Meyer, T. J.; Inorg. Chem. (1988) 27, 4478.

104. Burchfield, D. E.; Richman, R. M.; Inorg. Chem. (1985) 24, 852.

105. Clark, R. J. H.; Frank, M. L.; Turtle, P.C.; J. Am. Chem. Soc. (1977) 99, 2473.

106. Earlet, J. E.; Fealey, T.; Inorg. Chem. (1973) 12, 323.

107. Baumann, J. A.; Salman, D. J.; Wilson, S. T.; Meyer, T. J.; Inorg. Chem. (1978) 17, 3342.

108. Durhum, B.; Wilson, S. R.; Hodgson, D. J.; Meyer, T. J.; J. Am. Chem. Soc. (1980) 102, 600.

109. Sanders-Loehr, J.; "Binuclear Iron Proteins," In Iron Carrier and Iron Proteins (1989) Chap. 5, pp 373-466, Loehr, T. M., Ed., VCH, New York.

110. Popovych, O.; "Transfer Activity Coefficients (Medium Effects)," In Treatise of Analytical Chemistry, Part 1, Vol. 1, 2nd Ed., Chap. 12, Kolthoff, I. M. and Elving, P. J., Eds., John Wiley and Sons, New York.

111. Sahami, S.; Weaver, M. J.; J. Electroanal. Chem. Interfacial Electrochem. (1981) 122, 155.

112. Popovych, O.; Tomkins, R. P. T.; Nonaqueous Solution Chemistry (1981), Chap. 9, pp 372-422, John Wiley & Sons, New York.

113. Adams, D. M.; "Metal-Ligand and Related Vibrations," (1968) Chap. 5, St. Martin's Press, New York.

114. Ferraro, J. R.; "Low-Frequency Vibrations of Inorganic and Coordination Compounds," (1971) Chap. 5, pp 65-109, Plenum Press, New York.

115. Wing, R. M.; Callahan, K. P.; Inorg. Chem. (1969) 8, 871.

116. Hewkin, D. J.; Griffith, W. P.; J. Chem. Soc. A (1966) 472.

117. Cotton, F. A.; Wing, R. M.; Inorg. Chem. (1965) 4, 867.

118. Meyer, T. J.; J. Eletrochem. Soc. (1984) 131, 221c.

119. Comte, P.; Nazeeruddin, M. K.; Rotzinger, F. P.; Frank, A. J.; Grätzel, M.; J. Mol. Catalysis (1989) 52, 63.

120. Pauling, L.; "The Nature of the Chemical Bond," (1960) 3rd Ed. Chap. 7, pp 224, Cornell University Press, Ithaca, New York.

121. Nakanishi, K.; Solomon, P.; "Infrared Absorption Spectroscopy," (1977) 2nd Ed., Chap 3, , Holden-Day, Inc.

122. Conley, R. T. "Infrared Spectroscopy," (1972) 2nd Ed., Chap. 5, Allyn and Bacon, Inc.

123. Loehr, T. M.; Shiemke, A. K.; In Biological Applications of Raman Spectroscopy (1988) Vol. 3, Chap. 10, Spiro, T. G., Ed., Wiley, New York.

124. Fischer, B.; Eisenberg, R.; J. Amer. Chem. Soc. (1980) 102, 7361.

125. Haynes, L. V.; Sawyer, D.; Anal. Chem. (1967) 39, 332.

126. Sander-Loehr, J.; Wheeler, W. D.; Shiemke, A. K.; Averill, B. A.; Loehr, T. M.; J. Amer. Chem. Soc. (1989) 111, 8084.

128. Lincoln, S. E.; Loehr, T. M.; Inorg. Chem. (1990) 29, 1097.